Marlene Trindade

Maternal thyroid hormones role in zebrafish blood-hindbrain barrier development

Universidade do Algarve

Faculdade de Ciências e Tecnologia

2023

Marlene Trindade

Maternal thyroid hormones role in zebrafish blood-hindbrain barrier development

Doutoramento em Ciências Biológicas

Especialidade em Biologia do desenvolvimento

Trabalho efetuado sob a orientação de:

Doutor Marco António do Nascimento Sequeira de Jesus Campinho

Universidade do Algarve

Faculdade de Ciências e Tecnologia

2023

Título | Thesis title

Maternal thyroid hormones role in zebrafish blood-hindbrain barrier development

Declaração de autoria de trabalho:

Declaro ser a autora deste trabalho que é original e inédito. Autores e trabalhos consultados estão devidamente citados no texto e constam da listagem de referências incluída.

Declaration of authorship:

This work has not previously been submitted for a degree in any university. To the best of my knowledge and belief, the thesis contains no material previously published or written by another person except where due reference is made in the thesis itself.

Marlene Pacheco Trindade

ACKNOWLEDGEMENTS

This thesis is the result of the work where many people have contributed with their support, guidance, and friendship.

The journey of my PhD started in 2015 when Marco Campinho asked me if I would like to do this thesis. I can say that I am truly grateful for this opportunity and that it was really challenging. It was a real life-changing experience for me with a lot of ups and downs. I learned a lot from his experience and his theoretical and practical knowledge. I want to thank my supervisor Marco Campinho for his help in the lab and principally for his availability, support, and guidance during all this time.

A special thanks to Nádia Silva, for her support and friendship. Who always heard my complaints and my achievements. She had always a friendly word when times were tough.

I want to thank my friends Vilma Duarte, Sílvia Coelho, Xana Alves and Pasqualina Gaetano for the good time in the lab and their help, companionship, and friendship.

I want to thank Bruno Louro for his help in the transcriptomic analysis. His help and collaboration allowed to publish our first paper, together with Nadia Silva (author), Prof. Deborah Power and my supervisor Marco Campinho: *Transcriptomics reveal an integrative role for maternal thyroid hormones during zebrafish embryogenesis* (2017). doi.org/10.1038/s41598-017-16951-9.

I want to thank the AlfaScore project from the Algarve Biomedical Centre Research Institute (ABC Ri) that allowed me to finish writing my thesis while working on the project.

Thank you to my family for all the support.

Thank you Zé for everything. You joined my life during my darkest moments in life and brought the light and joy back. Afterwards, our son Tiago was born, and although it was difficult to conciliate the work and writing of this thesis, you had the patience to be there and hear my complaints and also my joy after finishing writing one more Chapter.

I dedicate this work to my son Tiago so that you know that everything in life is achievable with effort and determination and above all when you truly want it!

FUNDING

Marlene Trindade was supported by the Portuguese Foundation for Science and Technology (FCT) through the PhD grant SFRH/BD/108842/2015.

This study received Portuguese national funds from FCT - Foundation for Science and Technology through project PTDC/EXPL/MAR-BIO/0430/2013, UIDB/04326/2020, UIDP/04326/2020 and LA/P/0101/2020, and from the operational programmes CRESC Algarve 2020 and COMPETE 2020 through project EMBRC.PT ALG-01-0145-FEDER-022121.

I acknowledge the contribution of the Light Microscopy Unit of CBMR-UAlg. The Microscopy Unit was partially supported by national Portuguese funding FCT: UID/BIM/04773/2013 CBMR and PPBI-POCI-01-0145-FEDER-022122.

Dificuldades preparam pessoas comuns

para destinos extraordinários

C.S Lewis

ABSTRACT

Thyroid hormones (THs), thyroxine (T4) and 3,5,3'–triiodothyronine (T3), are key signalling molecules that regulate vertebrate development and physiology. In humans, an inadequate supply of THs during prenatal stages causes several neurological impairments, affecting a new-born' psychomotor and cognitive development. The most severe condition results from mutations of the monocarboxylate transporter 8 (MCT8), leading to a rare X-linked neurodevelopmental disorder, the Allan-Herndon-Dudley syndrome (AHDS). In zebrafish, knockdown of the T3 exclusive membrane transporter Mct8 phenocopies the symptoms observed in AHDS patients. An impaired blood-hindbrain barrier (BHB) was observed in zebrafish but has not yet been confirmed in humans. This thesis aimed to understand how maternal T3 (MT3) through Mct8 coordinates the development of the vascular system of the zebrafish hindbrain. Transcriptome analysis of 25 hours post fertilisation (hpf) CTRMO vs MCT8MO zebrafish embryos revealed that expression of several genes of the important angiogenic Vegf pathway was significantly regulated by MT3. At the cellular level, specific *vegfaa* signalling juxtaposed to the developing central arteries (CtAs) was identified and *vegfaa-165* mRNA rescues the majority of CtAs in MCT8MO zebrafish embryos. To identify the source of hindbrain *vegfaa* and, consequently, the cell identity dependent on MT3 signalling, neural cell markers were analysed. This revealed that *pax8* inhibitory interneurons and *cpne4* intrinsic digit-innervating motor neurons were under MT3 regulation but were not responsible for CtA development. *pax6a* neural progenitor cells (NPCs) were the source of hindbrain *vegfaa*, and a correlation between these cells and the migratory behaviour of the CtAs was found. Colocalisation analysis of *pax6a* NPCs with *thraa*, *thrab* and *mct8* demonstrated that these cells were regulated in a cell-autonomous way and showed that the spatiotemporal expression could be an indicator of the timely sprouting of each CtA during BHB development. Finally, *pax6a* loss-of-function CRISPR/Cas9 zebrafish embryos had a similar hindbrain vascular impairment as the MCT8MO zebrafish embryos, confirming that *pax6a* NPCs were the cells responsible for CtA ingression into the hindbrain. In conclusion, MT3 via Mct8 is important for the survival and proliferation of *pax6a* NPCs, which are the instructing source of *vegfaa* necessary for the timely development of the BHB CtAs.

KEYWORDS: angiogenesis; blood-hindbrain barrier development; central arteries; maternal T3; MCT8; zebrafish.

RESUMO

A contribuição das hormonas da tiroide (TH) para o desenvolvimento do sistema nervoso central (CNS) é reconhecido há muitos anos. Durante o primeiro trimestre, as TH são fornecidas pela gestante para o embrião, demonstrando que desde o início do desenvolvimento embrionário estas hormonas possuem um papel fundamental para a formação do embrião. Alias, concentrações inadequadas de TH nesta fase do desenvolvimento levam a malformações do CNS graves e irreversíveis para o descendente. Estas malformações podem ser devido a hipotiroidismo ou hipotiroxinemia gestacional, ou devido a mutações dos recetores nucleares da T3 ou dos transportadores das TH no embrião/feto. Em humanos, mutações no principal transportador da TH, o transportador monocarboxilato 8 (MCT8), causa a síndrome de Allan-Herndon-Dudley (AHDS). Esta doença rara provoca atrasos globais no desenvolvimento, ausência de fala e graves problemas a nível neuro motora. Neste trabalho utilizamos o modelo knockdown do Mct8 no peixe zebra. Neste modelo inibimos a tradução do transportador Mct8 durante o desenvolvimento embrionário e deste modo impedimos o transporte da hormona materna T3 (MT3) para as células alvo e consequentemente inibimos a ação da hormona. Este modelo possui características fenotípicas semelhantes a síndrome AHDS humana. Para além disso uma barreira hematoencefálica (BHB) comprometida foi detetada no rombencéfalo dos embriões de peixe zebra em que o Mct8 foi knockdown. Esta condição ainda não foi descrita nos doentes com AHDS. O objetivo desta tese consiste em compreender qual o papel da MT3 para a formação do sistema vascular do rombencéfalo no peixe zebra. A análise do transcriptoma do peixe zebra controlo morfolino (CTRMO) e MCT8MO às 25 horas pós-fertilização (hpf) por RNAseq permitiu determinar que vários genes envolvidos nos "pathways" Vegf, Wnt e Notch, que são essenciais à angiogénese, estão alterados na sua expressão. Selecionamos alguns destes genes e analisamos a expressão, no embrião inteiro, por uma série temporal desde o início da formação da BHB (28 hpf) até a vascularização completa (72 hpf) por qRT-PCR. No entanto verificamos que não existe nenhuma alteração a nível da expressão dos genes entre o grupo CTRMO e MCT8MO. Analisando a distribuição celular de alguns desses genes por hibridação *in situ* e/ou por imunohistoquímica demonstrou que a MT3 possui uma ação celular específica que não foi possível detetar na análise por qRT-PCR. Mostramos que entre os genes escolhidos, o *vegfaa* possui uma localização celular próxima das artérias cerebrais (CtAs), os quais estão maioritariamente ausentes nos embriões MCT8MO. O sinal do *vegfaa* nos embriões MCT8MO está significativamente reduzida ou ausente no rombencéfalo

do peixe-zebra. Demonstramos que é possível recuperar a maioria das CtAs nos embriões MCT8MO através de microinjeção com mRNA do *vegfaa-165*. Globalmente estes resultados mostram que a MT3 regula a ação do *vegfaa* no rombencéfalo para a formação das CtAs. De modo a determinar o tipo celular que está a ser regulado pela MT3, o qual é responsável pela expressão do *vegfaa*, usamos vários marcadores celulares neurais. Averiguamos alguns marcadores para neurónios, os quais foram previamente relatados estarem a ser regulados pelas TH. No entanto verificou-se que os neurónios *pax8*+ e o *cpne4*+ não estão envolvidos na formação da BHB. Durante o desenvolvimento embrionário, as primeiras células que promovem a formação da BHB são as células progenitoras neurais (NPC). Estas células são um alvo direto das TH, tanto para a sua sobrevivência como para a sua proliferação celular. Verificamos que as NPC *pax6a*+ estão significativamente reduzidos no rombencéfalo dos embriões MCT8MO. Demonstramos que estas células colocalizam com *vegfaa* durante vários estadios da formação da BHB. Também observamos que as células endoteliais dos CtAs migram na direção das células que co-expressam *pax6a* e *vegfaa*. A análise de colocalização das NPC *pax6a* com os recetores *thraa* e *thrab* e com o transportar *mct8* permitiu identificar que estas células são sensíveis e potencialmente reguladas pela MT3. Também se verificou que os diferentes componentes do metabolismo da T3 são expressos temporal e espacialmente durante o desenvolvimento da BHB, o que indica que a ação da hormona segue a ordem cronológica da formação das CtAs. De modo a confirmar o envolvimento das NPC *pax6a* para o desenvolvimento das CtAs, foi produzido um mutante com perda de função do *pax6a* com a tecnologia do CRISPR/Cas9. Verificou-se que este mutante possui um desenvolvimento das CtAs semelhante ao do embrião do MCT8MO, confirmando deste modo que as células progenitoras neurais *pax6a* são as células no rombencéfalo do peixe zebra responsável pelo desenvolvimento das CtAs. Em conclusão este trabalho mostra que a MT3 que entra nas células alvo através do Mct8 permite a sobrevivência e proliferação das células progenitoras neurais *pax6a* no rombencéfalo do peixe zebra, as quais são responsáveis pela formação das CtAs através da expressão de *vegfaa*.

PALAVRAS-CHAVE: angiogénese; artérias cerebrais; desenvolvimento da barreira hematoencefálica do rombencéfalo; MCT8; peixe zebra; T3 materna.

TABLE OF CONTENTS

LIST OF FIGURES

Chapter 1

Chapter 2

Chapter 3

Chapter 4

Chapter 5

LIST OF TABLES

LIST OF ABBREVIATIONS

A

A	Astrocytes
AC	Amniotic cavity
ACV	Anterior Cardinal Veins
ADAR	Adenosine deaminases acting on RNAs
AF	Amniotic fluid
AHDS	Allan-Herndon-Dudley syndrome
ALS	Amyotrophic lateral sclerosis
Ang-1	Angiopoietin-1
Ant	Anterior
ANT	Angiotensin
AP	Alkaline phosphatase
AQP4	Aquaporin-4

B

β-cat	Beta-catenin
BA	Basilar Artery
BBB	Blood-brain barrier
BCA	Basal Communicating Artery
BCIP	Bromo-chloro-indolyl-phosphate
BCSFB	Blood-cerebrospinal fluid barrier
BHB	Blood-hindbrain barrier
BMP	Bone morphogenetic proteins
bp	Base pair

C

C	Cerebellum
CaCl	Calcium chloride
cadherin-5	5-vascular endothelial cadherin
CCMAR	Centre of Marine Sciences
CDA	Confined Displacement Algorithm
CDN5	Claudin 5

cDNA	Complementary deoxyribonucleic acid
CF	Coelomic fluid
chb	Caudal hindbrain
cldn5a	*claudin-5a*
CNS	Central nervous system
CoA	Coactivators
CoBLs	Commissural bifurcating longitudinal interneurons
CoR	Corepressors
Cpne4	Copine 4
CRH	Corticotropin-releasing hormone
cRNA	Complementary ribonucleic acid
CSF	Cerebrospinal fluid
CtAs	Central Arteries
CTR	Control
CTRMO	Control morpholino
CV	Cardinal Vein
CVP	Choroid vascular plexus
Cxcl12b	C-X-C motif chemokine ligand 12b
Cxcr4a	C-X-C motif chemokine receptor 4a

D

DA	Dorsal Artery
DBD	DNA-binding domain
Dig	Digoxigenin
DIO1	Deiodinase type 1
DIO2	Deiodinase type 2
DIO3	Deiodinase type 3
DIT	Diiodotyrosine
DLL	Delta-like ligand 4
DNA	Deoxyribonucleic acid
dpf	Days post-fertilization
DUOX2	Dual oxidase type 2

E

E	Endothelium

EC	Endothelial cells
ECC	Exocoelomic cavity
ECM	Extracellular matrix
EDTA	Ethylenediamine tetra-acetic acid
EGFP	Enhanced green fluorescent protein
EU	European union
ey	Eye
F	
FDR	False Discovery Rate
FGF	Fibroblast growth factors
fli1	*friend leukemia integration 1*
Flt1	Fms Related Receptor Tyrosine Kinase 1
Flt4	Fms Related Receptor Tyrosine Kinase 4
Fluo	Fluorescein
FP	Floor plate
FPKM	Fragments per kilobase of exon per million mapped fragments
Fw	Forward
Fzd	Frizzled
G	
gad67a	*glutamic acid decarboxylase 67a*
gad67b	*glutamic acid decarboxylase 67b*
GFAP	Glial fibrillary acidic protein
GFP	Green fluorescent protein
glyt2a	*sodium- and chloride-dependent glycine neurotransmitter transporter 2a*
glyt2b	*sodium- and chloride-dependent glycine neurotransmitter transporter 2b*
GPCR	G protein-coupled receptor
gRNA	Guide ribonucleic acid
H	
h	Hour
H_2O_2	Hydrogen peroxide
Hb	Hindbrain
HCl	Hydrochloric acid
hpf	Hours post-fertilization

HuC	Hu protein C
HybMix	Hybridization mix
I	
I^-	Iodide
IgG	Immunoglobulin G
IHC	Immunohistochemistry
ISV	Intersegmental vessels
K	
KCl	Potassium chloride
kdrl	Kinase insert domain receptor like
KOH	Potassium hydroxide
L	
LAM	Leukocyte adhesion molecules
lamb1a	*laminin beta 1a*
lamb4	*laminin beta 4*
lamc1	*laminin gamma 1*
lamc2	*laminin gamma 2*
LAT	L-type amino acid transporters
LBD	Ligand-binding domain
LDA	Lateral Dorsal Aorta
M	
M	Microglia
MAB	Malic acid buffer
MABTr	Malic acid buffer plus Triton X-100
Mb	Midbrain
MCeV	Mid-cerebral Vein
MCT	Monocarboxylate transporters
MCT8	Monocarboxylic acid transporter 8
MCT8MO	Monocarboxylic acid transporter 8 morpholino
MCtAs	Mesencephalic Central Arteries
MeOH	Methanol
MFS	Major facilitator superfamily
$MgCl_2$	Magnesium chloride

$MgSO_4$	Magnesium sulphate
MHB	Midbrain-hindbrain boundary
MIT	Monoiodotyrosine
MN	Motorneurons
MO	Morpholino
mPax6	Monoclonal paired box 6
mRNA	Messenger ribonucleic acid
MT3	Maternal T3
MTH	Maternal thyroid hormone
N	
N	Neuron
NaCl	Sodium chloride
NBT	Nitro blue tetrazolium
ND	Non-identified differential expression
Neg	Negative
Neurog2	Neurogenin 2
NICD	Notch intracellular domain
NIS	Sodium-iodine symporter
nMDP	Normalised mean deviation product
NPC	Neural progenitor cells
Nrp1	Neuropilin-1
nrp1a	*neuropilin 1a*
nrp2a	*neuropilin 2a*
nt	Notochord
NTCP	Sodium/taurocholate cotransporting polypeptide
NVU	Neurovascular unit
O	
OATP	Organic anion-transporting polypeptides
P	
P	Placenta
Pax	Paired box
Pax6	Paired box 6
pax6a	*paired box 6a*

pax6b	*paired box 6b*
pax8	*paired box 8*
PBS	Phosphate-buffered saline
PBT	Phosphate-buffered saline plus Tween-20
PBTr	Phosphate-buffered saline plus Triton X-100
PCS	Posterior Communicating Segments
PCV	Posterior Cerebral Vein
PDGF	B - platelet-derived growth factor B
PDGFR	β - platelet-derived growth factor receptor beta
PDS	Pendrin
PEST domain	Proline (P), glutamate (E), serine (S) and threonine (T) repeats
PFA	Paraformaldehyde
PHBC	Primordial Hindbrain Channels
PICA	Primitive Internal Carotid Artery
PMBC	Primordial Midbrain Channels
PNVP	Perineural vascular plexus
POD	Peroxidase
Post	Posterior
PSM	Pre-somitic mesoderm
Ptc1	Patched 1
PTU	Propylthiouracil
PVN	Paraventricular nucleus
Q	
qRT-PCR	Quantitative real-time polymerase chain reaction
R	
r1 – r8	Rhombomeres 1 – 8
r^2	Coefficient of determination
RA	Retinoic acid
RAR	Retinoic acid receptor
RARE	Retinoic acid response elements
RBE4	Rat brain endothelial cells
RF	Roof plate
RIN	RNA integrity number

rMCT8	Rat Monocarboxylate transporters 8
RNA	Ribonucleic acid
RNAseq	Ribonucleic acid sequencing
rT3	Reverse T3 or 3,3',5'-triiodothyronine
Robo	Roundabout
Robo4	Roundabout 4
Rspo1	R-Spondin 1
RTHα	Resistance to Thyroid Hormone alpha
RTHb	Resistance to Thyroid Hormone beta
Rv	Reverse
RXR	Retinoid X receptors
rxrba	*retinoid x receptor, beta a*

S

S1pr	Sphingosine-1-phosphate receptor
S1PR1	Sphingosine-1-phosphate receptor 1
SD	Standard deviation
SDS	Sodium dodecyl sulfate
sey	Small eye
sFlt1	Soluble fms-like tyrosine kinase 1
SLC7A5	Solute carrier family 7 member 5 (LAT1)
SLC7A8	Solute carrier family 7 member 8 (LAT2)
SCL10A1	Solute carrier family 10 member 1 (NTCP)
SLC16A2	Solute carrier family 16 member 2 (MCT8)
SLC16A10	Solute carrier family 16 member 10 (MCT10)
SLCO1A2	Solute carrier organic anion transporter family member 1A2
SLCO1B1	Solute carrier organic anion transporter family member 1B1
SLCO1B3	Solute carrier organic anion transporter family member 1B3
SLCO1C1	Solute carrier organic anion transporter family member 1C1
SLCO2B1	Solute carrier organic anion transporter family member 2B1
SLCO3A1	Solute carrier organic anion transporter family member 3A1
SLCO4A1	Solute carrier organic anion transporter family member 4A1
SLCO4C1	Solute carrier organic anion transporter family member 4C1
SHH	Sonic hedgehog

SMAD4	Mothers against decapentaplegic homolog 4
SSC	Sodium chloride/sodium citrate buffer
SSCT	Sodium chloride/sodium citrate buffer plus Tween-20
SSeCKS	Src-suppressed C-kinase substrate
SYS	Secondary yolk sac
T	
T2	3,3'-diiodothyronine
T3	3,5,3’-triiodothyronine
T4	3′,5′,3,5-tetraiodo-L-thyronine or L-thyroxine
TAE	Tris-acetate-EDTA buffer
TBG	Thyroxine-binding globulin
TCF	T-cell factor
TE	Tris-EDTA buffer
TGF-β	Transforming growth factor-beta
TGF-βR2	Transforming growth factor beta receptor type-2
TH	Thyroid hormones
THRA	Thyroid hormone receptor alpha
thraa	*thyroid hormone receptor alpha a*
thrab	*thyroid hormone receptor alpha b*
THRB	Thyroid hormone receptor beta
TJ	Tight junction
TMD	Transmembrane domains
TPO	Thyroid peroxidase
TR	Thyroid hormone receptors
TRa1	Thyroid hormone receptor alpha-1
TREs	Thyroid response elements
TRH	Thyrotropin-releasing hormone
TSH	Thyroid-stimulating hormone
Triac	Triiodothyroacetic acid
TTR	Transthyretin
V	
VE-cadherin	Vascular endothelial cadherin
Vegf	Vascular endothelial growth factor

Vegf-A	Vascular endothelial growth factor-A
vegfaa	*vascular endothelial growth factor aa*
vegfab	*vascular endothelial growth factor ab*
VEGFR	Vascular endothelial growth factor receptor

W

WHO	World Health Organization
WISH	Whole mount in situ hybridisation
WNT	Wingless
wt	Wildtype

Z

ZO-1	Zonula Occludens-1
ZRF-1	Zuotin-related factor 1

Symbols

º C	Degrees Celsius
∅	Diameter
+	Positive

CHAPTER 1

Introduction and Objectives

1 GENERAL OVERVIEW

Diseases related to the thyroid gland, like goitre (enlargement of the thyroid gland due to iodine deficiency and hypothyroidism) and cretinism, have been described in the literature of ancient Greek, Indian and Egyptian medicine centuries ago. Still, the association of goitre to the thyroid gland was only discovered in the 19th-century (Niazi et al., 2011). In 1888 the Clinical Society of London published the first evidence that the thyroid gland has an important role in normal brain development. This conclusion came from observing patients with sporadic and endemic cretinism displaying mental retardation (Oppenheimer and Schwartz, 1997; Yen, 2001). A breakthrough came in 1907, by David Marine that proved that iodine is essential for the normal function of the thyroid gland and insufficiency is linked to the development of diseases, like Grave's disease and goitre (Niazi et al., 2011). The thyroid hormone L-thyroxine (T4) was isolated and chemically characterised in 1914 by Kendall and almost 40 years later, the thyroid hormone 3,5,3'-triiodothyronine (T3) was discovered by Jack Gross and Rosalind Pitt-Rivers (Kendall, 1919; Niazi et al., 2011; Yen, 2001). Only some years later, it was recognised that T4 is the pro-hormone of T3, the active hormone, that binds with the greatest affinity to the cognate nuclear receptor to regulate thyroid hormone (TH)-target gene transcription (Gereben et al., 2008; Oetting and Yen, 2007).

Since then, great advances have been made in understanding the thyroid gland's importance and the role of its hormones. THs are important in many biological processes, as they are involved and required in the differentiation, growth, and metabolism of practically every cell and organ. During adult life, they are involved in oxidative phosphorylation, protein, carbohydrate, lipid, and vitamin metabolism and are the signal that sets the basal metabolic rate of all vertebrates (Oetting and Yen, 2007; Yen, 2001). Recent evidence has revealed a central role for THs in post-partum neurodevelopment and they are critical for normal foetal central nervous system (CNS) development (De Escobar et al., 2004; Utiger, 1999).

TH-related diseases are recognised as major endocrine disorders worldwide. Efforts have been made to diagnose and clinically screen thyroid diseases to allow treatment as early as possible. However, iodine deficiency remains a public health issue in developing countries and Western industrialised countries due to a rising trend of consumption of processed food with non-iodised salt (Moog et al., 2017; Oppenheimer and Schwartz, 1997). Insufficient iodine dietary intake causes maternal and foetal hypothyroidism, the most common cause of preventable mental

retardation worldwide (Oetting and Yen, 2007; J. Patel et al., 2011). The World Health Organization (WHO) implemented universal salt iodisation as the main strategy to prevent iodine deficiency disorders (Andersson et al., 2007).

During embryonic development, THs are fundamental for normal neurodevelopment. In the human foetus, the thyroid gland reaches maturity between weeks 11 – 12 of gestation and starts to secrete THs by around week 16. But circulating THs are already present before the onset of foetal THs production through the maternal circulation to ensure normal neurological development (J. Patel et al., 2011). Only at the end of the 19th century was a consensus reached about the maternal transfer of THs to the foetus (De Escobar et al., 2004). For many years it was assumed that the placenta and foetal membranes are impermeable to THs, and the presence of the enzyme deiodinase DIO3, which catalyses inner ring deiodination and rapidly converts T4 and T3 to their inactive forms, prevents the passage of maternal THs to the foetus (de Escobar et al., 2004; Fisher et al., 1964; Vulsma et al., 1989). Despite studies with radiolabelled iodine that demonstrated circulating maternal THs are present in the foetus (Fisher et al., 1964), only in the mid-1980s did studies on rats establish maternal T4 placental transfer (Vulsma et al., 1989). Many studies have now elucidated the mechanism and importance of maternal THs for the neurodevelopment of the human foetus (Calvo et al., 2002; J. Patel et al., 2011; Utiger, 1999). An adequate amount of maternal THs is crucial since even a slight decrease in the maternal THs concentration impairs the offspring's cognitive and motor development. Given the importance of maternal THs levels for appropriate foetal neurodevelopment, it is essential to understand how it acts and regulates gene transcription and the nature, magnitude, time- and context-specificity of its effects on neurodevelopment (Moog et al., 2017).

1.1 CENTRAL REGULATION OF THYROID HORMONES

THs are iodinated amino acids produced in the thyroid follicles of the thyroid gland. The main hormone produced by the thyroid gland is 3′,5′,3,5-tetraiodo-L-thyronine (T4 or thyroxine), which functions mostly as a pro-hormone. The biologically active hormone is 3,3′,5-triiodothyronine (T3), a lesser product of the thyroid gland, and it has a high binding affinity to TH receptors (Braun and Schweizer, 2018; Oetting and Yen, 2007). T3 is essential for normal neurodevelopment, and in adults' it regulates many biological functions, including cardiovascular, bone, and liver function; food intake; and energy expenditure (Fekete and

Lechan, 2014; Yen, 2001). Therefore, in mammals, THs synthesis and secretion by thyrocytes in the thyroid gland is highly regulated via a feedback mechanism involving the hypothalamus and pituitary to maintain circulating THs levels within normal limits.

1.1.1 THE HYPOTHALAMUS-PITUITARY-THYROID AXIS

In mammals, serum THs levels are controlled by a negative feedback mechanism involving the hypothalamus, the pituitary, and the thyroid gland, known as the HPT axis (Fig. 1.1 A). Low circulating levels of THs are sensed by the paraventricular nucleus (PVN) localised in the hypothalamus, which synthesises thyrotropin-releasing hormone (TRH). TRH is then released to the median eminence via axons and transported to the anterior pituitary's thyrotropin cells via the hypophysial portal system. There it binds to TRH receptors on thyrotrophs and stimulates the synthesis and release of thyroid-stimulating hormone (TSH) into the circulatory system. TSH binds to G-coupled membrane receptors in the thyroid gland follicle cells (i.e. thyrocytes) stimulating the synthesis and secretion of THs (Ortiga-Carvalho et al., 2016; Yen, 2001; Zoeller et al., 2007). TSH-activated thyrocytes increase the uptake of iodide (I^-), and the expression of thyroglobulin and thyroid peroxidase (TPO). In the follicle colloid redox environment, in the presence of iodine and H_2O_2, TPO catalyses the iodination of tyrosine residues in thyroglobulin, forming monoiodotyrosine (MIT) and diiodotyrosine (DIT). These iodothyronines are enzymatically coupled to form mostly T4 and some T3. Thyroglobulin is then endocytosed into the follicular cells and degraded inside lysosomes releasing THs (mostly T4) into the blood circulation via membrane transporters (Fig. 1.1 B) (Citterio et al., 2019; Ortiga-Carvalho et al., 2016; Smallridge, 1980; Thanas et al., 2020).

Most T4 released by the thyroid gland binds preferentially to TH-binding proteins in the plasma due to its hydrophobic properties. Thyroxine-binding globulin (TBG) has a high affinity for THs and is the main TH-binding protein in humans. Transthyretin (TTR) and albumin are also TH-binding proteins with a higher capacity (due to their circulating concentration) but lower binding affinity for THs. The bindings of THs to the TH-binding proteins maintain the bioavailability of THs in blood circulation and increase the half-life of the hormones. Only a small percentage of THs circulate in a free form (Schussler, 2000).

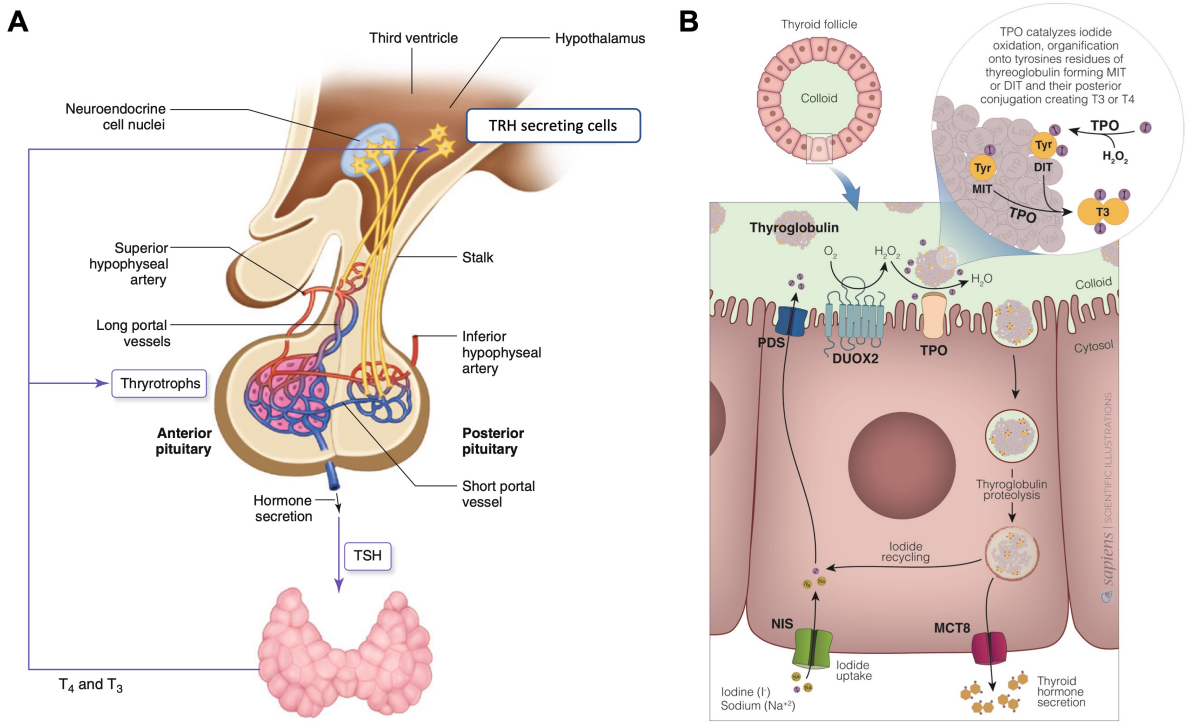

Figure 1.1 – Regulation of thyroid hormone synthesis. A) HPT feedback mechanism. A negative feedback mechanism between the hypothalamus, pituitary, and thyroid gland tightly controls the bioavailability of THs. THs production is triggered by the binding of TSH, secreted by the anterior pituitary gland in response to low circulating THs sensed by the hypothalamus neurons, which produce TRH. **B) Thyroid hormone synthesis.** The binding of TSH to its receptor in the thyroid follicular cells (thyrocytes) promotes TH synthesis. Signalling of TSH stimulates iodine intake by the sodium-iodine symporter (NIS), which is then transported from the cytosol to the colloid via Pendrin (PDS). In the colloid, iodide is oxidised to iodine. In the presence of iodine, H_2O_2 (generated by DUOX2) and thyroglobulin, thyroid peroxidase (TPO) catalyses the iodination of thyroglobulin's tyrosine residues, forming MIT and DIT. Later coupling of MIT and DIT generates T3 and T4. The cell incorporates iodinated thyroglobulin into vesicles containing proteolytic enzymes, which cleaves thyroglobulin to release free T4, and some T3, to the blood circulation by MCT8. DIT: diiodotyrosine; DUOX2: dual oxidase type 2; MCT8: monocarboxylic acid transporter 8; MIT: monoiodothyrosine; NIS: sodium-iodine symporter; PDS: Pendrin; TPO: thyroid peroxidase; TRH: thyrotropin-releasing hormone; TSH: thyroid stimulating hormone. Adapted from A) Styne, (2016) and B) Ortiga-Carvalho et al., (2016).

In vertebrates, the chemical structure of THs and their active metabolites are conserved, and the HPT axis and its mode of action are relatively conserved between vertebrates (Opitz and Köhrle, 2017; Song et al., 2021; Zoeller et al., 2007). In mammals, TSH secretion is stimulated by TRH, but in some teleosts, the specific role of TRH in stimulating TSH secretion is not well established (Blanton and Specker, 2007). *In vitro* studies have shown that in non-mammalian

species such as amphibians, corticotropin-releasing hormone (CRH) may act as a TSH stimulator by relieving T4 inhibition of TSH (De Groef et al., 2006). In a single study on the bighead carp (*Aristichthys nobilis*), *in vitro* studies have suggested that besides TRH, leptin, neuropeptide Y, β-endorphin and galanin can stimulate TSHβ mRNA expression (Chowdhury et al., 2004). Due to the lack of studies, it is unclear how TSH is stimulated in the zebrafish pituitary, nonetheless, overall the main function of the thyroid system is comparable with the mammalian system, and this is the support for its use as a model to study human conditions (Jia et al., 2016).

1.2 THYROID HORMONES CELLULAR SIGNALLING

Regulation of gene expression by THs is mediated by the nuclear receptors for T3. This requires TH transport into the cell, deiodination and nuclear transport. After intracellular transport, before hormone binding to nuclear receptors, the pro-hormone T4 must be converted into the active T3, mediated by deiodinases (Gereben et al., 2008; Marsili et al., 2011; Wu and Koenig, 2000). This signalling triad, that is, transmembrane transport, intracellular deiodination, and T3 receptor–mediated gene transcription, constitutes the basis for cellular THs signalling (Fig. 1.2), thus ensuring adequate concentrations of T3 at the right location and at the right time (Bianco et al., 2019; Opitz and Köhrle, 2017).

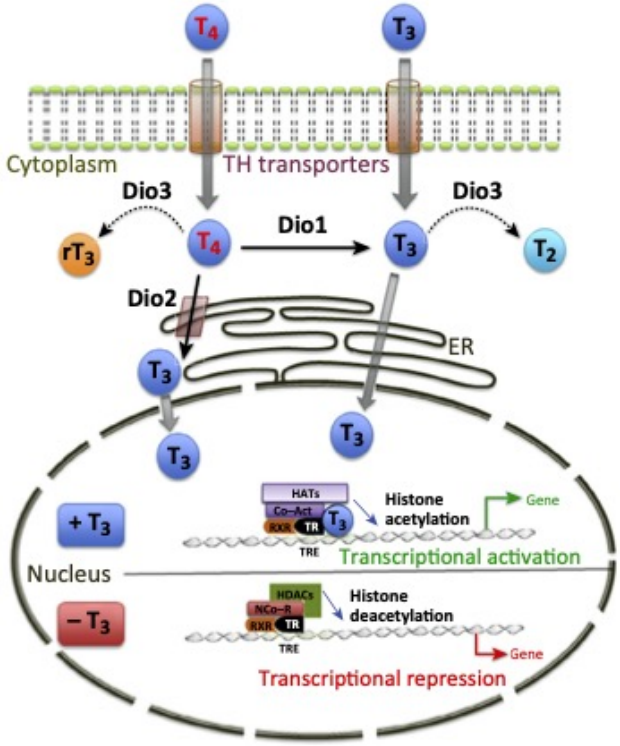

Figure 1.2 – Thyroid hormones signalling. THs enter target cells via TH membrane transporters present on the plasma membrane. Inside the cell, T4 can be activated (into T3) or inactivated (conversion of T4 to reverse T3 (rT3) or T3 to T2) by the action of iodothyronine deiodinases (Dio2, and Dio3, respectively). Intracellular T4 is converted mostly by Dio2 to its active form T3, which binds to TH receptors (TR) already bound to target gene promoter regions in the nucleus and transactivates gene transcription. In the absence of T3, gene transcription is repressed. Adapted from Sinha et al., (2014).

1.2.1 THYROID HORMONE MEMBRANE TRANSPORTER PROTEINS

It was assumed that THs crossed the cell membrane by simple diffusion for a long time. That was assumed, given that THs are lipophilic molecules and could easily cross the lipid-rich bilayer of the cell membrane (Hennemann et al., 2001; Robbins, J. and Rall, 1960). But this is untrue. Only after the 1970s did several studies demonstrate that THs transport into target cells is carrier-mediated, and energy- and Na^+-dependent. Over the years, several TH transporter families have been identified. These include the monocarboxylate transporters (MCT), the organic anion-transporting polypeptides (OATP), the L-type amino acid transporters (LAT) and the sodium/taurocholate cotransporting polypeptide (NTCP) (Table 1.1) (Bernal et al., 2015; Hennemann et al., 2001).

Table 1.1 – The main human thyroid hormone transporters in the brain vasculature. Transport of TH metabolites studied in parallel are listed in order of substrate preference. (,): equal affinity; (>): greater affinity. TH substrates that have not been studied in parallel are not listed in any specific order: (;). Reviewed in Groeneweg et al., (2020).

Gene name	*Protein name*	*TH substrates*	*Tissue distribution in humans*
SLC7A5	LAT1	3,3'-T2 > rT3 >T3 > T4; MIT	Brain, placenta, testis, liver, bone marrow.
SLC7A8	LAT2	3,3'-T2 > T3; MIT	Brain, kidney, placenta, spleen, prostate, testis, ovary.
SLCO1C1	OATP1C1	T4 > T4S > rT3 > T3	Brain, testis, ciliary body, adipose tissue.
SLC16A2	MCT8	T3 > T4 > rT3, 3,3'-T2	Brain, liver, kidney, thyroid, pituitary.
SLC16A10	MCT10	T3 > T2 ≥ T4, rT3	Brain, kidney, skeletal muscle, placenta, heart.

The NTCP (SCL10A1) is a Na^+-dependent organic anion transporter present exclusively in the liver's hepatocytes. It is principally involved in the transport of bile salts, but it can also

transport the sulphated derivatives of T4 and T3 (Hagenbuch and Dawson, 2004; Visser et al., 2010).

The L-type amino acid transporters comprise LAT1 (SLC7A5) and LAT2 (SLC7A8) and are sodium-independent transporters. Besides transporting neutral amino acids, such as leucine, phenylalanine and tyrosine, they can also transport THs (Friesema et al., 2001). They are present in many cell types, including the brain (Bernal et al., 2015).

The OATPs are a large family, and 8 members have been shown to have the ability to transport different iodothyronines: OATP1A2 (SLCO1A2), OATP1B1 (SLCO1B1), OATP1B3 (SLCO1B3), OATP1C1 (SLCO1C1), OATP2B1 (SLCO2B1), OATP3A1 (SLCO3A1, has 2 protein isoforms: V1 and V2), OATP4A1 (SLCO4A1) and OATP4C1 (SLCO4C1). These members also transport various organic compounds, such as steroids, bile salts, drugs, and anionic oligo peptides. OATP1A2 is expressed in the brain, liver, and kidney. OATP1B1 and OATP1B3 are specifically expressed in the liver. OATP1C1 is expressed exclusively in the brain and testis. OATP2B1 and OATP4A1 are expressed in many tissues. OATP3A1 is expressed in the brain, testis, ovary, and heart, and OATP4C1 is expressed specifically in the kidney. OATP1C1 is the most physiologically relevant of all family members as it has been shown to have a high specificity in transporting iodothyronines, particularly T4 and rT3 (Bernal et al., 2015; Friesema et al., 2005; Groeneweg et al., 2020; Karapanou and Papadimitriou, 2011).

The MCT family are proteins that transport monocarboxylates such as pyruvate and lactate. Two members of this family can transport THs in a sodium and proton-independent way: MCT8 (SLC16A2) and MCT10 (SLC16A10). MCT10 can transport aromatic amino acids and TH metabolites. It is expressed in many tissues, such as the kidney, liver, skeletal muscle, placenta, and heart. MCT8 is highly homologous to MCT10 but is instead a specific TH transporter. It specifically transports T3>T4>>rT3>T2. It is expressed in many tissues, including the brain and adult endothelial cells of the blood-brain barrier (BBB) (Bernal et al., 2015; Braun and Schweizer, 2018; Friesema et al., 2005; Groeneweg et al., 2020; Schweizer et al., 2014).

THs membrane transporters in the foetal brain during embryonic development are responsible for all intracellular hormone transport. So far, studies have shown that nine different transporters are present in the human foetal cerebral cortex from 7 weeks of gestation (OATP1A2, OATP1C1, OATP3A1.1, OATP3A1.2, OATP4A1, MCT8, MCT10, LAT1 and LAT2), showing the importance of THs uptake from the early 1st trimester (Chan et al., 2011).

Functional evidence suggests that only OATP1C1 and MCT8 have a physiological role in vertebrate neurodevelopment (Boccone et al., 2013; Novara et al., 2017; Remerand et al., 2019; Schwartz and Stevenson, 2007; Strømme et al., 2018).

1.2.1.1 THE MCT8 TRANSPORTER

The human *MCT8* gene was identified by Lafrenière et al. (1994) and is located on chromosome Xq13.2. The gene consists of six exons and five introns, and, depending on the translation start site used, it codes for a protein with 613- or 539- amino acids. It has 12 putative transmembrane domains (TMD), with the N- and C- terminus having a cytoplasmic localisation. The N-terminal region of the protein contains a PEST domain, characterised by proline (P), glutamate (E), serine (S) and threonine (T) repeats. Although its transported substrate was unknown, they identified it as a protein like a monocarboxylate transporter family. In humans, the *MCT8* mRNA is highly expressed in the liver, heart, brain, placenta, lung, and kidney (Lafrenière et al., 1994). The characterisation of the MCT8 transporter as a specific and active transporter for THs was only established in 2003 by Friesema et al. (2003) by studying rat *Mct8* (*rMct8*). They showed that rMCT8 transports different iodothyronines (T4, T3, rT3 and T2) but cannot transport sulfonated iodothyronine derivates, amino acids ligands of T-type and L-type transporters and monocarboxylates (lactate and pyruvate). These findings were afterwards confirmed for the human MCT8 transporter (Friesema et al., 2006, 2003).

MCT8 belongs to the major facilitator superfamily (MFS) of membrane transporters, where the Rocker switch model transports iodothyronines (Schweizer et al., 2014). In this model, the transporter contains two nearly symmetrical bundles of 6 transmembrane domains that can exert a rotary movement against each other. The binding of the iodothyronines on the transporter protein triggers conformational changes that allow the substrate to enter the cavity in the transporter from one side (outside-open) of the membrane and leave the cavity towards the other side (inside-open) (Fig. 1.3 A and B) (Kleinau et al., 2011; Schweizer et al., 2014). The transport of iodothyronines is bi-directional. Some highly conserved amino acids have been identified in the protein's cavity and are essential for the transport of T3, such as His192, His415, Arg445, and Asp498. T3 adheres alternately to these residues and is carried through the central part of the channel and released on the other side (Fig. 1.3 C) (Protze et al., 2017).

The MCT8 transporter is relevant for normal CNS embryonic development. Mutations of this transporter are responsible for the X-linked mental retardation condition known as the Allan-Herndon-Dudley syndrome (Friesema et al., 2004), which will be discussed later in this Chapter.

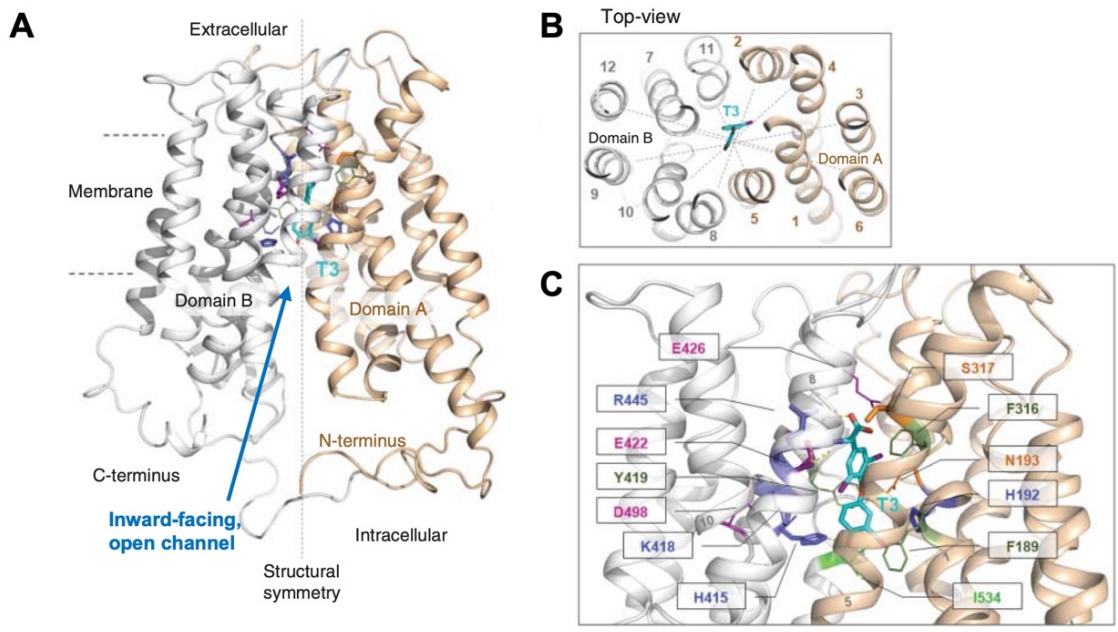

Figure 1.3 – Cristal structural model of the MCT8 transporter protein. A) 3D-structure of the MCT8 transporter protein. The protein is subdivided into domains A (beige) and B (white). Each domain comprises 6 helices in a mirror-like arrangement with centre-axis symmetry (dashed line). The N- and C-terminus are localised in the intracellular region. This model predicts the interaction of T3 (cyan colour) binding inside the translocation channel. **B) Top view of the binding interaction of T3 in the translocation channel.** The model predicts that T3 binds with high probability exactly at the symmetry axis between the two domains and helices. **C) Representation of the putative interaction of MCT8 and T3.** Hydrophilic and charged amino acids interact with the carboxy group of T3. Arg445 (R445) and Asp498 (D498) participate in the binding of T3 and presumably interact via H-bonds (shown as dotted yellow lines). His192 (H192) and His415 (H415) participate in substrate translocation. Other amino acids that may participate in the T3 translocation are shown. Adapted from Fischer et al., (2015).

1.2.1.2 THYROID HORMONE MEMBRANE TRANSPORTERS IN ZEBRAFISH

In zebrafish, the identification and characterisation of TH transmembrane transporters have been focused only on the three main TH transporters: *mct8*, *mct10* and *oatp1c1*. The high

sequence similarities and conserved protein motifs of these TH transporters between zebrafish and mammals suggest that the transport mechanism of THs is well conserved between fish and humans (Arjona et al., 2011; Vatine et al., 2013). Zebrafish *mct8* was the first TH membrane transporter to be cloned and characterised in zebrafish. The zebrafish Mct8 protein shares sequence identity with the human (57%), mouse (57%) and rat (56%) MCT8 protein. The protein structure is also highly conserved, presenting the 12 transmembrane domains, a PEST domain in the N-terminal region of the protein and the 2 amino acids, Arg445 and Asp498, that are the key players in the transport mechanism of iodothyronines. The zebrafish Mct8 transporter is fully functional and can transport iodothyronines in a temperature-dependent and Na^+-independent way. At the physiological zebrafish temperature (26 ºC), it specifically transports T3 but not T4. At human physiological temperature (37 ºC), the transport of T3 increases, and also T4 (Arjona et al., 2011). This evidence highlights the specific physiological role of Mct8 in transporting T3 and the exclusive role of T3 as the major TH signalling metabolite in zebrafish.

During early development, the relative expression of *mct8* in zebrafish was detected by real-time quantitative PCR (RT-qPCR), from 3 hours post-fertilization (hpf), with expression increasing during development until 72 hpf. The highest mRNA expression was detected at 48 hpf before the hatching of the embryos. In the adult zebrafish, *mct8* expression was detected ubiquitously in all tissues except female gonads. The highest expression levels were found in the brain, gills, pancreas, pituitary, heart, and gut (Arjona et al., 2011). Whole mount *in situ* hybridisation (WISH) of *mct8* during embryonic development showed that this transporter was mainly expressed in the nervous system. From 10 – 12 hpf, *mct8* expression was observed ubiquitously in the embryo. At 24 hpf, *mct8* expression was found in several brain regions, particularly in the hindbrain, spinal cord, and eyes. At 31 hpf, *mct8* expression was located in the brain and spinal cord, specifically in the outer lining of the first ventricle, the midbrain-hindbrain boundary and the eye. At 48 and 72 hpf, the expression of *mct8* was essentially observed in the brain's vascular system (Campinho et al., 2014; Vatine et al., 2013).

Expression analysis by WISH found that *mct10* and *oatp1c1* transporters were only detected from 48 hpf onwards. These observations suggest that Mct8 is the sole cellular transporter of zebrafish maternal-derived THs during embryogenesis. Nonetheless, zebrafish Mct10 and Oatp1c1 share 71% and 58% identity to their human homologues, respectively, strongly suggesting that these transporters also function as TH-specific transporters. At 48hpf, *mct10*

was expressed in the liver and trigeminal ganglia, while *oatp1c1* was localised in the vascular structures of the brain (Vatine et al., 2013).

1.2.2 IODOTHYRONINE DEIODINASES

After crossing the cell membrane, THs bioavailability inside the cells is tightly controlled by iodothyronine deiodinases. Deiodinases are selenoenzymes responsible for the activation or inactivation of THs in a time- and tissue-specific manner. They are important to maintain homeostatic levels of THs throughout life and are essential regulators of local THs levels during development (Bianco et al., 2019; Dentice and Salvatore, 2011).

Until now, three deiodinases have been identified and characterised to modify the local availability of THs and thus control the biological activity of TH action: deiodinase type 1 (DIO1), deiodinase type 2 (DIO2) and deiodinase type 3 (DIO3). DIO1 is a non-selective enzyme catalysing outer and inner ring deiodination, depending on the substrate. DIO2 is an outer ring deiodinase and catalyses the removal of iodine from the phenolic ring of the pro-hormone T4 into T3, the active TH. DIO3 inactivates TH action by catalysing inner ring deiodination by removing iodine from the inner tyrosyl ring from T4 or T3 to form the biological inactive 3,3',5'-triiodothyronine (reverse T3 (rT3)) or 3,3'-diiodothyronine (3,3'-T2), respectively (Fig. 1.4) (Reviewed in: Bianco et al., 2002a; Bianco and da Conceição, 2018).

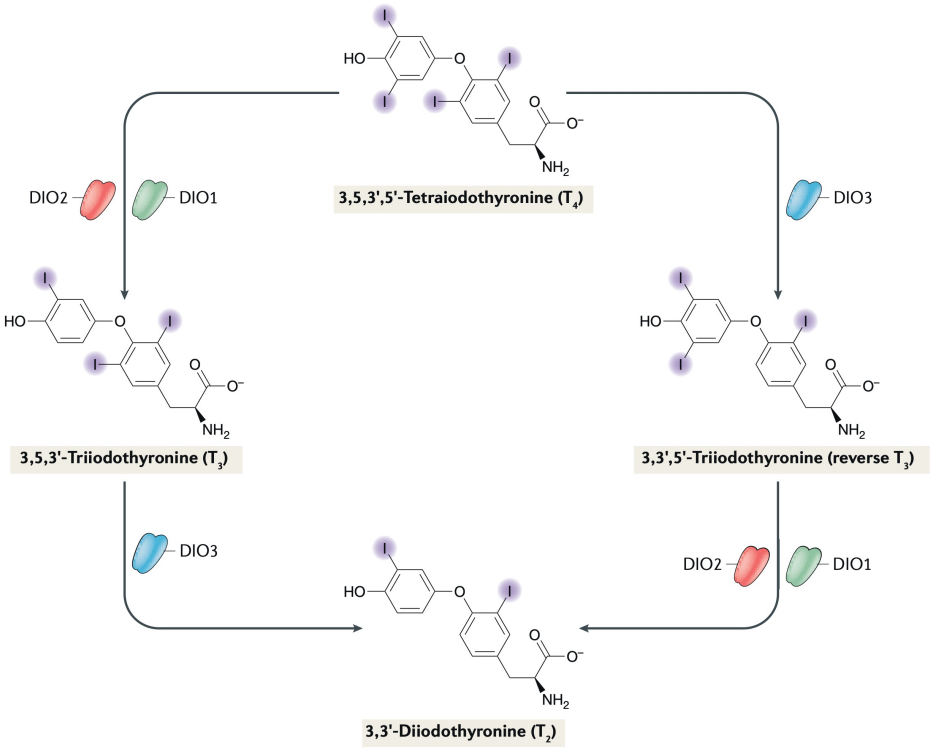

Figure 1.4 – Human thyroid hormones deiodinase metabolic pathway. In humans, the pro-hormone T4 is activated by outer ring deiodination of the phenolic thyronine ring by DIO1 or DIO2 to form T3. Inner ring deiodination of the tyrosyl ring by DIO1 or DIO3 inactivated T4 and T3. Additionally, rT3 can be deiodinated by DIO1 or DIO2 to T2. Adapted from Luongo et al., (2019).

Deiodinases are distributed in a wide range of tissues where they control THs availability in a cell-autonomous manner. In humans, most systemic T3 present in the circulation is produced by DIO2, although DIO1 also contributes (Maia et al., 2005). In adult humans, DIO1 activity is present in the liver, kidney, thyroid gland and pituitary. DIO2 activity has been found in the thyroid gland, heart, brain, spinal cord, skeletal muscle, and placenta (Bianco et al., 2002). DIO2 activity is especially important in the CNS, where it is the only deiodinase capable of activating T4 into T3 and responsible for local T3 availability (Campos-Barros et al., 1996). Dio3 is mostly expressed in adult tissues in the brain and placenta (Bianco et al., 2002; Campos-Barros et al., 1996; Roti et al., 1981; Tu et al., 1999). In the placenta, DIO3 plays an active role in controlling the availability of maternal THs to the developing foetus (Roti et al., 1981).

Studies conducted in rats have shown that DIO1 and DIO2 activity is low in most tissues during development. DIO1 activity only increases after birth (Bates et al., 1999; Bianco et al., 2002; Burrow et al., 1994). DIO2 activity increases before birth and during the perinatal period (Bates

et al., 1999). *Dio3*, in contrast to *Dio1* and *Dio2*, is highly expressed in most foetal tissues (Bianco et al., 2002; Roti et al., 1981; Tu et al., 1999). The timed and tissue-specific reduction of DIO3 during development, coordinated with the slow increase in DIO2 activity provides a tighter control of TH action during embryonic development (Bianco et al., 2002).

Recently, mutations in the human *DIO1* gene were identified and characterised in two unrelated families. Heterozygous family members presented abnormal THs metabolism with elevated serum rT3 levels and rT3/T3 ratios (França et al., 2021). Several polymorphisms in the *DIO* genes have been found that affect deiodinase activity or expression, which usually modify THs plasma levels (Luongo et al., 2019). In humans, three polymorphisms have been identified for DIO1 (rs2235544, Cys785Thr, and Ala1814Gly), and two polymorphisms have been identified for DIO2 (Panicker et al., 2008; Peeters et al., 2003; Verloop et al., 2014). The DIO2 Thr92Ala polymorphism occurs in about 15–30% of Caucasians and is associated with diabetes (Dora et al., 2010), mental retardation (Zhang et al., 2012), and hypertension (Gumieniak et al., 2007), among other conditions (Verloop et al., 2014). The DIO2 ORFa–G3A polymorphism has been reported to affect only THs metabolism (Peeters et al., 2005). For DIO3, only one polymorphism (Thr154Gly) has been identified in humans but does not affect TH plasma levels (Peeters et al., 2003).

1.2.2.1 DEIODINASES IN ZEBRAFISH

The zebrafish has 4 deiodinases genes: *dio1*, *dio2* and two paralogues of *dio3* (*dio3a* and *dio3b*) (Guo et al., 2014; Heijlen et al., 2014). The deiodinases are assumed to have the same catalytic activity as their mammalian counterparts. However, the zebrafish deiodinases show important differences in their enzymatic activity (Fig. 1.5). The zebrafish Dio3a and Dio3b both have inner ring activity. However, Dio3a has also the capacity to catalyse outer ring deiodination of rT3, which is absent in Dio3b and the human DIO3. *In vitro* studies of zebrafish Dio1 also showed that it differs from its mammalian homolog. Zebrafish Dio1 has minimal capacity to catalyse outer ring deiodination of T4 or inner ring deiodination of T3. In zebrafish, the main T4 to T3 converter is Dio2, while the main T3 inactivators are Dio3a/Dio3b (Fig. 1.5) (Guo et al., 2014).

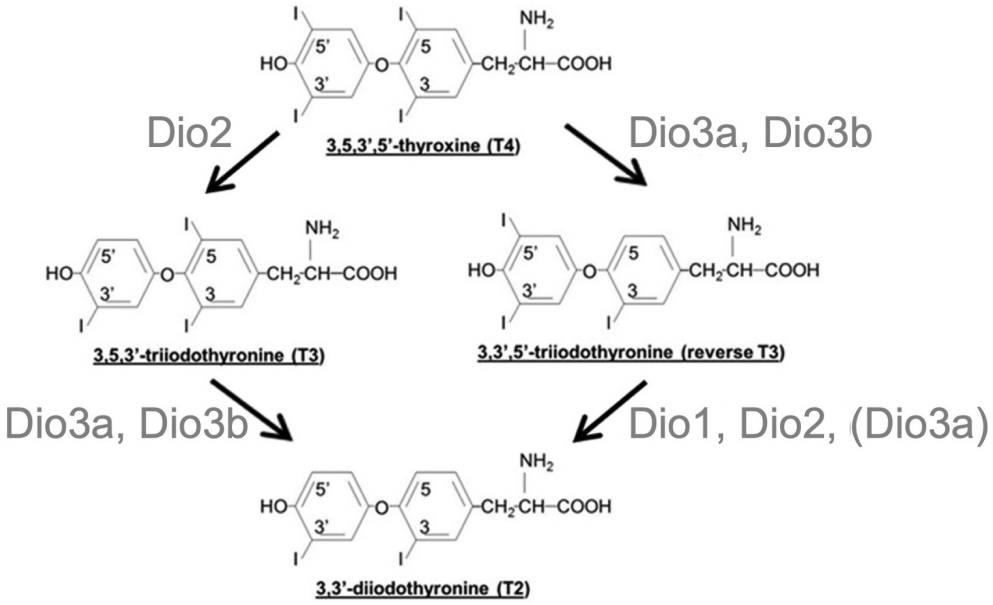

Figure 1.5 – Zebrafish thyroid hormones deiodinase metabolic pathway. The zebrafish has 4 iodothyronine deiodinases: Dio1, Dio2, Dio3a and Dio3b. T4 is activated by outer ring deiodination by Dio2 to form T3. The *dio3* gene was duplicated during teleost evolution, originating Dio3a and Dio3b. Both enzymes have inner ring deiodinase activity and inactivate T4 and T3. Additionally, rT3 can be deiodinated by Dio1, Dio2 or Dio3a (this enzyme also has outer ring activity but only on the rT3 subtract) to T2. Adapted from Guo et al., (2014).

In zebrafish development, the expression of *dio1* mRNA was detected by WISH from 2 cell-stage (0,75 h) ubiquitously. At 22 hpf, *dio1* expression was more abundant in the brain, at 48 hpf in the liver and at 96 hpf in the kidney and proximal intestine (Dong et al., 2013; Vatine et al., 2013). Expression of *dio1* by RT-qPCR was first detected at 12 hpf (first-time point collected in the experiment) and increased after 72 hpf until 5 days post-fertilization (dpf) (Walter et al., 2019). Expression of *dio2* by WISH was first weakly detected at 24 hpf in the retina and adenohypophysis. At 36 hpf, *dio2* expression was also detected in the intestinal bulb and at 96 hpf in the swim bladder (Dong et al., 2013; Thisse et al., 2003). *dio2* mRNA was first detected, by RT-qPCR at 12 hpf (first-time point collected in the experiment) and increased to the highest expression level at 72 hpf and 96 hpf (Walter et al., 2019). Gene expression analysis by RT-qPCR showed that *dio3a* and *dio3b* have a similar expression profile over the first five days of development. Expression of both *dio3* genes was detected at 24 hpf, with the highest expression level at 96 hpf (Walter et al., 2019). WISH revealed that *dio3a* and *dio3b* genes have different spatial-temporal expression patterns. From 24 hpf until 48hpf, expression of *dio3a*

was present in the dorsal hindbrain and otic vesicle (Guo et al., 2014). Expression of *dio3b* was detected at 24 hpf in the dorsal regions of the fore-, mid- and hindbrain and pronephric ducts. At 35hpf neural expression of *dio3b* was lost but its expression was maintained in the pronephric ducts up until 48 hpf. At 5 dpf, *dio3b* was expressed in the retina, liver and brain (Guo et al., 2014). Studies confirmed that both *dio3* genes contribute to Dio3 activity, but Dio3b activity shows a greater contribution during embryonic development (Guo et al., 2014; Heijlen et al., 2014). Notably, functional analysis of *dio3* paralogues showed that only *dio3b* loss of function apparently affects zebrafish development (Guo et al., 2014).

1.2.3 THYROID HORMONE RECEPTORS

The final step in THs signalling is T3 binding to chromatin-bound nuclear receptors, thus regulating the expression of target genes. According to cellular context, physiological status and cell identity, THs stimulate different cellular responses (Bernal, 2022; Stepien and Huttner, 2019). In target cells, gene transcription is mediated by TH receptors (TRs) that are members of the nuclear hormone receptor superfamily type II and function as a T3-inducible transcription factor (Cheng et al., 2010; Flamant et al., 2006).

In mammals, TRs are encoded by two genes, *thyroid hormone receptor alpha* (*THRA*) and *thyroid hormone receptor beta* (*THRB*), originating TRα and TRβ proteins, respectively. In mammals, these receptors give rise to different isoforms by alternative splicing, promoter usage, and different translation start site usage. These isoforms present different binding abilities for target DNA, ligand, and co-factor recruitment. THRA encodes one active T3-binding receptor in humans, the TRα1, and two splice variants, TRα2 and TRα3. The latter isoforms have different carboxy terminus and thus are not able to bind T3 (Fig. 1.6). *THRB* encodes two isoforms, TRβ1 and TRβ2, that have T3-binding activity and differ in their amino-terminal domain (Cheng et al., 2010; Harvey and Williams, 2002; Skah et al., 2017). In mice, there is a third TRβ isoform, the TRβ3, that also has T3-binding activity (Fig. 1.6) (Williams, 2000). In addition, truncated TRs have been identified (TRΔβ3, TRΔα1, and TRΔα2) that have the capacity to bind THs but cannot bind to thyroid response elements (TREs) (Fig. 1.6). TRα1 and TRβ1-3 are, as mentioned above, the isoforms with DNA and T3-binding capacity and therefore mediate the genomic effects of THs on target genes. The other isoforms act as

dominant-negative regulators or have non-genomic functions (Cheng et al., 2010; Davis et al., 2016).

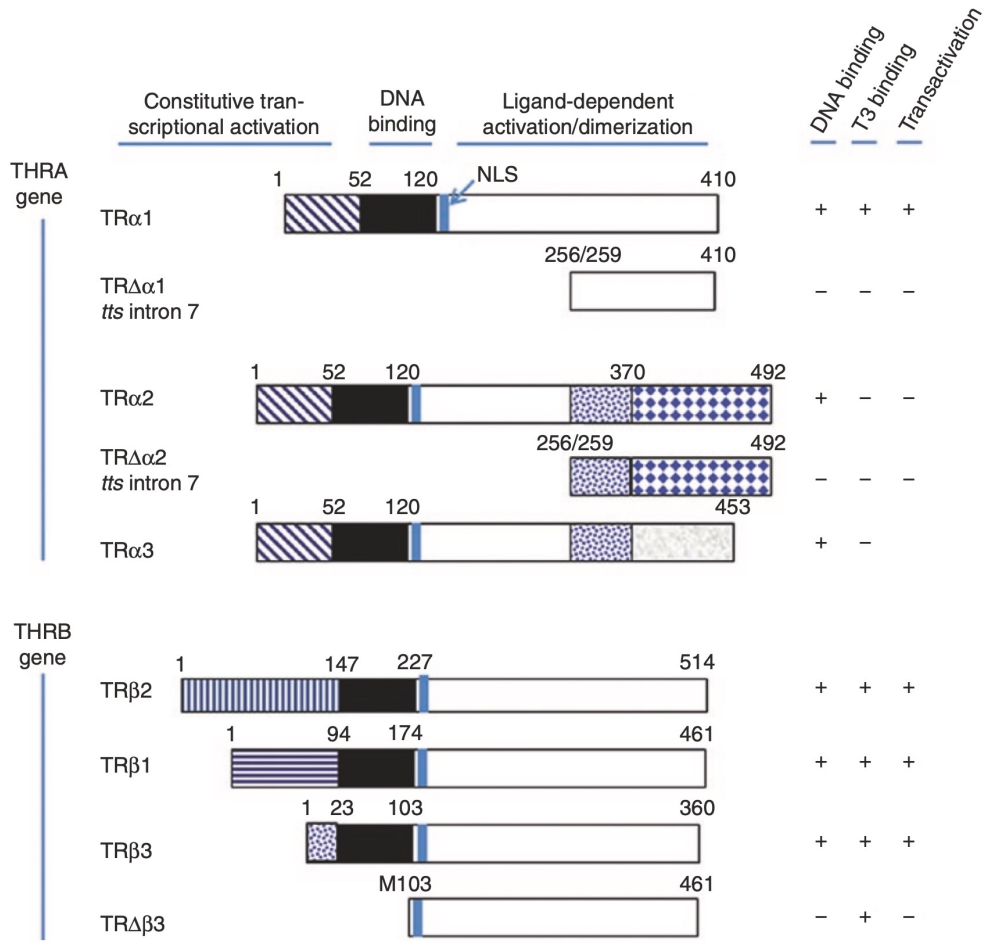

Figure 1.6 – Human thyroid hormone receptor isoforms. TRs are encoded by TRα and TRβ genes located on chromosomes 17 and 3, respectively. Alternative splicing of TRα gives rise to one functional isoform (TRα1), and of TRβ gives rise to three functional isoforms (TRβ1-3, where TRβ3 is specific for mice). TR isoforms share high sequence homology in the DNA binding domain (solid black bar) and in the hormone binding domain (white bar). The constitutive transcriptional activation domains or A/B domain are variable in length (Cheng et al., 2010). A different colour pattern illustrates regions with different amino acid sequences. Numbers indicate amino acid position. DNA-binding, T3-binding properties, and transactivation (+) or repression (−) are indicated. M: position of the methionine; NLS: nuclear localization signal; *tts*: transcriptional start site. Adapted from Gerdes and Ojamaa, (2016).

TR isoforms are differentially expressed in adult tissues and present developmentally specific expression and regulation (Cheng, 2000). In humans, *TRs* are detected in the developing brain between 7 to 8 weeks of gestation, which coincides with the detection of DIO2 activity in the

foetal cerebral cortex and also with the presence of circulating maternal THs (from 5 – 6 weeks of gestation), indicating a functional role of TRs during early development (Calvo et al., 2002; Chan et al., 2002; Landers and Richard, 2017). In mammals, *TRα1* is the dominant TR expressed during embryonic development, and in the developing brain, it is the major isoform expressed in neurons. *TRβ* isoforms are also present in early development, but expression levels are much lower. In the developing brain, they are more abundant in specific neuronal cell types such as hippocampal pyramidal and granule cells, paraventricular hypothalamic neurons and cerebellar Purkinje cells (Bernal and Pekonen, 1984; Bradley et al., 1992; Chan et al., 2002; Mellström et al., 1991).

TR isoforms are well conserved across species. They are constituted by 3 domains, an amino-terminal or A/B domain, a central DNA-binding domain (DBD), and a carboxy-terminal hormone-binding or ligand-binding domain (LBD) (Fig. 1.6) (Darras et al., 2011; Vella and Hollenberg, 2017). The A/B domain is the region that varies the most between TR isoforms and is involved in the target gene transcriptional regulation (Cheng et al., 2010).

TRs mediate gene expression by binding to specific DNA sequences, the thyroid-responsive elements (TREs), located in the promoter or enhancer regions of T3-responsive genes. The TRE has a canonical structure constituted by two-half sites AGGTCA separated by four random nucleotides (Chen and Young, 2010). TRs can bind DNA as monomers, homodimers (two identical monomers) or heterodimers (two different monomers) with retinoid X receptors (RXR) to the TREs (Bakker, 2004; Lazar et al., 1991). In a given TRE, TRs usually are found in a 3' position regarding RXR receptors (Fig. 1.7) (Lee and Privalsky, 2005).

TRs regulate gene expression, both bound and unbound to T3. This unique characteristic results from TRs being constitutively bound to chromatin, independently of T3 binding. When unbound to T3, the TR-dimer recruits several proteins that assemble into a corepressor complex. This complex recruits typically histone deacetylases and methylases that close the chromatin of target genes, leading to the silencing of gene transcription. After T3 binding, conformational changes in the TR results in the release of the corepressor factors and recruitment of coactivators and other associated proteins that modify the chromatin structure to facilitate transcriptional activation (Fig. 1.7) (Bakker, 2004; Takayama et al., 2008; Wu and Koenig, 2000). These findings indicate that TRs have a dual function on gene transcription. In the absence of ligand, TRs act as transcriptional repressors, whereas, in the presence of T3, they function as transcriptional activators. There are also other T3-target genes in that expression is

activated by TRs in the unliganded state, while in the ligand state TRs act as transcriptional repressor (Jho et al., 2005).

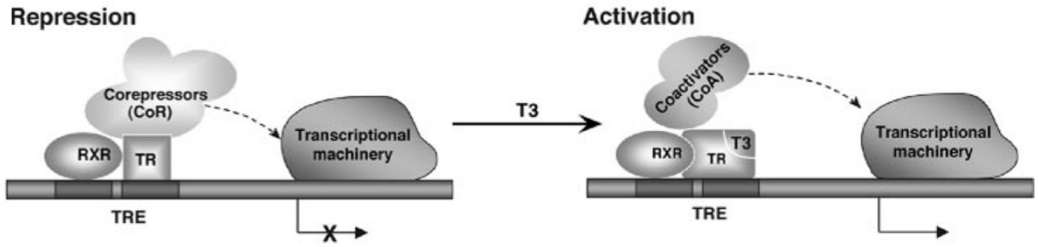

Figure 1.7 – Thyroid hormone receptor action. The best-described thyroid hormone receptor (TR) action is as a ligand-activated transcription factor. The unliganded TR interacts with corepressors (CoR), which leads to the repression of gene transcription. Binding of T3 (ligand) to the TR, which binds DNA as a heterodimer with retinoid-X-receptor (RXR) in the thyroid hormone response element (TRE), recruits' coactivators (CoA) and this interaction leads to transcriptional activation. Adapted from Cheng et al., (2010).

T3 is well established to be the biologically active form of THs. It binds to TRs with 10 to 15-fold higher affinity than T4 (Skah et al., 2017). T4 has been viewed only as a pro-hormone, to be locally converted by DIO2, to its active form T3. But studies in different organisms, such as rats (Yoshimasa and Hamada, 1983) and tadpoles (Anne Galton and Cohen, 1980), have shown that T4 has activity and binds to TRs under specific conditions, which also depends on the cell and tissue type. However, no *in vivo* studies have so far shown this and more studies are needed to understand *in vivo* T4 activity (Galton, 2017).

In humans, mutations in the TRs cause reduced responsiveness to T3 in the peripheral tissues, causing several disorders, such as Resistance to Thyroid Hormone alpha (RTHα) or beta (RTHβ) due to mutations in the *THRA* or *THRB* gene, respectively. These mutations lead to the inability of the receptor to bind T3 or to recruit protein complexes responsible for the transcriptional activation or repression of target genes (Machado et al., 2009; Refetoff et al., 2014). 85% of cases of resistance to THs are due to mutations in the *THRB* gene. These patients have cognitive disabilities, reduced IQ, and increased incidence of Attention Deficit and Hyperactivity Disorder (Refetoff and Dumitrescu, 2007). Mutations in the *THRA* gene are associated with growth retardation, delayed bone development, severe constipation, and mild cognitive deficits (Bochukova et al., 2012; van Mullem et al., 2012).

The vast majority of physiological effects of THs involve the binding of T3 to specific nuclear TRs (genomic effects). Still, TH action can also be mediated by non-genomic mechanisms, independent of nuclear uptake of T3 and intranuclear formation of T3-TR complexes with other nucleoproteins (Davis et al., 2016; Galton, 2017). The non-genomic action of THs is not the subject of this thesis and will not be further explored.

1.2.3.1 THYROID HORMONE RECEPTORS IN ZEBRAFISH

TRs protein structure and function are well conserved among vertebrate species, especially the DNA-binding and ligand-binding domains. The human and zebrafish receptors share 90 – 95% protein identity (Darras et al., 2011; Marelli et al., 2017). In zebrafish, two *trα* genes were identified, the *thraa* and *thrab*, and one *trβ* gene, the *thrb*. The *thraa* gene produces, by alternative splicing, two trα isoforms, the zTRαA1S (short) and zTRαA1L (long). zTRαA1S is very similar to the vertebrate TRα1 and differs from zTRαA1L in that it has 14 additional amino acids in the carboxy-terminal domain (Fig. 1.8) (Darras et al., 2011). The zebrafish zTRαB encoded by the *thrab* gene is structurally similar to the zTRαAS isoform but lacks a large part of the A/B domain and thus lacks transactivation activity (Fig. 1.8) (Marelli et al., 2016; Takayama et al., 2008). The zebrafish *thrb* gene produces two TRβ1 isoforms (zTRβ1S and zTRβ1L), which differs for the presence of an additional 9 amino acids in the ligand-binding domain, and one TRβ2 isoform (Fig. 1.8) (Darras et al., 2011; Marchand et al., 2001; Marelli et al., 2016).

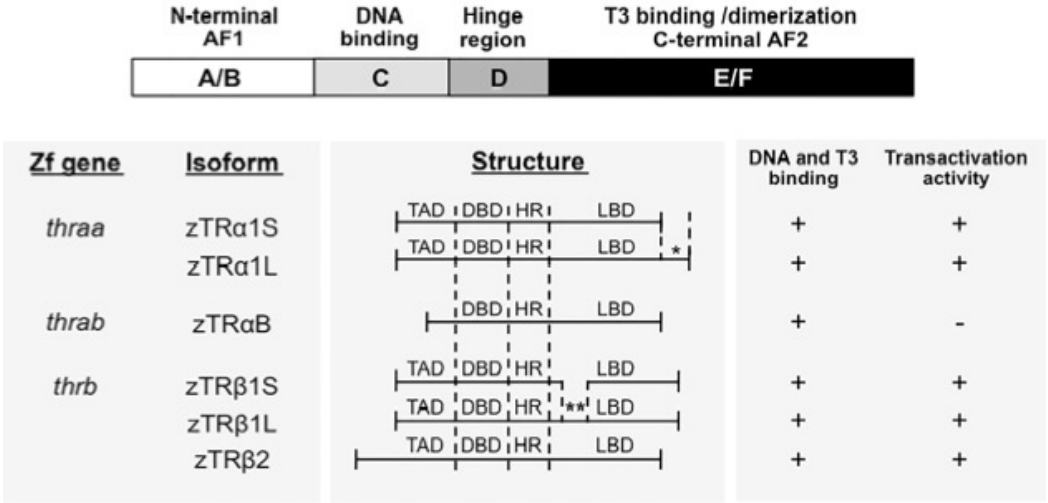

Figure 1.8 – Thyroid hormone receptor isoforms in zebrafish. The *thraa* gene gives rise to two functional isoforms: zTRα1S and zTRα1L. These isoforms differ for 14 amino acids in the C-terminus of the ligand-binding domain (LBD), represented in the figure with an (*). The *thrab* gene encodes the zTRαB receptor that can bind DNA and T3 but has no transactivation activity because it lacks a large part of the A/B domain. The *thrb* gene gives rise to 3 functional isoforms: zTRβ1S, zTRβ1L and zTRβ2. The two zTRβ1 isoforms differ for a 9 amino acid insert in the LBD represented in the figure with (**). TAD: transactivation domain; DBD: DNA binding domain; HR: hinge region; LBD: ligand binding domain. Adapted from Marelli et al., (2016).

The expression profile of the different zebrafish *TR* genes revealed that they are regulated in a spatiotemporal matter. Expression of *thraa* and *thrb* were detected by RT-qPCR from the first hour of development, demonstrating those are maternally derived transcripts. Zygotic expression of *thraa* and *thrb* were only detectable at 3 hpf (Essner et al., 1997; Liu and Chan, 2002). From 6hpf, the expression of both transcripts decreases and becomes almost undetectable. At 24hpf, expression increases and maintains similar expression levels until 5dpf. In the adult zebrafish, *thraa* was expressed in the brain, heart, kidney, gastrointestinal tract, liver, swim bladder, pectoral fins and gonads. Adult expression of *thrb* was present in the eye, muscles, swim bladder, pectoral fins and gonads (Marelli et al., 2016).

During embryonic development, expression of *thraa* was first detected by WISH at 24 hpf in the retina, brain, spinal cord and optic capsule. By 48hpf *thraa* expression increases, which was maintained until 72 hpf. At 5 dpf, expression of *thraa* was also present in the gastrointestinal tract (Campinho et al., 2014; Marelli et al., 2016). The expression of *thrab* was detectable at 12 hpf in the neural epithelia. At 24, 48 and 72 hpf high expression of *thrab* was present in the brain and spinal cord (Campinho et al., 2014). The expression of *thrb* was only visible at 31

hpf in the retina. At 48 hpf, expression increases in the retina, hindbrain and pituitary. At 5 dpf expression was also detected in the optic vesicle (Campinho et al., 2014; Marelli et al., 2016).

1.3 NEURODEVELOPMENT IN VERTEBRATES

Vertebrate neurodevelopment is a tightly regulated and complex process that starts early in embryonic development. The development of the CNS in vertebrates involves many coordinated cellular events, and internal and external cues in a precise temporal and spatial manner, to generate the diverse neuronal and glial cell types required for proper brain function (Gothié et al., 2020; Murao et al., 2016). The vast cell diversity in mammalian brains is generated during embryonic and early postnatal stages from a neural stem and progenitor cell pool. The transition of proliferative and multipotent progenitor cells to fully differentiated neurons is called neurogenesis (Urbán and Guillemot, 2014). Neurogenesis is followed by the migration and differentiation of neurons, formation of dendrites and axons, synaptogenesis, and the establishment of neuronal circuitry. However, non-neuronal processes are also part of vertebrate neurodevelopment, such as the development of glial cells by gliogenesis (radial glial cells, astrocytes and oligodendrocytes), myelination, vascularisation, and the development of the blood-brain barrier (BBB) (Taverna et al., 2014).

In vertebrates, development of the CNS starts during gastrulation (16 – 18 days post conception in humans) (Plessis and Volpe, 2018). Some cells from the primitive ectoderm ingress through the primitive streak (in amniotes) or through the embryonic shield (in teleosts) into the interior of the embryo and give rise to the mesodermal and endodermal germ layers (Stern, 2005). The remaining cells form the definitive ectoderm (Shparberg et al., 2019). At this stage, the definitive ectoderm covers the embryo's outer layer and gives rise to two different tissues. Ectodermal cells on the lateral side give rise to epidermal progenitors, while on the central side give rise to neural progenitors. This neural induction of the ectoderm is triggered by signals from the organizer (node in mice), giving rise to the neural plate. The main signalling involved in this neural event are the Fibroblast growth factors (FGF), Bone morphogenetic proteins (BMP), Wingless (Wnt) and Nodal (De Robertis and Kuroda, 2004; Stern, 2005; Weinstein and Hemmati-Brivanlou, 1999). However, the key regulatory mechanism for neural induction is the inhibition of the BMP pathway (particularly BMP4) by Noggin, Chordin, Follistatin, and Cereberus secreted by the organizer (reviewed in Rogers et al., 2009).

After neural plate establishment, the pseudostratified epithelium is constituted by a monolayer of neuroepithelial cells. It undergoes a series of morphogenetic events to fold into the neural tube by a process known as primary neurulation (Fig. 1.9). In amniotes, the lateral edge of the neural plate thickens and elevates into neural folds. This narrows the neural plate to form the neural groove. At the dorsal midline, the neural plate edges converge and close to form the neural tube. The anterior part of the neural tube will give rise to the brain, while the spinal cord forms at the posterior end (Colas and Schoenwolf, 2001).

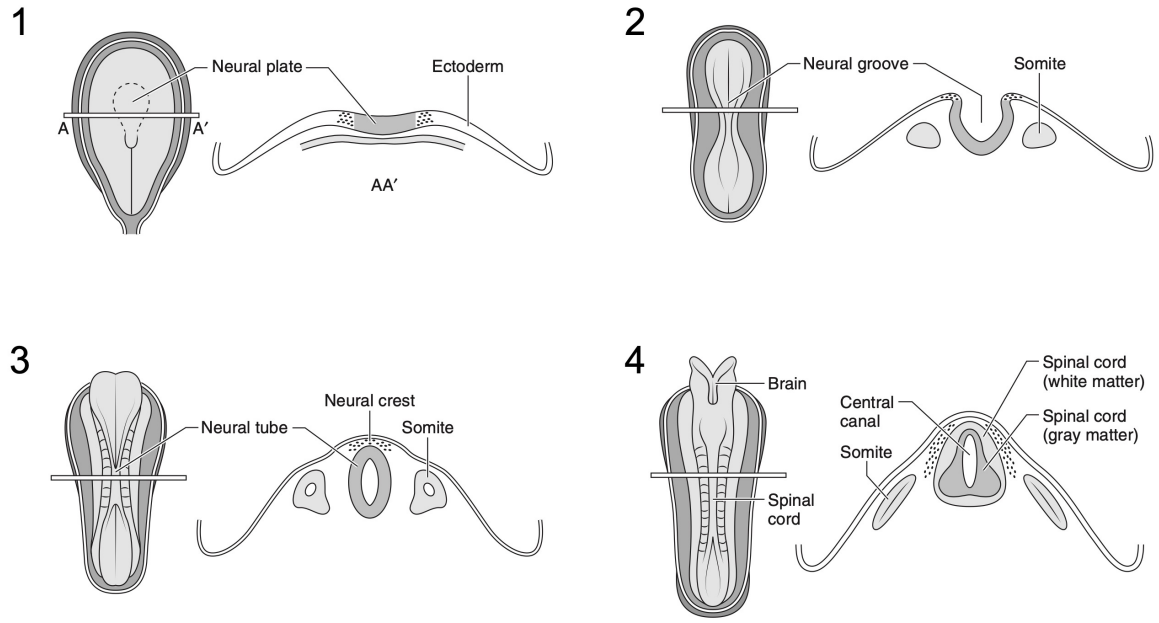

Figure 1.9 – Schematic representation of neural tube formation in the developing embryo. In each panel: external view (left) and corresponding cross-sectional view (right) at the middle of the future spinal cord. After neural plate establishment, the neuroectoderm folds. At the edges of the groove, neural crest cells form and separate from the neural fold giving rise to the peripheral nervous system. The neural plate continues to fold until the edges meet at the midline and form the neural tube. The anterior part of the neural tube will give rise to the brain, while the posterior part will give rise to the spinal cord. Adapted from Plessis and Volpe, (2018).

The basic mechanism involved in primary neurulation is conserved between vertebrates. However, some differences exist in the cellular movements involved in tube closure, resulting in differences in neural tube cavity appearances. In teleost, like zebrafish, and amphibians, primary neurulation starts with the neural plate, which is also a monostratified neuroepithelium. But after thickening the lateral edges of the neural plate, a transient structure, the neural keel, develops, consisting of a solid mass of rod of cells. Afterwards, the cells in the neural keel

reorganise in a neural rod, which is a solid tube. Later the tube lumen opens and forms the neural tube (Fig. 1.10) (Harrington et al., 2009; Lowery and Sive, 2004).

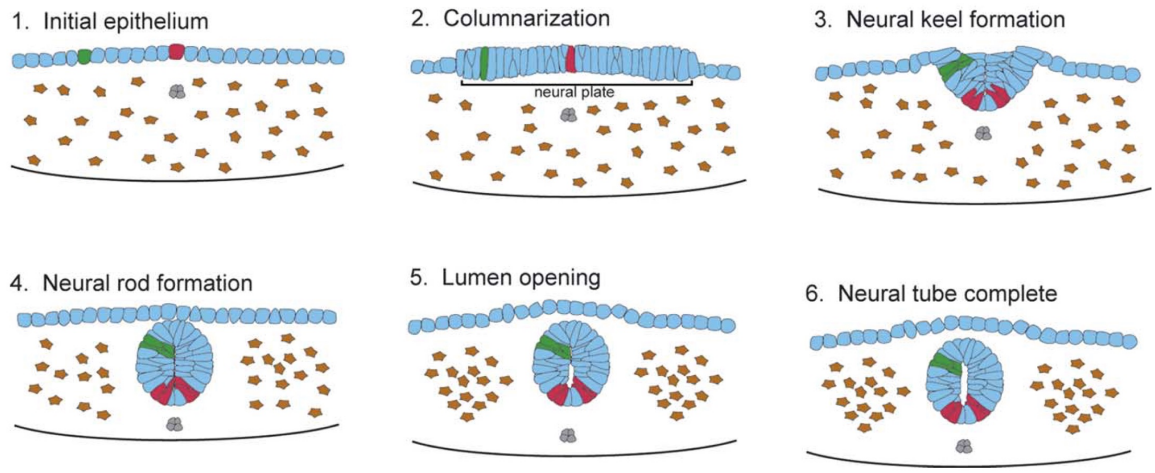

Figure 1.10 – Schematic representation of neural tube development during zebrafish embryonic development. The initial epithelium columnarizes and forms the neural plate, afterwards, the neural keel forms, followed by the formation of the neural rod. In the midline, the tube opens and forms the lumen. Cells labelled by red and green show that they maintain their relative position in the neural tube. Adapted from Lowery and Sive, (2004).

Neural progenitor cells of the neural tube divide and generate the large diversity of neurons and glia that comprise the CNS (Kintner and Koyano-Nakagawa, 2013). However, acquiring a specific neural cell fate of the neural progenitor cells depends on its position within the neural tube along the anterior-posterior and dorsal-ventral axis. This initial position determines the progenitor cell portfolio of expressed transcription factors, resulting from the different patterning signals to which it was exposed and guiding the neural cell fate and outcomes of the progenitor (Hernandez-Miranda et al., 2017; Le Dréau and Martí, 2012). Neural cell fate acquisition starts early during neural plate establishment, where the neural plate is patterned by specified Wnt, FGF and retinoic acid (RA) signalling gradients to establish the anterior-posterior axis of the CNS (Gaspard and Vanderhaeghen, 2010). The dorsal-ventral axis is established after neural tube development, where two sets of specialised cells behave as the organizer, the dorsal roof plate (RF) and the ventral floor plate (FP) (Fig. 1.11 A). The main morphogenic signals involved in this dorsal-ventral patterning are Sonic hedgehog (Shh) released from the FP and the notochord, and Wnt and BMP signalling gradients from the RP (Le Dréau and Martí, 2012). These morphogens set up concentration gradients that establish specific cues for the progenitor cells, leading to the expression of a distinct combination of

homeodomain genes and the activation of specific transcriptional programs that results in the rise of different population of neuronal cells (Gouti et al., 2015; Yan and Wang, 2021). Neural progenitor cells also require Notch signalling and action, besides the above-mentioned signalling pathways, for their proliferation and differentiation (Lara-Ramirez et al., 2019; Yeo and Chitnis, 2007).

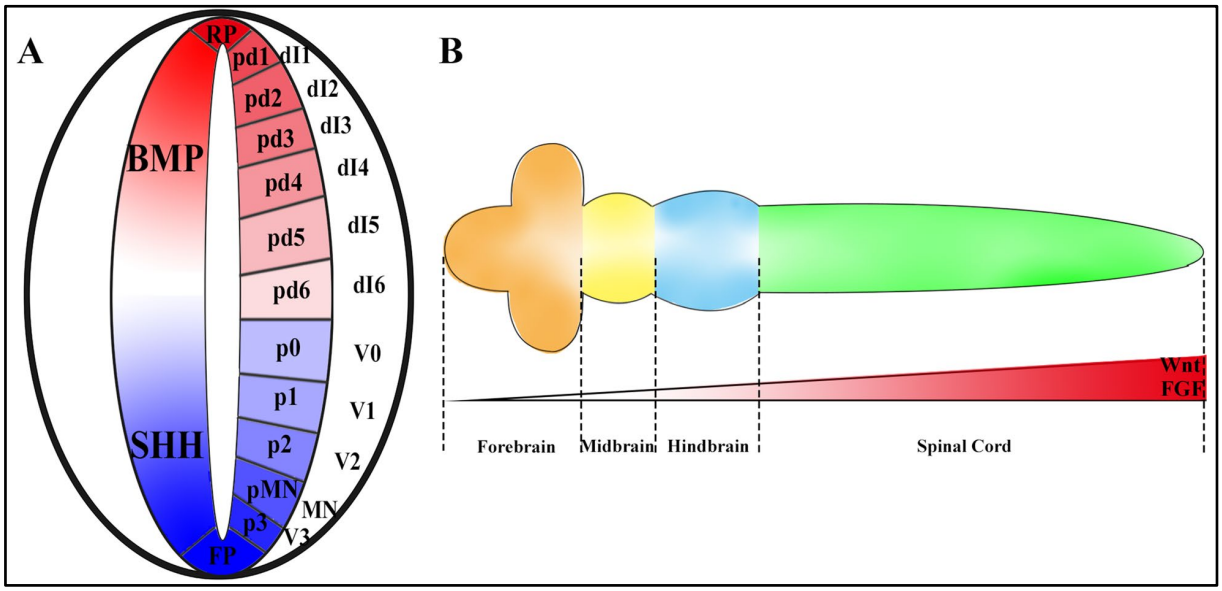

Figure 1.11 – Neural tube patterning during vertebrate development. A) The dorsal-ventral patterning. During neural tube development, Shh signalling is secreted by the ventral floor plate (FP) and notochord. In contrast, BMPs are secreted by the roof plate (RP), creating two opposing morphogenetic gradients that pattern the neural tube. In response to the morphogen gradient, the proliferative progenitor cells in the lumen of the neural tube differentiate into postmitotic neurons. The dorsal domain (coloured in red) contains six dorsal progenitor domains (dP1-dP6) that differentiate into the dorsal interneuron population (dI1-dI6). The ventral domain (coloured in blue) comprises five progenitor domains, that differentiate into the ventral interneurons (V0-V3, motorneurons (MN)). **B) The anterior-posterior patterning.** Retinoic acid (RA) signalling is released from the somites in the anterior region of the neural tube, while Wnt and FGF signalling gradients are released in the posterior part of the neural tube contributing for the anterior-posterior patterning. After neural tube formation, four domains arise: forebrain, midbrain, hindbrain, and spinal cord. Adapted from Wang et al., (2021).

The temporal sequences for CNS development and the morphogenetic signalling pathways for dorsal-ventral and anterior-posterior patterning are widely conserved between vertebrates (Okano and Temple, 2009; Yan and Wang, 2021).

The initial steps of vertebrate brain development are similar. Shortly after neural tube closure, the most anterior part of the tube undergoes morphological changes induced by differential proliferation of the neuroepithelial regions, forming the forebrain (prosencephalon), midbrain (mesencephalon), and hindbrain (rhombencephalon) (Fig. 1.11 B) (Ishikawa et al., 2012). The hindbrain is one of the most evolutionary conserved regions of the vertebrate brain. It will generate a complex neuronal circuit required for basic motor functions, such as respiration, facial expression and locomotion, and sensory information, such as audition, balance and heart rate (Gilland and Baker, 2005; Krumlauf and Wilkinson, 2022).

During development, the hindbrain is temporarily subdivided into seven to eight compartments named rhombomeres (r1 – r8) (Fig. 1.12), each expressing a distinct set of transcription factors, including *egr* (*krox20*), *mafb*, *Hnf1* and *Hox* genes, that underlie segmentation and anterior-posterior identity (Alexander et al., 2009; Moens and Prince, 2002). These rhombomeres become lineage-restricted cellular compartments that prevent the intermixing of cells with the neighbouring rhombomeres (Calzolari et al., 2014). This segmentation process is fundamental for specifying the neural developmental fate associated with the diverse functions of the hindbrain. So each rhombomere generates distinct neuronal cell types (Briscoe and Wilkinson, 2004). Each rhombomere has specific boundary cells regulated by the Eph/ephrin bidirectional signalling pathway. The Eph receptors are expressed in r3 and r5, whereas their ligands, the ephrins, are expressed in r2, r4 and r6, showing that the rhombomeres have an alternative two-segment periodicity (Mellitzer et al., 1999). This principle can also be observed in the formation of the branchiomotor nerves. The first neurons appear in the even-numbered rhombomeres r2, r4 and r6, forming the trigeminal (V), facial (VII) and glossopharyngeal (IX) branchiomotor nerves. Afterwards, the neurons differentiate in the odd-numbered rhombomeres (r3, r5 and r7), sending axons unidirectionally to the anteriorly adjacent even-numbered rhombomere (Chandrasekhar, 2004). This shows that the hindbrain's spatially and temporally controlled patterns set the early ground plan for an elaborative neuronal circuitry that constitutes the CNS (Chandrasekhar, 2004; Moens and Prince, 2002).

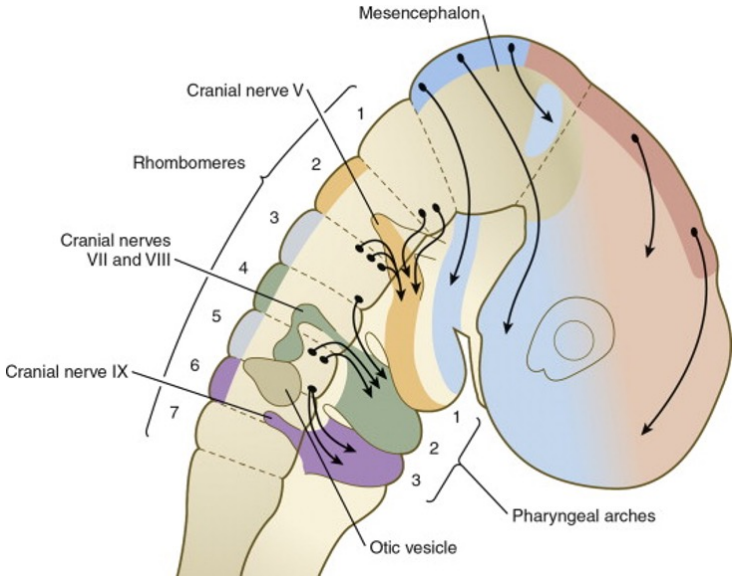

Figure 1.12 – Segmental organization of the vertebrate hindbrain. Illustration of the 7 rhombomeres (numbers 1 – 7) present during hindbrain development. The migration pathway of the branchiomotor nerves (V – X) into the first three pharyngeal arches is shown, illustrating the two-segment periodicity in the segmental organization. Adapted from "Development of the Neural Crest," (2014).

In zebrafish, the morphological segmentation of the hindbrain is transiently visible at 18 – 20 hpf (18 somite stage) (Kimmel et al., 1995). Rhombomere boundary formation is species-specific. In zebrafish, the first rhombomere boundaries appear between r3 and r4, and then between r4 and r5, defining first the r4 territory. Afterwards, the boundaries between r1/2, r2/3 and r6/7 are established. Boundaries between r7 and r8 have not been found (Moens and Prince, 2002). The most anterior rhombomere, r1, is the largest rhombomere, extending from the mid-hindbrain boundary to the r1/2 boundary. The most posterior rhombomere, r7 – r8, transitions to the spinal cord. This rhombomere differs morphologically from the other rhombomeres (r2 – r6) as it is more than twice as large (Lumsden, 1990; Ma et al., 2009).

1.4 THYROID HORMONES AND NEURODEVELOPMENT

Clinical and experimental studies have shown that THs are essential for normal human CNS development. The developmental timing of THs insufficiency can arise from maternal, foetal or infant origin (Zoeller and Rovet, 2004). Congenital hypothyroidism arises from an impaired foetal thyroid gland development and function. It can be primarily prevented by early postnatal TH substitution therapy, while insufficient THs from maternal origin lead to neurological

cretinism, which is irreversible after birth (Moog et al., 2017). An adequate amount of maternal THs is crucial since even a mild decrease in maternal THs levels during early pregnancy can impair the neurocognitive development of the offspring (Li et al., 2010). This shows that the timing and severity of THs insufficiency can lead to different types and severities of neurological deficits (Zoeller and Rovet, 2004).

1.4.1 THYROID HORMONE DELIVERY DURING DEVELOPMENT

The human foetal thyroid gland is the first endocrine organ to develop (at 5 – 6 weeks of gestation) and starts to secret low amounts of T4 around 14 – 16 weeks of gestation. Thus, during the 1st trimester of pregnancy, the foetus depends on the adequate and timely supply of maternal THs (Obregon et al., 2007; Jatin Patel et al., 2011). For maternal THs to reach the developing foetus they must first pass the placental barrier. The placenta is an active barrier that controls the amount of THs that reaches the foetus. Membrane transporters and local deiodinases achieve this (reviewed in Jatin Patel et al., 2011). DIO3 is the main deiodinase expressed in the placenta, thus protecting the foetus from excessive levels of maternal THs. DIO3 has a substrate specificity for T3, contributing to T4 being the main form of maternal THs reaching the foetus (Salvatore et al., 1995).

Maternal THs are actively transported through the placenta into the exocoelomic cavity from 5 – 6 weeks of gestation (Calvo et al., 2002; Landers and Richard, 2017). The exocoelomic cavity forms at 4 weeks of gestation, separating the placenta from the amniotic fluids (Fig. 1.13). It is an important compartment of molecular exchange between the mother and the foetus and a reservoir of nutrients (Jauniaux and Gulbis, 2000). Total levels of THs in foetal fluids are 100-fold lower compared to the concentration in the mother's serum. Nonetheless, free T4 levels in the foetal fluids are around one-third of those in the maternal circulation (Calvo et al., 2002; Contempré et al., 1993). During gestation, total foetal serum T4 levels gradually increase and reach adult levels at the beginning of the third trimester. In contrast, total foetal T3 levels remain low during development, increasing only at term (Thorpe-Beeston et al., 1991).

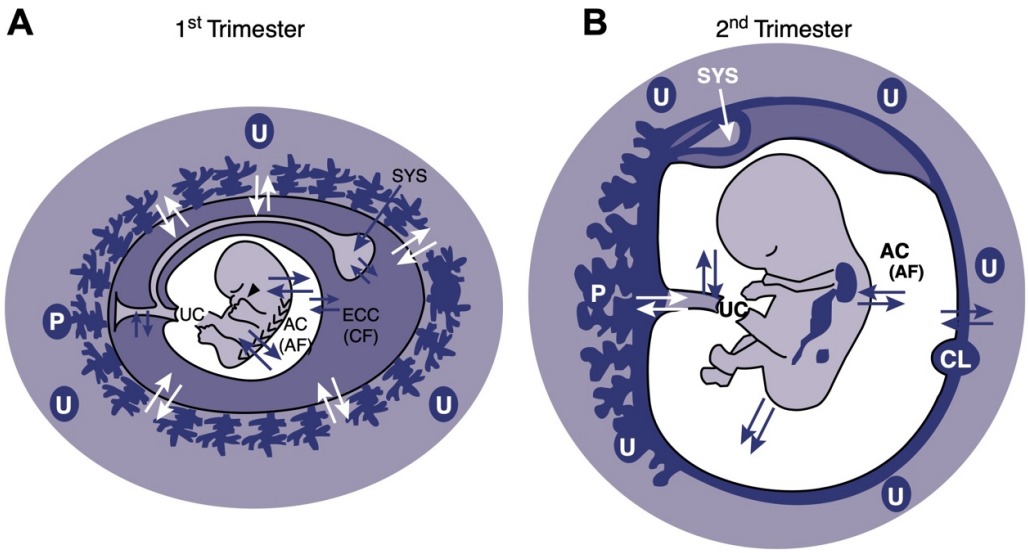

Figure 1.13 – Schematic representation of the maternal-foetal unit. A) 1st trimester. During the 1st trimester, the human foetus is surrounded by the amniotic cavity (AC) that contains the amniotic fluid (AF), the foetus and the exocoelomic cavity (ECC) that separates the AC from the placenta (P) and contains the secondary yolk sac (SYS). The SYS is directly connected to the foetal gut and circulation. The ECC contains the coelomic fluid (CF) that regulates the molecular exchange between the mother and the foetus. **B) 2nd trimester.** The SYS, the ECC and two-thirds of the placenta progressively degenerate, and the AC grows gradually. From 11 – 12 weeks of gestation onward, maternal nutrients are transferred directly from the placenta into the foetal circulation. AC: amniotic cavity, AF: amniotic fluid, CF: coelomic fluid, CL: chorion leave, ECC: exocoelomic cavity, P: placenta, SYS: secondary yolk sac, U: uterus, UC: umbilical cord. Adapted from de Escobar et al., (2004).

During the first trimester, maternal THs are transferred from the exocoelomic cavity into the foetal circulation through the secondary yolk sac (SYS) that communicates directly with the foetal gut (Fig 1.13 A). By 10 weeks of gestation, the exocoelomic cavity (ECC) gradually disappears, and maternal THs are transferred directly from the placenta (P) into the foetal circulation (Fig. 1.13 B) (Calvo et al., 2002; Contempré et al., 1993). Before neural tube closure, maternal THs can access the CNS directly. Afterwards, from 17 – 20 weeks of gestation, THs enter the brain through the BBB or the blood-cerebrospinal fluid barrier (BCSFB) (Chanoine et al., 1992; Wirth et al., 2014).

During mid-gestation, the foetal thyroid gland becomes fully functional. However, in cases of insufficient foetal production of THs, maternal THs transfer compensates for insufficient THs endogenous levels (Vulsma et al., 1989). However, the placenta lacks a compensatory

mechanism of maternal THs transfer in the case of the hypothyroid state of the mother (Chan et al., 2009).

1.4.2 THYROID HORMONE DELIVERY INTO THE BRAIN

The entry of THs into the developing CNS and its distribution into the different regions and cell types is crucial for normal development and differentiation. But it is also essential for maintaining and regulating brain activity and metabolism in the adult (Wirth et al., 2014). THs are delivered into the foetal brain mainly through the BCSFB or the BBB (Fig. 1.14).

The BCSFB is a barrier formed by epithelial cells of the choroid plexus located in the lateral, third and fourth cerebral ventricles that separates blood from the cerebrospinal fluid (CSF) (Redzic and Segal, 2004; Saunders et al., 2018). THs in the blood circulation enter the choroid plexus epithelial cells throughout TH transporters. MCT8 is the main transporter, but OATP1C1, MCT10 and LAT2 have also been identified in the foetal choroid plexus (Chan et al., 2011; Friesema et al., 2012; Roberts et al., 2008; Wirth et al., 2014). THs bind with intracellular transthyretin, and this complex is transported through the choroid plexus on the apical membrane into the CSF. Afterwards, THs enter the brain through the ependymal cells (Fig. 1.14 B) or the third ventricle tanycytes (Figure 1.14 C) (Chanoine et al., 1992). Ependymal cells are specialised glial cells that allow THs to enter the CNS from the CSF (Landers and Richard, 2017). THs enter into tanycytes through MCT8 or OATP1C1 (Friesema et al., 2012). Once inside, T4 is converted into T3 by DIO2 (Guadaño-Ferraz et al., 1997). Tanycytes are specialised ependymal cells which send processes to the hypothalamus, facilitating the access of T3 to hypothalamic nuclei, which are responsible for the release of TRH, thus having a fundamental role in the central HPT axis (Bolborea and Dale, 2013).

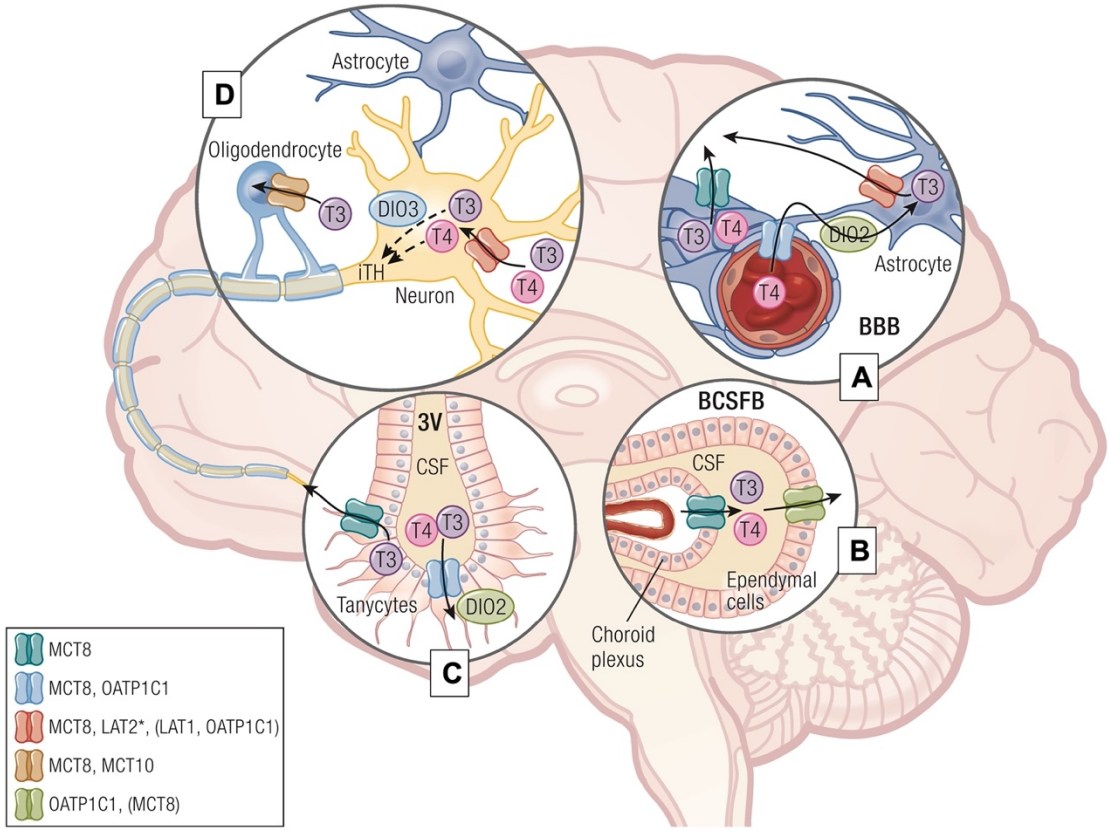

Figure 1.14 – Putative model of thyroid hormone transfer through the blood-brain barrier (BBB) and the blood-cerebrospinal fluid barrier (BCSFB) in the human brain. A) The BBB. Endothelial cells of the brain micro-vessels take up T4 and T3, preferably through OATP1C1 and MCT8, respectively. T4 is then transported into astrocytes end-feet via OATP1C1, where it can be locally converted to T3 by DIO2 and then exported through an unknown transporter. **B) The BCSFB.** THs in the bloodstream enter through the choroid plexus via MCT8. T4 binds with transthyretin and this complex is exported through the apical choroid plexus into the CSF. From the CSF, THs can enter the brain through the ependymal cells or the tanycytes. **C) Third ventricle tanycytes.** THs enter tanycytes through MCT8. T4 can be locally converted to T3 by DIO2 and exported via MCT8. **D) Neuron.** MCT8 mediates T3 entry into neuronal cells. It can bind to the nuclear TH receptors or be locally inactivated to T2 by DIO3. 3V: third ventricle; BBB: blood-brain barrier; BCSFB: blood-cerebrospinal fluid barrier; CSF: cerebrospinal fluid; iTH: inactive thyroid hormones. Adapted from Groeneweg et al., (2020).

THs enter the brain by passing the BBB through membrane transporters (Fig. 1.14 A). MCT8 is the main transporter present in the vascular endothelial cells of the BBB, while OATP1C1, LAT1 and LAT2 are present in lower quantities (De Boer et al., 2003; Roberts et al., 2008). Afterwards, T4 enters astrocytic end-feet via OATP1C1, which is then locally converted to T3 by DIO2. T3 is then exported via an unknown transporter and enters the neuronal cells via MCT8, where it binds to the nuclear TRs or can be inactivated by DIO3 (Fig. 1.14 D). T3 can

also enter directly into the neurons, via MCT8 transport, from the extracellular matrix (Bernal et al., 2015; Heuer, 2007; Landers and Richard, 2017). T4 can also enter target neurons. Nonetheless, T3 is the preferred substrate that enters neurons (Stepien and Huttner, 2019).

The majority of THs enters the brain through the BBB, whereas the uptake via the BCSFB is thought to be necessary to provide circumventricular areas with THs (Dratman et al., 1991).

1.4.3 CONGENITAL DISEASES CAUSED BY THYROID HORMONE DEFICIENCY DURING DEVELOPMENT

The mammalian CNS is highly sensitive to THs during the 1st trimester of pregnancy. Studies conducted in mice have shown that THs are involved in neurogenesis in the neocortex that starts in humans from weeks 5 – 6. Due to ethical issues, the exact timing remains to be defined (Ausó et al., 2004; Prezioso et al., 2018). THs deficiency does not cause major changes in brain anatomy. Still, it has an essential effect on processes involved in the formation of the cytoarchitecture of the brain, such as migration, proliferation and myelination (Ausó et al., 2004; Bernal and Nuncez, 1995; Lavado-Autric et al., 2003). During foetal development, THs signalling contributes to the formation of specific brain structures, such as the cortex, cochlea, hippocampus and cerebellum (Fig. 1.15) (Williams, 2008).

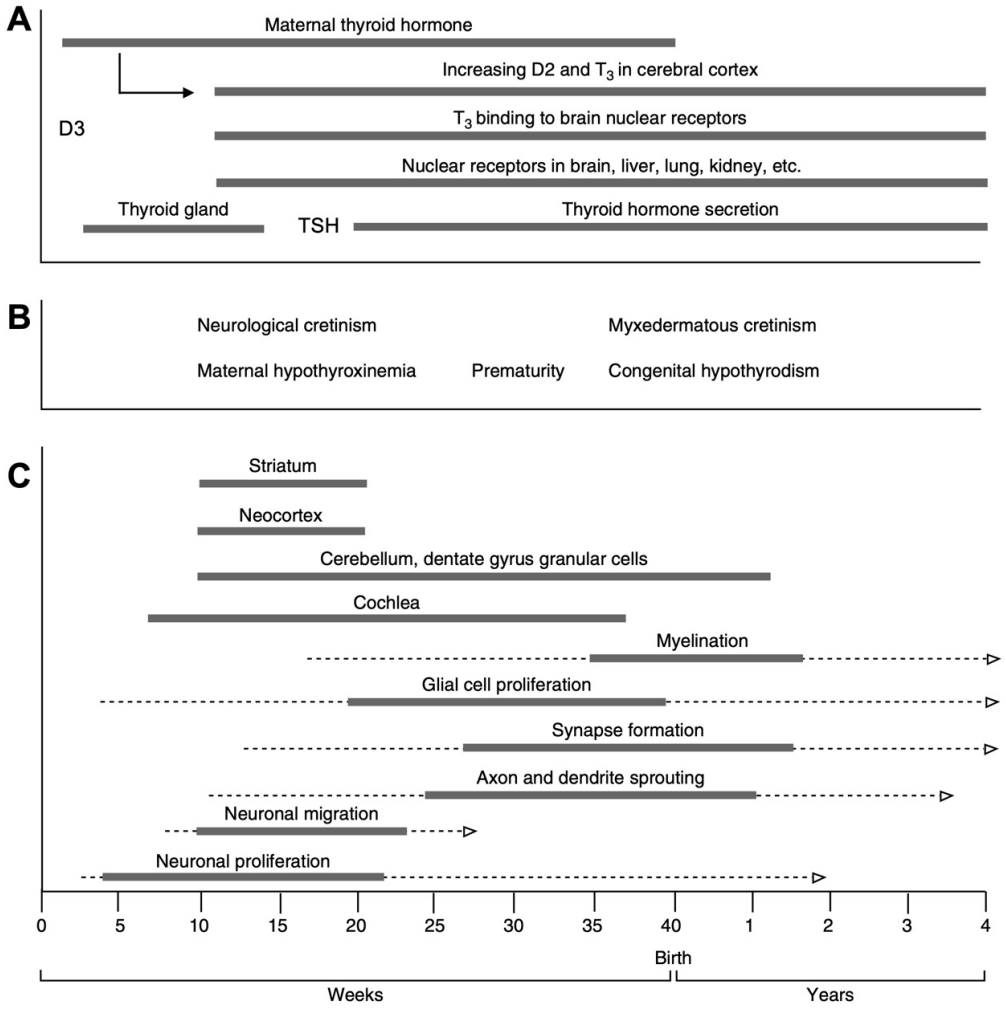

Figure 1.15 – Relationship between thyroid hormones action and human foetal and postnatal brain development. A) THs regulation. Ontogeny of the foetal thyroid gland, TSH, THs secretion, thyroid hormone receptors, and D2. D3 is abundant from the early stages of embryonic development. The foetus receives maternal THs from the early stages of development, being available during most of gestation. T4 from maternal origin is the main substrate of D2 in the brain, as illustrated by the black arrow. **B) THs-insufficiency-derived congenital conditions emerging during development.** The approximate timing of THs insufficiency that leads to neurological cretinism and myxedematous cretinism and the timing for maternal hypothyroxinaemia, prematurity, and congenital hypothyroidism. These features can be correlated with the developmental events shown in (A) and (C). **C) Neurodevelopmental processes dependent on THs.** The developmental timing of some relevant neurodevelopmental processes is presented. D2: deiodinase type 2; D3: deiodinase type 3; TSH: thyroid stimulating hormone. Adapted from Bernal, (2007); Patel et al., (2011).

An inappropriate supply of THs to the foetus in humans leads to developmental hypothyroidism (Fig. 1.15). Hypothyroid foetuses suffer various postnatal disorders that depend mostly on the

developmental time window of the neurological event if an adequate THs replacement therapy is not implemented. It can cause severe to irreversible neurological damage, leading to the inability to walk and speak, or mild to moderate impairments often associated with reduced intelligence and verbal development (Friesema et al., 2008; Ghassabian et al., 2014; Moog et al., 2017). For that reason, implementing systematic screening programs for THs deficiency in neonates has contributed to major progress in preventing neurological impairments and early treatment to improve infant life quality (Delange, 1997).

The main causes of THs deficiency during development are maternal and/or foetal hypothyroidism, iodine deficiency and congenital thyroid gland disorders. Worldwide, 2 – 5% of pregnant women are hypothyroid, while hypothyroxinaemia, a condition defined by low T4 in the presence of normal T3 and TSH, is present in 1.3 – 25.4% of pregnant women (Bernal, 2022; López-Muñoz et al., 2019; Teng et al., 2013).

Adequate levels of iodine from the mother are crucial during pregnancy. Iodine deficiency is the most severe cause of preventable neurodevelopmental disorder worldwide and impairs maternal and foetal THs synthesis during development (Zoeller et al., 2007). This condition gives rise to the syndrome known as endemic cretinism and can be divided into two conditions depending on the symptoms: neurological or myxedematous cretinism. In neurological cretins, the thyroid gland is normal and is clinically not hypothyroid. Nevertheless, they present severe mental retardation, deaf mutism and striatopallidal disorder with spastic diplegia affecting the lower limbs (Delong et al., 1985). Myxedematous cretins are clinically hypothyroid, have less severe mental defects than neurological cretins and present specific physical characteristics, such as short stature, poor sexual development, and craniofacial abnormalities. Usually, the neurological syndrome is more predominant, but a mixture of the two conditions has also been observed (Chen and Hetzel, 2010; Vanderpas et al., 1986). The differences between the two forms of cretinism are due to the different timing of THs action during foetal development (Fig. 1.15). Neurological cretinism results from deficient maternal THs supply during the first half of pregnancy, leading to defects in sensory, motor and cognitive functions (Fig. 1.15) (Bernal, 2022; Morreale De Escobar et al., 2000). Myxedematous cretinism results from an underactive thyroid gland of the foetus during the third trimester of pregnancy and in the postnatal life of infants (Fig. 1.15) (Bernal, 2022). Endemic cretinism and maternal hypothyroxinaemia can only be prevented by iodine supplementation before pregnancy. Otherwise, the insufficient THs supply leads to irreversible neurological impairments (Chen and Hetzel, 2010; de Escobar et al., 2004).

Congenital hypothyroidism is one of the most common diseases in paediatric endocrinology and affects 1/4000 newborns (Delange, 1997). This disease is caused by dysgenesis of the thyroid gland or by THs biosynthesis disorder (Rastogi and LaFranchi, 2010). Early treatment with L-thyroxine at birth increase infants' life quality to normal or near-normal neurocognitive outcome (Büyükgebiz, 2013; LaFranchi and Austin, 2007).

Infants born prematurely have a high risk of developing neurological impairment if not treated immediately (Reuss et al., 1996; Simic et al., 2009). Hypothyroidism is common in premature infants due to an immature HPT axis, an immature capacity to concentrate and synthesise iodine, and an immature TH metabolism (Van Wassenaer and Kok, 2004). In some cases, premature infants present a transient hypothyroxinaemia, occurring in 20 – 40% of premature infants before 34 gestational weeks (Delahunty et al., 2010). Premature infants also have a higher risk of congenital hypothyroidism, which is unpredictable in its evolution to transient or permanent (Vigone et al., 2014).

THs deficiency also results from mutations or polymorphisms of deiodinases and TRs, which have been already described in subsections 1.2.2 and 1.2.3, respectively. In the case of the TH membrane transporters, MCT8 and OATP1C1 are the only ones described to have a pathophysiological role (Schwartz and Stevenson, 2007; Strømme et al., 2018). To date, only one case has been reported with loss of function of the OATP1C1 membrane transporter due to a homozygous missense mutation that changed the highly conserved aspartic acid 252 to asparagine (D252N). The patient gradually developed dementia with spasticity and intolerance to cold. OATP1C1 is a specific T4-transporter, which is mostly expressed in astrocytes. *In vitro* studies of the mutated OATP1C1 resulted in reduced cellular T4 uptake and impaired plasma membrane localisation, leading to hypothyroidism in the brain and neurodegeneration. Treatment with the T3 analogue triiodothyroacetic acid (Triac) improved the clinical condition and well-being of the patient (Strømme et al., 2018).

1.4.3.1 THE ALLAN-HERNDON-DUDLEY SYNDROM

Mutations in the gene encoding the MCT8 transporter lead to a severe X-linked neurodevelopment disorder, known as the Allan-Herndon-Dudley syndrome (AHDS) (Friesema et al., 2004; Schwartz et al., 2005). Several mutations have been identified in the

MCT8 gene that range from large deletions, with loss of one or more exons, frameshift deletions and single amino acid deletions, insertions or substitutions (Friesema et al., 2004; Schwartz et al., 2005). From those mutations, the capacity of TH transport mediated by MCT8 has been classified into three pathogenic mechanisms. The first class of mutations comprises single amino acid deletions or insertions and missense mutations. It alters the transporter kinetics, which affects partially or completely the transporter capacity of MCT8, but it doesn't alter its expression levels at the cell membrane. The second class of mutations, which also results from single amino acid deletions or insertions and missense mutations, interfere with protein stability and/or trafficking toward the cell membrane, leading to residual transport of THs. These mutations result in reduced MCT8 protein levels at the plasma membrane. The third class of mutations fully inactivates the MCT8 protein by introducing a premature stop codon, large deletions, or frameshift mutations (reviewed in Groeneweg et al., 2020).

The diversity in mutations is associated with different phenotypic outcomes. Nevertheless, this syndrome affects males with mild to severe mental retardation and endocrine abnormalities. Although phenotypic plasticity exists, all affected males show low IQ levels (below 40), reduced communication capacity (speech is sometimes absent) and display movement disorders (Dumitrescu et al., 2004; Friesema et al., 2004; Masnada et al., 2022; Schwartz et al., 2005).

In terms of endocrine abnormalities, most patients have elevated serum T3 levels, reduced T4, free T4, and rT3 levels and high to normal TSH levels (Friesema et al., 2004). To date, heterozygous females do not present any neurological phenotype and have a minor alteration of THs levels, presenting only decreased serum T4 levels (Boccone et al., 2013; Dumitrescu et al., 2004; Heuer, 2007).

Histopathological analysis of the brain of MCT8 deficient male foetus and children revealed delayed cerebral cortex and cerebellum maturation, hypomyelination, altered neuronal differentiation, and underdeveloped synaptogenesis. The cerebral cortex of the foetuses was hypothyroid, presenting a 50% reduced concentration of THs. Nonetheless, TH levels in the liver were normal (López-Espíndola et al., 2014).

The pathogenic mechanism of MCT8 deficiency is not entirely understood, and some controversy exists. It is clear that THs are fundamental for brain development and that the lack of T3 transport through the BBB and/or neurons causes poor regulation of TH-dependent genes (Groeneweg et al., 2020; Kersseboom et al., 2014). Another proposed model suggests that the BBB is responsible for T3 entry into the brain and neural target cells. Thus MCT8 deficiency

affects THs supply into the brain, consequently remaining in a hypothyroid state (Bernal et al., 2015; Ceballos et al., 2009). Recent evidence in the zebrafish model of AHDS strongly argues that before BBB development, entry of maternal THs into neural cells is the determining factor giving rise to the neurodevelopmental phenotypes observed in these patients (Campinho et al., 2014; Silva and Campinho, 2023). Collectively, data from humans and zebrafish argue that MCT8-mediated THs transport constitutes the most determinant factor for adequate maternal THs-dependent neurodevelopment.

An effective treatment for AHDS that improves the thyrotoxicosis state in peripheral tissues and reverses cerebral hypothyroidism is unavailable. Several therapeutic approaches have been investigated, but so far, the only therapeutic approach that has alleviated the life quality of AHDS patients is the treatment with Triac (Groeneweg et al., 2020, 2019). Clinical trials using Triac alleviated thyrotoxicosis in peripheral tissues in paediatric and adult AHDS patients. Treatment with Triac in patients before age 4 also showed improved motor function. Nonetheless, the effects of Triac on neurodevelopment have not been studied in that trial, and if it reverses the neuro-motor phenotype can only be studied in young children whose developmental time window for brain development can be modulated (Groeneweg et al., 2019; Kersseboom et al., 2014; Zada et al., 2016).

1.5 THE ZEBRAFISH, A MODEL FOR THYROID HORMONE RESEARCH DURING EMBRYONIC DEVELOPMENT

Studies conducted in humans on the consequences of insufficient maternal THs supply during foetal brain development are mainly observational, focusing on relatively broad cognitive outcome measurements or the morphological changes of human brains (Bath et al., 2013; Noten et al., 2015; Willoughby et al., 2014). Due to the crucial role of THs action during CNS development, animal models have provided essential information to understand the molecular mechanism and behavioural changes depending on THs regulation (Bárez-López and Guadaño-Ferraz, 2017). Mammalian models, such as the mouse, have been largely used in biomedical research to understand human diseases because of their high homology between mammalian genomes and the similarity from anatomy to cell biology and physiology (Guénet, 2005; Lieschke and Currie, 2007). However, the difficulty in accessing the mammalian brain during

early embryonic development, given their in-utero development, and the difficulty to distinguish between the maternal and foetal THs contribution due to maternal compensatory mechanism upon experimental manipulation of the thyroid status, makes these models challenging to study THs action during embryonic neurodevelopment. For that reason, non-mammalian models, such as amphibian, teleost and avian, which develop externally, allow easier accessibility. The fact that during oogenesis, many maternal factors, including hormones and transcripts, are deposited into the egg ensures high control over TH status of the embryo during embryonic development (Abrams and Mullins, 2009; Préau et al., 2015; Vancamp and Darras, 2017).

The zebrafish (*Danio rerio*) is a small freshwater teleost fish, that emerged as a model organism in 1981 from work done by Streisinger et al. (1981) in molecular genetics and afterwards in its use for vertebrate embryology by Kimmel et al. (1989). The use of zebrafish in biomedical research has gained popularity because of the numerous advantages, such as simple maintenance, large number of progeny, rapid and external development, optical transparency, live imaging of all cell types, and targeted genetic manipulation, among others (Zada et al., 2017). Despite the anatomical differences between mammals and fish, as in all vertebrates, in zebrafish, the main regulators, such as TH transporters, deiodinases and TRs are also present in the zebrafish (Heijlen et al., 2013; Porazzi et al., 2009).

THs of maternal origin are deposited in high quantities in fish eggs. Freshwater fish, like zebrafish, have higher T4 levels than T3. These levels decrease during embryogenesis until endogenous production of THs starts (Chang et al., 2012). Maternal transfer of thyroid-related transcripts has also been confirmed in unfertilised zebrafish eggs (Vergauwen et al., 2018). This finding suggests an important role of THs during early embryonic development, such as those found in other mammalian species.

Zebrafish has widely been used to study the mechanism, function and defects of TH transporters (Arjona et al., 2011; Campinho et al., 2014; Vatine et al., 2013), iodothyronine deiodinases (Bagci et al., 2015; Dong et al., 2013; Guo et al., 2014) and TRs (Marelli et al., 2016). But also to study TH-related diseases, such as congenital hypothyroidism (Opitz et al., 2013), and thyroid cancer (Anelli et al., 2017).

The zebrafish has also become a suitable model for studying AHDS (Campinho et al., 2014; De Vrieze et al., 2014; Silva et al., 2017; Silva and Campinho, 2023; Vatine et al., 2013). Unlike the mouse model, which only phenocopies the peripheral endocrinological status of AHDS

patients, due to the compensatory mechanism of LAT2 and OATP1C1 in the BBB (Braun et al., 2011; Mayerl et al., 2014; Trajkovic et al., 2007; Wirth et al., 2009), the zebrafish phenocopies also the neurological and behavioural alteration as seen in AHDS patients (Campinho et al., 2014; De Vrieze et al., 2014; Vatine et al., 2013; Zada et al., 2014).

In zebrafish, *mct8* is abundantly expressed in the nervous system from the early stages of development and in the vascular system of the brain from 48 hpf (Campinho et al., 2014; Vatine et al., 2013). Expression of *oatp1c1* is restricted to vascular structures within the brain, and *mct10* is exclusively expressed in liver and trigeminal ganglia in 48 hpf embryos, suggesting that there is a relatively small possibility of full compensation for Mct8 loss of function in zebrafish, allowing for the development of Mct8-deficient zebrafish (Vatine et al., 2013). Using a morpholino-based system, which induces a transient gene knockdown of the Mct8 transporter, thus preventing the uptake of THs from the yolk into the cells. These animals present severe underdevelopment of the CNS. They exhibited a reduced number of trigeminal neurons, hindbrain interneurons, and *pax2a*- and *pax8*-expressing inhibitory neurons (Campinho et al., 2014). The zebrafish Mct8 knockdown embryo has a stiff axial body and impaired mobility, thus, phenocopies the locomotor consequences of AHDS observed in humans (Campinho et al., 2014; De Vrieze et al., 2014). Data from these models (Campinho et al., 2014) suggest that the impaired motor development observed in human AHDS patients is likely due to decreased inhibitory neurons in the hindbrain and spinal cord. Notably, recent evidence argues that maternal T3 generates the cellular diversity needed to achieve a fully functioning CNS (Silva and Campinho, 2023).

An unexpected observation made in these zebrafish models of AHDS is the impaired development of the blood-hindbrain barrier (BHB), with only three of the normal seven central arteries (CtAs) being formed (Campinho et al., 2014; De Vrieze et al., 2014)). The disadvantage of using this model is that morpholino penetrance will decrease by dilution as development progresses. Nonetheless, morpholino knockdown of target mRNAs is highly effective until 72 hpf and can be used to study gene function during the entire zebrafish embryonic development (Bedell et al., 2011; Timme-Laragy et al., 2012).

In summary, the zebrafish has been established as a model to study the role of Mct8 and the mechanism underlying AHDS (Campinho et al., 2014; Silva et al., 2017; Silva and Campinho, 2023; Zada et al., 2017).

1.6 VASCULARISATION OF THE VERTEBRATE CENTRAL NERVOUS SYSTEM

Initially, the neural tube is avascular, but after neurogenesis initiation, the neurons' high metabolic demand requires an increasing demand of nutrients and oxygen for its normal function (Attwell et al., 2010; Kurz, 2009). Vascularisation of the CNS starts at E8.5 – E9.5 in mice, where endothelial precursor cells (angioblasts) from the mesoderm are recruited by the neural plate to form a primitive vascular network around the neural tube named the perineural vascular plexus (PNVP) (Fig. 1.16 A) (Engelhardt and Liebner, 2014; Hogan et al., 2004). Afterwards, the neural tissue is vascularised by angiogenic sprouting from the PNVP (Breier et al., 1992; Hogan et al., 2004; Ruhrberg and Bautch, 2013). This angiogenic process is mainly mediated by neuronal progenitors, including neuroepithelial cells and radial glia cells, that secret morphogenetic cues, like the vascular endothelial growth factors (Vegfs) and Wnts, to promote vessel ingression into the neural tissue (Fig. 1.16 B) (Liebner et al., 2008; Raab et al., 2004). This angiogenic process happens in a precisely coordinated manner, where the timing and location of multiple cell types are fundamental to form a highly specialised vascular network with CNS vascular-specific BBB properties (Mancuso et al., 2008; Stamatovic et al., 2008). Angiogenesis of the CNS and barriergenesis of these cerebral endothelial cells occur simultaneously, demonstrating the pivotal role of the BBB in regulating the traffic of metabolites and signalling factors between the blood and the brain (Umans et al., 2017).

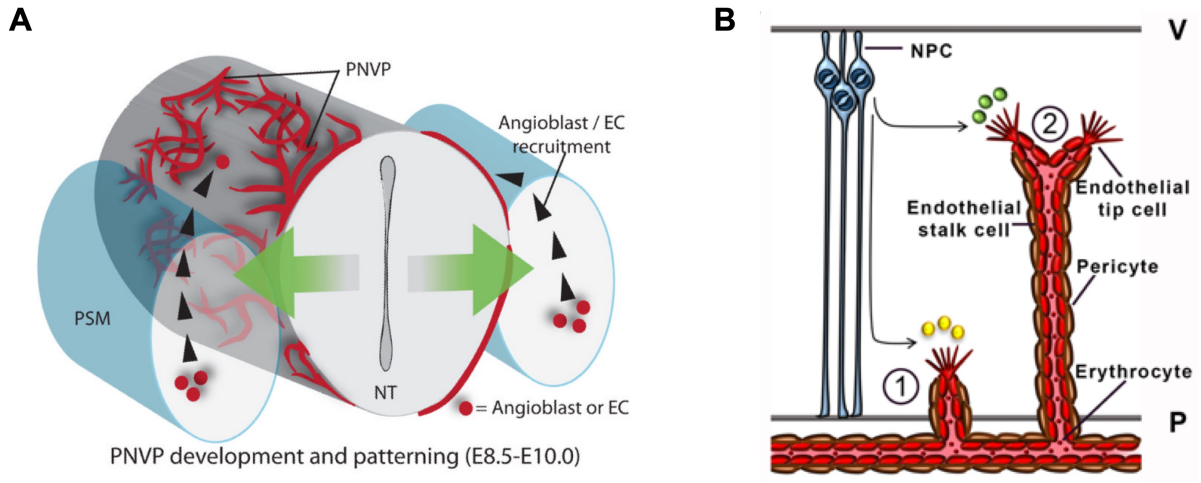

Figure 1.16 – Neural tube vascularisation. A) Schematic representation of perineural vascular plexus (PVNP) formation. In mice, at E8.5, guiding cues are secreted by the neural cells (green arrows) to induce angioblast and endothelial cells (EC) from the pre-somitic mesoderm (PSM) to differentiate, proliferate and migrate to the neural tube surface, forming the PVNP. **B) Brain vascularisation is mediated by**

neural progenitor cells. Schematic representation of the molecular mechanisms involved in the CNS vascularisation promoted by neural progenitor cells (NPC). NPCs secret angiogenic cues (yellow and green colour), such as VEGF and WNT ligands, that promote 1) vascular ingression and radial outgrowth, and 2) lateral branching. EC: endothelial cells; NPCs: neuro progenitor cells (light blue); NT: notochord; P: pial surface; PNVP: perineural vascular plexus; PSM: pre-somitic mesoderm; V: ventricular surface. Adapted from A) James and Mukouyama, (2011) and B) Tata and Ruhrberg, (2018).

1.6.1 BLOOD-BRAIN BARRIER DEVELOPMENT

In mammals, the development of the BBB can be subdivided into three stages: angiogenesis, differentiation, and maturation (Fig. 1.17). Development of the BBB begins early during neural tube development, where capillary sprouts from the PVNP penetrate the neuroepithelium by angiogenesis along an increasing VEGF concentration gradient (Fig. 1.17 A) (Potente et al., 2011; Raab et al., 2004; Risau et al., 1986). VEGF is secreted by neural progenitor cells of the ventricular neuroepithelium and serves as a directional cue for endothelial cells, which express the VEGF receptor (VEGFR) (Raab et al., 2004). Of the VEGF ligands, VEGF-A is the most potent angiogenic factor that mediates endothelial sprouting, migration and proliferation through the binding to the tyrosine kinase receptor VEGFR2 (FLK1 or KDR) (Bahary et al., 2007). Mutation of both ligand and receptor is embryonic lethal in mice (Carmeliet et al., 1996; Lee et al., 2007; Shalaby et al., 1995). In zebrafish, two *vegfa* paralogues exist, *vegfaa* and *vegfab* and both have been shown to be fundamental for BBB development. Zebrafish mutants for *vegfaa* displayed a reduced number of intra-cerebral vessels, called the central arteries (CtAs). In contrast, in *vegfab* mutants, the midline artery of the brain called the basilar artery (BA) does not develop (Lange et al., 2022).

Wnt signalling is important for endothelial cell migration into the embryonic neural tissue. Wnt ligands like Wnt7a, Wnt7b, and Wnt3a are secreted by the neural progenitor cells that bind to endothelium-expressed Frizzled (Fzd) receptors (Liebner and Plate, 2010). This interaction inhibits β-catenin degradation in the proteasome and leads to the accumulation of β-catenin in the cytoplasm, which afterwards translocates to the nucleus, where it induces transcription of BBB-related genes (Logan and Nusse, 2004), such as glucose transporter Glut-1 (Stenman et al., 2008), death receptors DR6 and TROY (Tam et al., 2012), and tight junction proteins (Liebner et al., 2008). In mice, deficiency in the Wnt/β-catenin pathway leads to reduced

vessels and brain haemorrhage due to vascular malformations and is embryonically lethal (Daneman et al., 2009; Stenman et al., 2008). During BBB development, Wnt7a and Wnt7b signalling differ from other Wnt ligands as they form a ligand-receptor complex with Reck, a GPI-anchored membrane protein Gpr124, an orphan G protein-coupled receptor (GPCR) (Cho et al., 2017). Wnt7a/b binds to Reck in the endothelial cells, and Gpr124 delivers this complex to Fzd (America et al., 2022). This complex signalling interaction of Wnt7a/b by Reck/Gpr124 results in a selective recruitment of Fzd receptors (Fzd1 and Fzd4), resulting in a more potent stimulation of BBB angiogenesis (America et al., 2022; Zhou and Nathans, 2014). Gpr124 deficient mice have vascular defects and haemorrhage in the CNS, thus being embryonically lethal (Zhou and Nathans, 2014). Gpr124 or Reck deficiency in zebrafish is associated with reduced CtAs that form the BBB (America et al., 2022; Ulrich et al., 2016).

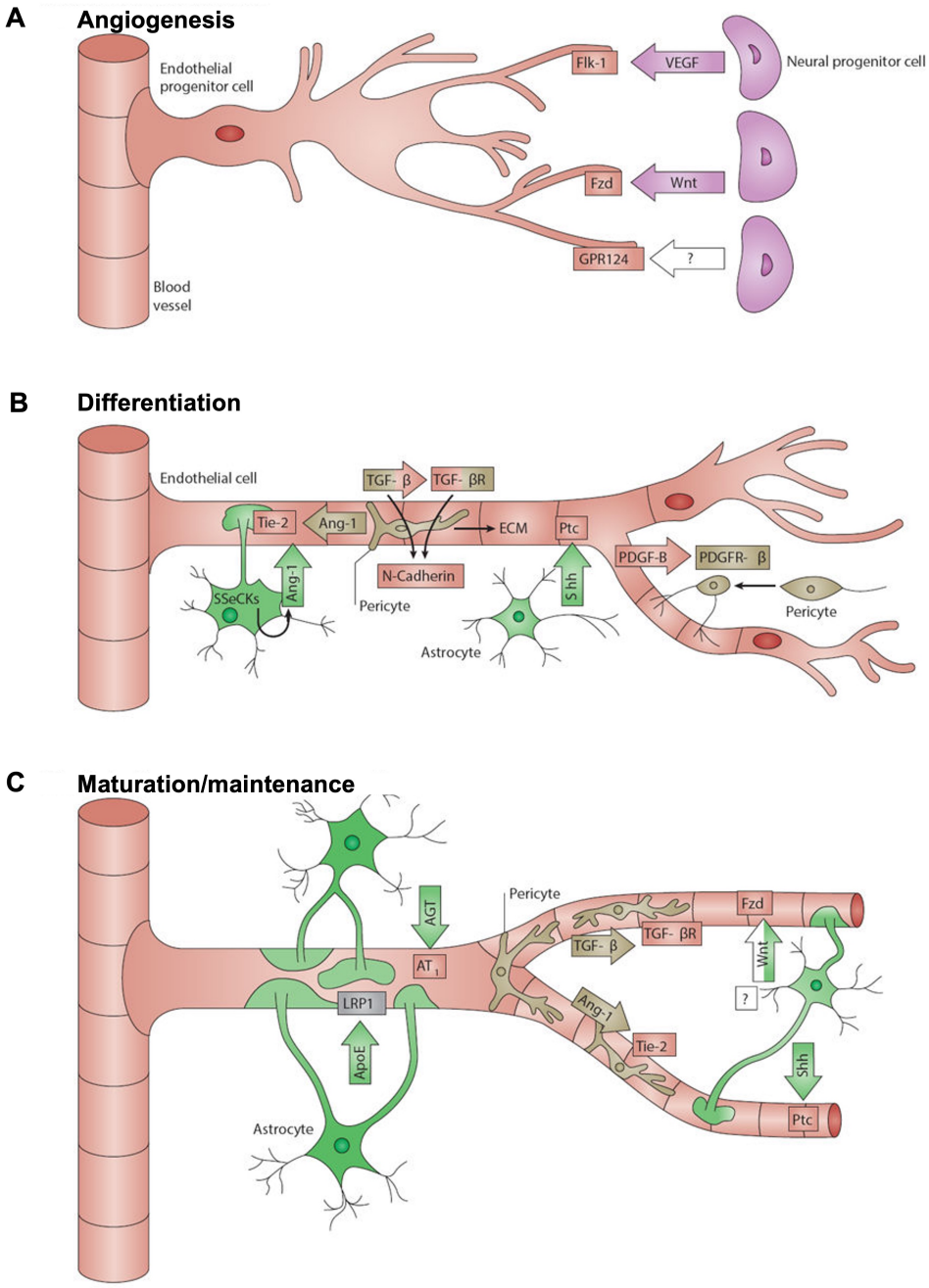

Figure 1.17 – Illustration of blood-brain barrier development stages. A) Angiogenesis. Neural progenitor cells release VEGF to induce endothelial cells to ingress the neural tissue according to an increased VEGF concentration gradient. Secretion of Wnt ligands by the neural progenitor also promotes endothelial cell migration. Binding of Wnt to endothelial Frizzled (Fzd) receptor, promotes the activation of β-catenin signalling and induces the expression of BBB-specific genes. The complex Wnt7a/b/Reck/Gpr124 highly stimulates the binding to specific Fzd receptors for BBB angiogenesis. **B) Differentiation.** As BBB development proceeds, pericytes are recruited by endothelial cells that secrete PDGF-B. This interaction induces TGF-β signalling (*TGF-β - TGF-βR2*), which promotes pericytes to deposit ECM components for basement membrane formation. TGF-β signalling also induces tight junction expression by the expression of Ang-1 in pericytes which bind to endothelial Tie-2 receptor. Recruitment of astrocytic end-feet induces the release of

SHH that binds to the Ptc endothelial receptor and contributes to the expression of tight junction proteins, increasing BBB permeability and maturation. The expression of ANT and ANG-1 in astrocytes also contributes to tight junction formation. **C) Maturation and maintenance.** Pericytes and astrocytic end-feet cover the vascular wall and secret ECM constituents for basement membrane formation. Sealing of interendothelial tight junctions by upregulation and redistribution of tight junction proteins is completed during maturation and is maintained throughout life by the pericytes and astrocytes. A: astrocytes; E: endothelium; EC: endothelial cell; M: microglia; N: neuron; NPC: neural progenitor cell; P: pericyte; TJ: tight junction; Ang-1: angiopoietin-1; ANT: angiotensin; β-cat: beta-catenin; VEGF: vascular endothelial growth factor; VEGFR: vascular endothelial growth factor receptor; FZD: frizzled; GPR124: G protein-coupled receptor A2; Shh: sonic hedgehog; Ptc: Patched 1; PDGF-B: platelet-derived growth factor B; PDGFR-β: platelet-derived growth factor receptor beta; TGF-β: transforming growth factor-beta; TGF-βR2: transforming growth factor beta receptor type-2. Adapted from Obermeier et al., (2013).

The notch signalling pathway is also involved in BBB development as it regulates, together with VEGF signalling, the cell phenotype of the endothelial cells (Fig. 1.18). During angiogenesis, the leading endothelial cell is the tip cell, which displays long and dynamic filopodia to guide the nascent vessel. The endothelial stalk cells proliferate to elongate the branch and form the vascular lumen (Blanco and Gerhardt, 2013; Gerhardt et al., 2003). Tip and stalk cell specification is induced through the Delta-Notch lateral inhibition mechanism (Geudens and Gerhardt, 2011). This mechanism prevents the neighbouring endothelial cells of a tip cell from having the same fate. The binding of VEGF to the endothelial VEGFR induces the expression of Delta-like ligand 4 (DLL4) in the tip cell. DLL4 binds to the Notch receptor in the neighbouring endothelial cell, leading to the proteolytic cleavage of Notch. The cleaved intracellular domain of Notch (NICD) translocates to the nucleus to modulate gene expression. This signalling cascade leads to the downregulation of VEGFR and DLL4 in the neighbouring cells, thus becoming a stalk cell (Blanco and Gerhardt, 2013; Herbert and Stainier, 2011). Deficient Notch signalling leads to increased sprouting of the tip cells, leading to hyper-branching of the blood vessels. Therefore, Notch signalling acts as a negative regulator on the endothelial sprouting (Sainson et al., 2005).

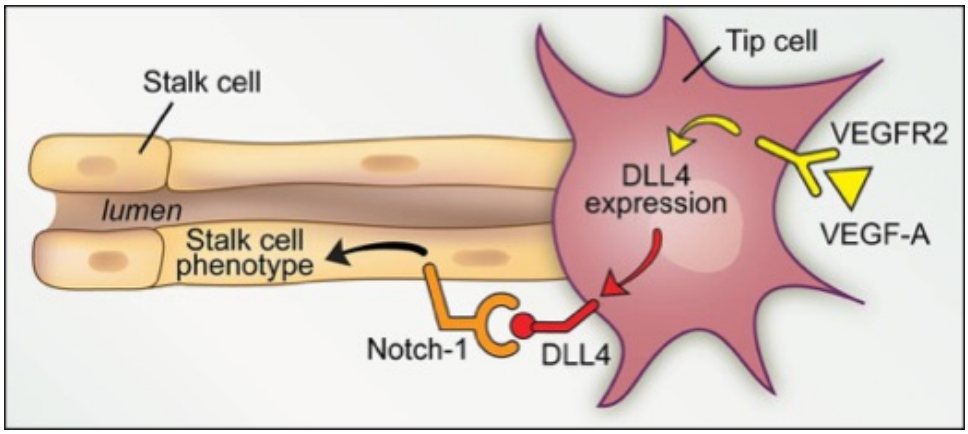

Figure 1.18 – Tip and stalk cell specification during angiogenesis. During angiogenesis, VEGF-A binds to endothelial VEGFR2. The binding of VEGF-A to its receptor induces DLL4 expression in the tip cell. DLL4 ligand activates Notch signalling in the stalk cell, suppressing the tip cell phenotype by reducing the expression of VEGFR2 in this cell. DLL4: Delta-like ligand 4; VEGF-A: Vascular endothelial growth factor A; VEGFR2: Vascular endothelial growth factor receptor 2. Adapted from Alabi et al., (2018).

During the differentiation phase (Fig. 1.17 B), endothelial cells induce anti-angiogenic signals and recruit pericytes and astrocytes to the newly formed blood vessels to promote barrier properties. Endothelial cells of the nascent vessels release platelet-derived growth factor b (Pdgf-b), thereby recruiting pericytes that express the receptor Pdgfr-β (Lindblom et al., 2003). This interaction leads to the expression of transforming growth factor-β (Tgf-β) and its receptor (Tgf-βR2) in pericytes and brain endothelial cells. The secretion of TGF, in coordination with Notch signal transduction, induces the production of N-cadherin by the endothelial cells, promoting cell adhesion between endothelial cells and pericytes. It also induces pericytes to deposit ECM components, contributing to the basement membrane formation (Winkler et al., 2014). Wnt/β-Catenin signalling is also involved in the regulation of N-cadherin. At this stage, Wnt/β-Catenin signalling is reduced, activating the Sphingosine-1-phosphate receptor (S1pr) signalling that mediates N-cadherin translocation to the endothelial cell surface (Hübner et al., 2018; Winkler et al., 2014). Tgf-β signalling also mediates the production of Angiopoietin-1 (Ang-1) (a strong anti-permeability factor) by the pericytes that bind to endothelial Tie-2 receptor and enhances tight junction formation and reduces the expression of leukocyte adhesion molecules (LAMs), thus limiting BBB permeability (Andreone et al., 2015; Daneman et al., 2010). Pericyte recruitment is critical for the development, maintenance, and function of the BBB. In mice, impaired *Pdgfr-β* expression and signalling or of its ligand *Pdgf-b* leads to a

lack of brain pericytes, resulting in erroneous tight junction distribution and increased vascular permeability, compromising BBB integrity (Armulik et al., 2010; Hellström et al., 2001). Nonetheless, this deficiency is only lethal when more than 90% of pericytes are reduced (Abramsson et al., 2003). Pericytes seem to recruit astrocytes to the BBB, promoting BBB formation and integrity (Alvarez et al., 2011; Armulik et al., 2010). Once recruited, astrocytes release SHH, which binds to the Patched-1 (Ptc1) receptor in endothelial cells. SHH signalling leads to the expression of the tight junction proteins occludin and claudin5, limiting BBB permeability and establishing barrier function (Alvarez et al., 2011; Xing et al., 2020). Src-suppressed C-kinase substrate (SSeCKS) is a factor astrocytes produce that increases during BBB maturation. SSeCKS acts as a negative regulator of angiogenesis by decreasing the expression of VEGF and stimulating the expression of tight junction proteins by enhancing the expression of astrocytic Ang-1 (Lee et al., 2003). Astrocytic end-feet, which encircle the abluminal side of cerebral vessels, are polarised structures containing the water channel aquaporin-4 (AQP4) and the ATP-sensitive potassium channel Kir4.1, which are involved in the water and ion regulation (Correale and Villa, 2009). Deficiency in SHH signalling leads to decreased expression of tight junction proteins, altering BBB permeability (Alvarez et al., 2011).

Finally, BBB formation is completed and maintained through life by the persistent expression of tight junction proteins and their distribution through the whole BBB structure (Fig. 1.17 C). This is ensured by the cross-talk between endothelial cells and pericytes, which mediate TGF-β – TGF-βR and Ang-1–Tie-2 signalling, and by astrocytes through SSeCKS expression and by Wnt signalling. Close contact between BBB's endothelial cells with pericytes, astrocytes, neurons, and microglia maintains BBB integrity and function, thus constituting the neurovascular unit (Obermeier et al., 2013).

The BBB is already formed and completely functional during late rodent gestation, but the exact timing is species-specific. Whether humans and /or other mammals are born with a full-function BBB is controversial. Although astrocytes are recruited only after birth for BBB integrity, some authors claim that the BBB is already functional during embryogenesis (Daneman et al., 2010; Hagan and Ben-Zvi, 2015; Malaeb et al., 2012; Saunders et al., 2014).

1.6.2 BLOOD-BRAIN BARRIER DEVELOPMENT IN ZEBRAFISH

In zebrafish, CNS angiogenesis begins later in embryonic development than in mammals. As described in the previous section, brain vascularisation starts with angiogenic sprouts that arise from the perineural vascular plexus of the neural tube and invade the nervous tissue (Ruhrberg and Bautch, 2013). The first perineural vessels are the Primordial Hindbrain Channels (PHBCs). These two veins run parallel to the ventral floor of the zebrafish hindbrain. Part of the hindbrain vasculature is the Posterior Communicating Segments (PCS) and the midline Basilar Artery (BA), the first and most important artery to develop in the hindbrain. Seven to eight loop-shaped Central Arteries (CtAs) penetrate the hindbrain and contribute to the irrigation of the brain (Fig. 1.19) (Gore et al., 2012; Isogai et al., 2001; Ulrich et al., 2011). The hindbrain PCS communicates with the midbrain through the basal communicating artery (BCA). Part of the midbrain vasculature is also the choroid vascular plexus (CVP) and several mesencephalic central arteries (MCtAs), which connect to the BCA to form a vascular loop (Fig. 1.19). The anterior midbrain vessels extend to the forebrain to irrigate the forebrain (Chen et al., 2012; Isogai et al., 2001).

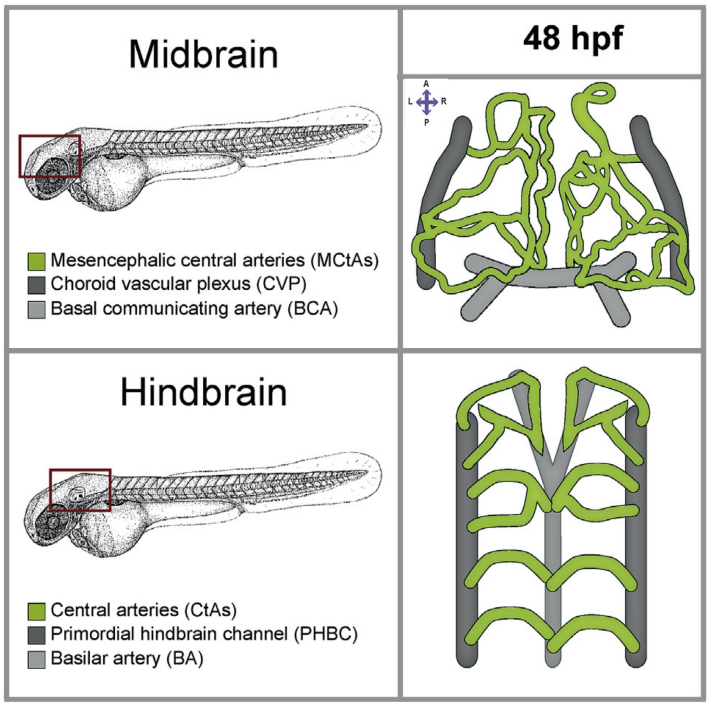

Figure 1.19 – Midbrain and hindbrain vascular structures in zebrafish embryos. Dorsal view of the midbrain and hindbrain vessels at 48 hpf. The red box indicates the midbrain and hindbrain localisation. Anterior to the top. A: anterior, P: posterior, L: left, R: right. Adapted from Quiñonez-Silvero et al., (2020).

The hindbrain vasculature structures are well-conserved among vertebrates (Fujita et al., 2011). In zebrafish, hindbrain vascular development follows a reproducible sequence, beginning with the formation of the PHBCs at 20 hpf (Fig. 1.20 A – B). These structures are formed by the ipsilateral fusion of angiogenic sprouts of the posterior extension of the Primordial Midbrain Channels (PMBCs) and the anterior extension of the Anterior Cardinal Veins (ACVs) that occurs from 24 to 28 hpf. At 28 hpf, two structures of the hindbrain vasculature develop, the PCSs and the BA (Fig. 1.20 B – D). The BA forms from lateral sprouting of the PHBC to the ventral midline of the hindbrain. Around 36 hpf, the BA and the PHBCs become separated structures, with only a few residual posterior connections between them. The PCSs arise from the caudal division of the two Primitive Internal Carotid Artery (PICA) in the midbrain, acquiring a V-shaped morphology, that, around 32hpf connect with the anterior end of the BA (Ulrich et al., 2011). Between 32 and 36 hpf, endothelial cells of the dorsal surface of the PHBC detach and sprout to the ventral half of the hindbrain, giving rise to the CtAs (Fig. 1.20 E – F). Initially, the CtAs grow dorsally until they are halfway along the dorsoventral axis of the hindbrain. Then, they turn ventrally to the midline to fuse with the PCS or BA, acquiring the characteristic arch-shaped form, or interconnect with their ipsilateral neighbours from 40 to 48 hpf. The anterior CtAs connect with the PCSs, while the posterior CtAs connect with the BA. At 72 hpf, seven to eight CtAs have normally formed along each side of the PHBC (Fujita et al., 2011; Ulrich et al., 2011). BA and CtAs are formed principally through PHBC-derived endothelial cell migration (Ulrich et al., 2011).

During development, the hindbrain is temporarily subdivided into seven to eight rhombomeres (r1 – r8) segments. Every single rhombomere develops one CtA through its centre (Moens and Prince, 2002; Ulrich et al., 2011). The order of CtA development is not random. In most 36 hpf zebrafish embryos, the first CtA to develop is in r3, r2 and then r5. The frequency of CtA invading r4 and r6 are lower; usually, r1, r7 or r8 have no CtAs. At 48 hpf, most embryos have all 7 to 8 rhombomeres vascularised, however, r7 and r8 are less frequently vascularised. At 72 hpf, all rhombomeres are vascularised with a 95-100% frequency (Ulrich et al., 2011).

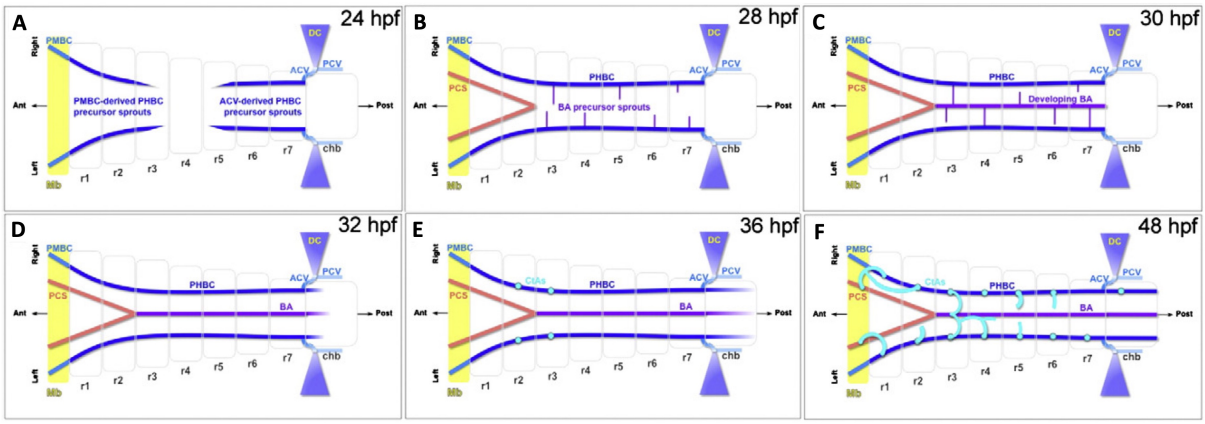

Figure 1.20 – Illustration of the zebrafish hindbrain vasculature development. A – B) Dorsal view of PHBCs formation via the ipsilateral fusion of the angiogenic sprouts of the PMBC and ACV. During this stage, the PCS arise from the PICA (not shown) to later fuse with the BA. **B – D)** Dorsal view of BA development after growth of PHBC-derived sprouts towards the ventral midline, where they coalesce. The sprouts gradually disappear, giving rise to an individual BA. **E – F)** CtA formation by angiogenic sprouting of the PHBC. The CtAs migrate dorsally to penetrate the ventral side of the rhombomeres via their centres. Later CtAs interconnect with their ipsilateral neighbours and with the PCS and BA. Drawings are not to scale. Colour-coding vasculature: BA: purple; CtAs: light blue; PHBCs: dark blue; PCS: light pink; Colour-coding non-hindbrain vessels: ACV, PCV and PMBC: other blue shades; Rhombomere boundaries: light grey lines; Mb: yellow. ACV: Anterior cardinal vein; Ant: Anterior; BA: Basilar artery; CtAs: Central arteries; Mb: Midbrain; chb: caudal hindbrain or r8; PCS: Posterior communicating segment; PCV: Posterior cerebral vein; PHBC: Primordial Hindbrain Channels; PICA: Primitive Internal Carotid Artery; PMBC: Primordial midbrain channel; Post: Posterior; r1 – r7: rhombomeres 1 – 7. Adapted from Ulrich et al., (2011).

The same angiogenic cues regulate vascularisation of the zebrafish hindbrain as in mammals (Hogan and Schulte-Merker, 2017). The VEGF signalling pathway is the main regulator of vascular development required for cerebral angiogenesis. It is involved in forming the PHBC, BA and CtAs (Bussmann et al., 2011; Covassin et al., 2006; Ulrich et al., 2011).

Canonical Wnt/β-Catenin signalling, through Wnt7a and Wnt7b, is also essential for zebrafish brain angiogenesis and BBB formation (Daneman et al., 2009). During the first angiogenic stage, activation of Wnt/β-Catenin, through the Gpr124/Reck, mediate vessel sprouting (America et al., 2022). At later stages, decreased Wnt signalling activates S1pr1 signalling to promote BBB maturation by regulating the junction molecules VE-cadherin and Esama (Hübner et al., 2018).

Chemokine signalling is also important during hindbrain vasculature development, particularly for the correct guidance of CtAs into the BA. In *cxcl12b* and *cxcr4a* mutants, CtAs fail to interconnect with the BA, thus having a defective circulatory hindbrain loop (Bussmann et al., 2011).

1.7 THE VERTEBRATE NEUROVASCULAR UNIT

The unique features of the BBB to control the traffic of compounds and metabolites between the blood and the CNS are not only due to the cerebral endothelial cells but also to a close interaction with pericytes, astrocytes, microglia, perivascular macrophages, basement membrane, and neuronal cells. This multicellular interaction is known as the neurovascular unit (NVU) (Fig. 1.21) (Obermeier et al., 2013). The NVU tightly regulates the local milieu in the brain and CNS, and each element has a fundamental role in maintaining proper BBB function.

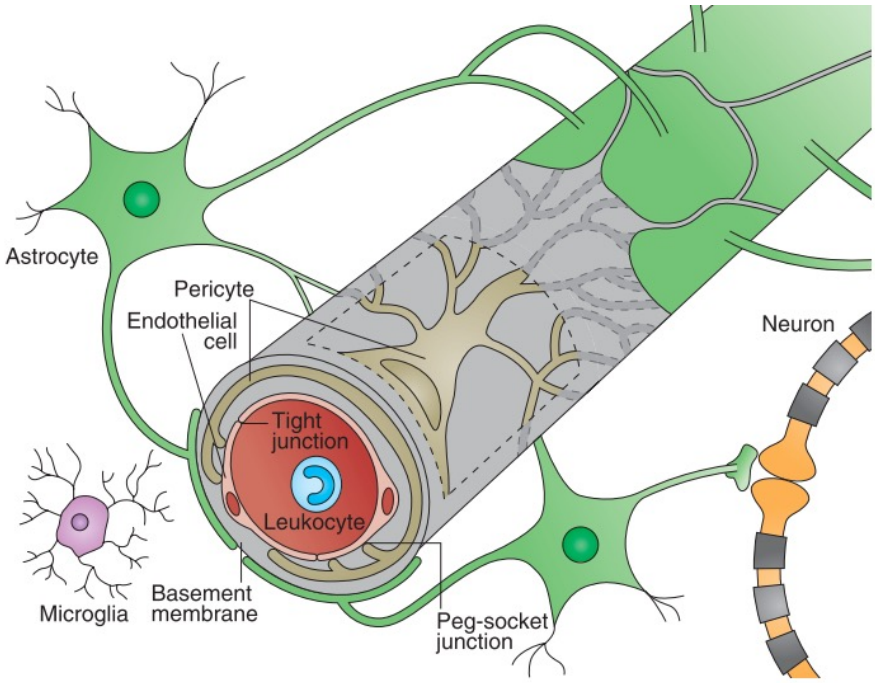

Figure 1.21 – The neurovascular unit. The NVU is constituted by the endothelial cells of the BBB that are in close association and physical contact with, astrocytic end-feet, pericytes and neurons. The abluminal surface of brain capillaries is ensheathed by a basement membrane that separates endothelial cells from pericytes and pericytes from astrocytes. Direct intercellular crosstalk between endothelial cells and pericytes is provided by peg-socket junctions. Astrocytic end-foots encircle the abluminal side of the vessels. This functional unit maintains brain homeostasis. Adapted from Obermeier et al.,(2013).

• **Vascular endothelial cells:** In mammals, the BBB is constituted by specialised endothelial cells, which have the function of separating blood components from the brain microenvironment, controlling the passage of molecules and compounds between the two interfaces to keep homeostatic balance (Obermeier et al., 2013). These vascular endothelial cells differ from their homologues in the peripheral tissues as they lack fenestration and undergo very low rates of transcytosis. Additionally, continuous intercellular tight and adherent junctions between adjacent endothelial cells limit molecules' paracellular movements across the BBB, acting as a 'physical barrier' (Abbott et al., 2006; Kooij et al., 2005; Pardridge, 2003). Besides providing a physical barrier, several membrane transporters in the BBB regulate the transcellular traffic of molecules. This provides a selective 'transport barrier', facilitating the influx of required nutrients and outflow of waste (Begley and Brightman, 2003). The BBB also functions as a 'metabolic barrier', as the presence of intracellular and extracellular enzymes metabolise unwanted molecules, including toxins (Tam and Watts, 2010). All these characteristics contribute to a selective barrier mechanism that regulates the in- and out-flux of nutrients and waste products and provides an adequate milieu for neuronal function by controlling the ionic and fluid movements between the blood and the brain (Abbott, 2004).

• **Brain pericytes:** Pericytes ensheath the abluminal surface of the cerebral vessel walls and are embedded in the basement membrane (Allt and Lawrenson, 2001). In areas lacking a basement membrane, pericytes can communicate directly with the cerebral endothelial cells through peg-socket contacts (Cuevas et al., 1984). Brain pericytes are important in improving the selective barrier permeability and provide the necessary cues for the astrocytic end-feet attachment to the cerebral endothelial cells (Armulik et al., 2010).

• **Astrocytes:** Astrocytes are star-shaped glial cells with extending processes, such as astrocytic end-feets to contact neurons and cerebral vessels. Astrocytes can interconnect with neighbouring astrocytes by gap junctions to facilitate long-range signalling (Alvarez et al., 2013; Nagy and Rash, 2003). Astrocytes are the most abundant cells in the brain, and around 90% of the abluminal surface of the rat cerebral endothelium is ensheathed by an astrocytic end-feed (Filosa et al., 2016; Mathiisen et al., 2010). Astrocytic end-feet shows several specialised features, such as the potassium channel Kir4.1, and the water-channel protein aquaporin-4 (AQP4), which are involved in ion and volume regulation (Abbott et al., 2006). During BBB development, the development of astrocytes and their subsequent ensheathment of the cerebral vessels only starts postnatally. Therefore the NVU is fully formed only after

birth (Caley and Maxwell, 1970; Daneman et al., 2010). Astrocytes maintain NVU homeostasis by providing nutrition for neurons, regulating the extracellular potassium and water balance, controlling immune reactions and for the clearance and recycling of neurotransmitters (Gee and Keller, 2005).

• **Neurons:** Neurons are also part of the NVU. Physical contact between neuronal processes and the BBB vasculature mediates the local increase of cerebral blood flow in response to neuronal activity (McConnell et al., 2017). This interaction is also essential for BBB maintenance. Neuronal activity maintains the adequate vascular network in the brain (Lacoste et al., 2014).

• **Basement membrane:** The basement membrane is formed by ECM molecules secreted by endothelial cells, pericytes and astrocytes. The principal constituents of the basement membrane are structural proteins (collagens, fibrillins, laminins, vitronectin, and fibronectin), soluble factors (growth factors and cytokines), matrix remodelling enzymes (metalloproteinases) and proteins that bind to ECM (lectins and semaphorins) (Carvey et al., 2009; Lu et al., 2011; McConnell et al., 2017). It maintains the NVU elements in the right place and mediates the intercellular crosstalk between them (Obermeier et al., 2013). In the BBB, two types of basement membranes can be found, i) the endothelial and ii) the parenchymal basement membrane, which are separated by pericytes (Hallmann et al., 2005). The endothelial and parenchymal basement membranes differ by their distribution of laminin isoforms which depends on the type of vessels (artery, arteriole, capillary, postcapillary venule, and venule) (Fig. 1.22) (Joutel et al., 2016). The endothelial basement membrane contains laminin isoforms α4 and α5 derived from endothelial cells. The parenchymal basement membrane contains laminin isoforms α2 derived from astrocytes and α1 derived from the pia mater epithelium cells (Sixt et al., 2001).

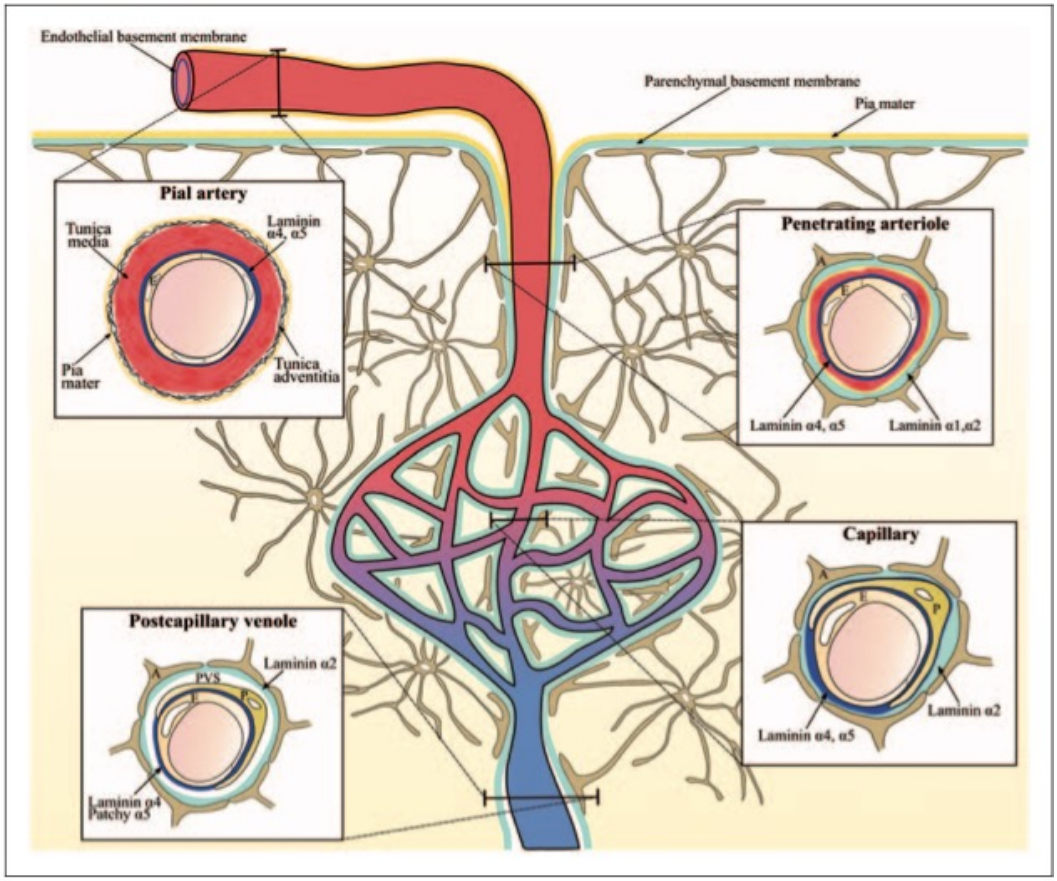

Figure 1.22 – Illustration of the different laminin expression along the cerebrovascular tree. The parenchymal (light blue) and the endothelial (dark blue) basement membranes are shown in the different vessels of the brain. Laminin α1 and α2 are expressed by the pia mater epithelium cell (yellow line) and astrocytes, respectively, which can be found in the parenchymal basement membrane of the penetrating arterioles. In these vessels laminin α4 and α5 can be found which are secreted by the endothelial cells, thus constituting the endothelial basement membrane. In the capillaries and postcapillary venules, only astrocytes contribute for the parenchymal basement membrane (laminin α2). In the capillaries, the endothelial and parenchymal basement membranes have no separation between them and appear as a single entity that covers the pericytes. A perivascular space between the two basement membranes exists in the postcapillary venule. The pial artery is only constituted by the endothelial basement membrane. A: Astrocytic end-feet; E: endothelial cells; P: pericytes. Adapted from Thomsen et al., (2017).

• **Microglia and perivascular macrophages:** Microglial cells and perivascular macrophages are immune cells also part of the NVU. Perivascular macrophages are the first line of innate immunity due to their capacity to phagocytose unwanted particles from the CNS quickly. They also contribute to the contact and crosstalk between the members of the NVU. Microglial cells are the major immune cells present in the CNS. Microglia cells migrate into the CNS during

development and interact with the sprouting vessels to facilitate angiogenesis (Correale and Villa, 2009; Daneman and Prat, 2015; Zenker et al., 2003).

1.7.1 NEUROVASCULAR UNIT IN ZEBRAFISH

The function of the BBB is evolutionarily conserved between vertebrates (Bundgaard and Abbott, 2008). Still, the cellular nature of the barrier and the NVU constituents varies across taxa (O'Brown et al., 2018). In teleosts, like zebrafish, the BBB is formed by endothelial cells, like in mammals and other amniotes, and the NVU shares several features with their mammalian counterparts (Bundgaard and Abbott, 2008).

The zebrafish endothelial barrier presents several endothelial cell markers that characterise the mammalian cerebral vasculature. This includes the tight junction proteins Zonula Occludens-1 (ZO-1) and Claudin-5 (Jeong et al., 2008) and BBB-related genes such as the nutrient transporter Glut1 and death receptors DR6 and TROY (Tam et al., 2012). That suggests that the zebrafish BBB endothelial cells function similarly to the mammalian BBB endothelium (O'Brown et al., 2018). Due to the fast development time of zebrafish, it develops a functional endothelial-based BBB, with comparable characteristics to mammals, as early as 3 dpf (Jeong et al., 2008).

Pericytes are present in the zebrafish BBB and are in close contact with the endothelial cells, as in mammals (Wang et al., 2014). In zebrafish, arterial endothelial cells recruit pericytes by expressing *pdgfb*, which induces proliferation and migration of pericytes, covering the arterial blood vessels until 5 dpf (Ando et al., 2016). Pericytes are mural cells that can develop from mesodermal-derived mesenchymal or neural crest cells. In the mammalian brain, pericytes in the forebrain derive from cranial neural crest origin, while midbrain, hindbrain, and spinal cord pericytes derive from mesodermal origin (Korn et al., 2002; Reyahi et al., 2015; Yamanishi et al., 2012). In zebrafish, brain pericytes also arise from neural crest or mesodermal developmental precursors. Still, most hindbrain vascular structures are covered by mesodermal-originating pericytes, whereas pericytes recruited into the CtAs derive from the neural crest (Ando et al., 2016). Therefore, zebrafish pericytes share several characteristics with mammalian pericytes, but the precise role in zebrafish BBB is still largely unknown (O'Brown et al., 2018).

In zebrafish, astrocyte-like cells, similar to the mammalian astrocytes, have been found recently (Chen et al., 2020). These zebrafish astrocytes express the same marker genes as humans and mice, like the glutamate transporters *slc1a2b* (*EAAT2a*/*GLT-1*), *slc1a3b* (*EAAT1b*/*Glast*), the GABA transporter *slc6a11b* (*GAT-3*) (Chen et al., 2020), the *glial fibrillary acidic protein* (*gfap*) (Johnson et al., 2016), the water channel *aqp4* (Gleiser et al., 2016) and several tight junction markers (Grupp et al., 2010). However, the cellular distribution of these markers may not be the same as in mammals. In mammals, *Aqp4* is present in the highly polarised astrocytic end feet. In zebrafish, there is a lack of polarization since the expression of *aqp4* can be found through the entire radial glia processes. Besides that, this *aqp4*$^{+}$ radial glia processes rarely contact the cerebral vasculature, suggesting that these radial glia cells regulate water flow in zebrafish brains differently than in mammals and thus may have a different role in the BBB (Gleiser et al., 2016; Grupp et al., 2010).

Microglia are also present in the zebrafish BBB and are involved in CNS vascularisation by interacting with the tip cells during angiogenesis, as seen in mammals (Fantin et al., 2010).

The zebrafish has several advantages regarding mammalian species. The external development from the mother, the optical transparency and the availability of endothelial-specific fluorescent reporters provide a powerful model to analyse *in vivo* the development of cerebral vasculature. The fact that the zebrafish has an endothelial barrier with an evolutionarily conserved function makes it a powerful system for studying the molecular and cellular mechanism of the barrier (O'Brown et al., 2018; Ulrich et al., 2011).

1.7.2 THYROID HORMONES DURING NEUROVASCULATURE DEVELOPMENT

The NVU is constituted by the vascular and nervous cells of the brain. The close interaction between the members of the NVU is fundamental for maintaining the brain's normal function (Obermeier et al., 2013). During development, many signalling factors are shared between the vascular and nervous systems, and they can even influence the development of each other (Paredes et al., 2018; Tam and Watts, 2010). For example, neural progenitor cells are the ones responsible for VEGF secretion and direct angiogenesis for ingression into the brain (Liebner et al., 2008; Raab et al., 2004), while the vascular system provides a microenvironment for the

survival, proliferation and differentiation of neural progenitor cells (Tata and Ruhrberg, 2018). This crosstalk between members of the NVU is fundamental, and malfunctioning of this crosstalk or lack of one NVU member leads to an imbalance of the functional NVU, consequently leading to several vascular and neuronal disorders (Segura et al., 2009; Tam and Watts, 2010). Indeed, several studies have shown that the BBB is disrupted in many CNS diseases, including neurodegenerative diseases, Alzheimer's disease, Parkinson's disease, amyotrophic lateral sclerosis, and others (Zlokovic, 2008).

Studies conducted in animal models have shown that diseases related to THs deficiency also show impaired development of the BBB. In zebrafish, knockdown of the specific TH transporter Mct8 leads to the development of only 3 of the 7 ingressing hindbrain CtAs (Campinho et al., 2014), and studies conducted in hypothyroid rats showed decreased brain angiogenesis, with reduced complexity and density of microvessels (Zhang et al., 2010). However, most developmental studies on THs deficiency have focused on the effects on neural cells, myelination, and TH-regulated genes, while the role of THs on angiogenesis in the CNS remains poorly understood (Bernal, 2005; Zhang et al., 2010). Whether THs regulate endothelial cells' ability to migrate or regulate specific neuronal progenitor cells mediating via angiogenic factors, endothelial migration and ingression, or both, remains to be elucidated.

1.8 OBJECTIVES

This PhD thesis tests the hypothesis that maternal thyroid hormone (MTH) acts as an integrator during zebrafish development that enables the coordinated development of the brain and its vascular support system to give rise to the blood-hindbrain barrier (BHB). A morpholino-based approach was implemented whereby the specific TH transporter Mct8 was knocked down. Here the role, cells and genetic networks regulated by MTHs in zebrafish BHB development were functionally tested.

To test this hypothesis, three main objectives were defined:

1. Identification of TH-dependent hindbrain/angiogenic genes putatively involved in BHB development.

2. Identification of TH-dependent hindbrain cells involved in BHB development.

3. Functional evaluation of MTH-dependent genetic factors involved in BHB development.

CHAPTER 2

Angiogenic genes and pathways under the regulation of maternal thyroid hormones during zebrafish blood-hindbrain barrier development

ABSTRACT

The physiological and developmental effects of thyroid hormones (THs) are mostly due to the interaction of T3 with the nuclear receptors that regulate gene expression. During development, T3 is essential for embryonic brain development. During this period, maternal T3 (MT3) supply is the only source to the embryo and deficient levels lead to several neurological impairments in the offspring. The monocarboxylate transporter 8 (Mct8) is the main T3 transporter present in the brain and blood-brain barrier during embryonic stages in zebrafish and the determinant of MT3 developmental function. In humans, mutations of this TH-specific membrane transporter cause the Allan-Herndon-Dudley syndrome (AHDS), a rare X-linked neurodevelopmental disorder, which is characterised by severe mental retardation, lack of speech and movement disorders. In zebrafish, knockdown of the Mct8 transporter also leads to an impaired blood-hindbrain barrier (BHB) development, which has not yet been confirmed in humans. To understand the role of MT3 on neurovascular development we used an established zebrafish Mct8 knockdown model to understand the genes and gene networks that were regulated by T3 during specific stages of BHB development. The transcriptome of 25 hours post-fertilization (hpf) zebrafish embryos was characterised, and differentially expressed genes were mapped into Reactome pathway analysis. The analysis revealed that genes involved in angiogenesis, including *vegf* pathway components, were regulated by MT3. Further gene expression analysis by qRT-PCR during BHB angiogenesis was analysed followed by *in situ* expression analysis and immunohistochemistry. We show that maternal THs regulate BHB angiogenesis mostly through *vegfaa* expression in a cell context-dependent manner.

2.1 INTRODUCTION

The importance of an appropriate supply of maternal thyroid hormones (MTHs) for neurodevelopment in humans is highlighted by the X-linked Allan-Herndon-Dudley syndrome (AHDS), which is caused by mutations in the thyroid hormone (TH)-specific membrane transporter *monocarboxylate transporter 8* (*MCT8*; *SLC16A2*) gene. Several mutations have been identified that affect, with different degrees, the capacity of TH cellular uptake, giving rise to different phenotypic outcomes in patients (Friesema et al., 2004; Schwartz and Stevenson, 2007). Nonetheless, AHDS is characterised by developmental delay, low IQ, poor language and walking skills and hypotonia (Remerand et al., 2019).

Several studies have shown that the blood-brain barrier (BBB) is disrupted in many central nervous system (CNS) diseases, including neurodegenerative diseases, Alzheimer's and Parkinson's disease, amongst others (Zlokovic, 2008). In the case of AHDS, there are no reports on human brain vasculature impairment in these patients, but studies conducted in Mct8 deficient zebrafish have impaired development of the BBB (Campinho et al., 2014; De Vrieze et al., 2014). Given that the zebrafish Mct8-knockdown model of AHDS recapitulates the neurodevelopmental effects observed in human AHDS patients (Campinho et al., 2014; De Vrieze et al., 2014; Silva and Campinho, 2023), it is hypothesised that incorrect BBB development might also occur in those patients.

The formation of a complex vascular system involves two distinct morphogenetic processes: vasculogenesis and angiogenesis. Vasculogenesis is defined as the *de novo* formation of vessels, while angiogenesis involves sprouting of existing blood vessels that expand, fuse and remodel into a functional vascular network (Adams and Alitalo, 2007; Ellertsdóttir et al., 2010; Kolte et al., 2016). Vascularisation of the brain is particularly important, and establishing a functional BBB is essential for normal brain homeostasis. In the zebrafish, the major vessels vascularising the hindbrain during development, and that form the blood-hindbrain barrier (BHB), are the primordial hindbrain channels (PHBC), the basilar artery (BA) and the central arteries (CtAs) (Isogai et al., 2001; Ulrich et al., 2011). These hindbrain vasculature structures form in a reproducible sequence, as indicated in Table 2.1.

Table 2.1 – Zebrafish hindbrain vasculature development during embryogenesis. Adapted from Quiñonez-Silvero et al., (2020) and Ulrich et al., (2011).

Time (hpf)	Event
24 - 28	Formation of the PHBC that runs along each side of the hindbrain anterior-posterior axis.
28	PHBC begins to sprout to the ventral midline to give raise to the BA.
32	PHBC dorsal sprouts initiate CtAs development and ingression into the ventral hindbrain.
36	BA and PHBC are individual structures.
40 - 48	Some CtAs interconnect with their ipsilateral neighbours, while others migrated to the midline and fuse with the BA to acquire a characteristic "M" shape form.
48	Seven to eight CtAs have formed along each side of the hindbrain and all CtAs have a functional lumen.
72	~ 95 – 100% of the rhombomeres are vascularised.

Vascular endothelial growth factor-A (Vegf-A) is a major angiogenic regulator and is secreted from neural progenitor cells and serves as a cue for endothelial cells which express tyrosine kinases receptors (Vegfr1/Flt1 and Vegfr2/Kdrl) (Bussmann et al., 2008; Liang et al., 1998; Raab et al., 2004). In zebrafish two Vegfa paralogs exist, *vegfaa* and *vegfab*, and both are required for sprouting CtAs from the PHBC through Vegfr2/Kdrl (Bahary et al., 2007; Bussmann et al., 2011). Genetic models have shown that CtA development strictly depends on *vegfaa* but that *vegfab* might also have accessory functions (Rossi et al., 2016). In zebrafish, *vegfaa* encodes two main isoforms Vegfaa-121 and -165 (Bahary et al., 2007). Vegfaa-121 is a diffusible isoform with low extracellular matrix (ECM) affinity that binds to Vegfr1/Flt1 and Vegfr2/Kdrl. In contrast, the Vegfaa-165 isoform has a high ECM affinity and binds to a co-receptor complex of Vegfr2/Kdrl and Neuropilin-1 (Nrp1) (Ferrara et al., 2003; Parker et al., 2012). Both *vegfaa* isoforms are expressed during zebrafish embryogenesis (Liang et al., 2001), and studies conducted in mice revealed that both VEGFA isoforms are required for proper brain vascular morphogenesis (Haigh et al., 2003; Ruhrberg et al., 2002). Nonetheless, of zebrafish Vegfa isoforms, Vegfaa-165 is the most potent stimulator of angiogenesis (Ferrara et al., 2003). The binding of Vegfaa-165 with the co-receptor complex Vegfr2/Kdrl and Nrp1 potentiates Vegfa signalling (Soker et al., 2002). Although Vegfa does not require Nrp1 to promote

angiogenesis during brain development, Nrp1 is essential for brain vascularisation since it promotes endothelial tip cell filopodia extension and actin cytoskeletal reorganisation via integrin-associated signalling pathways (Fantin et al., 2015; Gelfand et al., 2014). Vegfa isoforms can also bind to the Vegfr1/Flt1. However, this interaction negatively regulates angiogenesis, as it serves as a decoy receptor for Vegf (Chappell et al., 2009). In zebrafish, a soluble form of Flt1 (sFlt1) coordinates vascularisation of the spinal cord (Wild et al., 2017) and prevents hypersprouting of the venous intersegmental vessels (ISV) (Matsuoka et al., 2016). Vegfc is also important for embryonic blood vessel development. In zebrafish, Vegfc signalling through Vegfr3/Flt4 promotes the formation of the PHBC by vascularisation (Covassin et al., 2006).

During angiogenesis, endothelial cells coordinate the formation of a vascular system. The leading endothelial or tip cell has long and dynamic filopodia that navigate the nascent sprout, and the endothelial stalk cells, proliferate to elongate the branch and form the vascular lumen (Gerhardt et al., 2003; Gore et al., 2012; Phng and Gerhardt, 2009). Tip and stalk cell selection are regulated by VEGF and Notch signalling cross-talk (Blanco and Gerhardt, 2013). VEGF/VEGFR-2 signalling is important for tip cell specification and filopodia formation (Phng and Gerhardt, 2009). This interaction induces the upregulation of the Notch receptor Delta-like-4 (DLL4) in the tip cell, which upregulates Notch activity in the neighbouring stalk cells. Several Notch receptors are expressed in the endothelial cells. Nonetheless, Notch1 is critical for suppressing tip cell behaviour in stalk cells after downregulating VEGFR-2 and VEGFR-3 (Betsholtz, 2018; Phng and Gerhardt, 2009; Siekmann and Lawson, 2007; Tammela et al., 2008). The interplay between Vegfa and Notch1b signalling in zebrafish is important for brain arterial vasculature formation. Loss of Vegf signalling or activation of Notch signalling leads to a loss of BA and CtA sprouting (Bussmann et al., 2011; Leslie et al., 2007; Rossi et al., 2016).

Leading the sprouting blood vessels to the right place is mediated by chemo-attractive and chemo-repulsive signalling pathways, such as the interaction between the Robo receptor and Slit ligands (Fujiwara et al., 2006; Park et al., 2003). Of the Robo family, Roundabout 4 (Robo4) is a vascular endothelial-specific receptor, and it binds to slit ligands, Slit2 and Slit3, which generate repulsive or attractive cues, respectively, during endothelial cell migration (Park et al., 2003; Zhang et al., 2009). In zebrafish, *robo4* is essential for ISV's coordinated symmetric and directed sprouting, and defects in its expression misdirect sprouting of the ISV and abort vessel formation (Bedell et al., 2005).

The development of a complete hindbrain capillary network in the zebrafish is orchestrated by ligand-receptor interaction between chemokine, Cxcl12b and Cxcr4a. During development, expression of *cxcr4a* was found in the tip cells of the sprouting CtAs, while *cxcl12b* expression, and possible secretion, were found immediately above the BA. This chemokine-receptor interaction regulates the guidance of the sprouting CtAs to the BA, but not their ingression into the hindbrain. Mutations in *cxcr4a* or *cxcl12b* lead to the normal development of CtAs but fail in the migration towards the BA, leading to an increase in CtA interconnections (Bussmann et al., 2011).

Vessel maturation and stabilisation involve the recruitment of mural cells and deposition of ECM (Jain, 2003). Mural cells include pericytes, which contact directly with the endothelial cells in capillaries and immature vessels, and vascular smooth muscle cells, which ensheath the vascular lumen of arteries and veins and are separated from endothelial cells by a matrix (Gaengel et al., 2009). Notch3 signalling controls the maturation and differentiation of arterial vascular smooth muscle cells (Gridley, 2010) and also regulates brain pericyte proliferation by promoting *platelet-derived growth factor receptor-b* (*Pdgfrb*) expression (Jin et al., 2008; Wang et al., 2014). In zebrafish, *notch3* is a marker for brain pericytes and mutations in the *notch3* gene cause a deficit in brain pericytes and impaired BBB function, which results in intracranial haemorrhages (Wang et al., 2014). Sphingosine-1-phosphate receptor 1 (S1PR1) signalling also controls the interaction between endothelial and mural cells (Liu et al., 2000). In zebrafish, signalling through S1pr1 has been shown to inhibit the angiogenic sprouting mechanism and to be essential for normal trunk vascular development (Mendelson et al., 2013).

In zebrafish, Mct8 transports exclusively T3 at physiological zebrafish temperature (26 ºC) (Arjona et al., 2011) and knockdown of this T3-specific transporter by a morpholino (MO)-based system causes severe disruption of brain development similar to AHDS (Campinho et al., 2014; De Vrieze et al., 2014; Vatine et al., 2013). Also, it leads to impaired development of the BHB, since only 3 of the 7 penetrating hindbrain CtAs develop (Campinho et al., 2014). The present study used the same approach to impede maternal T3 (MT3) uptake by target cells in developing zebrafish embryos. Transcriptome differences between 25 hours post-fertilisation (hpf) control morpholino (CTRMO) and *mct8* morpholino (MCT8MO) zebrafish embryos were used to gain insight into the role of MT3 on BHB angiogenesis and development. Genes and genetic networks under the regulation of MT3 were identified, and the expression pattern of differentially expressed hindbrain/angiogenic genes was analysed during zebrafish BHB development (from 28 – 48 hpf). The outcome of this study indicated that Mct8 knockdown

and, consequently the absence of MT3 uptake only affected the angiogenic events mediating CtA development and that MT3 action on BHB angiogenesis was hindbrain specific.

2.2 RESULTS

2.2.1 Zebrafish *mct8* morphant hindbrain vasculature characterisation

In a previous study Campinho et al., (2014) showed that the MCT8MO zebrafish embryo at 48 hpf had impaired BHB development since only 3 of the 7 CtAs formed. To understand if these are the only hindbrain vascular structures affected by MT3 deprivation, a *Tg(fli1:EGFP)* zebrafish line (Lawson and Weinstein, 2002), which expresses EGFP under the regulatory region of the *fli1* promotor, and labels endothelial cells during zebrafish vascular development, was used. At 48 hpf, MCT8MO zebrafish embryos developed the PHBC and the BA but had a reduced number of CtAs compared to the CTRMO zebrafish embryos (Fig. 2.1). No apparent malformations in the fore- and midbrain vasculature were detected in MCT8MO zebrafish embryos. The mid-cerebral vein (MCeV) also developed normally (Fig. 2.1). This shows that the only vasculature structures affected by MT3 deprivation were the CtAs during zebrafish brain vascular development.

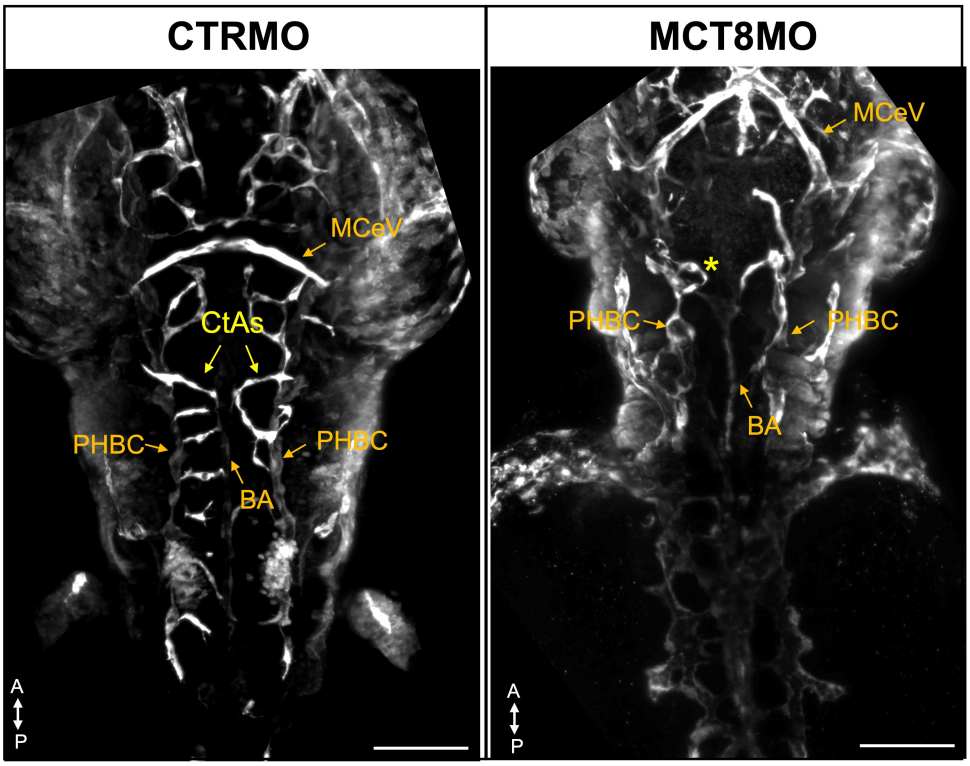

Figure 2.1 – Central arteries development is disrupted in MCT8MO zebrafish embryos. Dorsal view of maximum projection images of *Tg(fli1:EGPF)* zebrafish embryos after immunohistochemistry (IHC) against GFP (endothelial marker) at 48 hpf. A – Anterior; BA – Basilar Artery; CtAs – Central Arteries; MCeV – Mid-cerebral Vein; P – Posterior; PHBC – Primordial Hindbrain Channels. Asterisks denote reduced CtA sprouting. A minimum of 10 zebrafish embryos were analysed per experimental condition. Scale bar: 100 µm.

2.2.2 MT3 regulates several developmental pathways during zebrafish embryogenesis

The whole-embryo transcriptome of 25 hpf MCT8MO and CTRMO was obtained after mRNA sequencing (RNA-seq). More than 21 million pair-end sequences were generated for each sample (n=7/experimental group), and 2.2% of the sequences were removed after quality control editing. Comparisons of 85,652 paired assembled transcripts between the MCT8MO and CTRMO samples generated 53,350 primary transcripts sharing transcription start sites, of which 4,343 had a differential PFKM (FDR < 0.05, p< 0.01) (Fig. 2.2 A). Although the majority of differentially expressed genes between CTRMO and MCT8MO embryos were less than 2-fold different, they have a high statistical significance (Fig. 2.2 A; $p < 0.01$; FDR < 0.05).

Differentially expressed genes were submitted to pathway analysis using the Reactome V58 (www.reactome.org) human-curated database (Croft et al., 2014). It revealed that MT3 was involved in regulating 1681 pathways that are distributed over all Reactome mother category pathways. The percentage of MT3-regulated genes varied from 35% in the Reactome mother category pathway of Extracellular matrix organisation to 3.2% in the Reactome mother category pathway of Reproduction (Fig. 2.2 B). The Reactome analysis also revealed that 15 pathways were highly regulated by MT3, with more than 55% of their members affected by MT3 deprivation (Fig. 2.2 C). Moreover, of these pathways, MT3 influenced expression of all genes involved in regulating commissural axon pathfinding by Slit and Robo, loss of function of SMAD4 in cancer, amplification of the signal from kinetochores, and formation of editosomes by ADAR proteins (Fig. 2.2 C, Table 2.2).

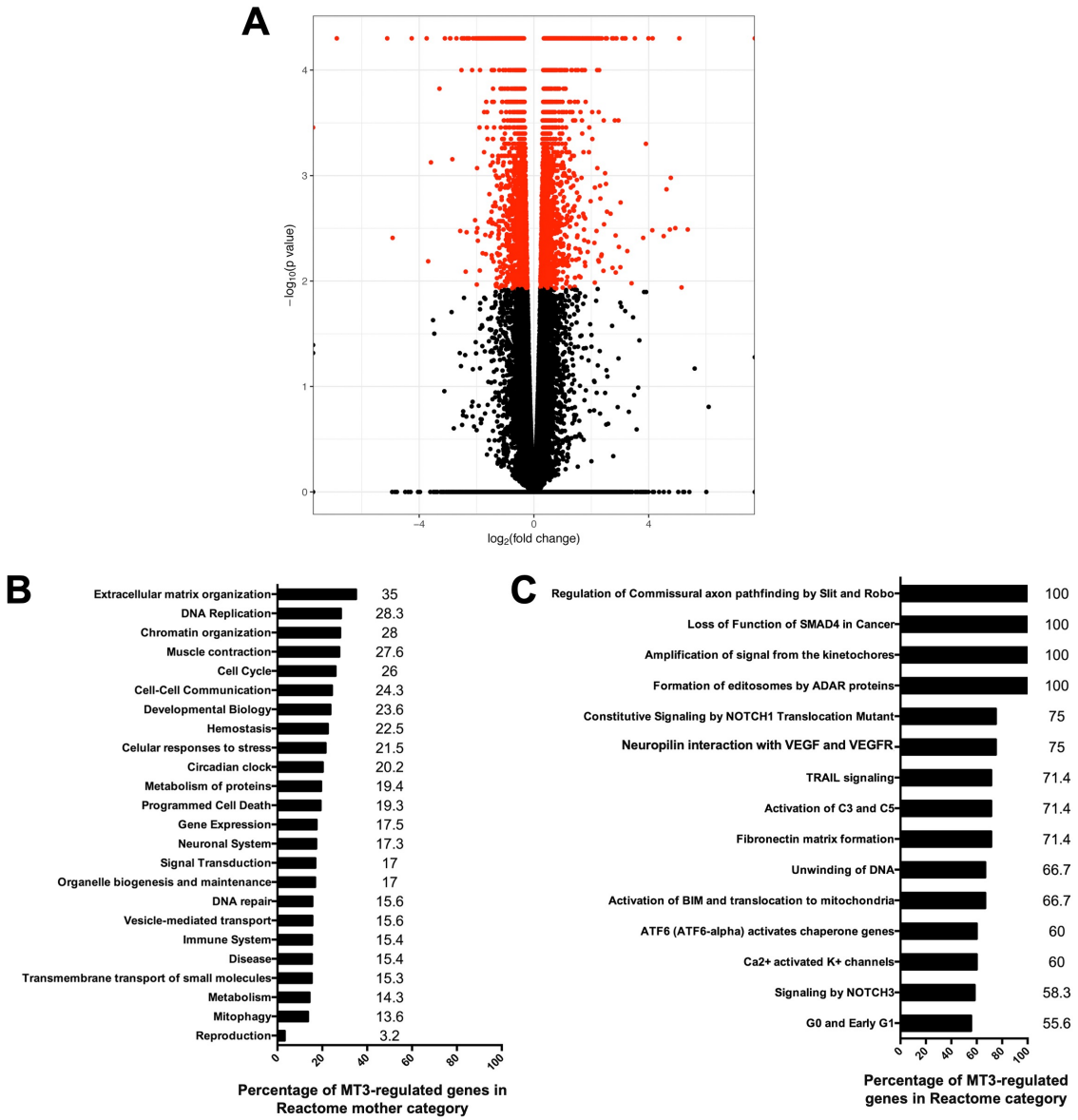

Figure 2.2 – Zebrafish genes and pathways under the regulation of MT3 at 25hpf. **A)** Volcano plot showing the differentially expressed genes (red points; $p<0.01$; FDR<0.05) between CTRMO and MCT8MO zebrafish embryos at 25hpf. **B)** Graphical representation of the ratio of MT3-regulated genes in the Reactome mother pathways of 25hpf zebrafish embryos. The numbers near the bars indicate the exact numeric value. **C)** Graphical representation of the Reactome pathways with the most populated genes regulated by MT3. The exact numerical value is indicated near the bar.

Pathways related to angiogenesis, such as VEGF, Notch and Wingless (WNT) belong to the Signal Transduction mother category. The sub-pathway Neuropilin interaction with VEGF and VEGFR has 75% of the genes regulated by MT3 (Fig. 2.2 C, Fig. 2.3 and Table 2.2 - R-HSA-194306). NOTCH pathways also showed a high number of MT3-dependent genes, such as

NOTCH3 signalling (58.3%; Fig 2.2 C, Fig.2.4 B, Table 2.2 – R-HSA-1980148), NOTCH1 signalling (32%; Fig. 2.4 A, Table 2.2 – R-HSA-1980143) and pre-NOTCH receptor expression and processing (26%; Table 2.2 – R-HSA-1912422). WNT signalling pathways involved in angiogenesis showed fewer MT3-dependent genes, this included the sub-pathways of WNT ligand biogenesis and trafficking with 36% of genes regulated by MT3 (Fig. 2.5, Table 2.2 – R-HSA-3238698), TCF dependent signalling in response to WNT with 19% of MT3 dependent genes (Table 2.2 – R-HSA-201681) and the sub-pathway Beta-catenin independent WNT signalling also with 19% of genes regulated by MT3 (Table 2.2 – R-HSA-3858494). WNT ligand biogenesis and trafficking was the most affected sub-pathway and had all genes and gene complexes regulated by MT3.

Table 2.2 – REACTOME pathways involved in angiogenesis. The percentage of MT3-regulated genes is shown for the selected pathway.

Pathway identifier	Pathway name	#Entities found	#Entities total	% of MTHs-regulated genes in Reactome categories
R-HSA-428542	Regulation of Commissural axon pathfinding by Slit and Robo	4	4	100
R-HSA-194306	Neuropilin interactions with VEGF and VEGFR	3	4	75
R-HSA-1980148	Signalling by NOTCH3	7	12	58
R-HSA-3238698	Regulation of WNT ligand biogenesis and trafficking	10	28	36
R-HSA-1980143	Signalling by NOTCH1	26	82	32
R-HSA-1912422	Pre-NOTCH Expression and Processing	20	76	26
R-HSA-201681	TCF dependent signalling in response to WNT	41	215	19
R-HSA-3858494	Beta-catenin independent WNT signalling	31	163	19

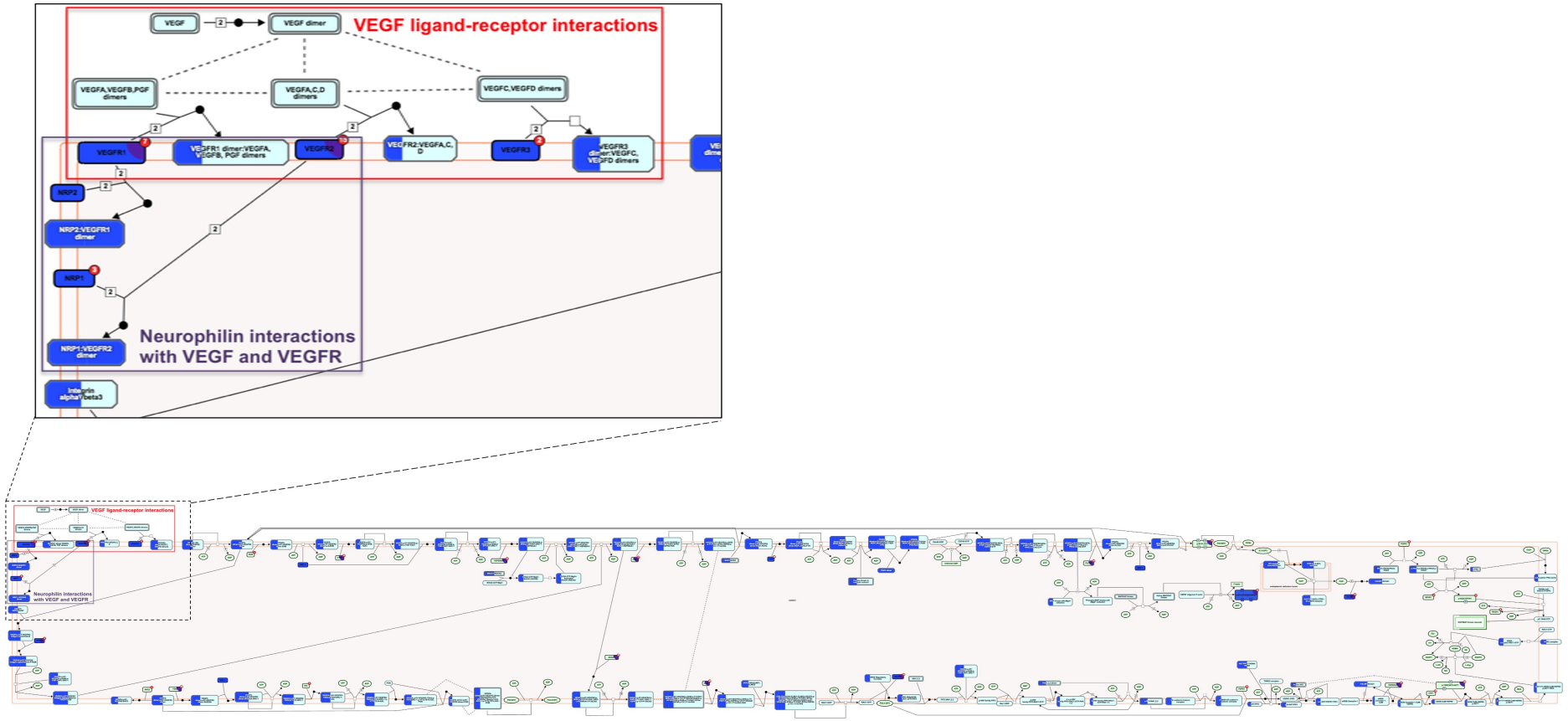

Figure 2.3 – Reactome human pathway for VEGFA-VEGFR2 pathway. The VEGFA-VEGFR2 pathway belongs to the Reactome mother category Signal Transduction, which is divided into two subcategories: VEGF ligand-receptor interaction (red box) and Neuropilin interaction with VEGF and VEGFR (violet box) which is highlighted in the black box. These two subcategories represent the binding of VEGF ligands (VEGFA, B, C, D, PGF) to VEGF receptors (VEGFR1, 2, 3) and co-receptors Neuropilin (NRP1, NRP2). Proteins or protein complexes highlighted in blue contain differentially expressed genes in the maternal thyroid hormone dataset. The VEGFR1, 2 and 3 and the co-receptors NRP1 and 2 have a highly modified expression level in MCT8MO. Neuropilin interaction with VEGF and VEGFR has 75% of genes regulated by MT3, the most affected part of the VEGFA-VEGFR2 pathway. For a detailed diagram key, please refer to Reactome (http://www.reactome.org/PathwayBrowser/#/R-HSA-194138).

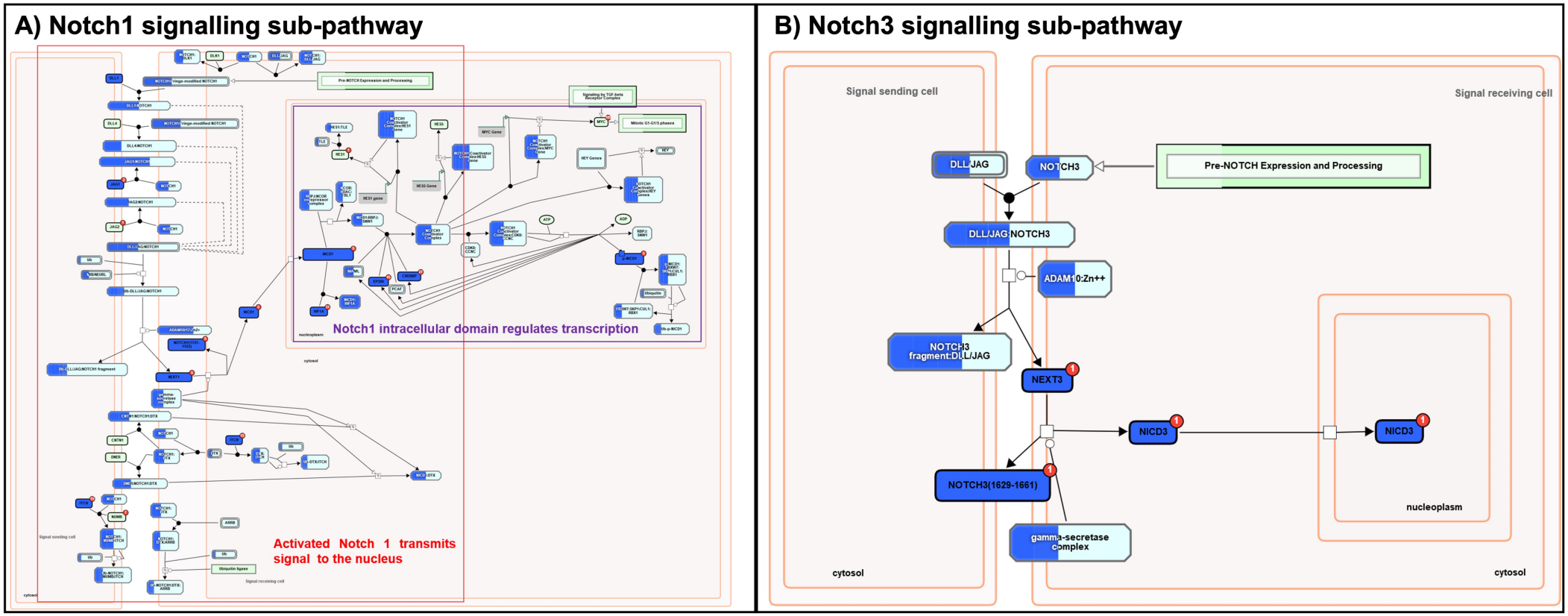

Figure 2.4 – Reactome human pathways for Notch signalling. A) Activated Notch1 signalling. The activated Notch1 transmits the signal to the nucleus, 42% of the entities involved were modified by the lack of maternal thyroid hormone. Inside the nucleoplasm, Notch1 intracellular domain regulates the transcription of a series of target genes, here, the outcome of *mct8* "knockdown" is reflected in a change in expression of 30% of the entities involved. **B)** Notch3 signalling. This image depicts the activation of NOTCH3, followed by cleavage and release of the intracellular domain NICD3 that traffics to the nucleus, where it acts as a transcriptional regulator. Many of the entities involved have corresponding genes that were differentially expressed in MCT8MO zebrafish embryos. Proteins or protein complexes highlighted in blue correspond to differentially expressed genes in the maternal thyroid hormone dataset. For detailed diagram key, please refer to Reactome A) (http://www.reactome.org/PathwayBrowser/#/R-HSA-1980143) and B) (http://www.reactome.org/PathwayBrowser/#/R-HSA-1980148).

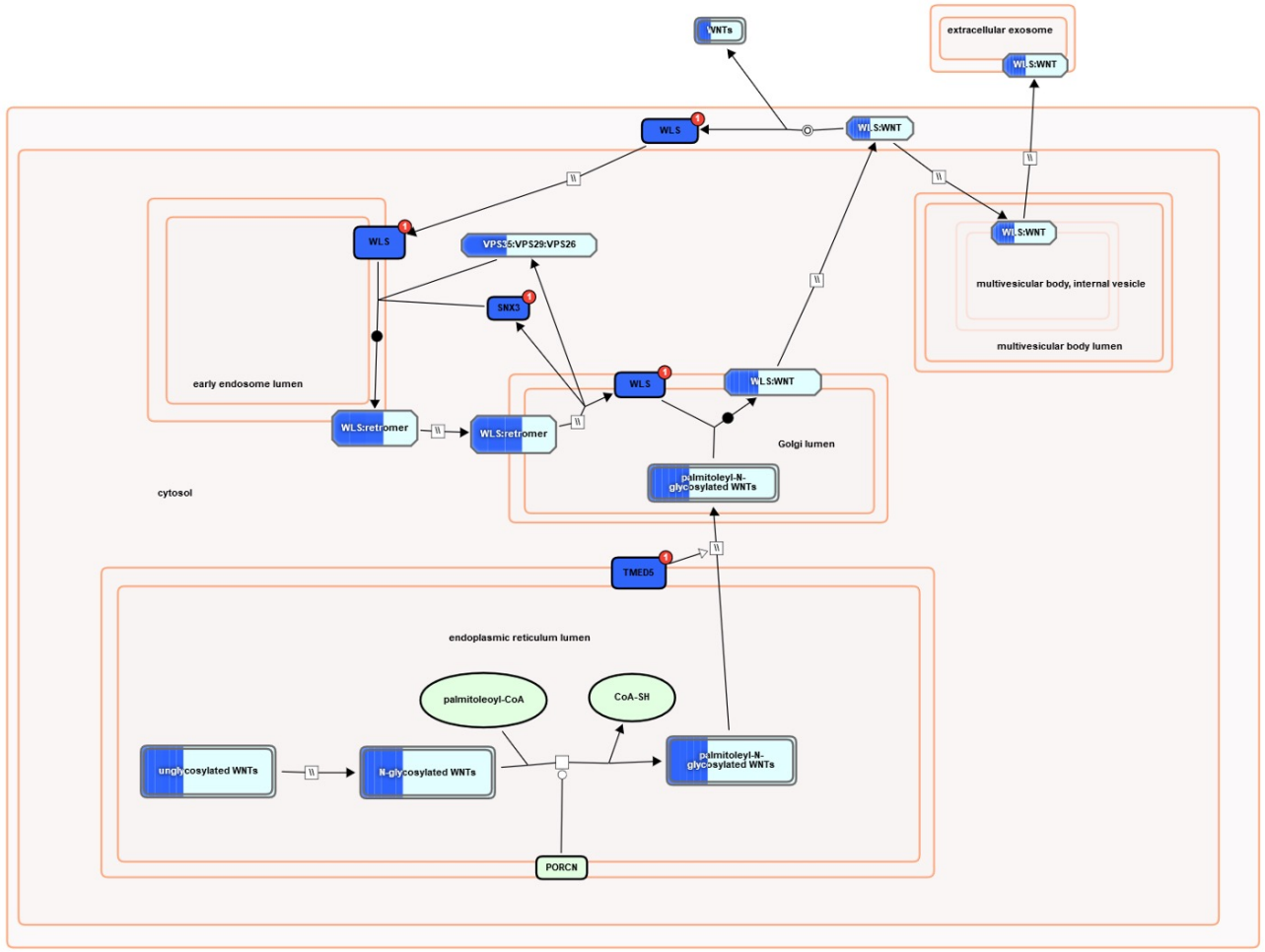

Figure 2.5 – Reactome human pathway for WNT ligand biogenesis and trafficking. Besides affecting the expression of several WNT ligands, MCT8MO zebrafish embryos showed differences in proteins involved in different aspects of WNT trafficking and release from expressing cells. Proteins or protein complexes highlighted in blue correspond to differentially expressed genes in the maternal thyroid hormone dataset. For a detailed diagram key please refer to Reactome (http://www.reactome.org/PathwayBrowser/#/R-HSA-3238698).

2.2.3 MT3 is involved in angiogenic development during zebrafish embryogenesis

The initial stage of angiogenesis involves releasing angiogenic factors such as Vegf and Wnt ligands from neural progenitor cells (Obermeier et al., 2013). To analyse the involvement of MT3 in zebrafish angiogenic development, we selected differentially expressed genes ($p<0.01$; FDR 5%) involved in Vegf and Wnt pathways; *flt4* (log2fold 0.431, $p<0.01$, FDR<0.05) and *rspo1* (log2fold 1.06, $p<0.01$, FDR<0.05). Both genes were upregulated at 25 hpf in the MCT8MO RNA-seq data. Vegf receptor *flt4* is highly expressed in endothelial tip cells in zebrafish (Siekmann and Lawson, 2007). In zebrafish, the expression of the *flt4* ligand, *vegfc*, is promoted by the canonical Wnt/β-catenin pathway through *rspo1* (Gore et al., 2011). Given the relation of these genes in both pathways, whole-mount *in situ* hybridization (WISH) was performed and the expression of these genes at 25 and 48 hpf during zebrafish embryogenesis was analysed.

WISH analysis of *flt4* revealed that the transcriptional response in *mct8* morphants was not generalized to the whole embryo but rather localised in the hindbrain region of the zebrafish embryo (Fig. 2.6). At 25 hpf *flt4* expression in the hindbrain region in the MCT8MO was lost compared to CTRMO zebrafish embryos (Fig. 2.6 A). The PHBC (green arrowhead in Fig. 2.6) was incompletely developed, and the mid- and forebrain structures were significantly disrupted (Fig. 2.6 A). In the trunk of 25 hpf MCT8MO embryos, the ISV (black arrowheads in Fig. 2.6) appeared to be normal, but *flt4* expression slightly increased in the dorsal artery (DA) and the cardinal vein (CV) compared to CTRMO zebrafish embryos (Fig. 2.6 A). At 48 hpf, expression of *flt4* in MCT8MO embryos, increased in the head vasculature and the PHBC was fully developed (Fig. 2.6 B). The slight increase in expression of *flt4* in the DA and CV was still evident at 48 hpf in MCT8MO zebrafish embryos (Fig. 2.6 B). The effects of Mct8 knockdown on *flt4* at 25 hpf were fully rescued in embryos co-injected with MCT8MO + 100 pg of *mct8* mRNA mutated in the seeding region of the morpholino (silent mutations were introduced) (Fig. 2.6 A).

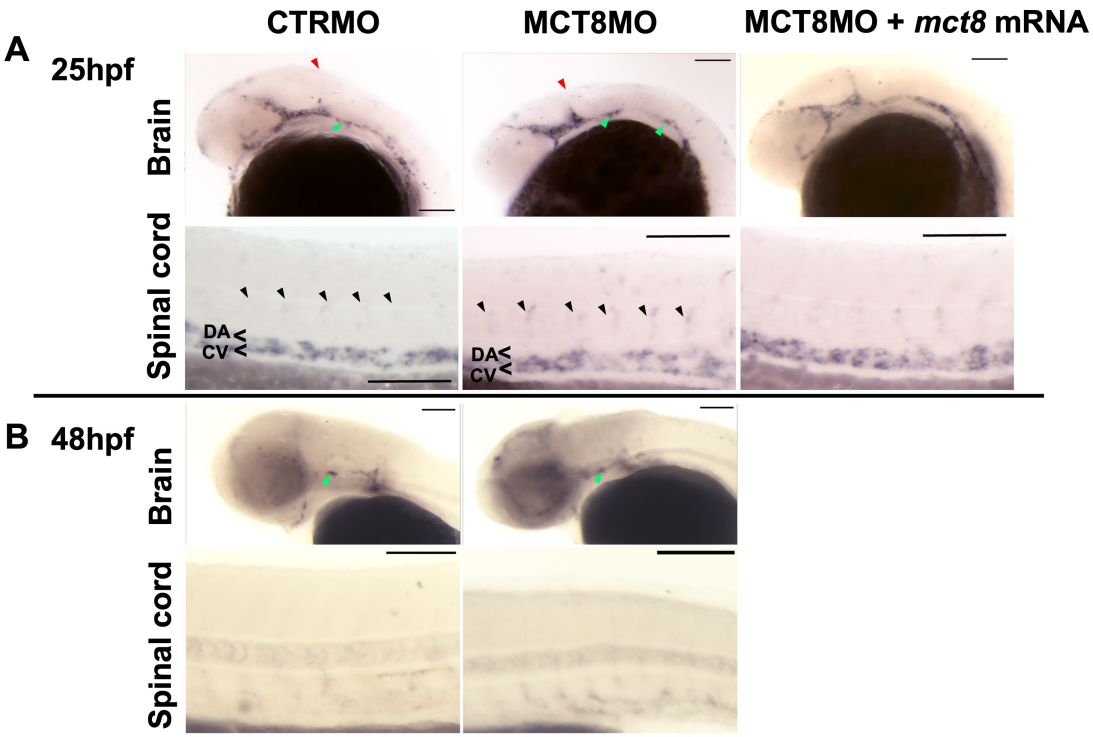

Figure 2.6 – MT3 regulates *flt4* gene expression during zebrafish development. A) WISH of *flt4* at 25 hpf and **B)** at 48 hpf in CTRMO, MCT8MO and co-injection of MCT8MO and *mct8* mRNA (MCT8MO + *mct8* mutated mRNA) zebrafish embryos are presented. WISH expression analysis show that MT3 regulates *flt4* expression in a context-dependent manner. An exogenous supply of *mct8* mutated mRNA rescued the expression of *flt4* to control levels in 25 hpf zebrafish embryos. Lateral images of the head (brain) and trunk (spinal cord) are shown. The red arrowhead indicates the mid-cerebral vein (MCeV), the green arrowhead indicates the primordial hindbrain channels (PHBC), and the black arrowhead indicates the intersegmental vessels (ISV). CV – Cardinal Vein; DA – Dorsal Artery; hb – hindbrain; mb – midbrain; nt – notochord. A minimum of 10 zebrafish embryos per condition and time points were analysed. Scale bar: 100 µm.

WISH analysis of *rspo1* revealed that the transcriptional response in *mct8* morphants was not generalised to the whole body but context-specific (Fig. 2.7), as observed previously for *flt4*. At 25hpf, *rspo1* expression was localised in the fore- and midbrain boundary (red arrowhead in Fig. 2.7 A), whereas, in MCT8MO zebrafish embryos, the expression was generalised in the head, eye, and brain (Fig. 2.7 A). At 48 hpf, *rspo1* expression in CTRMO embryos was more intense in the brain vasculature of the fore- and midbrain (Fig. 2.7 B). In MCT8MO embryos, the expression pattern was similar to the CTRMO embryos, but the expression was more intense (Fig. 2.7 B). This increase in the expression found in MCT8MO zebrafish embryos by WISH agrees with the results of the RNA-seq data.

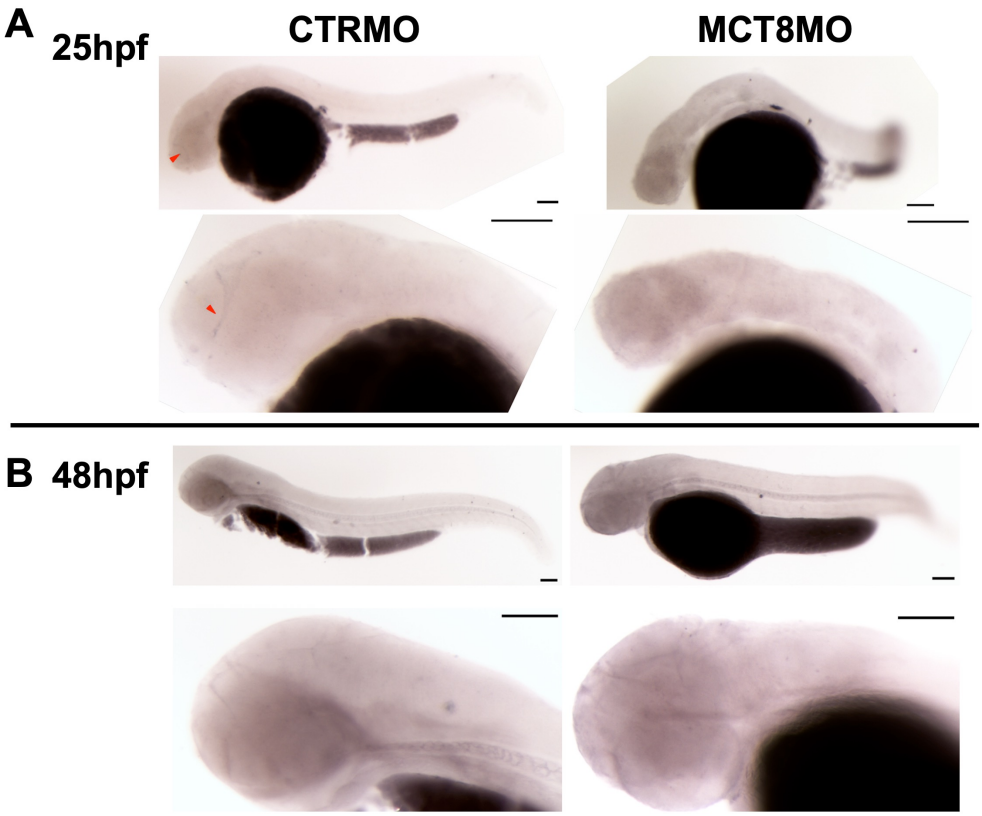

Figure 2.7 – MT3 regulates *rspo1* gene expression during zebrafish development. A) WISH of *rspo1* at 25 hpf and **B)** at 48 hpf in CTRMO and MCT8MO zebrafish embryos are presented. In the first panel the whole embryo is shown, while in the second panel, the head region is highlighted. During zebrafish development, *rspo1* expression was localised in the vasculature of the head, where it shows to have a role in BHB development. The red arrowhead indicates the forebrain-midbrain boundary. A minimum of 10 zebrafish embryos per condition and time points were analysed. Scale bar: 100 µm.

2.2.4 MT3 action during blood-hindbrain barrier development

Reactome pathway analysis and WISH expression analysis of *flt4* and *rspo1* demonstrated that knockdown of Mct8 and the consequent ablation of MT3 cellular uptake strongly suggest an involvement of MT3 in angiogenesis. To understand the requirements for MT3 in angiogenesis and zebrafish BHB development, differentially expressed genes between 25 hpf CTRMO and MCT8MO zebrafish embryos ($p<0.01$; FDR 5%) (Fig. 2.8) were analysed by qRT-PCR. However, angiogenic-related genes had low representation in the differential transcriptome (log2[fold-change] values), possibly because brain vascularisation had not started at 25 hpf. For

that reason, genes with non-identified differential expression (ND) in the transcriptome but reported to be important for BHB development (Fig. 2.8) were also analysed.

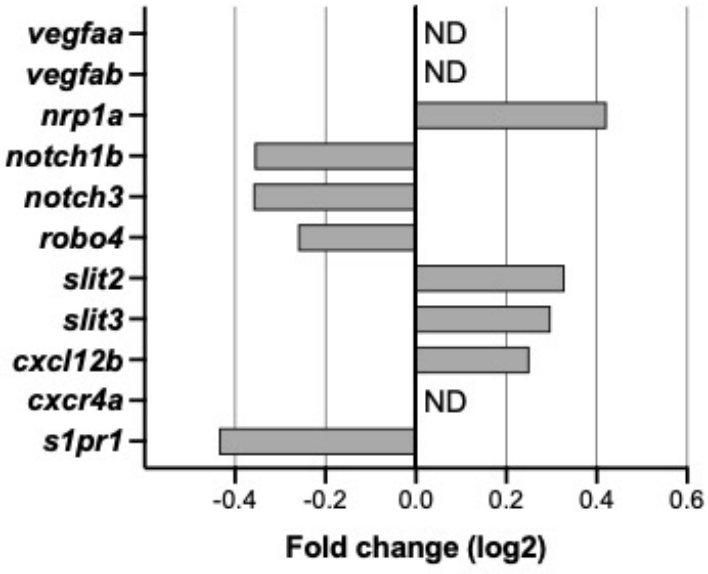

Figure 2.8 – Genes of interest involved in zebrafish hindbrain angiogenic development. Differentially expressed genes quantified by RNA-seq between CTRMO and MCT8MO zebrafish embryos are represented as Log2 or fold change (n = 7, $p < 0.01$, FDR < 0.05). ND – Not differentially expressed in RNA-seq but included in qRT-PCR analysis.

The formation of a vascular network involves a spatiotemporal sequence of angiogenic sprouting, guidance, remodelling, and maturation (Geudens and Gerhardt, 2011). The initial stage of angiogenesis involves releasing angiogenic factors such as Vegf. In mice, VEGF-A is required for endothelial tip cell induction and, together with Notch1, establishes an appropriate ratio between tip and stalk cells required for blood vessel formation and function (Gerhardt et al., 2003; Hellström et al., 2007). To determine if MT3 affects the initial events of the angiogenic sprouting mechanism, the two zebrafish *vegfa* paralogs, *vegfaa* and *vegfab*, the co-receptor *nrp1a*, and the *notch1b* receptor were analysed. The *vegfa* paralogs were not differentially expressed in the RNA-seq data, and whole-embryo gene expression analysis by qRT-PCR revealed that both genes were unaltered in MCT8MO zebrafish embryos during BHB development (Fig. 2.9 A and B). These results suggest that MT3 was not regulating *vegfa* expression or that the approach taken was not sufficiently sensitive to detect changes in the BHB.

Reactome analysis of the RNA-seq results revealed that the co-receptor *nrp1a* was a target of MT3. Besides that, it enhances Vegfa-dependent angiogenesis in zebrafish (Soker et al., 2002) and in mice, it is important for filopodia formation in endothelial tip cells (Fantin et al., 2015; Gelfand et al., 2014). In the 25 hpf MCT8MO transcriptome *nrp1a* was upregulated (Fig. 2.8), while gene expression analysis during BHB developmental time window shows a downregulation at 44 hpf (Fig. 2.9 C), a time window where the CtAs are connecting with the BA or with their ipsilateral neighbour (Table 2.1). The results suggest that MT3 regulates *nrp1a* during the final steps of BHB development.

Expression of *notch1b* was downregulated at 25 hpf MCT8MO embryos (Fig. 2.9 D). However, gene expression analysis by qRT-PCR revealed no significant differences in expression between CTRMO and MCT8MO zebrafish embryos among the different embryonic stages (Fig. 2.9 D). The results suggest that MT3 does not play a role in the coordinated interplay between endothelial tip and stalk cell selection or that whole-embryo analysis cannot detect changes only in the BHB. This is consistent with a lack of action of MT3 directly in CtAs, given that neither *mct8* nor TH receptors *thraa*, *thrab*, *thrb* are expressed in endothelial cells until 48 hpf (Campinho et al., 2014).

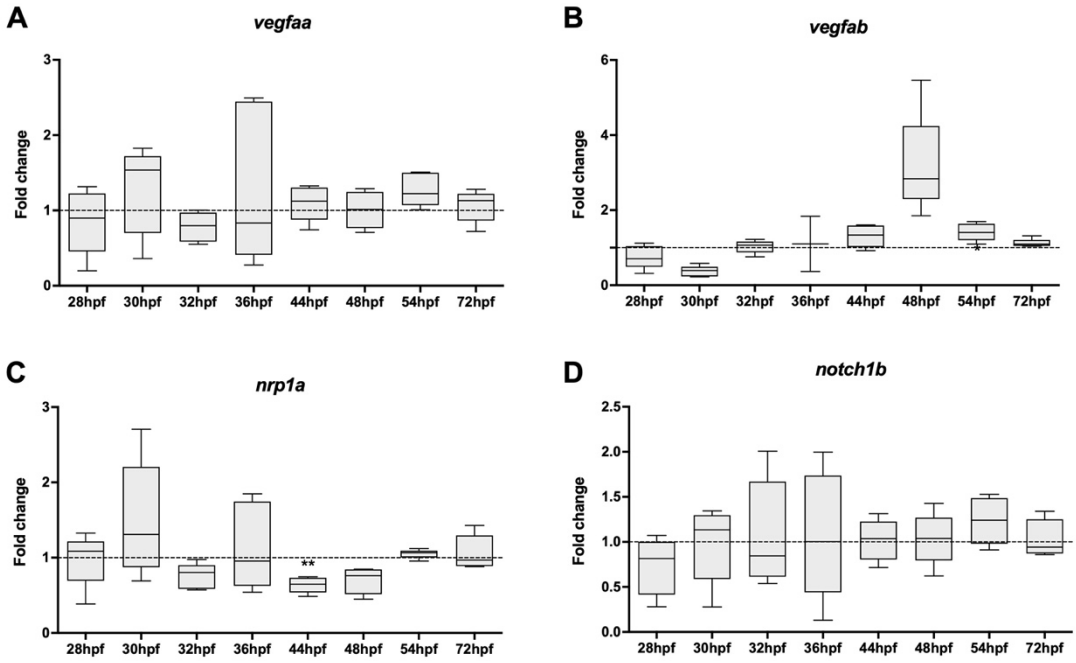

Figure 2.9 – Whole-embryo gene expression analysis suggests that MT3 is not involved in the endothelial tip and stalk specification but regulates *npr1a* during late BHB development. A) *vegfaa* and **B)** *vegfab* expression were not modified during BHB development between CTRMO and MCT8MO zebrafish embryos. **C)** The expression of the co-receptor *nrp1a* was downregulated only at 44 hpf in MCT8MO.

D) *notch1b* expression was unaffected by MT3 levels. Data are represented as fold change of MCT8MO expression relative to the CTRMO. Boxes represent the interquartile range ± SD. Dashed horizontal line represents no change in gene expression. Statistical significance was determined using a t-test: two-samples, assuming equal variance (n = 5; except for 36 hpf MCT8MO *vegfab* samples: n = 2). ** $p<0.01$.

Gene expression analysis revealed no significant changes between CTRMO and MCT8MO zebrafish embryos. To confirm the results obtained by qRT-PCR, WISH for *vegfaa* and *vegfab* were performed, genes that have previously been shown to be essential for CtA development in zebrafish (Jin et al., 2017; Rossi et al., 2016). WISH expression analysis of *vegfaa* at 36 hpf in MCT8MO embryos was decreased in the mid- and hindbrain compared to CTRMO embryos (Fig. 2.10 A). Specific *vegfaa* expression was observed in the anterior hindbrain region where CtAs are expected to sprout (green arrowheads in Fig. 2.10 A). MCT8MO embryos had a similar expression pattern, but the signal was much weaker (green arrowheads in Fig. 2.10 A). At 48 hpf, *vegfaa* expression was still reduced in MCT8MO compared to CTRMO embryos (Fig. 2.10 B). WISH analysis for *vegfab* revealed that the gene was much more expressed in the brain region than *vegfaa* (Fig. 2.10). The expression pattern of *vegfab* between CTRMO and MCT8MO zebrafish embryos was maintained. Still, the signal was less intense in MCT8MO than in CTRMO zebrafish embryos (Fig. 2.10 C and D).

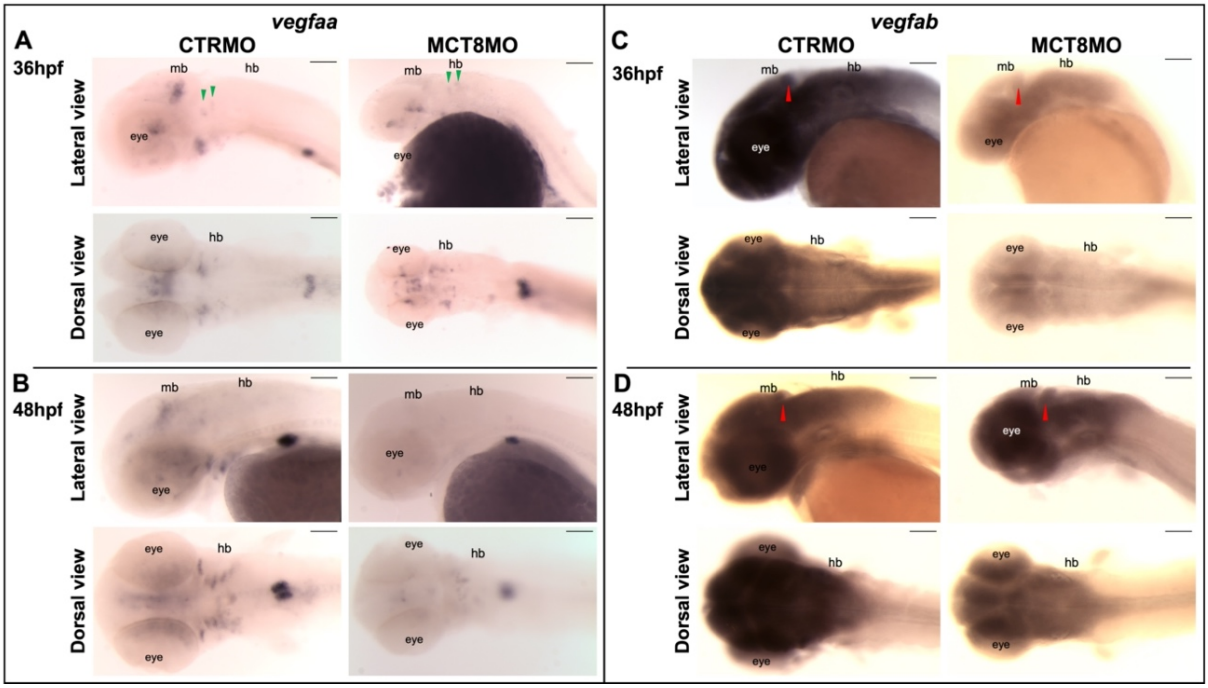

Figure 2.10 – MT3 regulates *vegfaa* and *vegfab* expression. WISH expression analysis between CTRMO and MCT8MO zebrafish embryos at 36 and 48 hpf are presented for *vegfaa* and *vegfab*. **A)** WISH expression analysis for *vegfaa* at 36 hpf and **B)** at 48 hpf shows a clear decrease of expression in MCT8MO compared to CTRMO zebrafish embryos. Specific *vegfaa* signalling is indicated by green arrowheads of putative CtA location. **C)** WISH expression analysis for *vegfab* at 36 hpf and **D)** at 48 hpf shows that the expression pattern was maintained between CTRMO and MCT8MO zebrafish embryos. The red arrowhead indicates the midbrain-hindbrain boundary (MHB). hb – hindbrain; mb – midbrain. A minimum of 10 zebrafish embryos per condition, time points and genes were analysed. Scale bar: 100 µm.

The results revealed that whole-embryo qRT-PCR gene expression analysis on angiogenic-related genes probably masked the real effect of MT3 on hindbrain angiogenesis and that, indeed, MT3 is required for appropriate *vegfaa* and *vegfab* expression in the hindbrain. In future work, WISH expression analysis for *notch1b* and *nrp1a* must be done.

After the initial sprouting, several signalling pathways interact to ensure angiogenic growth of the complex vascular network in the developing zebrafish embryo (Schuermann et al., 2014). The Slit/Robo and chemokine signalling pathways were analysed to determine if MT3 was involved in the guidance or migration of the cerebral blood vessels.

Reactome pathway analysis revealed that the "Regulation of commissural axon pathfinding by Slit and Robo" was under the regulation of MT3 (Fig.2.2 C). Although this pathway is specific

for the correct guidance of axons during neurogenesis (Dickson and Gilestro, 2006), this family of molecules also guides endothelial cell migration during angiogenesis (Fujiwara et al., 2006). The vascular-specific *robo4* receptor was downregulated at 25 hpf MCT8MO embryos, while the slit ligands *slit2* and *slit3* were upregulated (Fig. 2.8), indicating a possible role for MT3 in regulating these genes. Whole-embryo qRT-PCR gene expression analysis of all 3 genes revealed no significant differences between MCT8MO and CTRMO zebrafish embryos (Fig. 2.11 A-C), suggesting that MT3 was not regulating the Robo4 pathway or that using whole embryos for qRT-PCR was not able to detect changes occurring in the BHB.

The small chemokine *cxcl12b* and *cxcr4a* ligand-receptor pair were also analysed for their specific role in the correct pathfinding of the sprouting brain capillaries (Bussmann et al., 2011). RNA-seq data showed that *cxcl12b* was upregulated at 25hpf MCT8MO embryos (Fig. 2.8), but by qRT-PCR from 28 to 72 hpf, no significant change in *cxcl12b* gene expression was observed in MCT8MO embryos relative to CTRMO embryos (Fig. 2.11 D). The receptor *cxcr4a* was not differentially expressed in the RNA-seq data. Analysis of the *cxcr4a* gene across the BHB development revealed that expression was significantly upregulated in MCT8MO compared to CTRMO at 72 hpf (Fig.2.11 E). At 72hpf, the hindbrain vasculature was completely formed, showing that MT3 was unlikely to regulate *cxcr4a* during BHB development or that using whole embryos for qRT-PCR cannot detect changes occurring in the BHB.

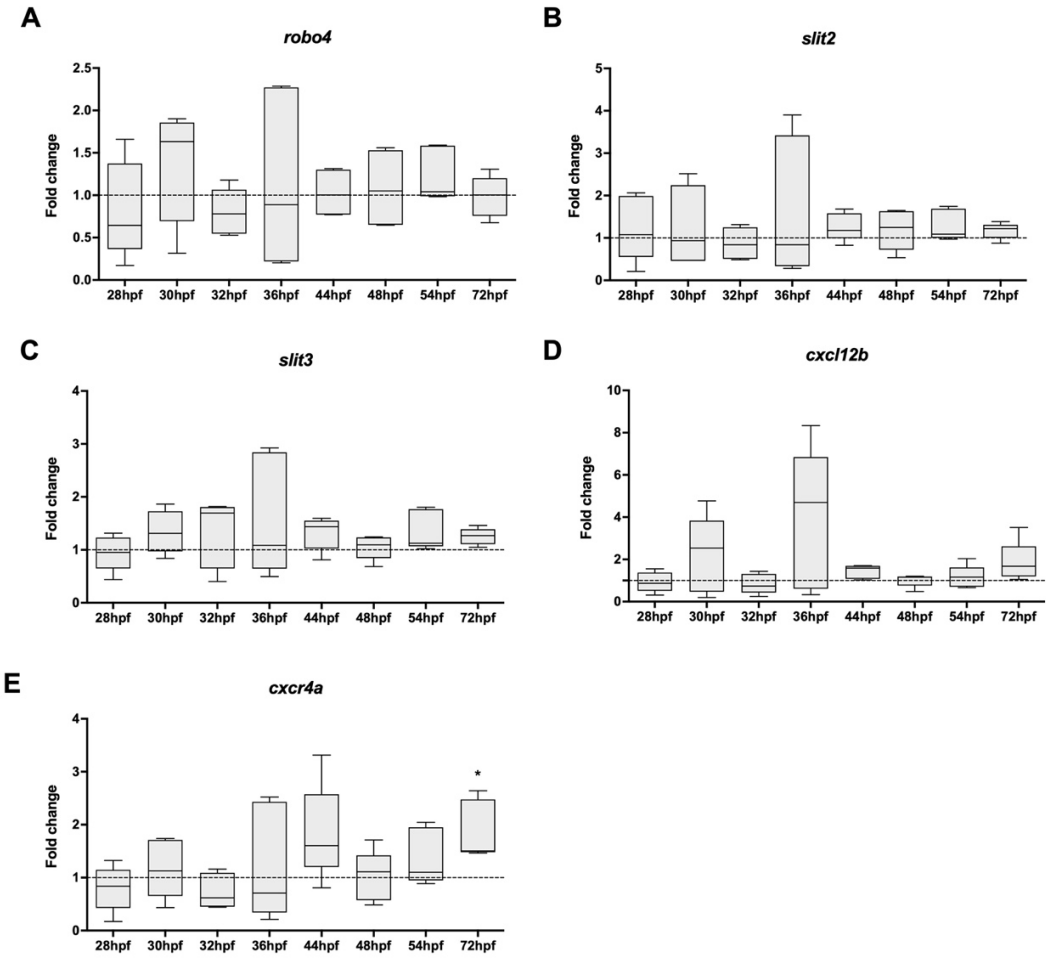

Figure 2.11 – Whole-embryo gene expression analysis suggests that MT3 is not regulating the Robo4 pathway or chemokine signalling during BHB development. **A)** *robo4* gene expression was not modified during BHB development between CTRMO and MCT8MO zebrafish embryos. The Robo4 ligands **B)** *slit2* and **C)** *slit3* were not altered by MT3 levels during BHB development. **D)** *cxcl12b* expression was unaffected by MT3 levels, while **E)** *cxcr4a* expression was only significantly upregulated at 72hpf. Boxes represent the interquartile range ± SD. Dashed horizontal line represents no change in gene expression. Statistical significance was determined using a t-test: two-samples, assuming equal variance (n = 5). * $p<0.05$.

WISH expression analysis of *robo4*, *slit2*, *slit3*, *cxcl12b* and *cxcr4a* were not performed in this thesis and needs to be conducted in future work.

As embryonic development proceeds, vessels need to mature to become functional (Potente et al., 2011). This relies on the recruitment of mural cells (pericytes) and deposition of ECM (Jain, 2003). Two genes, *s1pr1* and *notch3*, were selected to identify if MT3 regulates mural cell recruitment. RNA-seq data revealed that the expression of *notch3* and *s1pr1* were downregulated in 25 hpf MCT8MO embryos (Fig. 2.8), indicating a possible role for MT3 in

pericyte recruitment. Gene expression analysis by qRT-PCR during BHB development revealed that the only significant difference between MCT8MO and CTRMO embryos occurred for *notch3* at 72hpf (Fig. 2.12 A). This suggests that MT3 does not regulate *s1pr1* and *notch3* or that using whole embryos for qRT-PCR cannot detect changes occurring in the BHB.

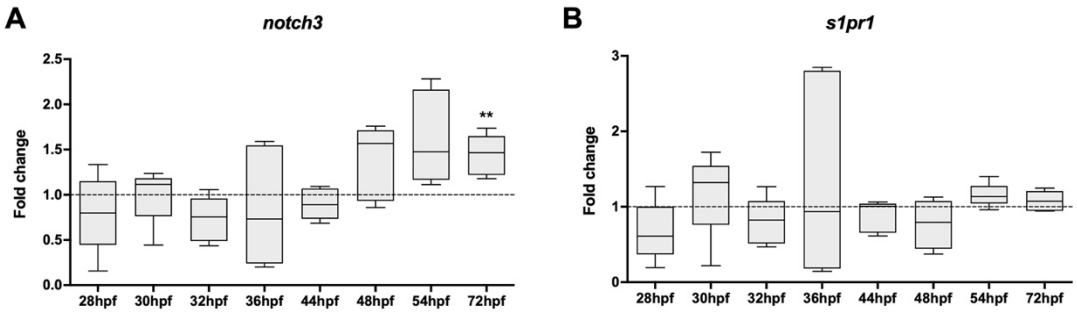

Figure 2.12 – Whole-embryo gene expression analysis suggests that MT3 is not involved in mural cell recruitment. A) *notch3* expression was only significantly upregulated at 72hpf. **B)** *s1pr1* was unaffected by MT3 levels. The data are represented as fold change of MCT8MO expression relative to the CTRMO. Boxes represent the interquartile range ± SD. Dashed horizontal line represents no change in gene expression. Statistical significance was determined using a t-test: two-samples, assuming equal variance (n = 5). ** $p<0.01$.

Both *notch3* or *s1pr1* genes are involved in the recruitment of pericytes for vessel maturation (Potente et al., 2011). Although there was no apparent change in *notch3* or *s1pr1* expression in MCT8MO, WISH and immunohistochemistry (IHC) analysis was performed on brain pericytes during BHB development to corroborate the results with qRT-PCR and RNA-seq. *pdgfrb* is a specific marker for pericytes in zebrafish, and this gene was not differentially expressed in the RNA-seq data. So, to establish if MT3 might be involved in brain pericyte recruitment for BHB development, the *Tg(fli1:EGFP)* transgenic zebrafish line (Lawson and Weinstein, 2002) was used to view the different hindbrain vascular structures and the number of pericytes in two different conditions was quantified: 1) increasing the concentration of T3 availability to the developing zebrafish embryos by treating them with 20 nM T3 (Sigma, Aldrich, USA) and 2) knocking-down the Mct8 transporter, to prevent TH entry into the brain by a morpholino-based system. The results show that brain pericytes were present in the main hindbrain vascular structures, the PHBC, the BA and the CtAs (Fig. 2.13). Pericytes only were observed in the CtAs at 48hpf (Fig. 2.13 C, F, I, L). Treatment with T3 during development did not significantly modify the number of pericytes in the different hindbrain vascular structures (Fig. 2.13 G-I). In contrast, the knockdown of the Mct8 transporter caused an altered number of pericytes to be

recruited to the different hindbrain vascular structures (Fig. 2.13 J-L). This evidence suggests that T3 is unlikely to act directly on pericytes. In the PHBC of MCT8MO zebrafish embryos, the number of pericytes was significantly reduced at 48hpf ($p<0.0001$) (Fig. 2.13 D-F, J). In the BA, the number of pericytes increased significantly at 36hpf ($p<0.0001$) and then decreased significantly at 48hpf ($p<0.01$) (Fig. 2.13 D-F, K). Interestingly, was the observation that at 36hpf the BA in the MCT8MO was not yet completely formed, and the pericytes formed agglomerates in the posterior region of the BA (Fig. 2.13 E). Nevertheless, the BA continued to develop and was formed entirely by 48hpf in MCT8MO embryos but fewer pericytes were identified (Fig. 2.13 F, K). This observation strongly suggested that impaired pericyte migration in MCT8MO embryos was not due to a direct effect on these cells, but due to the delayed BA development. In the case of the CtAs, impaired development of the CtAs in the MCT8MO embryos was observed (Fig. 2.13 D-F), as has been reported previously by Campinho et al., (2014). As mentioned, in CTRMO zebrafish embryos, pericytes were only observed at 48hpf, while in MCT8MO embryos no pericytes were observed (Fig. 2.13 F, L).

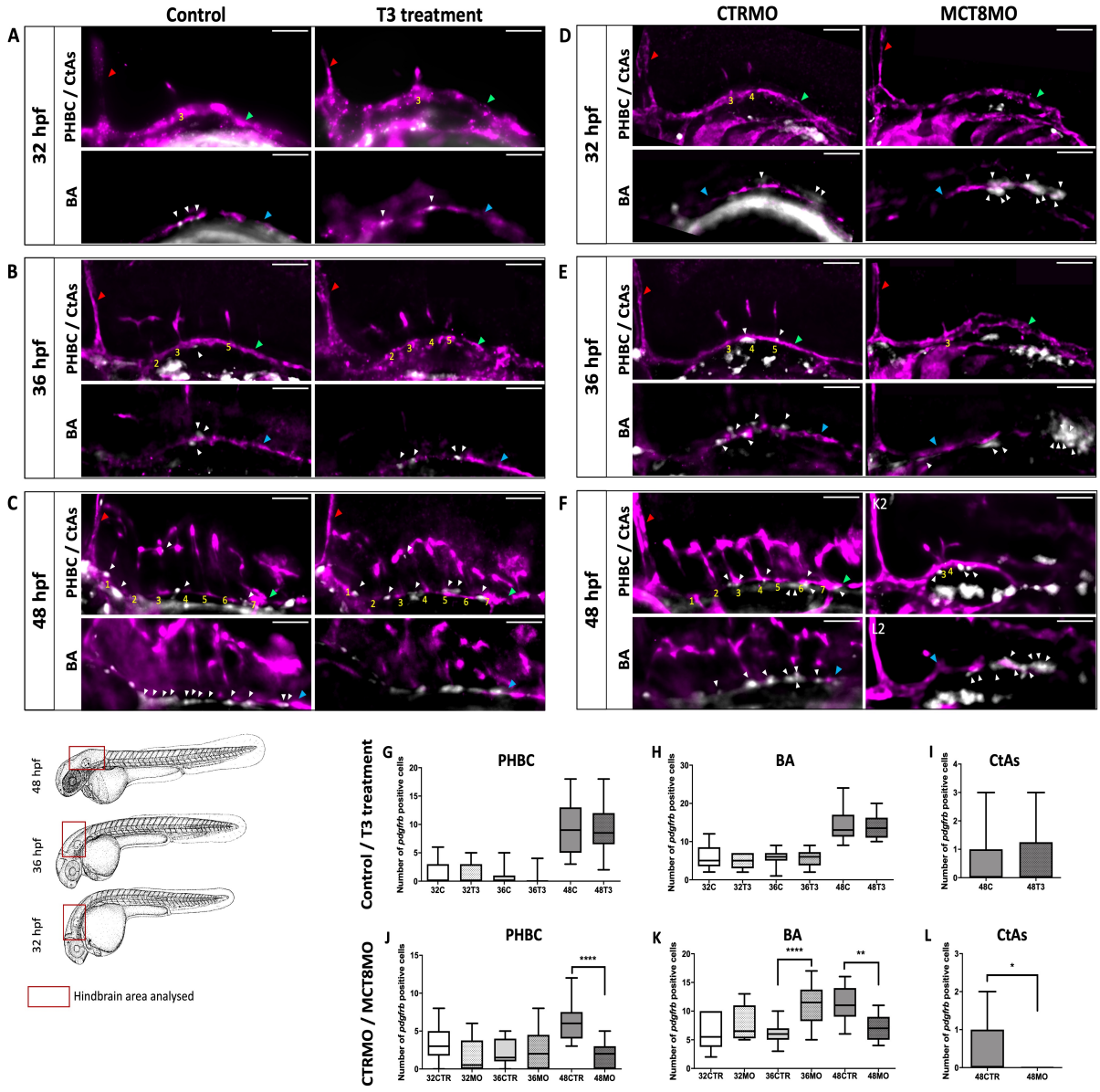

Figure 2.13 – MT3 affects pericyte number indirectly due to impaired development of the hindbrain vascular structures. Lateral view of *Tg(fli1:EGFP)* zebrafish embryos submitted to WISH for *pdgfrb* (pericyte marker – white colour) and IHC against GFP (endothelial marker – magenta colour) at 32, 36 and 48 hpf are represented. Zebrafish embryos were submitted to two experimental conditions: **A - C)** Increase of T3 availability in the medium (Control vs. T3 treatment) and **D - F)** Knockdown of the Mct8 transporter by a morpholino-based system (CTRMO vs. MCT8MO). The red box indicates the analysed hindbrain area for every embryonic stage. The red arrowhead indicates the mid-cerebral vein (MCeV), the green arrowhead indicates the primordial hindbrain channels (PHBC), the blue arrowhead indicates the basilar artery (BA), and the white arrowhead indicates pericytes. Yellow numbers 1-7 indicate the central arteries (CtAs) in their respective rhombomere. Scale bars: 100 µm. **G – L)** Quantification of the pericyte numbers in the PHBC, BA, and CtAs for **G – I)** the Control and T3 treatment condition and **J – L)** for CTRMO and MCT8MO condition. Results are presented as mean ± SD; statistical significance determined by t-test (n = 8 – 22). * $p<0.05$; ** $p<0.01$; *** $p<0.0001$.

2.2.5 MT3 regulates central arteries development through *vegfaa* expression

WISH analysis showed that *vegfa* genes were under MT3 regulation, but the specific expression of *vegfaa* in the hindbrain marking the position of CtA ingression makes it a suitable MT3-dependent candidate gene for BHB development. For that reason, the *Tg(fli1:EGFP)* transgenic zebrafish line (Lawson and Weinstein, 2002) was used to view the expression pattern of *vegfaa* concerning CtAs development between CTRMO and MCT8MO zebrafish embryos (Fig. 2.14). Expression of *vegfaa* during the different developmental stages (32, 36 and 48 hpf) was clearly reduced in MCT8MO embryos compared to CTRMO embryos (Fig. 2.14). During development, *vegfaa* expression can be observed in the hindbrain juxtaposed to specific CtAs, showing the importance of *vegfaa* for CtA sprouting and migration. At 32 and 36 hpf *vegfaa* expression was predominantly observed juxtaposed to CtAs 2, 3 and 4 in CTRMO zebrafish embryos (Fig. 2.14 A-C). As the embryo develops, *vegfaa* expression can also be observed juxtaposed to CtAs 1 and 5 (Fig. 2.14 A, D). In MCT8MO embryos, *vegfaa* expression was not lost but significantly reduced (Fig. 2.14 A). Some *vegfaa* expression was still evident in the rhombomeres where CtAs are supposed to sprout and migrate, but it was much reduced compared to CTRMO embryos (Fig. 2.14 A). At 32 hpf, knockdown of Mct8 significantly reduced the expression of *vegfaa* in rhombomeres 2, 3 and 5 (Fig. 2.14 B). At 36 hpf, *vegfaa* expression was significantly reduced in rhombomeres 2, 3 and 4 (Fig. 2.14 C). At 48 hpf, *vegfaa* expression was significantly reduced in rhombomeres 1 to 5 (Fig. 2.14 D). These results clearly link MT3, *vegfaa* expression, and CtA development.

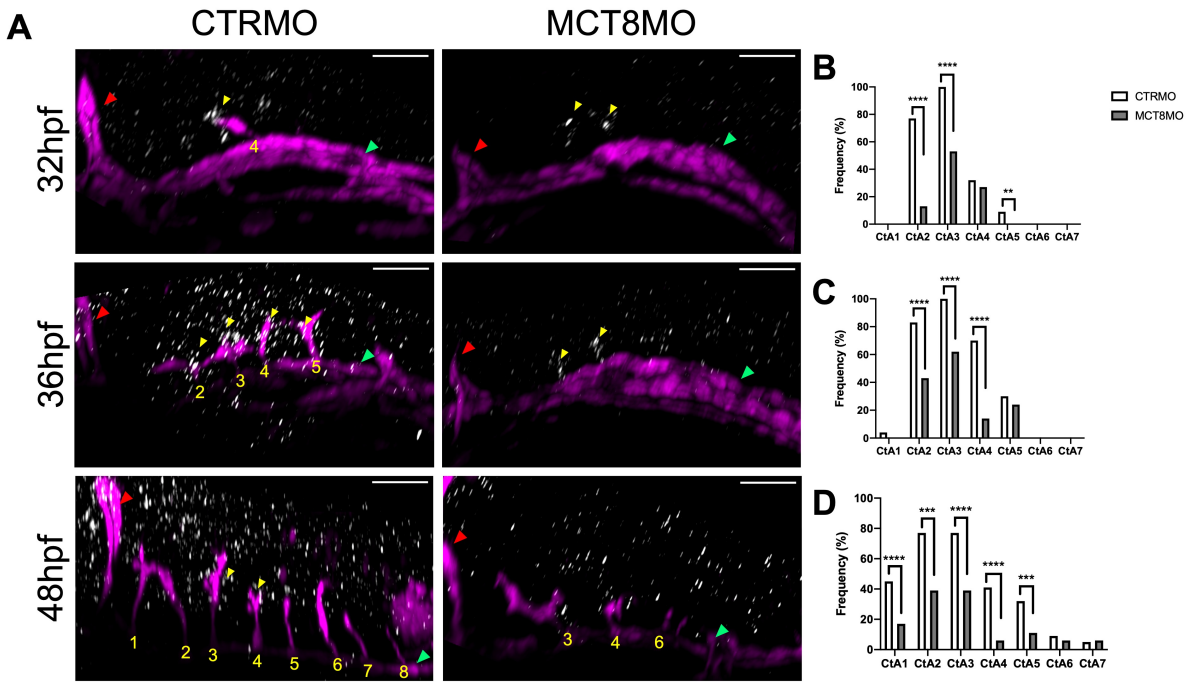

Figure 2.14 – *vegfaa* expression is decreased in MCT8MO zebrafish embryos during BHB development. A) Maximum projection of lateral images of the hindbrain of *Tg(fli1:EGFP)* submitted to WISH for *vegfaa* (white colour) and IHC against GFP (endothelial marker, magenta colour) of CTRMO and MCT8MO zebrafish embryos at 32, 36 and 48 hpf are represented. The red arrowhead indicates the mid-cerebral vein (MCeV), the green arrowhead indicates the primordial hindbrain channels (PHBC), and the yellow arrowhead indicates agglomeration of *vegfaa* expression around a CtA or the location where a CtA is supposed to develop. Numbers in yellow 1 – 8 indicate the CtA in its respective rhombomere. Scale bar: 50 µm. **B – D)** Graphical representation of the frequency of *vegfaa* expression visualised around a specific CtA or where a CtA is supposed to develop at **B)** 32 hpf, **C)** 36 hpf, **D)** 48 hpf. Statistical significance was determined using Fisher's exact test (n = 15 – 23). ** $p<0.01$; *** $p<0.001$; **** $p<0.0001$.

We observed that during BHB development several CtAs fail to sprout, possibly due to the lack of *vegfaa* signalling that is missing in MCT8MO zebrafish embryos. To further confirm that *vegfaa* signalling is involved in CtAs development downstream of MT3 signalling, we co-injected, together with the MCT8MO, the zebrafish *vegfaa-165* mRNA and analysed the number of CtAs present using the *Tg(fli1:EGFP)* transgenic zebrafish line (Lawson and Weinstein, 2002) to visualise the hindbrain vascular structures (Fig. 2.15). Embryos injected with CTRMO have 5 to 7 CtAs present, as expected at this developmental stage (Fig. 2.15 A and B). The number of CtAs significantly reduces in the MCT8MO with an average of 2 CtAs present at 48 hpf (Fig. 2.15 A and B). Analysing the frequency of each CtA to develop between

CTRMO and MCT8MO embryos shows that all 7 CtAs were significantly affected (Fig. 2.15 C). Exogenous supply of *vegfaa-165* mRNA significantly increased the number of CtAs to an average of 4 CtAs compared to MCT8MO (Fig. 2.15 B), being able to rescue CtAs 1, 2, 3 and 7 (Fig. 2.15 C). The embryos co-injected with MCT8MO and *vegfaa-165* mRNA partially rescued the control phenotype (Fig. 2.15 A and B). CtAs 5 and 6 were partially recovered by the exogenous supply of *vegfaa-165* mRNA, while CtA 4 could not be recovered (Fig. 2.15 C).

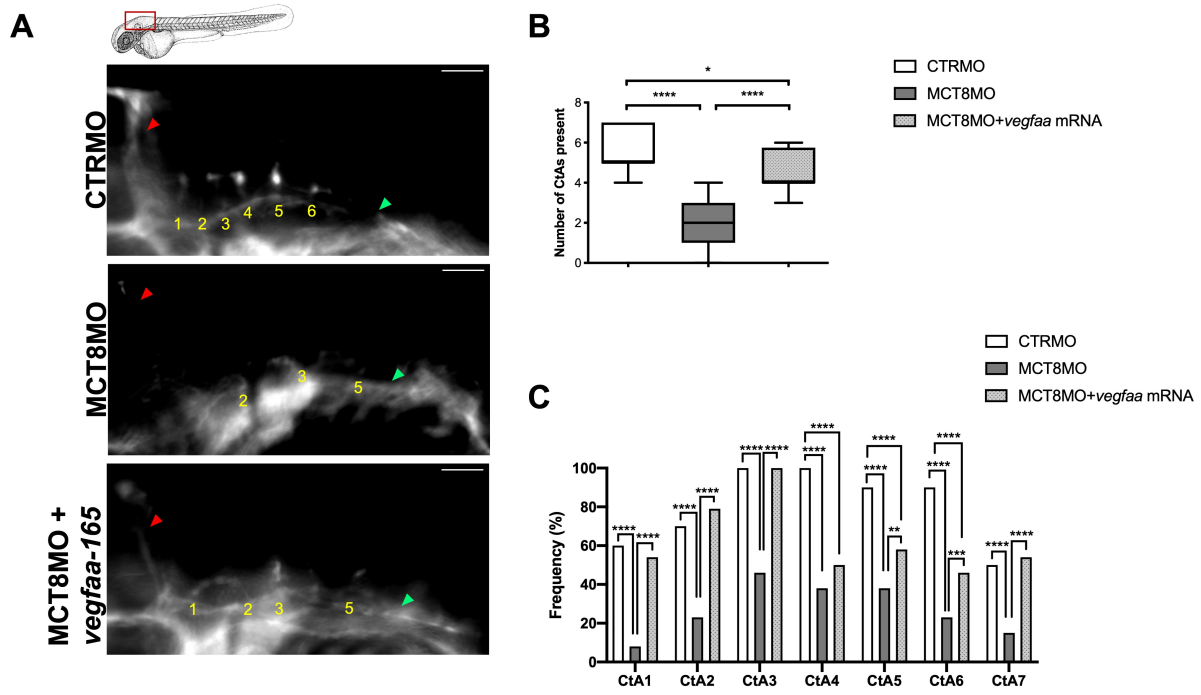

Figure 2.15 – *vegfaa* overexpression partially rescues the MTC8MO blood-hindbrain barrier phenotype. A comparison between CTRMO, MCT8MO and MCT8MO co-injected with *vegfaa-165* mRNA (rescue) zebrafish embryos at 48 hpf is presented. **A)** GFP staining (endothelial marker, white colour) of the hindbrain (lateral view) in 48 hpf injected CTRMO, MCT8MO and rescue zebrafish embryos are shown. The red arrowhead indicates the mid-cerebral vein (MCeV), and the green arrowhead indicates the primordial hindbrain channels (PHBC). Numbers in yellow 1 – 7 indicate the central arteries (CtAs) in their respective rhombomere. Scale bar: 50 µm. **B)** Statistical analysis of the number of CtAs present in each experimental group. Control embryos have an average of 5 CtAs at 48 hpf. This number was significantly reduced in MCT8MO embryos, as they have only an average of 2 CtAs at 48 hpf. Rescued zebrafish embryos have an average of 4 CtAs. This experimental group was significantly different from the MCT8MO group and also from the CTRMO group. Statistical significance was determined using One-way ANOVA followed by Bonferroni's multiple comparison analysis (n = 10 – 24). **C)** Frequency of each CtA to develop in each experimental group. All CtAs development were significantly reduced in MCT8MO embryos compared to CTRMO embryos. Co-injection of MCT8MO with *vegfaa-165* mRNA was able to rescue CtAs 1, 2, 3 and 7, but was not able to rescue CtA 4. CtAs 5 and 6 were partially rescued since they were significantly different from the MCT8MO but still significantly different from the CTRMO.

Statistical significance was determined using Fisher's exact test (n = 10 – 24). * p<0.05; **p<0.01; *** p<0.001; **** p<0.0001.

2.3 DISCUSSION

In this Chapter, it was aimed to investigate the involvement of MT3 in angiogenic-related gene regulatory networks and processes during zebrafish embryogenesis. The transcriptome of 25 hpf MCT8MO and CTRMO zebrafish embryos was analysed to achieve this. The involvement of MT3 in different angiogenic-related pathways and differentially expressed genes were identified. MT3-regulated genes involved in angiogenic events were identified and selected for a more detailed analysis during BHB development using qRT-PCR and WISH. Overall, MT3 acts in the angiogenic event mediating CtA ingression into the hindbrain during zebrafish embryogenesis. Our analysis suggests that the effect of MT3 on CtA angiogenesis is not direct but indirect.

2.3.1 MT3 regulates several genes in angiogenic-related genetic pathways

Transcriptome analysis revealed that 4,343 genes were significantly affected by MTH deprivation at 25 hpf, indicating that MT3 regulates various processes during zebrafish development. Reactome pathway analysis revealed that MT3 regulates genes in all Reactome mother categories (Fig. 2.2 B), demonstrating the relevance of this hormone for many cell signalling processes that are fundamental for zebrafish development. Extracellular matrix (ECM) organization was the most populated Reactome mother category, where MT3 regulates 35% of genes. Transcriptome analysis of primary cerebrocortical cells of mice also identified ECM proteins as one of the major groups regulated directly by T3 (Gil-Ibañez et al., 2015), concordant with our zebrafish Mct8 transcriptome results. ECM proteins are involved in many processes during brain development, such as neurogenesis (Bernal, 2017) and angiogenesis (Martino et al., 2015). The angiogenic growth factor Vegfa has several spliced isoforms (Bowler and Oltean, 2019). In zebrafish, Vegfaa-165 and the two Vegfab isoforms, Vegfab-171 and Vegfab-210, bind to the ECM (Lange et al., 2022). The spatial localization of these

angiogenic signals in the ECM ensures that the blood vessels are formed in the correct place (Martino et al., 2015). Alteration of ECM constituents may directly affect the binding capacity of the different Vegfa isoforms, thus leading to a defective vascular morphogenesis (Ruhrberg et al., 2002).

The major angiogenic-related pathways belong to the Reactome Signal Transduction mother category. In the VEGFA-VEGFR2 and NOTCH sub-pathways, MT3-regulated genes were present in almost all reactions, while MT3-regulated genes were more variable in the WNT sub-pathways. Although these developmental pathways are involved in angiogenesis, they also contribute to the development of the CNS. Many molecular pathways are shared between the vascular and nervous systems (Tam and Watts, 2010). From our analysis, it is uncertain whether MT3 regulates angiogenesis, whether it is acting only in neurogenesis or both. Nonetheless, given that neither *mct8* nor TH receptors (*thraa*, *thrab* and *thrb*) are expressed in the vascular tissue at these stages (Campinho et al., 2014) it is likely that the effect of MT3 on BHB development is due to neurodevelopmental effects.

All 3 pathways have previously been linked to TH signalling. Vegfa has been shown to be regulated by T3 *in vitro* to promote angiogenesis (Zhang et al., 2010) and transcriptome analysis of C17 neuronlike cells (obtained from mouse cerebellum) expressing Thra and Thrb revealed an upregulation of Vegfa expression (Chatonnet et al., 2013). Notch and Wnt pathway components have also been shown to be regulated by T3. Transcriptome analysis of cultured astrocytes isolated from the postnatal mouse cerebral cortex has shown that Notch ligands Dll1 and Dll3 and receptors Notch1, Notch3 and Notch4 were downregulated by T3 (Chatonnet et al., 2013; Morte et al., 2018). In the Wnt signalling pathway, Wnt7b was downregulated and Wnt7a was transcriptionally upregulated by T3 (Morte et al., 2018). In our transcriptome analysis, at 25 hpf, most of these genes were not differentially expressed, except for Notch1 and Notch3, which were downregulated at this developmental stage in MCT8MO zebrafish embryos. These differences might reflect differences in T3 action in these species when compared to zebrafish, different developmental stages, or even that cell-specific action of T3 on these genes cannot be resolved by the whole-embryo analysis carried out.

2.3.2 MT3 action in hindbrain angiogenesis

The spatial-temporal mapping of selected MT3-regulated angiogenic genes revealed that during zebrafish development MT3 has a role in hindbrain vascularisation. Expression of *flt4* (0.43 log2fold increase, $p < 0.01$, FDR < 0.0001) and *rspo1* (1.06; Log2fold increase, $p < 0.01$, FDR < 0.0001) were increased in MCT8MO embryos (Fig. 2.6 and 2.7), which were also upregulated in the RNA-seq data. Both genes are involved in Wnt-Vegfc-Flt4 signalling during zebrafish angiogenesis (Gore et al., 2011). The fact that both genes were upregulated in *mct8* morphants suggests that MT3 may modulate blood vessel development via Rspo1-Wnt-Vegfc-Flt4 signalling pathway. But how MT3 is regulating this signalling pathway remains to be clarified. However, given that no component of the TH signalling pathway (transporters, deiodinases and receptors (Campinho et al., 2014)) are expressed in zebrafish brain vessels at these early developmental stages suggests that these changes are likely due to indirect effects on endothelial cells.

Afterwards, we wanted to identify at which stage MT3 is involved in hindbrain angiogenesis by conducting whole-embryo gene expression analysis. However, no significant differences were observed in the different angiogenic-related genes over BHB developmental time window in whole-embryo analysis. A huge variance was observed in all genes analysed at 36 hpf suggesting that these genes expressions might be modified in BHB angiogenesis. Although we did not analyse the gene expression at 25 hpf, this analysis showed no correlation between the RNA-seq data and qRT-PCR analysis. Previous studies have shown that 15-20% of the genes analysed between RNA-seq data and qRT-PCR showed non-concordant results, either by showing opposite differential expression or that one method showed differential expression while the other does not (Coenye, 2021; Everaert et al., 2017). This happens frequently in genes that have a fold change lower than 2 or 1.5, as it happens for the genes that were selected for qRT-PCR analysis (Fig. 2.8). Another fact that contributes to the non-differential expression observed in the qRT-PCR analysis is that during zebrafish embryogenesis, MCT8MO zebrafish embryos do not show any malformation in the trunk vasculature, as the ISV developed normally (Fig. 2.6), and in the hindbrain, the PHBC and BA show an altered formation over developmental time but were completely formed at 48 hpf (Fig. 2.1 and Fig. 2.13). The only vascular structures disrupted by Mct8 deprivation were the CtAs (Fig. 2.1) (Campinho et al., 2014). Given these facts, gene expression analysis conducted in the whole-embryo masked the real effect of MT3 on hindbrain angiogenesis. This was confirmed by WISH expression

analysis conducted on *vegfaa* and *vegfab* which showed that MT3 was regulating these genes in the hindbrain (Fig. 2.10).

Several studies using the zebrafish as a model have shown that *vegfaa* signalling is important for CtA development (Jin et al., 2017; Rossi et al., 2016). In the MCT8MO zebrafish embryo, *vegfaa* expression was significantly downregulated, indicating that MT3 regulates *vegfaa* expression (Fig. 2.14). Interestingly was the observation that in CTRMO zebrafish embryos, specific *vegfaa* expression appeared juxtaposed to the location of CtA development and that this expression appeared diminished in MCT8MO embryos, indicating a possible role of MT3 in regulating CtA development through *vegfaa* expression. To date, it is known that TH influences angiogenesis, but most studies in the field are focused on the non-genomic action of T4-induced angiogenesis through the integrin αvβ3/protein kinase D/histone deacetylase 5 signalling pathway for cardiac angiogenesis (Liu et al., 2014; Luidens et al., 2010). Only a few *in vitro* and *in vivo* studies have shown that in induced hypothyroid mice, the expression of *Vegfa* was reduced in the cerebral cortex. These mice presented a deficient microvasculature development in the dentate gyrus (Zhang et al., 2010). These results corroborate our findings, showing that *vegfaa* signalling is likely a target of MT3, at least in specific regions of the CNS.

Co-injection of *vegfaa-165* mRNA with MCT8MO showed the capacity and importance of *vegfaa* for CtA development (Fig. 2.15). In these embryos, CtAs 1, 2, 3 and 7 were rescued by *vegfaa-165* mRNA, while CtAs 5 and 6 were partially rescued. In rhombomeres 2 and 3 of MCT8MO embryos, *vegfaa* expression although diminished, was still present, so the exogenous supply of *vegfaa-165* mRNA rescued completely the vascularisation of those two rhombomeres. Rhombomeres 1 and 7 are usually the last ones that vascularise (Ulrich et al., 2011) and were also completely recovered by exogenous *vegfaa-165* mRNA. Vascularisation of rhombomeres 5 and 6 were partially rescued by exogenous *vegfaa-165* mRNA, indicating that other endothelial guidance factors are required for the complete rescue of these CtAs. Since these two rhombomeres are neighbours, a common guidance factor may be involved in the sprouting and growth of these CtAs. In rhombomere 4, *vegfaa-165* mRNA could not rescue CtA sprouting, indicating that another angiogenic factor or a combination of factors is required for the sprout and development of this CtA. Although we restored *vegfaa-165* mRNA levels, the ECM components were still modified, leading to a putative reduced capacity of *vegfaa-165* binding to the ECM, diminishing the effect of *vegfaa-165* on CtA sprouting. In this study, we did not investigate the effect of *vegfab* on CtA development. Zebrafish mutants for *vegfab* display minor angiogenic defects, with a slightly reduced number of CtAs (Rossi et al., 2016).

Since both *vegfa* paralogs are involved in CtA sprouting, it might be an interesting target gene to study the recovery of the remaining CtAs in MCT8MO or to see if both *vegfa* paralogs are needed for the full recovery of the Mct8 BHB phenotype.

The effect of Mct8 deficiency significantly affected the sprouting and growth of all 7 CtAs during zebrafish BHB development (Fig. 2.15). However, in MCT8MO embryos, CtA development was variable, with CtA 3 development having the highest frequency to develop (50%) in MCT8MO embryos, followed by the development of CtAs 4 and 5 in almost 40% of MCT8MO embryos. The lowest frequencies were observed for the development of CtAs 1, 2, 6 and 7 (Fig. 2.15 C). This shows clearly that some CtAs were more susceptive to MT3 signalling in the hindbrain than others. We have shown that *vegfaa* expression was still present in some rhombomeres in MCT8MO embryos, but recent data from Silva, (2020) has shown that the rhombomere boundaries were anomalously formed. This might lead to developing a neighbouring rhombomere vascularisation that is not dependent on *vegfaa* signalling.

This study indicates that the action of MT3 in BHB development is likely focused on hindbrain cells involved in the attraction and ingression of CtAs into the brain rather than a direct effect of MT3 on endothelial cells (Fig. 2.16). Moreover, the action of MT3 signalling on these putative hindbrain cells likely precedes Vegf-signalling borne in those cells.

2.3.3 MT3 regulates indirectly pericyte recruitment to the hindbrain blood vessels

The consequence of the indirect regulation of MT3 on the hindbrain vascular endothelial cells was also observed for the recruitment of the pericytes to the different hindbrain vascular structures. Pericytes are important for blood vessel maturation and BBB stabilization as they express tight junction proteins to promote vascular permeability (Daneman et al., 2010) to allow the establishment of a competent neurovascular unit. In MCT8MO zebrafish embryos, pericyte numbers were significantly reduced in the PHBC, BA and CtAs at 48 hpf (Fig. 2.13). But treating the embryos with an exogenous supply of T3 did not affect the numbers of pericytes in the different hindbrain vascular structures. As already mentioned, the PHBC and BA have a defective formation during BHB development but manage to completely develop at 48 hpf, while the number of CtAs was reduced in MCT8MO zebrafish embryos at 48 hpf. In this way,

MT3 was not directly regulating pericyte recruitment by inducing *pdgfrb* expression, but rather it was affecting pericyte recruitment as a consequence of the impaired hindbrain vasculature development.

2.4 CONCLUSIONS

In this study, we investigated how MT3 is affecting the angiogenic events during BHB development and concluded that:

1) MT3 modulates several developmental pathways including angiogenic-related pathways such as the VEGFA-VEGFR2 pathway;

2) MT3 affect the development of the CtAs during zebrafish BHB development, although not directly on the endothelial cells, but indirectly by regulating the chemoattraction of the CtA sprouting and growth;

3) MT3 signalling occurs upstream of *vegfaa* signalling which mediates CtA ingression in the zebrafish hindbrain.

The loss of CtAs has been reported in *vegfaa* mutant zebrafish embryos (Jin et al., 2017; Rossi et al., 2016) although in these mutants other vasculature structures of the trunk and brain are dependent on *vegfaa* signalling. Given the fact that in MCT8MO zebrafish embryos only the CtAs are affected indicates that MT3 is regulating specific hindbrain cells that are responsible for *vegfaa* hindbrain expression. Therefore, we propose a model whereby hindbrain CtAs ingression is instructed by MT3-dependent hindbrain cells (Fig. 2.16). In human AHDS patients, this phenotypic outcome has not been confirmed, but it would not be surprising that the hypoxic levels in the brain due to the lack of blood vessels could also participate in brain underdevelopment and consequently impact on neurological problems of these patients.

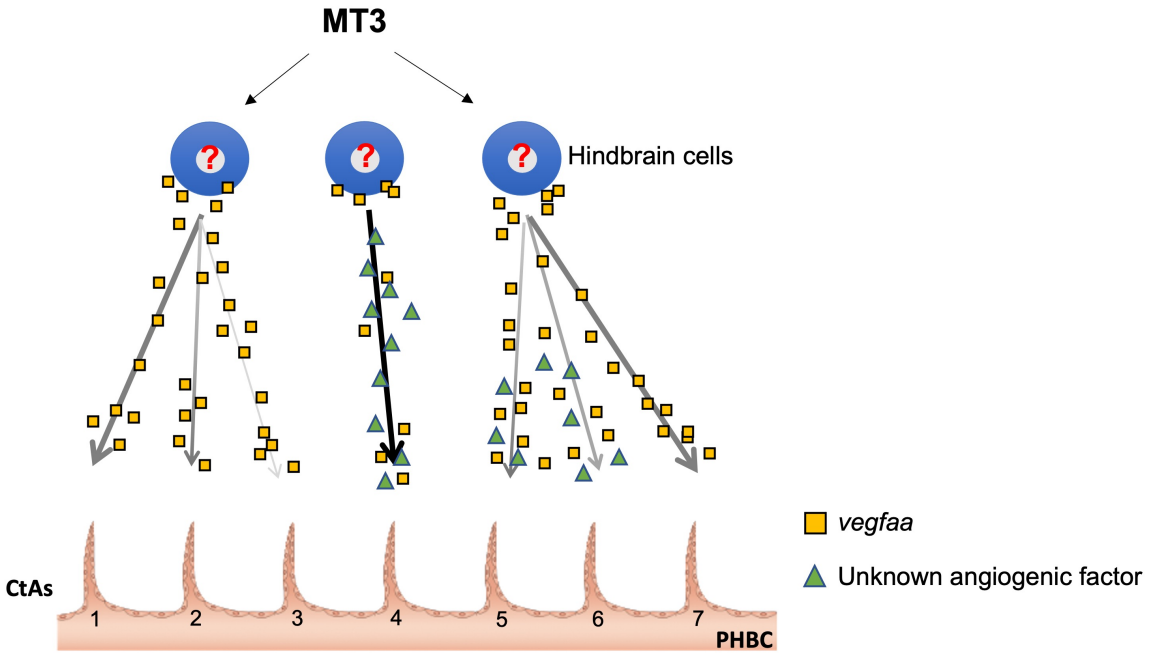

Figure 2.16 – Schematic representation of maternal T3 regulation on central arteries development. MT3 acts on specific hindbrain cells, that are responsible for the release of *vegfaa* and/or other angiogenic cues for central arteries (CtAs) ingression into the hindbrain. In MCT8MO zebrafish embryos, these MT3-dependent cells are absent and impairs CtAs development. The dependency on MT3 signalling for CtA development is indicated by colour-shaded arrows. Dark-coloured arrows for more dependent and light-grey coloured arrows for less dependent. CtAs: Central arteries; MT3: maternal T3; PHBC: Primordial hindbrain channels.

2.5 MATERIALS AND METHODS

2.5.1 Zebrafish maintenance

Adult wildtype (AB strain) and transgenic *Tg(fli1:EGFP)* (Lawson and Weinstein, 2002) zebrafish were maintained in a ZebTEC zebrafish housing system (Tecniplast, Italy) at 28 ºC in a 14h/10h light/dark cycle, in a fish facility laboratory at CCMAR, in the University of Algarve (Faro, Portugal). The breeding stocks were fed twice a day with granulated food (Tetra granules, Germany) and once with *Artemia nauplii*. The night before egg collection, adult couples (wildtype × wildtype or wildtype × *Tg(fli1:EGFP)*) were placed in breeding tanks with a perforated bottom (Techniplast) and separated by a transparent barrier. The barrier was removed on the following day at the beginning of the light phase cycle. All experiments were

carried out in accordance with the EU Directive 2010/63/EU on the protection of animals used for scientific purposes.

2.5.2 Morpholino injection and sampling

Upon spawning, embryos were immediately collected and microinjected at the 1-2-cell stage with 1 nL of morpholino solution containing either 0.8 pmol CTRMO (control morpholino) or MCT8MO (*mct8* morpholino) (Gene Tools, USA) as described in Campinho et al., (2014). Embryos were distributed on plastic Petri dishes (∅ 100mm) containing E3 medium (5 mM NaCl, 0.17 mM KCl, 0.33 mM CaCl, 0.33 mM MgSO4) and reared until sampling time at 28.5 ºC in an incubator (Sanyo, Germany) under 12h:12h light:dark cycles. Staging was done after Kimmel et al., (1995) by observing developmental landmarks in CTRMO embryos.

2.5.3 T3 treatment

Upon spawning, embryos were immediately collected and distributed on plastic Petri dishes (∅ 100mm) containing E3 medium (5 mM NaCl, 0.17 mM KCl, 0.33 mM CaCl, 0.33 mM $MgSO_4$) and maintained at 28.5 ºC in an incubator (Sanyo, Germany). After 10 hours the experimental group embryos were transferred to E3 medium containing 20 μM 3,3',5-Triiodo-L-Thyronine (T3, Sigma-Aldrich, USA), while the control embryos were maintained in E3 medium. Embryos were reared until sampling time at 28.5 ºC in an incubator (Sanyo, Germany) under 12h:12h light:dark cycles. Staging was done after Kimmel et al., (1995) by observing developmental landmarks in control embryos.

2.5.4 Isolation of total RNA from experimental embryos for transcriptomic analysis

For each biological replicate (n = 7) experimental embryos (MCT8MO and CTRMO embryos) at 25hpf were manually dechorionated, pooled (~50 embryos per replicate) and preserved in RNAlater reagent (Sigma-Aldrich, USA) and stored at -20 °C until use.

Collected embryos were removed from RNAlater reagent and homogenised with a glass homogeniser and RNA was extracted using an E.Z.N.A® Total RNA extraction kit I (OMEGA Biotek, USA) as described by the manufacturer. Total RNA was subjected to DNase treatment using an Ambion Turbo DNA-free™ kit (Life Sciences, USA) as described by the manufacturer. The quality (RIN > 8) and quantity of total RNA were verified with a BIO-RAD Experion Total RNA chip following the manufacturer's instructions. Ten micrograms of total RNA per sample were shipped on dry ice to the Oklahoma Medical Research Foundation NGS core facility for Illumina RNA-seq sequencing (USA). One microgram of total RNA per sample was amplified using a TrueSeq stranded pair-end Illumina kit following the standard protocol. Sequencing of mRNA was conducted on an Illumina HiSeq instrument and 50 base paired-end reads were generated. cDNA libraries from each of the 14 biological samples (n = 7 CTRMO and n = 7 MCT8MO zebrafish at 25hpf) were randomized and then sequenced in two lanes of the HiSeq instrument, following an experimental balanced block design.

2.5.5 Transcriptome assembly, annotation and analysis

Quality control of raw reads and editing was performed with Trimgalore wrapper script version 0.3.3 (bioinformatics.babraham.ac.uk/projects/trim_galore) producing simple descriptive statistics and edited reads. Edited and cleaned reads were mapped to the zebrafish reference genome (zfish_GRCz10.80) with Tophat version 2.0.13 (Trapnell et al., 2013) using the sequence aligner bowtie2 version 2.2.4 (Langmead and Salzberg, 2012), and the fasta and respective annotation file (.gtf) were downloaded from the Ensembl Genome Browser (http://ensembl.org). Assembled transcripts and gene transcript estimated abundance were generated in the Cufflinks workflow, version 2.2.1 (Trapnell et al., 2013) and used to establish

differential gene expression using EdgeR version 3.12.1 (Robinson et al., 2009; Trapnell et al., 2013). Expression plots were designed using CummeRbund version 2.16.0.

Pathway analysis was carried out using the Reactome V58 (www.reactome.org) (Croft et al., 2014) curated pathway resource. Mapping of differentially expressed genes and their expression fold change between CTRMO and MCT8MO was established using human pathway data. Pathways under the regulation of MTH were taken to be significant at $p<0.05$.

2.5.6 qRT-PCR analysis of mRNA expression

Five independent biological replicates (n = 5), pools of 10 wildtype embryos each, were sampled at 28, 30, 32, 36, 40, 44, 48, 54 and 72 hpf for each experimental condition (MCT8MO and CTRMO). Embryos were manually dechorionated, snap-frozen in liquid nitrogen and stored at -80 ºC until use.

RNA from the embryos were extracted manually with a glass mortar and E.Z.N.A® Total RNA kit I (Omega Biotek, USA) following the manufactures instructions. In order to remove contaminating DNA, total RNA was then treated with Ambion Turbo DNA-free™ kit (Life Sciences, USA) as described by the manufacturer. Afterwards RNA concentration and purity were determined using a NanoDrop ND-1000 spectrophotometer (NanoDrop Technologies Inc., USA). RNA with an A250/A280 ratio between 1.8 – 2.2 was considered satisfactory and used for further analysis. RNA quality was visualised on a 1% agarose gel containing 1× TAE buffer stained with SYBR Green nucleic acid gel stain (Thermo Fisher Scientific, USA). Immediately before electrophoresis, 200 ng of RNA sample was mixed with 100% formamide in the amount giving a final concentration of at least 50% (v/v) formamide. The samples were denatured by heating for 5 min at 65 ºC, immediately chilled on ice for 5 min, and loaded on the agarose gel.

500 ng of purified total RNA was reverse transcribed to complementary DNA (cDNA) in 20 µL of reaction using RevertAid First Stranded cDNA Synthesis kit and random hexamer primer (Thermo Fisher Scientific, USA) following the manufacturer's instructions. cDNA quality was confirmed by amplification of 18S ribosomal RNA (Forward primer: 5’-TCAAGAACGAAAGTCGGAGG-3’ and Reverse primer: 5’-GGACATCTAAGGGCATCACA-3’) using DreamTaq DNA Polymerase (Thermo Fisher

Scientific, USA) according to the manufacturer's instructions. Afterwards, synthesized cDNA was diluted 1/5 in ultrapure water (Sigma-Aldrich, USA) and stored at -20 ºC.

Primers of the target genes were designed as follows: sequence variants obtained from RNAseq data were aligned in BioEdit (Hall, 2011) and primers were designed using Primer 3 Plus (Untergasser et al., 2012) in a common region of all sequence variance. Primers were produced by Stabvida (Portugal). Specificity and temperature optimization of primers for each gene was tested by PCR using DreamTaq DNA Polymerase (Thermo Fisher Scientific, USA) according to the manufacturer's instructions. Afterwards, PCR products were amplified, purified using E.Z.N.A. Gel Extraction kit (Omega Biotek, USA), quantified by NanoDrop ND-1000 spectrophotometer (NanoDrop Technologies Inc., USA), and sequenced at the Molecular Biology facility at CCMAR in the University of Algarve (Faro, Portugal) to confirm gene identity. Confirmed genes were used as templates for the standard curve. Table 2.2 provides primer sequences and amplicon size for each gene for quantitative real-time PCR (qRT-PCR) analysis.

Table 2.3 – List of primers for qRT-PCR analysis.

Gene		Sequence 5' → 3'	Product size (bp)	Efficiency (r^2)
cxcl12b	*Forward*	ACACACACACACTCGCTCTTG	188	100.7% (r^2=0.995)
	Reverse	GGGAGTGTGGAGGAACTTGAT		
cxcr4a	*Forward*	GGTCAGTCACGACTTCCAGAG	150	96.5% (r^2=0.998)
	Reverse	GAGAGGTGCAGACGGTACTTG		
notch1b	*Forward*	CCTGTCATACTGGAGCCACAT	149	83% (r^2=1.000)
	Reverse	GACTGGGTTGGTGTCACAGTT		
notch3	*Forward*	GCAGTAACAAGAACCGCAGAG	133	98.7% (r^2=0.998)
	Reverse	TTAGCCTCTGGGCAGTCTGTA		
nrp1a	*Forward*	ATTACAGCTCCAGGACCCAAC	105	97.9% (r^2=1.000)
	Reverse	GCCGTCTCTCACTTCCACATA		
robo4	*Forward*	GGGGGCACTAGACTGAGAGAC	170	96.2% (r^2=0.996)
	Reverse	GAGCGATACAGCACCTCAAAG		

Continuation of Table 2.3

Gene		Sequence 5' → 3'	Product size (bp)	Efficiency (r^2)
s1pr1	*Forward*	CTCTTCATCCTGCTCCTCCTT	132	98.6% (r^2=0.994)
	Reverse	GCTGGTCAGGGTGTAGATCAG		
slit2	*Forward*	GCATCAGTAACCCCTGTCAGA	169	97.3% (r^2=0.999)
	Reverse	ATACCGTCCACGCATGTAGAG		
slit3	*Forward*	AGAGGAGCATTTGAGGGTCTC	192	91% (r^2=1.000)
	Reverse	GTCCAGTTGCAGGTTCTTGAC		
vegfaa	*Forward*	TCTCCTCCATCTGTCTGCTGT	173	93.7% (r^2=0.999)
	Reverse	GGATGTACGTGTGCTCGATCT		
vegfab	*Forward*	CATACCGTCCTGTGTGGTTCT	81	81.4% (r^2=0.994)
	Reverse	CACCCTGATGACGAAGAGGT		

qRT-PCR for the target genes was performed in a CFX Touch Real-Time detection system (Bio-Rad, Portugal). Samples were run in a 384-well plate (Axygen, Life Sciences, USA) with 6 μL of reaction mixture per well. The final concentration of the reaction mixture consisted of 1 × SensiFAST™ SYBR, No-ROX Kit (Bioline, USA), 150 nM forward primer, 150 nM reverse primer, 1 μL cDNA (1/5), and ultrapure water (Sigma-Aldrich, USA). PCR cycling condition consisted of 95 ºC for 3 min, followed by 44 cycles of 95 ºC for 10 s and 60 ºC for 15 s. A standard melting curve was included, that consisted in a gradient temperature increment of 0.5 ºC for 5 s from 60 ºC to 95 ºC, to confirm the production of a single amplicon and the absence of primer dimers. A negative control was included to detect genomic DNA contamination. Each cDNA sample was run as two technical replicates and averaged for expression analysis. Every gene was analysed using a standard curve prepared from a purified PCR product of the target template and normalised to the input of the total RNA. Values are represented as fold change of relative gene expression between CTRMO and MCT8MO. PCR efficiency and coefficient of determination (r^2) were established and are listed in Table 2.2.

2.5.7 Riboprobe preparation

The *flt4* plasmid was kindly provided by Professor Schulte-Merker, the *rspo1*, *vegfaa* and *vegfab* plasmids were kindly provided by Professor Brant Weinstein and the *pdgfrb* plasmid was kindly provided by Professor Ching-Ling Lien. Five micrograms of plasmids were linearized with NotI (Thermo Fisher Scientific, USA) restriction enzyme followed by phenol-chloroform extraction, sodium acetate and ethanol precipitation. 300 ng of purified linearized plasmid were used to prepare Digoxigenin labelled antisense probes. These were synthesized by *in vitro* transcription with DIG RNA Labelling mix (Roche, Switzerland) and RNA polymerase (Fermentas, USA) according to the manufacturer's instructions. Integrity of probes was determined by gel electrophoresis and stored in 50% RNAlater (Sigma-Aldrich, USA) at -20 ºC.

2.5.8 Whole-mount *in situ* hybridization (WISH)

WISH was carried out according to Thisse and Thisse (2008) with adaptations. One-cell stage embryos microinjected with either 0.8 pmol CTRMO or 0.8 pmol MCT8MO, were fixed at selected stages in ice-cold 4% paraformaldehyde (PFA)/1×PBS overnight at 4 ºC. Samples were washed 2 × 5 min in 1×PBS/0.1% Tween-20 (1×PBT), depigmented with 0.3% H_2O_2/0.5% KOH/1×PBS, transferred into 100% methanol (MeOH) and stored at -20 ºC until use. Samples were brought to room temperature and hydrated through a graded series of MeOH/1×PBS (100% to 0% MeOH) and afterwards washed 3 × 5 min in PBT. Embryos were permeabilized by digestion with proteinase K (1 μg/ml) in 1×PBS from 1 to 15 min, depending on the embryonic stage. Proteinase K digestion was stopped by incubating the embryos for 20 min in 4% PFA/1×PBS. Samples were washed 4 × 5 min with PBT to remove the residual PFA and then pre-hybridized for 3 hours at 68 ºC in pre-heated hybridization mix (HybMix). HybMix was discarded and replaced with pre-heated HybMix containing 0.25 ng/ml of Dig-labelled cRNA probe and hybridised overnight at 68 ºC. Samples were subjected through a series of stringency washes at 68 ºC for 10 min in Hyb(–)/2×SSC (75%, 50% and 25% of Hyb(–)), 2×SSC/0.1% Tween-20 and finally washed twice in 0.2×SSC/0.1% Tween-20 (0.2×SSCT) for 30 minutes. Samples were then washed through a graded series in 0.2×SSCT/Malic acid buffer

(MAB, Sigma-Aldrich, USA) (75%, 50% and 25% of 0.2×SSCT) and then washed 3 × 10 min in MAB/0.1% Triton X-100 (MABTr, Sigma-Aldrich, USA). Embryos were preincubated in blocking solution MAB/0.1% Triton X-100/10% sheep serum (Sigma-Aldrich, USA)/2% Blocking solution (Roche, Switzerland) for 2 hours at room temperature. Afterwards, the blocking solution was discarded and replaced with blocking solution containing anti-Dig-AP Fab fragments serum (1/5000, Roche, Switzerland) and incubated overnight at 4 ºC. Samples were washed 6 × 30 min in MABTr. Afterwards, embryos were washed 3 × 5 min in staining buffer (100 mM Tris HCl pH 9.5, 50 mM $MgCl_2$,100 mM NaCl, 2 mM Levimasol and 0.1% Tween-20) and then incubated with labelling solution containing nitro blue tetrazolium (NBT)/bromo-chloro-indolyl-phosphate (BCIP) diluted in staining solution for colour development. When the desired staining intensity was reached, the reaction was stopped by washing the samples in stop solution (1× PBS pH 5.5, 1 mM EDTA, 0.1% Tween-20). For image analysis samples were transferred to 100% glycerol and photographed under a stereoscope (Olympus) coupled to an OPTICA 3.0 digital colour camera. At least ten animals per stage and experimental condition were analysed.

2.5.9 Fluorescent immunohistochemistry (IHC)

One-cell stage embryos microinjected with either 0.8 pmol CTRMO or 0.8 pmol MCT8MO, were fixed at selected stages in ice-cold 4% PFA/1×PBS overnight at 4 ºC. Samples were washed 2 × 5 min in 1×PBT, depigmented with 0.3% H_2O_2/0.5% KOH/1×PBS, transferred into 100% MeOH and stored at -20 ºC until use. Samples were brought to room temperature and hydrated through a graded series of MeOH/1×PBS (75%, 50%, and 25% MeOH) for 5 min each, followed by 3 × 5 minutes in 1×PBS/0.1% Triton X-100 (Sigma-Aldrich, USA). Embryos were preincubated in 1×PBS/10% sheep serum (Sigma Aldrich, USA) /0.5% Triton X-100 at room temperature for 3 hours. Samples were incubated overnight at 4 ºC in rabbit anti-GFP (1/1000, abcam, UK) primary antibody diluted in preincubation solution. Embryos were washed 6 × 30 minutes in 1×PBS/0.5% Triton X-100 (PBTr0.5%) and then blocked for 1 hour with preincubation solution. Samples were incubated overnight at 4 ºC in goat-anti-rabbit 488HL (1/400, Jackson Laboratory, USA) secondary antibody and then washed 6 × 30 minutes in PBTr0.5%. Afterwards, samples were transferred to 100% glycerol and imaged using a

fluorescent stereoscope (Olympus) coupled to an OPTICA 3.0 digital colour camera. At least ten animals per stage and experimental condition were analysed.

2.5.10 Fluorescent whole-mount *in situ* hybridization with immunohistochemistry

WISH was performed as described previously using *Tg(fli1:EGFP)* positive samples at 32, 36 and 48 hpf with some minor modifications. After the overnight incubation with blocking solution containing anti-Dig-AP Fab fragments serum (1/5000, Roche, Switzerland), samples were subjected to probe detection. **For *pdgfrb* probe detection:** Samples were washed 6 × 30 min in MABTr. Afterwards, samples were incubated in FastRed TR/ Naphthol AS-MX tablets (Sigma-Aldrich, USA) for colour development, according to the manufacturer's instructions, followed by several washes in PBT. **For *vegfaa* probe detection:** Samples were washed 2 × 30 min in MABTr. Afterwards, samples were washed 4 × 30 min with PBT. Probe detection was performed by incubating the samples in fluorescein Tyramide 1:100 in amplification reagent (Perkin Elmer, USA) for fluorescent colour development, according to the manufacturer's instructions, followed by several washes in PBT.

For the immunohistochemistry, the samples were re-fixated in 4% PFA/1×PBS for 15 min and then washed 4 × 15 min in PBT. Embryos were preincubated in 1×PBS/10% sheep serum/0.5% Triton X-100 at room temperature for 1:30 hours. Samples were incubated overnight at 4 ºC with rabbit anti-GFP (1/500, abcam, UK) primary antibody diluted in preincubation solution. Samples were washed 6 × 30 minutes in 1×PBS/0.5% Triton X-100 (PBTr0.5%) and then blocked for 1 hour with preincubation solution. **Samples detected with *pdgfrb* probe:** Samples were incubated overnight at 4 ºC with goat anti-rabbit IgG-488 HL (1:400, Jackson Labs) fluorescent labelling secondary antibody. **Samples detected with *vegfaa* probe:** Samples were incubated overnight at 4 ºC with goat anti-rabbit 594 (1:400, Sigma-Aldrich, USA). Samples were then washed 6 × 30 minutes in PBTr0.5%.

Fluorescent imaging of the hindbrain was carried out using a Zeiss Z2 microscope coupled to a Zeiss digital camera or a Lighsheet Z1 microscope (Zeiss, Germany). Samples for Z2 imaging were mounted in 0.3% agarose (Sigma-Aldrich, USA) and imaged using a 20× lens and a z step of 0.850 μm. Afterwards, images were deconvoluted in SCI Huygens software 4.4 (Scientific

Volume Imaging, The Netherlands, http://svi.nl). Maximum projections were generated in Fiji (Schindelin et al., 2012). Samples for Z1 imaging were mounted in 1% low melt agarose (CarlRoth, Germany) and imaged using a 10× lens, dual illumination and a z step of 1.5 μm (optimal distance option) to acquire the complete hindbrain using 1× zoom. After image acquisition, dual illumination images were merged using Dual side Fusion (Zen Black, Zeiss, Germany). Images were then imported into Fiji (Schindelin et al., 2012) and analysed.

2.5.11 Rescue experiments

Rescue experiments were carried out for *mct8* mutant mRNA (insertion of 5 silence mutations on the MCT8MO target region) and *vegfaa*-165 mRNA. One-cell stage embryos were injected with either 0.8 pmol CTRMO, 0.8 pmol MCT8MO or 0.8 pmol MCT8MO + 100 pg *mct8* or *vegfaa-165* mRNA as described in Campinho et al., (2014). Production of *mct8* mutant mRNA is described in Campinho et al., (2014). The *vegfaa-165* gene was isolated from the pCR®4-TOPO plasmid using EcoRI (Thermo Fisher Scientific, USA) restriction enzyme according to the manufacturer's instruction and then cloned into the pCS2+ plasmid. Insert orientation was confirmed and afterwards 5 μg of pCS2+ *vegfaa-165* were linearized with NotI (Thermo Fisher Scientific, USA) restriction enzyme and purified by phenol-chloroform, sodium acetate and ethanol precipitation. 1 μg of the linearized pCS2+ *vegfaa-165* was used as the template for *in vitro* transcription using the mMESSAGE mMACHINE® Kit (Ambion, UK) following the manufacturer's instructions. mRNA was quantified and stored at -80 ºC until use.

2.5.12 Statistical analysis

Student's t-test was performed to determine significant differences in absolute expression levels by qRT-PCR analysis between CTRMO and MCT8MO groups in stage-specific time points. Fisher's exact test was performed to determine the frequency of *vegfaa* expression or CtA development between experimental groups in stage-specific time points. One-way ANOVA was performed in order to determine significant differences between 3 experimental groups.

Data analysis was performed using GraphPad Prism version 8.4.0 software for Mac (San Diego, USA, www.graphpad.com).

2.5.13 Data availability

All RNA-seq data generated is available through the BioProjects portal at the NCBI website with the accession number PRJNA381309.

CHAPTER 3

Is blood-hindbrain barrier development regulated by maternal T3-dependent hindbrain neurons?

ABSTRACT

Maternally derived T3 (MT3) is crucial for embryonic neurodevelopment. Impaired MT3 transport causes several neurological impairments in offspring. The most severe condition observed in humans is caused by mutations in the specific thyroid hormone (TH) transporter *monocarboxylate transporter 8* (*MCT8*) gene, which causes the Allan-Herndon-Dudley syndrome (AHDS) in males. Patients with this syndrome present a severely underdeveloped central nervous system (CNS) with cognitive and locomotor impairments. Using the zebrafish as a model, knockdown of the Mct8 transporter phenocopies the symptoms observed in AHDS patients. In the zebrafish AHDS model, the findings of underdeveloped vascularisation of the hindbrain have been reported. That suggests an unreported consequence of impaired MT3 signalling in AHDS patients is likely impaired brain vascularisation. However, how this occurs and the cells mediating brain vascularisation are unknown. Moreover, this evidence suggests an unknown function of MT3 in CNS development.

Developing a CNS-specific vasculature during embryogenesis requires cross-talk between the developing nervous tissue and specialised endothelial cells. Several studies have reported that vascular deficiency causes neurodegeneration and dementia. In zebrafish, vascular development is regulated by *vascular endothelial growth factor aa* (*vegfaa*) signalling. Previous studies on zebrafish spinal cord vascularisation have pointed to neurons as the source of attraction of blood vessels into the CNS. Here we exploit the hypothesis that MT3-dependent neurons are the cells instructing the ingression of hindbrain vessels. We use different genetic models to demonstrate that hindbrain neurons, in close physical proximity to sprouting hindbrain central arteries (CtAs), were not responsible for instructing blood-hindbrain barrier (BHB) development.

3.1 INTRODUCTION

Formation of the vascular system during vertebrate embryonic development is fundamental, as it permits the delivery of oxygen and nutrients to all tissues and organs, ensuring proper growth and function of the organism (Larrivée et al., 2009). In the central nervous system (CNS), adequate vascular network patterning is required for its development and neuronal survival, while disturbance results in neuronal dysfunction (James and Mukouyama, 2011; Zacchigna et al., 2008). During vascular development, the Vascular endothelial growth factor A (Vegfa) plays a pivotal role (Álvarez-Aznar et al., 2017; Koch and Claesson-Welsh, 2012).

During embryonic development, the CNS is vascularised by sprouting angiogenesis from the surrounding perineural vascular plexus (PNVP) (Ruhrberg and Bautch, 2013). In several vertebrate species, such as chicken, mouse, and zebrafish, the initial formation of the PNVP and the sprouting of the blood vessels into the neural tissue is promoted by neural progenitor cells that secret Vegf-A (Hogan et al., 2004; James et al., 2009; Matsuoka et al., 2017). After the ingression of the blood vessels into the neural tissues, blood vessels sprout and grow in a very precise manner and location by following a defined path for blood vessel patterning. However, the cells and signalling mechanism involved in this blood vessel patterning remains largely unknown (Himmels et al., 2017; Takahashi et al., 2015). In the developing spinal cord of chicken and quail embryos, studies have shown that the invading blood vessels tend to avoid the neural progenitor zone and migrate toward the differentiation zone (Takahashi et al., 2015). In the developing spinal cord of mice embryos, *Vegf* was expressed uniformly at the beginning of spinal cord vascularisation (E9.5). But between E10.5 – E12.5, this expression pattern in the ventral spinal cord becomes restricted to neuronal progenitor and differentiated neuron domains, such as motor neuron columns (Himmels et al., 2017). These motor neurons regulate blood vessel sprouting in a precise and coordinated manner, as they express *Vegf* for blood vessel invasion and growth but also regulate the timing as they express a soluble form of VEGF receptor-1 (*sFlt1*) to prevent premature blood vessel ingression into the motor neuron columns (Himmels et al., 2017). This has also been observed during zebrafish spinal cord vascularisation (Wild et al., 2017). Spinal cord neurons in the neural tube regulate venous intersegmental vessel (ISV) sprouting by regulating the expression of neuronal-derived *vegfaa* and *sflt1* (Wild et al., 2017). This mechanism of attractive and repulsive angiogenic guidance cues promoted by the same cellular source shows that the proper temporal and spatial vascularisation of the CNS is crucial (Himmels et al., 2017).

Thyroid hormones (THs) are essential for brain development and function (Williams, 2008). In humans, an inadequate supply of T3 during prenatal stages causes several neurological impairments, affecting newborns' psychomotor and cognitive development if not adequate treatment is undertaken (de Escobar et al., 2004; Zoeller and Rovet, 2004). These conditions include iodine deficiency, maternal hypothyroxinaemia and hypothyroidism, congenital hypothyroidism, nuclear T3 receptor mutations or TH transporter mutations (Bernal, 2022; de Escobar et al., 2004; Zoeller and Rovet, 2004). Mutations in the TH transporter *monocarboxylate transporter 8* (*MCT8*) gene cause one of the most severe conditions of TH deficiency, known as the Allan-Herndon-Dudley syndrome (AHDS) (Schwartz et al., 2005). This rare disease results in brain morphological changes, delayed cerebral cortex and cerebellum maturation, hypomyelination, altered neuronal differentiation, and deficient synaptogenesis (López-Espíndola et al., 2014).

The zebrafish has become a valid model organism to study the developmental effects of Mct8-deficiency (Campinho et al., 2014; Silva et al., 2017; Vatine et al., 2013; Zada et al., 2017). This zebrafish model of AHDS phenocopies the neurological and locomotor impairments observed in human AHDS patients (Campinho et al., 2014; De Vrieze et al., 2014). Additionally, an impaired blood-hindbrain barrier (BHB) was observed in the developing zebrafish embryo, affecting the ingression of several central arteries (CtAs) into the zebrafish hindbrain (Campinho et al., 2014, Chapter 2). Previously we showed that maternal T3 (MT3) acting through Mct8 affects the CtA sprouting mechanism by regulating the expression of *vegfaa* (Chapter 2). However, the cells responsible for the expression of *vegfaa*, and thus mediating CtA sprouting from the venous primordial hindbrain channels (PHBC), remain to be elucidated. Is MT3 acting on hindbrain neurons, like spinal cord neurons, responsible for vascularising the zebrafish trunk?

In this Chapter, we used the Mct8 knockdown AHDS model to exploit the hypothesis that the loss of specific MT3-dependent hindbrain neurons is responsible for impaired BHB development. Cell-specific zebrafish reporter lines for *pax8* (Ikenaga et al., 2011) and *copine4* (*cpne4*) (Cowland et al., 2003; Creutz et al., 1998; Molyneaux et al., 2009) were used to question the involvement of MT3-dependent neurons in the ingression of the CtAs during BHB development. The outcome of this study indicated that MT3 regulates *pax8* and *cpne4* cells, but these cells were not involved in the attraction of the CtAs during BHB development. This study suggests that in zebrafish, the mechanism involved in the attraction of blood vessels differs between the spinal cord and the hindbrain.

3.2 RESULTS

3.2.1 Maternal T3-dependent *pax8* expression is not responsible for central arteries development

Previously Campinho et al., (2014) found that a key neuronal hindbrain population dependent on MT3 to develop were *pax8* interneurons. These neurons occupy positions that are topologically close to developing CtAs. Therefore, we argued that *pax8* positive (+) neurons could be the source of signalling involved in the ingression of CtAs into the hindbrain.

Pax8 is a transcription factor that belongs to the Paired box (Pax) family that influences cell lineage specification of glycinergic and GABAergic inhibitory interneurons (Batista and Lewis, 2008; Blake and Ziman, 2014). *pax8* is expressed early during zebrafish development (10 hpf) (Feijóo et al., 2009), and in the hindbrain, the first *pax8*-expressing cells were detected at 31 hpf (Campinho et al., 2014), a time point that precedes the first CtA sprouts from the PHBC (Ulrich et al., 2011). Previous studies have shown that knockdown of the Mct8 transporter by a morpholino (MO)-based system reduced the expression of *pax8* in the midbrain-hindbrain boundary (MHB) and the hindbrain at 31 hpf. This expression was mostly absent in MCT8MO zebrafish embryos at 48 hpf (Campinho et al., 2014). To understand if there is a relationship between *pax8* and the developing CtAs, the transgenic zebrafish line *Tg(fli1:EGFP)* (Lawson and Weinstein, 2002) was used to visualise the hindbrain vascular structures during three time points of BHB development. Namely at 32 hpf, which is the beginning of the sprouting of the first CtA; 36 hpf, an intermediate stage where usually three CtAs ingress the hindbrain; and 48 hpf, a time point where all seven CtAs have formed and the BHB is fully developed (Quiñonez-Silvero et al., 2020; Ulrich et al., 2011). In CTRMO embryos, *pax8* expression at 32 and 36 hpf was located in the posterior region of the hindbrain and in the MHB (Fig. 3.1). At 48 hpf, *pax8* was expressed in the hindbrain juxtaposed to CtAs 4 to 7. Some *pax8* expression was located near CtA 3, but it was not juxtaposed to the CtA, as it occurs for CtAs 4 to 7 (Fig. 3.1 A1). In MCT8MO embryos, some *pax8* expression was detected at 32 and 36 hpf in the MHB, but in the hindbrain, only at 48 hpf *pax8* expression was present but in a more reduced expression field. Most of the remaining *pax8*-expressing cells were located more ventrally in MCT8MO embryos than in CTRMO embryos, suggesting a spatial redistribution of these cells and likely a different identity and function of these cells (Fig. 3.1 A and B). That observation suggests a

relation between the lack of or reduced *pax8* expression in the posterior region of the hindbrain in MCT8MO zebrafish embryos and the lack of sprouting CtAs from rhombomeres 4 to 7.

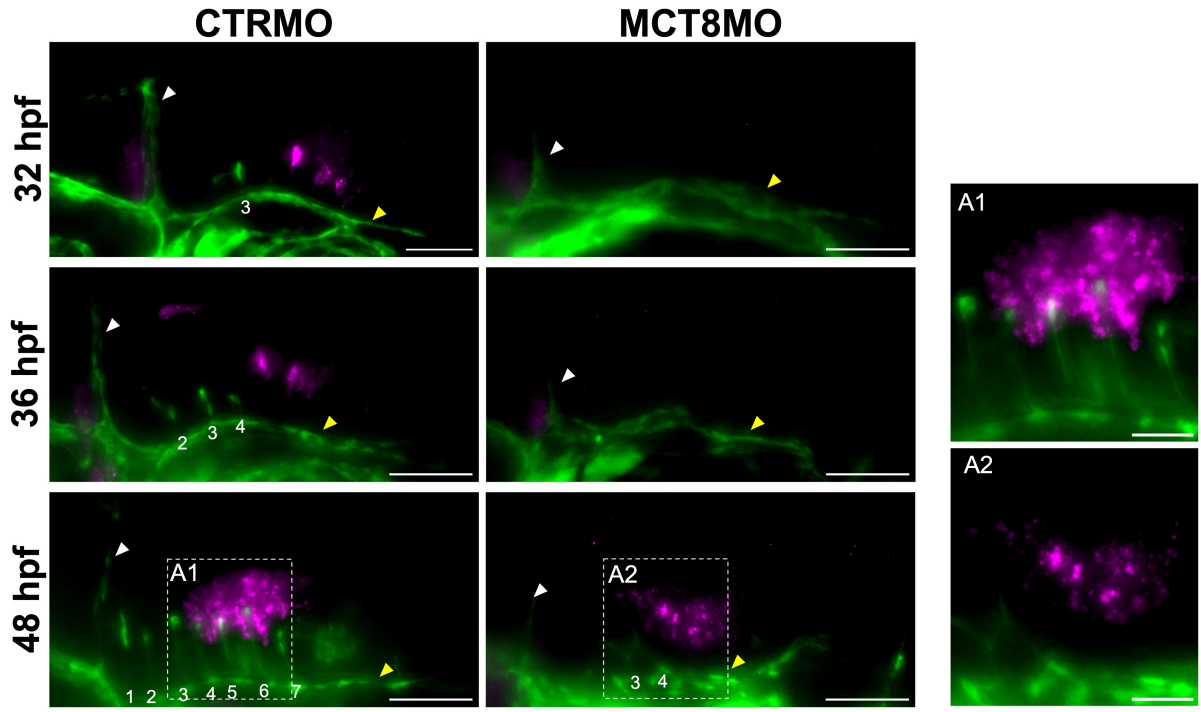

Figure 3.1 – *pax8* expression is downregulated in MCT8MO zebrafish embryos. Lateral view of fluorescent maximum projections of the hindbrain vasculature structures at 32, 36 and 48 hpf in *Tg(fli1:EGFP)* (endothelial cell marker – green colour) submitted to whole-mount *in situ* hybridization (WISH) of *pax8* (magenta colour) in CTRMO and MCT8MO zebrafish embryos are shown. In CTRMO zebrafish embryos *pax8* expression appears in the posterior hindbrain region, juxtaposed to CtAs 4 to 7. In MCT8MO zebrafish embryos *pax8* expression was clearly reduced and only appears at 48 hpf. The white arrowhead indicates the mid-cerebral vein (MCeV), and the yellow arrowhead indicates the primordial hindbrain channels (PHBC). White numbers 1 – 7 indicate the developed CtA in its respective rhombomere. n = 9 – 18. Scale bar: 50 µm. Magnification of the selected area in 48 hpf **A1)** CTRMO and **A2)** MCT8MO embryos are shown. Scale bar: 20 µm.

To understand if *pax8*-neurons are involved in CtA development, the transgenic *Tg(pax8:DsRed)* zebrafish line (Ikenaga et al., 2011) was used to knockout *pax8* gene function. In this transgenic zebrafish line, homozygous embryos lose Pax8 function and are considered hypomorph *pax8*$^{-/-}$ mutant embryos (Ikenaga et al., 2011). Whole-mount *in situ* hybridization (WISH) analysis between heterozygous *pax8*$^{+/-}$ (control) and hypomorph *pax8*$^{-/-}$ embryos for the *vascular endothelial cadherin* (*VE-cadherin* or *cadherin-5*), which is expressed specifically in endothelial cells, shows that *pax8*$^{-/-}$ hypomorph mutants developed a normal BHB (Fig. 3.2

A). Comparison analysis of the length of the PHBC (Fig. 3.2 B) and CtAs (Fig. 3.2 C) between control *pax8*$^{+/-}$ and hypomorph *pax8*$^{-/-}$ mutant embryos showed no significant differences between them, except for CtA 7. However, CtA 7 is usually the last to develop (Ulrich et al., 2011) and that can lead to variance in its length at 48 hpf. These results demonstrate that *pax8*-neurons are not involved in BHB development.

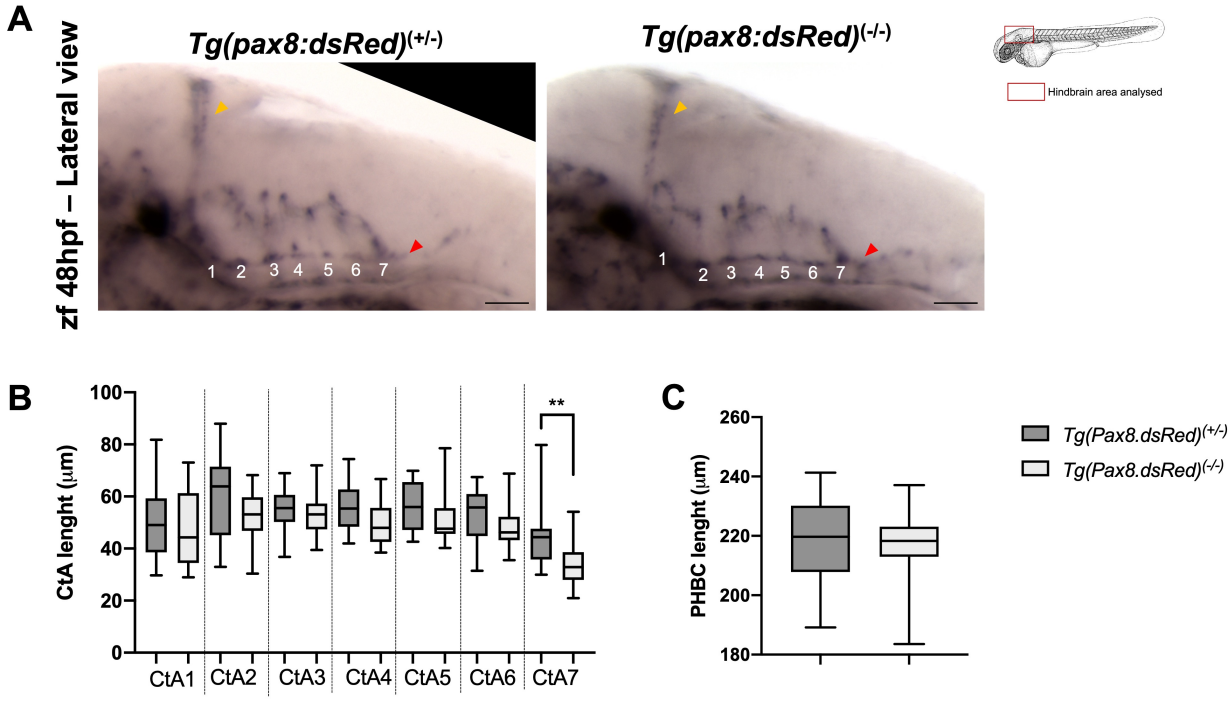

Figure 3.2 – *pax8*-neurons are not involved in BHB development. A) Lateral view of the hindbrain of *Tg(pax8:dsRed)*$^{+/-}$ (heterozygote – control *pax8*$^{+/-}$) and *Tg(pax8:dsRed)*$^{-/-}$ (homozygote – hypomorph *pax8*$^{-/-}$ mutant) zebrafish embryos submitted to WISH with *cadherin-5* at 48 hpf are represented. All 7 CtAs were present in control *pax8*$^{+/-}$ and hypomorph *pax8*$^{-/-}$ zebrafish embryos. The yellow arrowhead indicates the mid-cerebral vein (MCeV), and the red arrowhead indicates the primordial hindbrain channels (PHBC). White numbers 1 – 7 indicate the developed CtA in its respective rhombomere. Scale bar: 50 µm. Image J software was used to measure the length of **B)** each CtA and **C)** the PHBC between control *pax8*$^{+/-}$ and hypomorph *pax8*$^{-/-}$ zebrafish embryos. Statistical significance was determined using unpaired t-test (Mann-Whitney test) (n = 14 – 18). ** $p<0.01$.

3.2.2 Inhibitory interneurons are unlikely involved in central arteries development

Since *pax8* gene function was lost in hypomorph *pax8*$^{-/-}$ mutant embryos and they developed a normal BHB, this raises the question of whether other glycinergic and GABAergic interneurons (from now on called "inhibitory") in the hindbrain can be behind CtA ingression. For that, we conducted double WISH for DsRed (*pax8* lineage marker), *gad67a* and *gad67b* (GABAergic markers) and *glyt2a* and *glyt2b* (glycinergic markers) in 48 hpf control *pax8*$^{+/-}$ and hypomorph *pax8*$^{-/-}$ mutant zebrafish embryos. The GABAergic and glycinergic markers are, from now on denominated as inhibitory cell markers. In the *pax8*$^{-/-}$ hypomorph mutants, DsRed expressing cells were not lost but reduced compared to control *pax8*$^{+/-}$ zebrafish embryos (Fig. 3.4 A). In control, *pax8*$^{+/-}$ embryos, colocalisation between DsRed expressing cells and inhibitory cells can be observed, while in hypomorph *pax8*$^{-/-}$ mutant zebrafish embryos, most of this colocation was lost (Fig. 3.3 A). That indicates that the remaining DsRed cells in *pax8*$^{-/-}$ mutants are likely not neurons. We used the confined displacement algorithm (CDA) for colocalisation significance analysis to compute the Pearson correlation coefficient between control *pax8*$^{+/-}$ and hypomorph *pax8*$^{-/-}$ mutant zebrafish embryos. The distribution of correlation coefficients in the control *pax8*$^{+/-}$ group follows a weak positive correlation [0.0107 – 0.1280], while the hypomorph *pax8*$^{-/-}$ mutant group follows a weak negative correlation [0.0432 – -0.1503] (Fig. 3.3 B). This result suggests that the inhibitory cell fate in hypomorph *pax8*$^{-/-}$ mutant embryos has diverged from that of the control *pax8*$^{+/-}$ zebrafish embryos. These results indicate that, although the inhibitory cell fate may have changed, it does not seem to affect CtA development, indicating that these cells are not responsible for CtA ingression into the hindbrain.

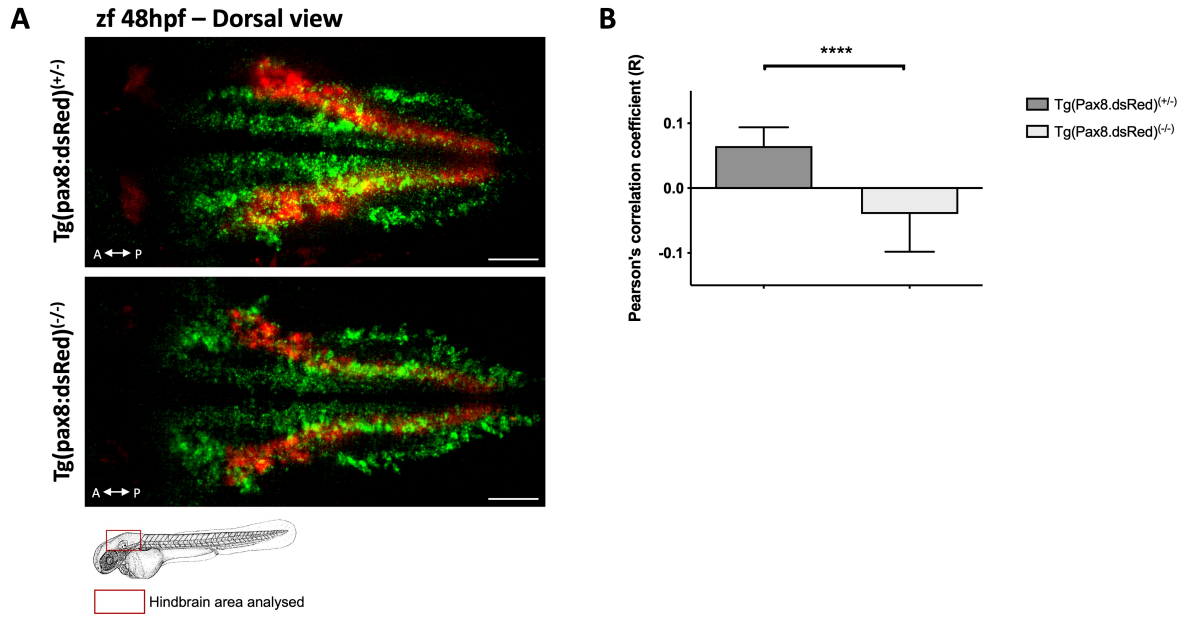

Figure 3.3 – Inhibition of *pax8* gene function modifies cell fate determination of the inhibitory interneurons. A) Dorsal view of fluorescent maximum projection images of the hindbrain of *Tg(pax8:DsRed)*$^{+/-}$ (heterozygote – control embryo) and *Tg(pax8:DsRed)*$^{-/-}$ (homozygote – hypomorph mutant embryo) zebrafish embryos at 48 hpf are represented. Embryos were submitted to double WISH for markers of DsRed (*pax8* lineage marker – red colour), glycinergic (glyt2A and glyt2B) and GABAergic (GAD67A and GAD76B) (labelled "inhibitory", probes were mixed – green colour). Scale bar: 50 µm. **B)** Image j plugin for Confined displacement algorithm (CDA) was used to analyse colocalisation significance to compute the Pearson correlation coefficient between control *pax8*$^{+/-}$ and hypomorph *pax8*$^{-/-}$ mutant zebrafish embryos. Results show a weak positive correlation of DsRed cells with inhibitory cells in the control group [0.0107 – 0.1280], and a weak negative correlation in the hypomorph *pax8*$^{-/-}$ mutant group [0.0432 - -0.1503]. Statistical significance was determined using Fisher's exact test (n = 7 – 11). ** $p<0.01$; $p<0.001$; **** $p<0.0001$.

3.2.3 MT3 regulates *cpne4* hindbrain cells

Given that *pax8*-neurons do not seem important for CtAs ingression, we argued that another neuron population might be responsible for instructing BHB development.

During a screening program for transgenic zebrafish lines from the Kawakami Laboratory (Japan), we accessed a transgenic zebrafish line generated by *Tol2*-based gene trap and enhancer trap constructs (Kawakami et al., 2010) named *gSA2AzGFF306A*. This zebrafish line expresses GFP under the regulatory region of the native *cpne4* promoter (https://shigen.nig.ac.jp/zebrafish/strain/strainTopJa.jsp). In 48 hpf zebrafish embryos, GFP

expression has been found in cells in the hindbrain, spinal cord, eye and fin (https://ztrap.nig.ac.jp/ztrap/). In an initial study conducted by the host lab, zebrafish *gSA2AzGFF306A* embryos were treated with 20 μM 3,3',5-Triiodo-L-Thyronine (T3, Sigma) at 10 hpf until 48 hpf. Densitometry analysis of the spinal cord and hindbrain between untreated and T3-treated zebrafish embryos showed a significant decrease in GFP expression in the spinal cord but not in the hindbrain (unpublished result from Campinho, M.). This showed that the Cpne4/GFP-positive (+) cells were responsive to T3. Notably, in the hindbrain, Cpne4/GFP(+) cells were located in the same spatial region where ingression of the CtAs occurs. Given these results, we argued if these Cpne4 cells could constitute the neuronal cell population responsible for CtAs ingression.

To understand if these Cpne4/GFP(+) cells are involved in MT3-dependent BHB development, double-transgenic zebrafish embryos expressing GFP under the regulation of the *cpne4* promoter (https://shigen.nig.ac.jp/zebrafish/strain/strainTopJa.jsp) and mCherry in endothelial cells under the regulation of the *kdrl* promoter (Fujita et al., 2011) was used. In the hindbrain of CTRMO embryos, Cpne4/GFP(+) cells were located dorsally to the PHBCs and juxtaposed to the developing CtAs (Fig. 3.4 A). It is visible that the number of Cpne4/GFP(+) cells increases over development in CTRMO embryos (Fig. 3.4 A and B). In MCT8MO embryos at 36 hpf, the number of Cpne4/GFP(+) cells reduced significantly in rhombomeres 5 and 7, compared to CTRMO embryos (Fig. 3.4 B). That was also evident at 48 hpf, where the number of Cpne4/GFP(+) cells was significantly reduced in rhombomeres 2, 4, 5, 6 and 7 (Fig. 3.4 B). Given the close location of these cells with the CtAs and the fact that these cells were significantly reduced in MCT8MO embryos, the correlation between the presence of Cpne4/GFP(+) cells and the presence of CtAs in CTRMO and MCT8MO at 48 hpf was analysed. The data showed a positive correlation between Cpne4/GFP(+) cells and the development of CtAs 4, 6 and 7 in the hindbrain (Fig. 3.4 C).

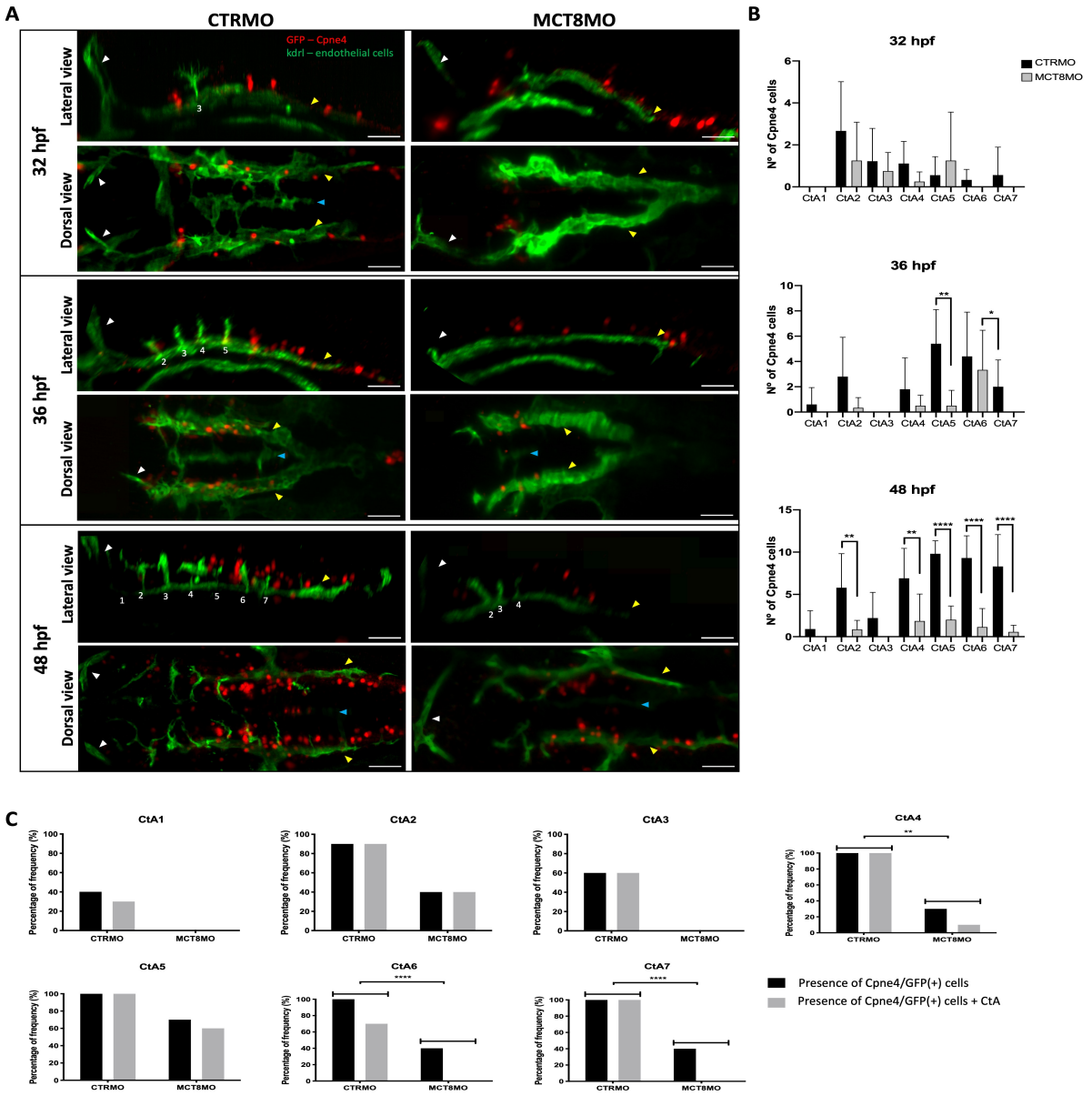

Figure 3.4 – MT3 regulates Cpne4 cells during BHB development. A) Maximum projection of the hindbrain vasculature structures in double transgenic zebrafish embryos expressing mCherry (endothelial cell marker – green colour) and GFP (Cpne4 cells – red colour) submitted to double IHC are shown. In CTRMO zebrafish embryos, Cpne4/GFP(+) cells were in close contact with the central arteries (CtAs), while in MCT8MO zebrafish embryos some Cpne4/GFP(+) cells were lost. The white arrowhead indicates the mid-cerebral vein (MCeV), the yellow arrowhead indicates the primordial hindbrain channels (PHBC), and the blue arrowhead indicates the basilar artery (BA). White numbers 1 – 7 indicate the developed CtA in its respective rhombomere. Scale bar: 50 µm. **B)** The number of Cpne4/GFP(+) cells between CTRMO and MCT8MO zebrafish embryos was analysed at 32, 36 and 48 hpf. Statistical significance was determined by Unpaired t-test (n = 7 – 11). **C)** Graphical view of the correlation between the presence of Cpne4/GFP(+) cells and the presence of each CtAs in CTRMO and MCT8MO at 48 hpf, shows that a correlation between these two conditions exists for CtAs 4, 6 and 7. Statistical significance was determined using Fisher's exact test (n = 7 – 11). * $p<0.05$; ** $p<0.01$; **** $p<0.0001$.

We then further characterised these hindbrain Cpne4/GFP(+) cells. Cpne4 is expressed in human brain tissue (Cowland et al., 2003), and in mice, it is involved in developing the callosal projection neurons during neurodevelopment (Molyneaux et al., 2009). First, we aimed to characterise these cells in zebrafish by using specific cell markers for neurons (labelling HuC proteins), glial cells (labelling glial fibrillary acidic protein (GFAP) also called ZRF-1) and radial glial progenitor cells (*pax6a*). Cpne4/GFP(+) cells colocalise mostly posteriorly and ipsilaterally in the hindbrain, at 32 and 36 hpf, with the mature neurons marker HuC (Fig. 3.5 A). No colocation of these cells was observed when labelled with ZRF-1 (Fig. 3.5 B) or *pax6a* (Fig. 3.5 C). This evidence confirms that Cpne4/GFP(+) cells are post-mitotic neurons.

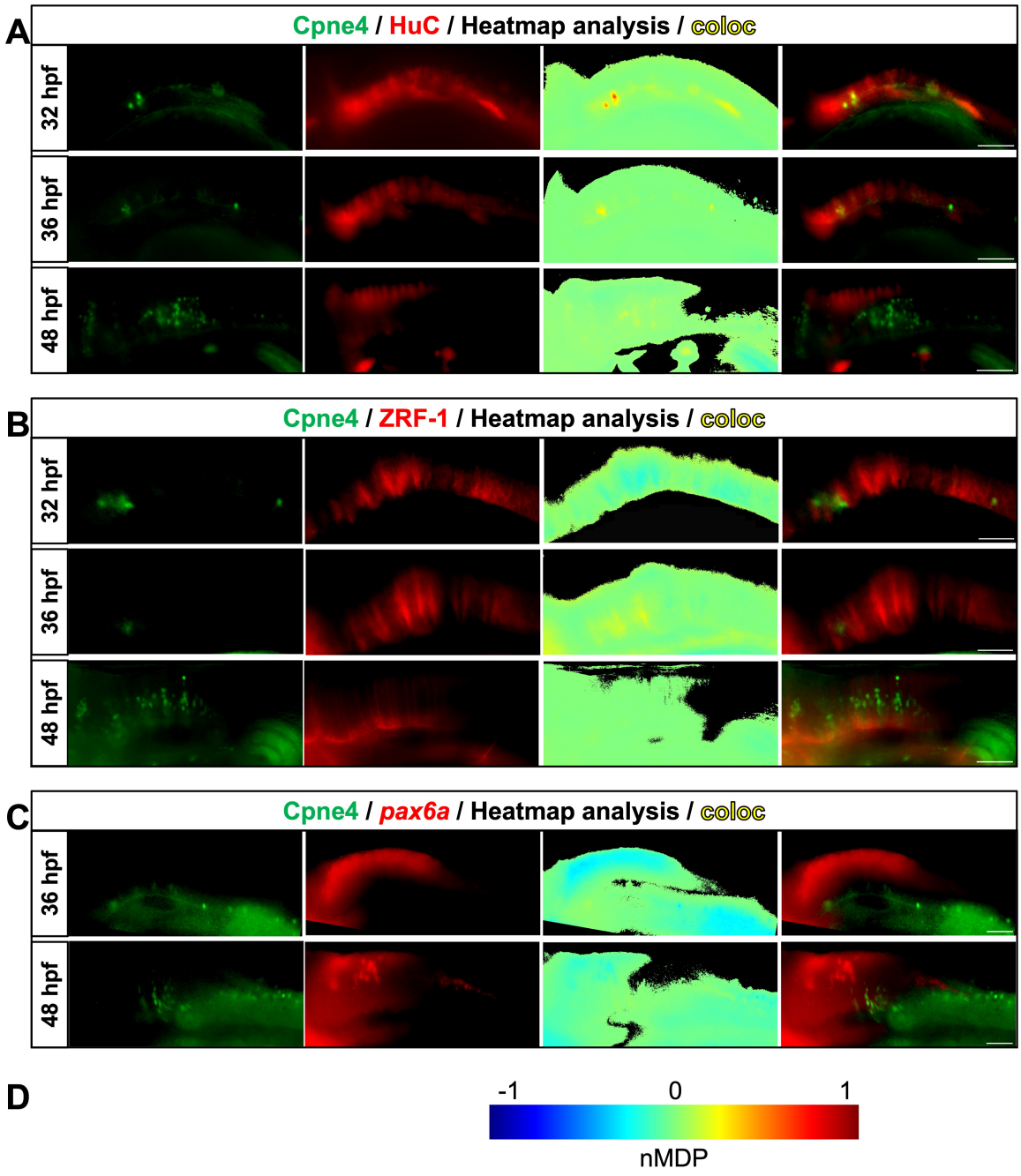

Figure 3.5 – Characterisation of GFP-positive Cpne4 cells. Lateral view of the hindbrain of transgenic *gSA2AzGFF306A* zebrafish embryos at 32, 36 and 48 hpf are shown. Heatmap colocalisation analysis was used to identify cell identity. **A)** Double IHC against GFP (Cpne4 cells – green colour) and HuC (mature neurons – red colour), their heatmap using normalised mean deviation product (nMDP) values and colocalisation (yellow). **B)** Double IHC against GFP (Cpne4 cells – green colour) and ZRF-1 (glial cells – red colour), their heatmap using nMDP values and colocalisation (yellow). **C)** IHC against GFP (Cpne4 cells – green colour) and ISH of *pax6a* (red colour), their heatmap using nMDP values and colocalisation (yellow). **D)** Colorbar chart indicating no colocalisation (-1, blue colour) to colocalisation (1, red colour).

3.2.4 Zebrafish *cpne4*$^{+}$ hindbrain cells are not the source of neuronal derived *vegfaa*

Cpne4/GFP(+) cells have a particular pattern in the zebrafish hindbrain, located ipsilaterally and dorsally juxtaposed above the PHBC and the developing CtAs. We also found a correlation between Cpne4/GFP(+) cells and CtAs 4, 6 and 7. Therefore, we wanted to understand if these cells are responsible for CtA ingression into the hindbrain by the expression of *vegfaa*. Colocalisation analysis of Cpne4/GFP(+) and *vegfaa* in control zebrafish embryos, showed no colocalisation at any developmental time (Fig. 3.6), arguing that these cells are not involved in instructing CtA ingression into the hindbrain.

Together, this evidence argues that neurons were likely not the neuronal cells instructing the ingression of CtAs into the hindbrain.

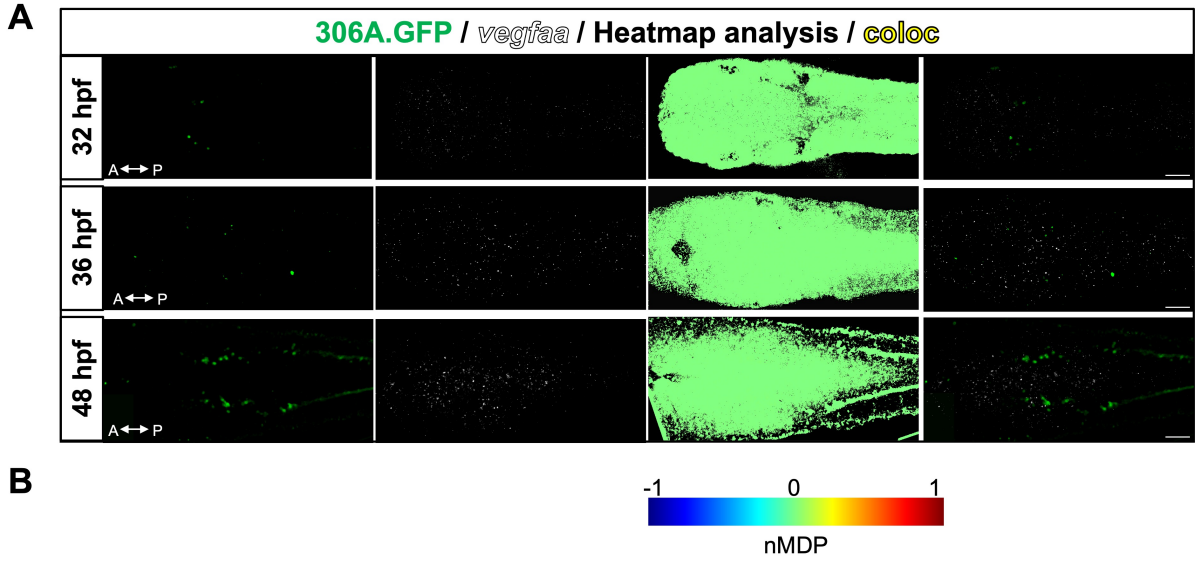

Figure 3.6 – Cpne4/GFP(+) cells do not colocalise with *vegfaa* expression. A) Dorsal view of the hindbrain of transgenic *gSA2AzGFF306A* zebrafish embryos at 32, 36 and 48 hpf submitted to ISH of *vegfaa* (white colour) and IHC against GFP (Cpne4 cells – green colour) are shown. Heatmap colocalisation analysis was used using nMDP values and a combined image between GPF and *vegfaa* expression is shown. **B)** Colorbar chart indicating no colocalisation (-1, blue colour) to colocalisation (1, red colour).

3.3 DISCUSSION

The vascular and nervous systems are functionally different but share anatomical similarities and cross-talk (Tam and Watts, 2010). The interface between these two organs is known as the neurovascular unit in the CNS. It establishes a life-long relationship that is essential for the functioning of the brain and is susceptible to ageing and disease (Bautch and James, 2009). During embryonic development, neural stem cells differentiate into mature neurons. Due to the high metabolic demand of these neurons, a highly vascularised network of blood vessels arises to provide nutrients and oxygen to the CNS (Watts et al., 2018). In zebrafish larvae, vascularisation of the CNS from intersegmental vessels (ISV) into the spinal cord is promoted by neurons that coordinate vessel growth by regulating the expression of neuron-derived Vegfaa and sFlt1 (Wild et al., 2017). In the hindbrain, CtA development is regulated by Vegfaa (Jin et al., 2017; Rossi et al., 2016), although the neuronal cell identity involved in instructing blood vessel ingression is unknown.

Here, we used the zebrafish Mct8 knockdown model to identify two different types of neuronal cells dependent on MT3 that are physically interacting with CtAs, namely *pax8*-expressing inhibitory interneurons, and *cpne4*-expressing intrinsic digit-innervating motor neurons. We hypothesised that due to their proximity with CtAs, they are the instructing guides for CtA ingression into the hindbrain during zebrafish embryogenesis.

3.3.1 Neurons topologically associated with CtAs are not involved in vessel ingression

Mutations in the MCT8 transporter impair MT3 signalling and compromises the maturation of several types of neurons (Bernal, 2022). In humans and mice, inhibitory interneurons are reduced in the cerebellar cortex (Bárez-López et al., 2019; López-Espíndola et al., 2014), which are involved in sensation, movement, and cognition (Swanson and Maffei, 2019). The transcription factor Pax8 labels a subpopulation of inhibitory interneurons in the zebrafish hindbrain and spinal cord (Batista and Lewis, 2008; Ikenaga et al., 2011). Here we hypothesise that if *pax8*-expressing cells are lost after Mct8 knockdown, are they responsible for instructing CtA ingression into the hindbrain during zebrafish embryonic development? Consistent with

previous results, we found that *pax8*-expressing cells in the hindbrain were reduced in the MCT8MO zebrafish embryo (Fig.3.1) (Campinho et al., 2014). We observed that in CTRMO embryos, *pax8*-expressing cells were near the posterior CtAs (CtAs 4 to 7, Fig. 3.1) and that this interaction was lost in MCT8MO embryos, either due to the loss of CtA development or due to the loss of these *pax8*-expressing cells or both.

To investigate the involvement of *pax8*$^{+}$ cells in BHB development, we conducted a *pax8* gene loss-of-function study, using the transgenic *Tg(pax8:DsRed)* (Ikenaga et al., 2011) hypomorph mutant zebrafish embryo. Surprisingly we observed that homozygous *pax8*$^{-/-}$ hypomorph mutant zebrafish embryos form a complete BHB. Statistical analysis between heterozygous *pax8*$^{+/-}$ control embryos and homozygous *pax8*$^{-/-}$ hypomorph mutant zebrafish embryos showed no significant changes in PHBC length between the two experimental groups. The lengths of CtAs 1 to 6 were also not significantly different between control *pax8*$^{+/-}$ and hypomorph *pax8*$^{-/-}$ mutant zebrafish embryos. Only the length of CtA 7 was statistically different between control *pax8*$^{+/-}$ and hypomorph *pax8*$^{-/-}$ mutant zebrafish embryos. These differences in lengths are most probably due to the fact that rhombomere 7 is usually the last one to vascularise and at 48 hpf the frequency of vascularisation is low (Ulrich et al., 2011).

In the hindbrain of 48 hpf control *pax8*$^{+/-}$ zebrafish embryos, some DsRed-expressing cells (*pax8*-lineage cell marker) colocalise with glycinergic (*glyt2a* and *glyt2b* markers) and GABAergic (*gad67a* and *gad67b* markers) inhibitory interneurons. These findings agree with previous studies from Ikenaga et al., (2011), in which they demonstrated that DsRed-expressing cells in the zebrafish hindbrain are mainly neurons and include interneurons. Although in hypomorph *pax8*$^{-/-}$ mutant zebrafish embryos, DsRed-expressing cells were not lost (Fig 3.3A), the expression pattern of DsRed-expressing cells between control *pax8*$^{+/-}$ and hypomorph *pax8*$^{-/-}$ zebrafish embryos were different (Fig. 3.3A) and colocalisation between DsRed-expressing cells and inhibitory glycinergic and GABAergic markers was reduced in hypomorph *pax8*$^{-/-}$ mutant zebrafish embryos. The quantitative analysis further confirmed these observations by confined displacement algorithm (CDA) for colocalisation significance analysis by computing the Pearson correlation coefficient between control *pax8*$^{+/-}$ and hypomorph *pax8*$^{-/-}$ mutant zebrafish embryos. The distribution of correlation coefficient between the two experimental groups diverged in opposite directions, indicating two possible outcomes, 1) the DsRed-expressing cells in hypomorph *pax8*$^{-/-}$ mutant zebrafish embryos changed their neuronal cell fate or 2) the cells maintained a neuronal progenitor state. According to Ikenaga et al., (2011), the spinal network in hypomorph *pax8*$^{-/-}$ mutant embryos

is maintained. The location and density of Pax2-expressing cells are maintained, and the commissural bifurcating longitudinal interneurons (CoBLs) differentiated normally in hypomorph *pax8*$^{-/-}$ mutant embryos (Ikenaga et al., 2011). Previous studies conducted in mice have shown that in the forebrain, GABAergic interneurons migrate in close proximity to the periventricular vascular network, indicating that the preformed vascular network serves as a guide for their migration (Won et al., 2013). Other studies in mice also indicated that vascular-derived VEGF-A promotes the migration of the cortical interneurons near the vasculature. The authors also suggested that an intact vasculature is required for migrating interneurons into the dorsal cortex (Barber et al., 2018). Another study conducted in the mouse brain has shown that blood vessels in the ventral telencephalon are required to differentiate radial glial progenitors into inhibitory interneurons (Tan et al., 2016). Thus, this data suggests that MT3 regulates *pax8*+ inhibitory interneurons, but the additional effect of the defective vasculature development in the hindbrain of MCT8MO zebrafish embryos is likely not dependent on these interneurons (Fig.3.1 A2). Considering these results, we suggest that the DsRed-expressing cells maintained a neuronal precursor state. Due to the defective vascular network, these cells cannot differentiate into mature neurons and migrate to their target location. These results indicate that *pax8*$^{+}$ interneurons are not responsible for CtA ingression in the zebrafish hindbrain.

In an unrelated study, screening transgenic zebrafish zTrap lines (Kawakami et al., 2010) for MT3-responsive neural cells (Campinho and Kawakami, unpublished results), we identified the *gSA2AzGFF306A* line, which presents a discrete population of hindbrain GFP(+) cells that are located dorsally juxtaposed and perfectly aligned along the PHBC. These cells are highly responsive to MT3 and genomic data from these fish indicated that the enhancer trap construct containing GFP locates in the *cpne4* locus (https://shigen.nig.ac.jp/zebrafish/strain/strainTopJa.jsp). Here our analysis identified these Cpne4/GFP(+) MT3-sensitive cells as neurons. Notably, in mice *Cpne4* is an embryonically expressed gene specific for hand and foot motor neurons, labelling specifically the intrinsic digit-innervating motor neurons (Alkaslasi et al., 2021; Mendelsohn et al., 2017). *Cpne4* in mice has also been characterised as excitatory glutamatergic neurons (Das Gupta et al., 2021; Häring et al., 2018). Since these reports came out after our study, we did not confirm these results with IHC for islet1 (motor neuron marker). We further confirmed that Cpne4/GFP(+) neurons were regulated by MT3 (Fig. 3.4 A and B). In the last few years, some studies have shown that motor neurons in mice's developing spinal cord regulate blood vessel development

by a combination of attractive and repelling signalling cues (Himmels et al., 2017; Martins et al., 2022). VEGF is the attractive factor in regulating blood vessel development in a long-range signalling manner (Himmels et al., 2017; Martins et al., 2022). We analysed *vegfaa* expression in Cpne4/GFP(+) cells, however, no colocalisation was found between them. This signifies that Cpne4/GFP(+) cells were not the source of the signal instructing the ingression of CtAs into the hindbrain.

One of the most characteristic features present in AHDS patients is movement disorders (Masnada et al., 2022). AHDS patients present muscular hypotonia of the limbs (Masnada et al., 2022; Schwartz et al., 2005). They have abnormal hand positioning, usually in a clubbed position (Ono et al., 2016; Schwartz et al., 2005). The toes are in a clawed position (Schwartz et al., 2005). Although zebrafish don't have tetrapod-like digits, and the fin and limbs are structurally different, a common ancestrally origin of motor neurons has been suggested by Ma et al., (2010) and Murakami and Tanaka, (2011). In zebrafish, motor neurons originating from the hindbrain and/or spinal cord innervate the pectoral fins (Ma et al., 2010; Murakami and Tanaka, 2011), whereas, in tetrapods, the limbs are innervated by motor neurons of the lateral motor column of the spinal cord (Murakami and Tanaka, 2011). This data in mice corroborates the identity of the zebrafish Cnpe4+ cells and presents a functional nexus with AHDS phenotypes in patients.

3.3.2 Hindbrain central nervous system resident cells responsible for central artery development

This study's selected hindbrain neurons are not responsible for CtAs development. Previous studies using the zebrafish as model organism have shown that spinal cord vascularisation is negatively regulated by radial glial cells that, through the expression of sFlt1, prevents hypersprouting of the venous ISVs (Matsuoka et al., 2016). But it also regulates the development of the vertebral arteries of the trunk by regulating the expression of Vegfab (Matsuoka et al., 2017). This shows that also radial glial cells have a dual function for blood vessel development, as observed for spinal cord neurons (Himmels et al., 2017; Martins et al., 2022). In the hindbrain, CtA development is majorly regulated by Vegfaa (Jin et al., 2017; Rossi et al., 2016). The defects observed in CtA development in zebrafish mutants for *vegfaa* resemble the ones observed in MCT8MO zebrafish embryos. We suggest that CNS-resident

radial glial progenitor cells in the hindbrain might be the cell type instructing BHB development through the expression of *vegfaa*.

3.4 CONCLUSIONS

Knockdown of Mct8 leads to the loss of *pax8*$^{+}$ and Cpne4^{+} neurons in the hindbrain. Both cell markers label populations of inhibitory glycinergic and GABAergic interneurons and digit-innervating glutamatergic motor neurons, respectively. In this Chapter, we conclude that the development of these neurons was MT3-dependent, although not responsible for CtA sprouting into the zebrafish hindbrain. We suggest that CNS angiogenesis in the zebrafish hindbrain and spinal cord have developed different strategies for blood vessel ingression. While in the zebrafish spinal cord, spinal neurons are responsible for the ingression of the ISV for trunk vascularisation, the hindbrain neurons are not involved in BHB development. Our results open the hypothesis that in the hindbrain, neural progenitors might be the cell type instructing BHB development.

3.5 MATERIALS AND METHODS

3.5.1 Zebrafish maintenance

Adult zebrafish (*Danio rerio*) were maintained in a ZebTEC zebrafish housing system (Tecniplast, Italy) at 28 ºC in a 14h/10h light/dark cycle, in a fish facility laboratory at CCMAR, in the University of Algarve (Faro, Portugal). The breeding stocks were fed twice a day with granulated food (Tetra granules, Germany) and once with *Artemia nauplii*. Zebrafish lines used for egg production were wildtype (AB strain), *Tg(fli1:EGFP)* (Lawson and Weinstein, 2002), *Tg(kdrl:CaaX-mCherry)* (Fujita et al., 2011), *gSA2AzGFF306* (Kawakami et al., 2010), and *Tg(pax8:DsRed)* (Ikenaga et al., 2011). The night before egg collection, adult couples were placed in breeding tanks with a perforated bottom (Techniplast) and separated by a perspex screen. The separator was removed on the following day at the beginning of the light phase cycle. All experiments were carried out in accordance with the EU Directive 2010/63/EU on the protection of animals used for scientific purposes.

3.5.2 Morpholino injection and sampling

Upon spawning, embryos were immediately collected and microinjected at the 1-2-cell stage with 1 nL of morpholino solution containing either 0.8 pmol CTRMO (control morpholino) or MCT8MO (*mct8* morpholino) (Gene Tools, USA) as described in Campinho et al., (2014). Embryos were distributed on plastic Petri dishes (∅ 100mm) containing E3 medium (5 mM NaCl, 0.17 mM KCl, 0.33 mM CaCl, 0.33 mM $MgSO_4$) and reared until sampling time at 28.5 ºC in an incubator (Sanyo, Germany) under 12h:12h light:dark cycles. Staging was done after Kimmel et al., (1995) by observing developmental landmarks in control embryos. Embryos were fixed at 32, 36 and 48 hpf in ice-cold 4% paraformaldehyde (PFA)/1×PBS overnight at 4 ºC. Samples were washed 2 × 5 min in 1×PBS/0.1% Tween-20 (PBT), depigmented with 0.3% H_2O_2/0.5% KOH/1×PBS and transferred into 100% methanol (MeOH) and stored at -20 ºC until use.

3.5.3 Double fluorescent immunohistochemistry

gSA2AzGFF306 or *Tg(gSA2AzGFF306; kdrl:CaaX-mCherry)* embryos were injected with 0.8 pmol CTRMO and MCT8MO at 1 cell stage and sampled at 32, 36 and 48 hpf for double fluorescent immunohistochemistry.

Samples were brought to room temperature and hydrated through a graded series of MeOH/1×PBS (75%, 50%, and 25% MeOH) for 5 min each, followed by 3 × 5 minutes in 1×PBS/0.1% Triton X-100 (Sigma-Aldrich, USA). Embryos were preincubated in 1×PBS/10% sheep serum (Sigma Aldrich, USA)/0.5% Triton X-100 at room temperature for 3 hours. Samples were incubated overnight at 4 ºC with primary antibody diluted in preincubation solution. Primary antibodies used are listed in Table 3.1. Samples were washed 6 × 30 minutes in 1×PBS/0.5% Triton X-100 (PBTr0.5%) and then blocked for 1 hour with preincubation solution. Samples were incubated overnight at 4 ºC with fluorescent labelling secondary antibody that are listed in Table 3.1. Samples were then washed 6 × 30 minutes in PBTr0.5%. Afterwards, the protocol was repeated for the second primary antibody, as described above.

Table 3.1 – List of antibodies used for double fluorescent immunohistochemistry.

1st primary antibody	1st secondary antibody	2nd primary antibody	2nd secondary antibody
rabbit anti-GFP (1:1000, ab290, abcam, UK)	goat anti-rabbit IgG-488 HL (1:400, Jackson Labs)	mouse anti-mCherry-Tag (1:100, STJ34373 – St John's Laboratory, UK)	goat anti-mouse IgG-CF594 (1:400, Sigma, USA)
		mouse anti-Zrf1 (1:100, ZIRC, USA)	
		mouse anti-HuC (1:500, Invitrogen, USA)	

Fluorescent imaging of the hindbrain was carried out using a Zeiss Z2 microscope coupled to a Zeiss digital camera or using a Lighsheet Z1 microscope (Zeiss, Germany). Samples for Z2 imaging were mounted in 0.3% agarose (Sigma-Aldrich, USA) and imaged using a 20× lens and a z step of 0.850 μm. Afterwards, images were deconvoluted in SCI Huygens software 4.4 (Scientific Volume Imaging, The Netherlands, http://svi.nl). Maximum projections were generated in Fiji (Schindelin et al., 2012). Samples for Z1 imaging were mounted in 1% low melt agarose (CarlRoth, Germany) and imaged using a 10× lens, dual illumination and a z step of 1.5 μm (optimal distance option) to acquire the complete hindbrain using 1× zoom. After image acquisition, dual illumination images were merged using Dual side Fusion (Zen Black, Zeiss, Germany). Images were then imported into Fiji (Schindelin et al., 2012) and analysed.

3.5.4 Riboprobe preparation

The *vegfaa* plasmid was kindly provided by Professor Brant Weinstein, the *gad67a*, *gad67b*, *glyt2a* and *glyt2b* plasmids were kindly provided by Professor Wolfgang Driever, the *cadherin5* plasmid was kindly provided by Professor Wiebke Herzog, and the *dsRed-1* plasmid was kindly provided by Professor Raquel Andrade. The zebrafish *pax8* (XM 001339857.2) riboprobe was generated by PCR amplification and cloned as described in Campinho et al., (2014). The *pax6a* primers (Table 3.2) were designed using as template the sequences from the assembled transcriptome (NCBI – BioProjects: PRJNA381309). Isolation of the cDNA of *pax6a* was carried out using a DreamTaq PCR kit (Thermo Fisher Scientific, USA) following the manufacturer's recommendation, and the amplified fragment was isolated by agarose gel band extraction after electrophoresis and cloned into a pGemT easy vector (Promega) as described

by the manufacturer. Isolated plasmid DNA was sequenced to confirm the identity and orientation.

Table 3.2 – Primer sequences used to isolate the zebrafish *pax6a* cDNA.

Gene	Primer Forward (5' → 3')	Primer Reverse (5' → 3')
pax6a	AGGCTGTTGGAACTATGCCTC	CGTCGCGTTCTCACTGTAGTC

Ten nanograms of plasmid DNA for zebrafish *pax8*, *pax6a* and *dsRed-1* were used to PCR amplify the template and the T7 and SP6 RNA polymerase promoter in the flanking multiple cloning site using universal M13 forward and reverse primers. PCR protocol was 95 ºC for 5 min, 35 cycles of 95 ºC for 30 sec, 60 ºC for 30 sec and 1 min at 72C, followed by a final extension of 5 minutes at 72 ºC. PCR products were purified by agarose gel and extracted using a GFX gel band extraction kit (Omega Biotek, USA) according to the manufacturer's instructions. For the other zebrafish plasmids, five micrograms of plasmid DNA were linearized with Thermo Fisher Scientific (USA) fast digest EcoRI (*gad67a*, *gad67b*, *glyt2b*), XhoI (*glyt2a*), or NotI (*vegfaa, cadherin5*), followed by phenol-chloroform extraction and sodium acetate and ethanol precipitation.

300 ng of purified linearized plasmid were used to prepare Digoxigenin or Fluorescein labelled antisense probes. These were synthesized by *in vitro* transcription with DIG-RNA labelling kit or Fluorescein-RNA labelling kit (Roche, Switzerland) according to the manufacturer's instructions. Probes for *vegfaa*, *cadherin5*, *gad67a*, *gad67b*, *glyt2b*, and *glyt2a* were produced with T3 RNA polymerase (Fermentas, USA), *pax8* and *pax6a* probes were produced with SP6 RNA polymerase (Fermentas, USA), and *dsRed-1* probe was *in vitro* transcribed using T7 RNA polymerase (Fermentas, USA). Integrity of probes was determined by gel electrophoresis and stored in 50% RNAlater (Sigma, USA) at -20 ºC.

3.5.5 Whole-mount *in situ* hybridization (WISH)

WISH was carried out according to Thisse and Thisse (2008) with adaptations. Heterozygote and homozygote *Tg(pax8:DsRed)* zebrafish embryos at 48 hpf were brought to room temperature and hydrated through a graded series of MeOH/1×PBS (100% to 0% MeOH) and

afterwards washed 3 × 5 min in 1×PBS/0.1% Tween-20 (PBT). Embryos were permeabilized by digestion with proteinase K (1 μg/ml) in 1×PBS for 15 min. Proteinase K digestion was stopped by incubating the embryos for 20 min in 4% PFA/1×PBS. Samples were washed 4 × 5 min with PBT to remove the residual PFA and then pre-hybridized for 3 hours at 68 ºC in pre-heated hybridization mix (HybMix). HybMix was discarded and replaced with pre-heated HybMix containing 0.25 ng/ml of Dig-labelled cRNA *cadherin5* probe and hybridized overnight at 68 ºC. Samples were subjected through a series of stringency washes at 68 ºC for 10 min in Hyb(−)/2×SSC (75%, 50% and 25% of Hyb(−)), 2×SSC/0.1% Tween-20 and finally washed twice in 0.2×SSC/0.1% Tween-20 (0.2×SSCT) for 30 minutes. Samples were then washed through a graded series in 0.2×SSCT/Malic acid buffer (MAB, Sigma-Aldrich, USA) (75%, 50% and 25% of 0.2×SSCT) and then washed 3 × 10 min in MAB/0.1% Triton X-100 (MABTr, Sigma-Aldrich, USA). Embryos were preincubated in blocking solution MAB/0.1% Triton X-100/10% sheep serum (Sigma-Aldrich, USA)/2% Blocking solution (Roche, Switzerland) for 2 hours at room temperature. Afterwards, the blocking solution was discarded and replaced with blocking solution containing anti-Dig-AP Fab fragments serum (1/5000, Roche, Switzerland) and incubated overnight at 4 ºC. Samples were washed 6 × 30 min in MABTr. Afterwards, samples were washed 3 × 5 min in staining buffer (100 mM Tris HCl pH 9.5, 50 mM $MgCl_2$,100 mM NaCl, 2 mM Levimasol and 0.1% Tween-20) and then incubated in labelling solution containing nitro blue tetrazolium (NBT)/bromo-chloro-indolyl-phosphate (BCIP) diluted in staining solution for colour development. When the desired staining intensity was reached, reaction was stopped by washing the samples in stop solution (1× PBS pH 5.5, 1 mM EDTA, 0.1% Tween-20). For image analysis, samples were transferred to 100% glycerol and photographed under a stereoscope (Olympus) coupled to an OPTICA 3.0 digital colour camera.

3.5.6 Double fluorescent whole-mount *in situ* hybridization

Heterozygote and homozygote Tg(*pax8:DsRed*) zebrafish embryos at 48 hpf were brought to room temperature and hydrated through a graded series of MeOH/1×PBS (100% to 0% MeOH) and afterwards washed 3 × 5 min in 1×PBS/1×PBT. Embryos were permeabilized by digestion with proteinase K (1 μg/ml) in 1×PBS for 15 min. Proteinase K digestion was stopped by

incubating the embryos for 20 min in 4% PFA/1×PBS. Samples were washed 4 × 5 min with PBT to remove the residual PFA and then pre-hybridized for 3 hours at 68 ºC in pre-heated HybMix. HybMix was discarded and replaced with pre-heated HybMix containing 0.25 ng/ml of Dig-labelled cRNA probes (*gad67a*, *gad67b*, *glyt2a* and *glyt2b*, probes were mixed and labelled "inhibitory") and 0.5 ng/ml of Fluorescein-labelled cRNA probe (*dsRed-1*) and hybridized overnight at 68 ºC. Samples were subjected through a series of stringency washes at 68 ºC for 10 min in Hyb(−)/2×SSC (75%, 50% and 25% of Hyb(−)), 2×SSC/0.1% Tween-20 and finally washed twice in 0.2×SSC/0.1% Tween-20 (0.2×SSCT) for 30 minutes. Samples were then washed through a graded series in 0.2×SSCT/Malic acid buffer (MAB, Sigma-Aldrich, USA) (75%, 50% and 25% of 0.2×SSCT) and then washed 3 × 10 min in MAB/0.1% Triton X-100 (MABTr, Sigma-Aldrich, USA). **1st probe detection – anti-Fluo-AP + FastRed detection:** Samples were preincubated in blocking solution containing MAB/0.1% Triton X-100/10% sheep serum (Sigma-Aldrich, USA)/2% Blocking solution (Roche, Switzerland) for 2 hours at room temperature. Afterwards, the blocking solution was discarded and replaced with blocking solution containing preabsorbed anti-Fluorescein-AP Fab fragments serum (1/8000, Roche, Switzerland) and incubated overnight at 4 ºC. Samples were washed 6 × 30 min in MABTr. Afterwards, samples were incubated in FastRed TR/ Naphthol AS-MX tablets (Sigma, USA) for colour development, according to the manufacturer's instructions, followed by several washes in PBT. **2nd probe detection – anti-Dig-POD + Fluorescein TSA detection:** Samples were pre-incubated for 1:30 hours in blocking solution. Afterwards, the blocking solution was discarded and replaced with blocking solution containing anti-DIG-POD Fab fragments serum (1/500, Roche, Switzerland) and incubated overnight at 4 ºC. Samples were washed 2 × 30 min in MABTr. Afterwards, samples were washed 4 × 30 min with PBT. Probe detection was performed by incubating the samples in Fluorescein Tyramide 1:100 in amplification reagent (Perkin Elmer, USA) for fluorescent colour development, according to the manufacturer's instructions, followed by several washes in PBT.

Lightsheet Z1 microscope (Zeiss, Germany) was used to acquire images. Samples were mounted in 1% low melt agarose (CarlRoth, Germany) and imaged using 10× lens, 1× zoom, dual illumination and a z step of 1.4 μm (optimal distance option) to acquire the complete hindbrain. After image acquisition, dual illumination images were merged using Dual side Fusion (Zen Black, Zeiss). Images were then imported into Fiji (Schindelin et al., 2012) and analysed.

3.5.7 Fluorescent *in situ* hybridization with immunohistochemistry

WISH was performed as described previously using *gSA2AzGFF306* GFP positive samples at 32, 36 and 48 hpf with some minor modifications. Samples were incubated in pre-heated HybMix containing 0.5 ng/ml of Dig-labelled cRNA probe (*pax8, pax6*a or *vegfaa*) and hybridized overnight at 68 ºC. After the stringency washes probes were subjected to probe detection. **For *pax8* or *pax6a* probe detection:** Samples were washed 6 × 30 min in MABTr. Afterwards, samples were incubated in FastRed TR/ Naphthol AS-MX tablets (Sigma, USA) for colour development, according to the manufacturer's instructions, followed by several washes in PBT. **For *vegfaa* probe detection:** Samples were washed 2 × 30 min in MABTr. Afterwards, samples were washed 4 × 30 min with PBT. Probe detection was performed by incubating the samples in fluorescein Tyramide 1:100 in amplification reagent (Perkin Elmer, USA) for fluorescent colour development, according to the manufacturer's instructions, followed by several washes in PBT.

For the immunohistochemistry, the samples were re-fixated in 4% PFA/1×PBS for 15 min and then washed 4 × 15 min in PBT. Embryos were preincubated in 1×PBS/10% sheep serum/0.5% Triton X-100 at room temperature for 1:30 hours. Samples were incubated overnight at 4 ºC with rabbit anti-GFP (1/500, abcam, UK) primary antibody diluted in preincubation solution. Samples were washed 6 × 30 minutes in 1×PBS/0.5% Triton X-100 (PBTr0.5%) and then blocked for 1 hour with preincubation solution. **Samples detected with *pax6a* probe:** Samples were incubated overnight at 4 ºC with goat anti-rabbit IgG-488 HL (1:400, Jackson Labs) fluorescent labelling secondary antibody. **Samples detected with *vegfaa* probe:** Samples were incubated overnight at 4 ºC with goat anti-rabbit 594 (1:400, Sigma). Samples were then washed 6 × 30 minutes in PBTr0.5%.

Fluorescent imaging of the hindbrain was carried out using a Zeiss Z2 microscope coupled to a Zeiss digital camera or using a Lighsheet Z1 (Zeiss, Germany). Samples for Z2 imaging were mounted in 0.3% agarose (Sigma-Aldrich, USA) and imaged using a 20× lens and a z step of 0.850 µm. Afterwards, images were deconvoluted in SCI Huygens software 4.4 (Scientific Volume Imaging, The Netherlands, http://svi.nl). Maximum projections were generated in Fiji (Schindelin et al., 2012). Samples for Z1 imaging were mounted in 1% low melt agarose (CarlRoth, Germany) and imaged using a 10× lens, dual illumination and a z step of 1.5 µm (optimal distance option) to acquire the complete hindbrain using 1× zoom. After image

acquisition, dual illumination images were merged using Dual side Fusion (Zen Black, Zeiss, Germany). Images were then imported into Fiji (Schindelin et al., 2012) and analysed.

3.5.8 Colocalisation analysis

Images acquired with a Zeiss Z1 microscope were imported into Fiji (Schindelin et al., 2012). The ImageJ "Colocalisation Colormap" plugin was used to find areas of the colocalisation (Gorlewicz et al., 2020). At least 3 individuals per condition were analysed.

3.5.9 Statistical analysis

Statistical analysis was performed using GraphPad Prism version 8.4.0 software for Mac (San Diego, USA, www.graphpad.com). Values are represented as means ± SD. Statistical significance was determined by unpaired t-test or by Fisher's exact test.

CHAPTER 4

Maternal T3 regulates hindbrain neural progenitor cells responsible for the chemoattraction of the central arteries during zebrafish blood-hindbrain barrier development

ABSTRACT

Thyroid hormone (TH) signalling is important and necessary for proper neurodevelopment. Inadequate levels of maternally derived T3 (MT3) supply affects target gene expression profiles, which are fundamental for the brain's normal growth, maturation, and function. One of the first embryonic events for central nervous system (CNS) development is the differentiation and proliferation of neural progenitor cells (NPC), which are a direct target of MT3. Deficient MT3 levels lead to reduced NCP expansion, fewer neurons, and reduced neuronal cell diversity. This can also impact CNS vascularisation since NPC releases angiogenic cues, such as VEGF, for neural tube vascularisation. We reported previously that in zebrafish, MT3 deficiency causes impaired hindbrain central arteries (CtAs) development, resulting in an abnormal blood-hindbrain barrier (BHB) development. We identified that MT3 regulates the expression of hindbrain *vegfaa*, although the cellular identity of the MT3-dependent cells remained to be identified. We show here that during BHB developmental time window, a restricted population of *pax6a* progenitor cells in the hindbrain were lost in MCT8MO zebrafish embryos and that these cells express *vegfaa*. Colocalisation analysis between 30 hpf – 48 hpf, shows that hindbrain *pax6a* progenitor cells express the *mct8* transporter and the receptors *thraa* and *thrab*, indicating a direct regulation of MT3 over *pax6a* progenitor cells. However, the presence of the transporter and the receptors varies for each rhombomere and timing, demonstrating the importance of the timely sprouting of each CtA during embryonic development. These results highlight the importance of MT3 in the maintenance and proliferation of a restricted population of *pax6a* progenitor cells in the zebrafish hindbrain for the correct and coordinated development of the CtAs.

4.1 INTRODUCTION

Thyroid hormone (TH) signalling is important and necessary for proper neurodevelopment and for the regulation of cognitive functions in children and adults (Williams, 2008). Inadequate levels of maternally derived T3 supply affect target gene expression profiles, which are fundamental for the brain's normal growth, maturation and function (Brunton and Russell, 2011; De Escobar et al., 2004). One of the most severe conditions caused by TH deficiency is caused by mutations in the TH-specific *monocarboxylate transporter 8* (*MCT8*) gene, which causes the Allan-Herndon-Dudley syndrome (AHDS) in humans (Dumitrescu et al., 2004; Schwartz and Stevenson, 2007). The zebrafish has been shown to mimic the psychomotor and neurodevelopmental disorders found in human AHDS patients (Campinho et al., 2014; Silva et al., 2017; Vatine et al., 2013; Zada et al., 2016). Besides that, an impaired blood-hindbrain barrier (BHB) has been linked to the disease (Campinho et al., 2014; Chapter 2).

During embryonic development, the formation of a complex central nervous system (CNS) involves multiple cellular and molecular interactions between the neural and vascular systems (Ridaura et al., 2021). Formation of the CNS begins early during vertebrate development. After ectodermal germ layer specification, the neural ectoderm develops into the neuroepithelium (neuroepithelial cells), that are highly proliferative neural progenitor cells (NPC) (Kintner and Hemmati-Brivanlou, 2013). These cells can renew themselves (by non-terminal symmetrical division), increase the NPC pool, and latter divide asymmetrically to generate NPC or differentiate into neurons (Götz and Huttner, 2005; Paridaen and Huttner, 2014). After the onset of neurogenesis, the morphology of the neuroepithelial cells changes, and the cells acquire radial processes and are referred as radial glial cells (Tramontin et al., 2003). These cells will give rise to the large variety of neurons and glia that comprise the CNS (Hardwick et al., 2015; Kintner and Koyano-Nakagawa, 2013; Pinto and Götz, 2007). As the neural tissue grows, NPC, including neuroepithelial cells and radial glia secret morphogenetic cues, like Vascular endothelial growth factors (Vegfs) and Wingless (Wnts), to promote vessel ingression into the neural tissue to sustain the high metabolic demand of the NPCs and the neuronal progeny (Liebner et al., 2008; Raab et al., 2004; Tata and Ruhrberg, 2018; Watts et al., 2018). Vascularisation of the CNS begins with angiogenic sprouting of the perineural vascular plexus (PNVP) into the neural tissues (Bautch and James, 2009; Hogan et al., 2004). The invading blood vessels within the brain expand into a large network, concomitantly with the growing neural tissue, forming a hierarchical vascular tree (Tata et al., 2015).

Previous studies have shown that THs regulate NPC behaviour during vertebrate life (reviewed in Fanibunda et al., 2018). Studies conducted in NPC of the developing cortex of mice have shown that the TH machinery, such as the MCT8 transporter, Deiodinase type 2 (Dio2), and the Thrα1 receptor, is present, indicating a direct regulation of maternal T3 (MT3) on NPC (Mohan et al., 2012). They showed that in maternal TH-deficient mice, the rate of NPC proliferation and consequent neuronal differentiation was impaired in the developing cortex. The pool of NPC was significantly reduced, and due to a delay of the cell cycle exit for neurogenesis, all neurons, early- and late-borne neurons, were reduced, leading to a reduction of the cortical thickness (Mohan et al., 2012).

Pax6, a paired homeobox transcription factor, influences neural stem cell proliferation, multipotency, and neurogenesis in many regions of the CNS (Bel-Vialar et al., 2007; Sansom et al., 2009). In humans and mice, it has been shown that *PAX6* expression undergoes dosage variation, which is critical for cellular fate (Lacomme et al., 2018). During eye development, mutations in one allele of the *PAX6* gene leads to congenital aniridia (lack of iris) in humans and small eye in mouse and zebrafish. In contrast, mutations in both alleles cause the absence of eyes (Cvekl and Callaerts, 2017; Hill et al., 1991; Lesaffre et al., 2007; Nornes et al., 1998). In the hindbrain and spinal cord of small eye (sey) mice, the patterning of the neural tube was modified. They showed that a population of ventral progenitor cells expressing *Pax6* are influenced by Sonic Hedgehog (SSH) morphogen, which establishes different progenitor domains, giving rise to specific motor neurons and ventral interneurons (Ericson et al., 1997). Consequently, the loss of Pax6 function leads to a change in the neuronal fate (Ericson et al., 1997) or a delayed differentiation (Sun et al., 1998) of the ventral interneurons and motor neurons. In the developing spinal cord of chicken and mice embryos, it has been shown that repressing *Pax6* maintains NPC proliferation while increasing *Pax6* leads to cell cycle exit and neuronal commitment. *Pax6* expression must be repressed in committed neuronal precursor cells to enable neuronal differentiation (Bel-Vialar et al., 2007). The main molecular players involved in the temporal expression of *Pax6* are fibroblast growth factor (FGF) and retinoic acid (RA) signalling, and neurogenin 2 (Neurog2) (Bel-Vialar et al., 2007; Bertrand et al., 2000; Diez del Corral et al., 2003). In the developing spinal cord, *Pax6* expression is absent in the stem cell zone of the caudal neural plate, by the repressive action of FGF signalling (Bertrand et al., 2000). Afterwards, *Pax6* expression is activated in NPC during neural tube closure by RA signalling (Diez del Corral et al., 2003), which in turn up-regulates *Neurog2*. Consequently, it represses *Pax6* expression in neuronal precursor cells (Bel-Vialar et al., 2007).

In Chapter 2, we demonstrated that MT3 acting through Mct8 is involved in the development of the BHB, specifically in the development of the hindbrain central arteries (CtAs). We also uncovered that MT3 acting through Mct8 regulates the expression of *vegfaa* in the ventral hindbrain, which is responsible for the chemoattraction of specific CtAs for BHB development. In Chapter 3, we addressed the hypothesis that mature neurons could be responsible for CtA ingression, as observed in the vascularisation of the zebrafish spinal cord (Wild et al., 2017). However, that is not the case. Previous studies have shown that in zebrafish larvae, PNVP formation for spinal cord vascularisation is regulated by radial glia, regulating the expression of *vegfab* (Matsuoka et al., 2017). These NPC are positive regulators of vascularisation of the zebrafish spinal cord (Matsuoka et al., 2017).

In the present Chapter, we address the hypothesis that an appropriate supply of MT3 is necessary for the survival of a population of NPC in the zebrafish hindbrain, which are responsible for the release of *vegfaa* and consequently responsible for the sprouting, ingression and growth of the CtAs. For that, we used the zebrafish *mct8* morpholino (MCT8MO) model to study the effect of MT3 deficiency to determine its effect on specific ventral hindbrain NPC. Pax6 is a specific marker for NPC. In zebrafish, two *pax6* genes exist, *pax6a* and *pax6b*, and both are markers for progenitor cell state (Tambalo et al., 2020; Thummel et al., 2010). During development, *pax6a* expression is specifically localised in the zebrafish brain, including telencephalon, diencephalon, hindbrain, spinal cord, and eye (Kleinjan et al., 2008; Thisse et al., 2001), and thus we decided to focus on *pax6a*. Here we show that *pax6*a-positive (+) hindbrain cells were lost before BHB development and that *pax6a*+ cells colocalise with *vegfaa* expression, indicating that these cells might be responsible for CtA ingression into the hindbrain. Colocalisation analysis of *pax6a* with *thraa*, *thrab* and *mct8* mRNA was performed to determine if MT3 action is direct/cell autonomous. Functional studies using the *pax6a* loss-of-function crispant zebrafish embryos showed a similar CtA impairment as observed in MCT8MO zebrafish embryos. The outcome of this study indicates that the deficient supply of MT3 caused by Mct8 knockdown affects the development of a population of *pax6a*+ hindbrain progenitor cells, which are responsible for the expression of *vegfaa* and thus mediate CtA ingression into the hindbrain.

4.2 RESULTS

4.2.1 MT3 regulates *pax6a* expression during embryogenesis

Pax6 expression is activated in ventral neural progenitors during neural tube development by RA signalling. This has been observed in several vertebrate species, such as humans, mice and chickens (Diez del Corral et al., 2003; Novitch et al., 2003). RA regulates gene expression through heterodimerisation of the retinoic acid receptor (RAR) with the retinoid X receptor (RXR) that binds to specific RA response elements (RAREs) in the regulatory region of target genes (Janesick et al., 2015). The RXR is also an auxiliary protein for thyroid receptors (Zhang et al., 1992). In zebrafish four *rxr* genes exist (Tallafuss et al., 2006), but in the 25 hpf MCT8MO transcriptome data (NCBI – BioProjects: PRJNA381309), only *rxrba* was differentially expressed, and it was downregulated (-0.234, $p<0.01$; FDR 5%). In 25 hpf MCT8MO zebrafish embryos, *pax6a* was downregulated (-0.575, $p<0.01$; FDR 5%). To further explore this relation, whole-embryo gene expression analysis of *rxrba* and *pax6a* from 28 hpf until 72 hpf in CTRMO and MCT8MO was conducted (Fig. 4.1). During the BHB developmental time window, whole-embryo gene expression analysis did not found differences in expression of both genes between CTRMO and MCT8MO zebrafish embryos. Curiously, the expression of both genes, along the time window analysed, follows a similar trend (Fig. 4.1 A and B).

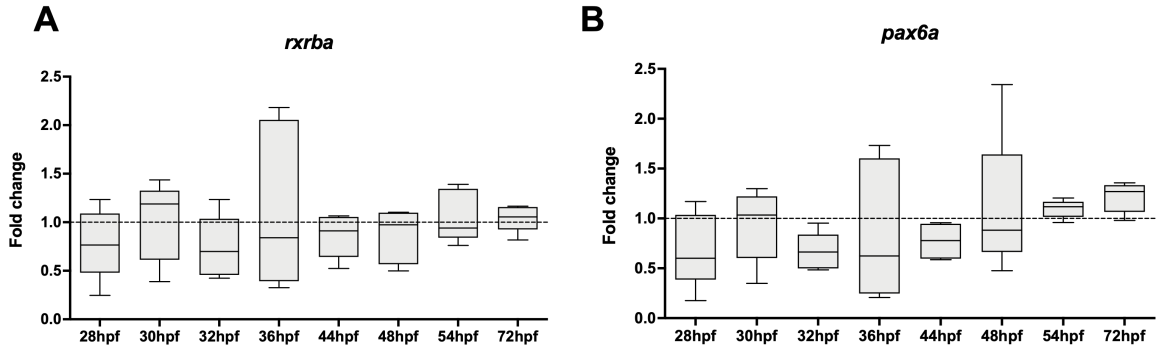

Figure 4.1 – Whole-embryo gene expression analysis suggests that MT3 is not regulating *rxrba* and *pax6a*. A) *rxrba* and **B)** *pax6a* expression were not modified during BHB development between CTRMO and MCT8MO zebrafish embryos. The data are represented as fold change of MCT8MO expression relative to the CTRMO. Boxes represent the interquartile range ± SD. Dashed horizontal line represents no

change in gene expression. Statistical significance was determined using a t-test: two-samples, assuming equal variance (n = 5).

In Chapter 2, we saw that whole-embryo qRT-PCR gene expression analysis was not able to reflect hindbrain specific expression changes. Therefore, whole-mount *in situ* hybridization (WISH) of *pax6a* in 25 and 48 hpf CTRMO and MCT8MO zebrafish embryos was conducted. In 25 and 48 hpf MCT8MO zebrafish embryos, *pax6a* was downregulated in a cell-specific manner in the brain and spinal cord (Fig. 4.2). In the brain, the most affected region, by the absence of MT3, was the hindbrain (Fig. 4.2 first and second panel). The spinal cord was severely affected by the absence of MT3, especially the most dorsal *pax6a*-positive (+) cells, which seemed to be more dependent on MT3 signalling than the more ventral *pax6a*+ cells (Fig. 4.2 last panel). *pax6a* expression also outlines rhombomere boundaries (black asterisks in Fig. 4.2 second panel) (Choe et al., 2002; Takahashi and Osumi, 2011). At 25 hpf, CTRMO embryos revealed seven rhombomere boundaries. In MCT8MO embryos, rhombomere boundaries were still visible, however rhombomere boundaries r1/r2, r2/3 and r6/7 show lower staining. Rhombomere boundaries r3/r4, r4/5 and r5/6 have stronger staining. Collectively, RNAseq and WISH data indicated that MT3 regulates *pax6a* hindbrain expression in a cell-specific manner. However, the exact identity of the *pax6a*+ MT3-dependent cells is not yet clear.

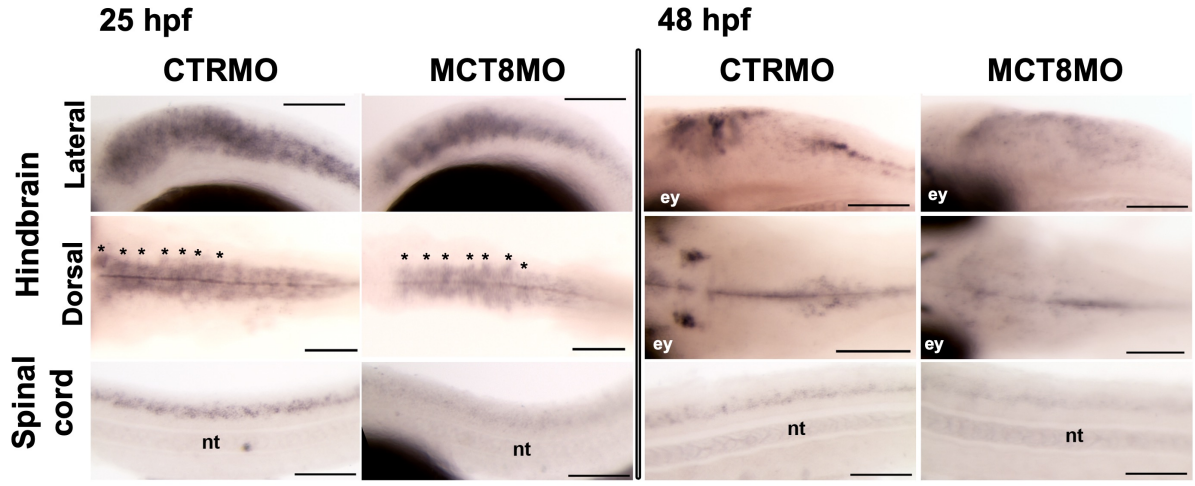

Figure 4.2 – MT3 regulates *pax6a* during zebrafish embryogenesis. WISH expression analysis of the neural progenitor marker *pax6a* in CTRMO and MCT8MO zebrafish embryos at 25 and 48 hpf are represented. Lateral and dorsal view of the hindbrain (first and second panels) and lateral view of the spinal cord (lower panel). Black * marks rhombomere boundaries from left to right r1/2, r2/3, r3/4, r4/5, r5/6, r6/7 and r7/r8. Expression of *pax6a* was reduced in the hindbrain and spinal cord of

25 and 48 hpf MCT8MO zebrafish embryos. ey – eye, nt – notochord. A minimum of 10 zebrafish embryos per condition and time points were analysed. Scale bar: 100 µm.

In the present study, we did not analyse by WISH the expression of *rxrba* in the zebrafish hindbrain and spinal cord, which will be analysed in future work.

4.2.2 MT3 regulates ventral *pax6a*+ cells in the zebrafish hindbrain

To analyse the expression pattern of *pax6a* during BHB development, particularly during CtA development, three time points were selected: 32 hpf (beginning of the sprouting of the first CtA), 36 hpf (an intermediate stage where usually three CtAs are growing into the hindbrain), and 48 hpf (usually all seven CtAs have sprouted and a complete BHB has formed) (Quiñonez-Silvero et al., 2020; Ulrich et al., 2011). The transgenic *Tg(fli1:EGFP)* zebrafish line (Lawson and Weinstein, 2002) was used to visualise the hindbrain vascular structures in CTRMO and MCT8MO zebrafish embryos (Fig. 4.3). In CTRMO zebrafish embryos, *pax6a*+ cells were found along the hindbrain (Fig. 4.3 A, C and E). The ventral *pax6a*+ cells were near the developing CtAs (Fig. 4.3 C and E). In MCT8MO embryos, *pax6a*+ cells were less abundant, and at 36 and 48 hpf the ventral *pax6a*+ cells were lost (Fig. 4.3 D and F).

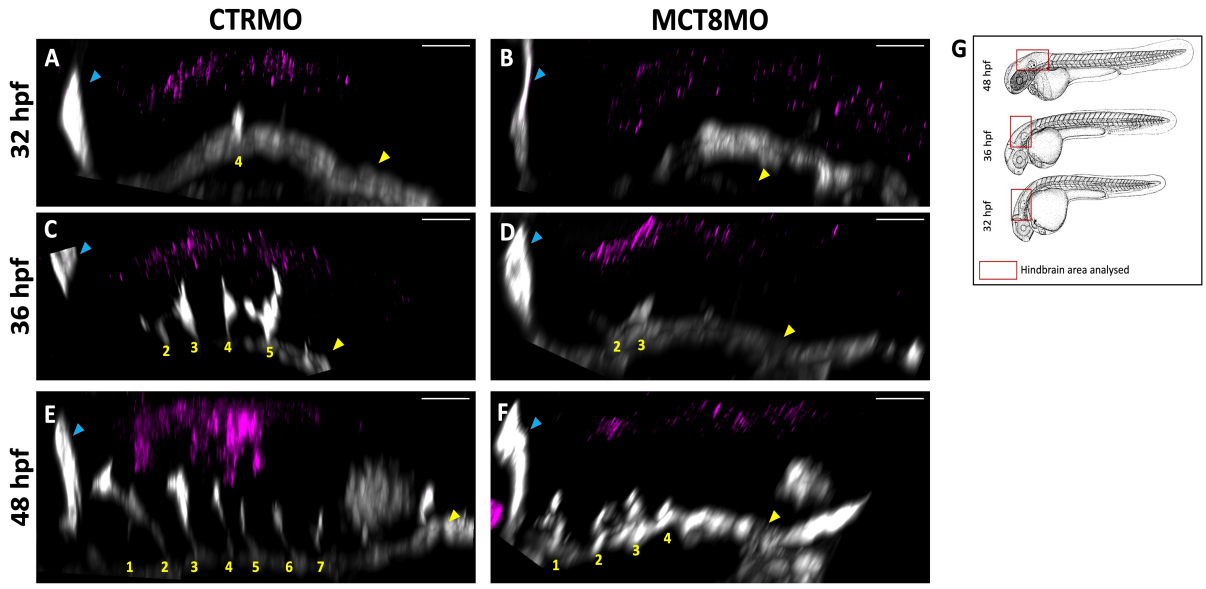

Figure 4.3 – Ventral *pax6a*+ cells are lost in MCT8MO zebrafish embryos. A – F) Lateral view of the hindbrain in CTRMO and MCT8MO zebrafish embryos at 32, 36

and 48 hpf are represented. WISH of *pax6a* (magenta) and immunohistochemistry (IHC) against GFP (endothelial marker, white). The ventral population of *pax6a* expressing cells were lost in MCT8MO zebrafish embryos, compared to CTRMO embryos. The blue arrowhead represents the mid-cerebral vein (MCeV), and the yellow arrowhead represents the primordial hindbrain channels (PHBC). Yellow numbers 1 – 7 indicate the CtA in its respective rhombomere. Scale bar: 50 µm. **G)** Schematic representation of the hindbrain area analysed in 32, 36 and 48 hpf zebrafish embryos.

4.2.3 Hindbrain *pax6a*+ cells express *vegfaa*

Afterwards, we wanted to know if these *pax6a*+ hindbrain cells express *vegfaa* and are thus responsible for CtA sprouting into the zebrafish hindbrain. Colocalisation analysis, using the image J plugin Colourmap (Gorlewicz et al., 2020) shows that some hindbrain *pax6a*+ cells express *vegfaa* (Fig. 4.4). This is evident at the five-time points analysed, 30, 32, 36, 42 and 48 hpf. Before CtA development, at 30 hpf, some *pax6a*+ cells colocalise with *vegfaa* (Fig. 4.4 A and B). Analysing the surrounding area of every CtA in every stage shows that colocalising *pax6a/vegfaa* cells exist near the developing CtAs (Fig. 4.4 individual images of the CtAs). Notable was the observation that the developing CtAs seem to migrate towards these *pax6a/vegfaa* colocalising cells (individual images of 4.4 C, E, G and I), indicating that these cells might be responsible for the chemoattraction of the developing CtAs.

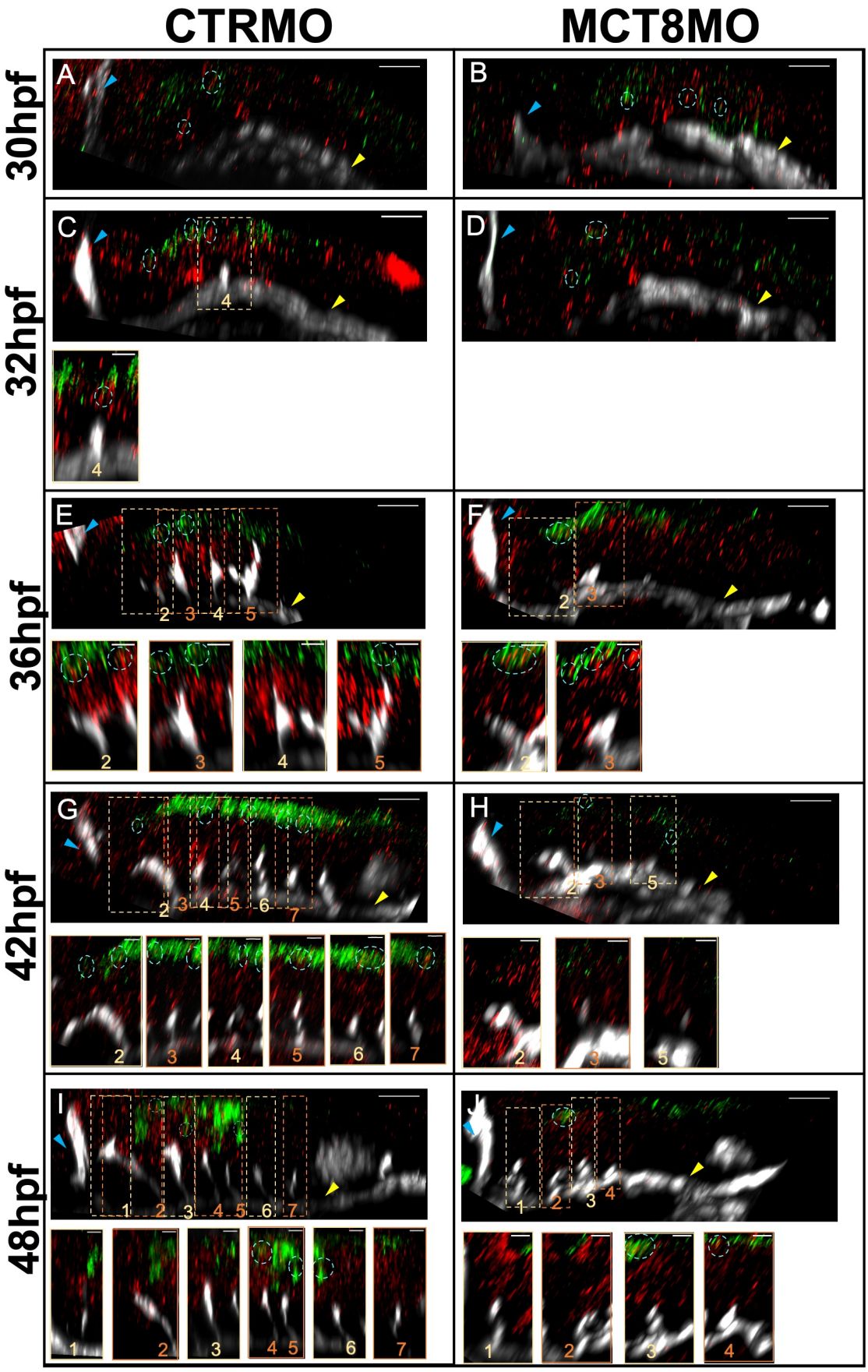
CTRMO
MCT8MO
30hpf
32hpf
36hpf
42hpf
48hpf
A
B
C
D
E
F
G
H
I
J

Figure 4.4 (previous page) – *pax6a* and *vegfaa* expression colocalise during BHB development. A – J) Fluorescent maximum projection images of double ISH of *pax6a* (green colour) and *vegfaa* (red colour) and IHC against GFP (endothelial cell marker, white colour) in CTRMO and MCT8MO zebrafish embryos at 30, 32, 36, 42 and 48 hpf are represented. The hindbrain of CTRMO and MCT8MO zebrafish embryos were analysed for colocalisation of *pax6a* and *vegfaa* co-expressing cells (cyan dotted circles) during BHB development at different time points. Colocalisation was determined by using the colourmap colocalisation plugin of Fiji software in the region of every CtA. Under each full hindbrain image, a maximum projection of the CtA, which is highlighted by a yellow or an orange dotted box, is represented to show the colocalisation of *pax6a* and *vegfaa* expressing cells in the plane of the CtA migration. The blue arrowhead represents the mid-cerebral vein (MCeV), and the yellow arrowhead represents the primordial hindbrain channels (PHBC). Yellow/orange numbers 1 – 7 indicate the CtA in its respective rhombomere. n = 8 – 10. Scale bar: 50 μm and 10 μm.

Afterwards, we wanted to understand if there is a relationship between the developing CtAs and the co-expressing *pax6a* and *vegfaa* cells between CTRMO and MCT8MO zebrafish embryos (Fig. 4.5). CtA 1 develops later during BHB (Ulrich et al., 2011). The statistical analysis revealed no relationship between CtA 1 development and *pax6a/vegfaa* co-expressing cells in the different time points analysed. Development of CtA 2 in CTRMO embryos showed that *pax6a/vegfaa* co-expressing cells were present from 30 hpf onwards. In MCT8MO embryos, these *pax6a/vegfaa* expressing cells were absent; at 48 hpf only 30% of the embryos developed CtA 2. Statistical analysis revealed that the existence of *pax6a/vegfaa* co-expressing cells might favour the development of CtA 2. CtA 3 developed in most CTRMO and MCT8MO zebrafish embryos. However, this CtA develops later in MCT8MO embryos. This explains the statistical significance observed at 32 hpf. Nonetheless, *pax6a/vegfaa* co-expressing cells were present in MCT8MO zebrafish embryos in rhombomere 3 and at 36 hpf, this rhombomere starts to be vascularised in some MCT8MO embryos. This might indicate that the fact that *pax6a/vegfaa* co-expressing cells were present in this rhombomere leads to the successful development of CtA 3 in MCT8MO embryos. CtA 4 is one of the first CtAs to develop (Ulrich et al., 2011), but in MCT8MO zebrafish embryos, only at 42 hpf 10% of the embryos analysed managed to develop this CtA. In MCT8MO zebrafish embryos in which CtA 4 developed were the same with *pax6a/vegfaa* co-expressing cells, showing a dependency of CtA 4 development and *pax6a/vegfaa* co-expressing cells. This was also evident from the statistical analysis showing that CtA 4 development and *pax6a/vegfaa* co-expressing cells were required. In rhombomere 5, *pax6a/vegfaa* co-expressing cells were present in CTRMO and MCT8MO zebrafish embryos from 30 hpf. Between 32 and 42 hpf, the presence of CtAs and *pax6a/vegfaa*

co-expressing cells between CTRMO and MCT8MO embryos differed significantly, showing that *pax6a/vegfaa* co-expressing cells were needed for CtA development. In rhombomere 6, *pax6a/vegfaa* co-expressing cells were present in CTRMO and MCT8MO zebrafish embryos from 30 hpf. The statistical analysis showed a dependency between CtA 6 development and *pax6a/vegfaa* co-expressing cells at 36 and 42 hpf. However, analysing the frequency of *pax6a/vegfaa* co-expressing cells in CTRMO and MCT8MO zebrafish embryos, they don't differ significantly. This might indicate that another angiogenic factor is involved in developing this CtA. CtA 7 forms later during BHB development (Ulrich et al., 2011). In CTRMO zebrafish embryos, *pax6a/vegfaa* co-expressing cells were present in this rhombomere early during BHB development, while in MCT8MO embryos, *pax6a/vegfaa* co-expressing cells were only present from 42 hpf. At 42 hpf, the statistical analysis revealed a significant relationship between *pax6a/vegfaa* co-expressing cells and CtA 7 development. In summary, *pax6a/vegfaa* co-expressing cells might be required to develop CtAs 2, 4, 5 and 7.

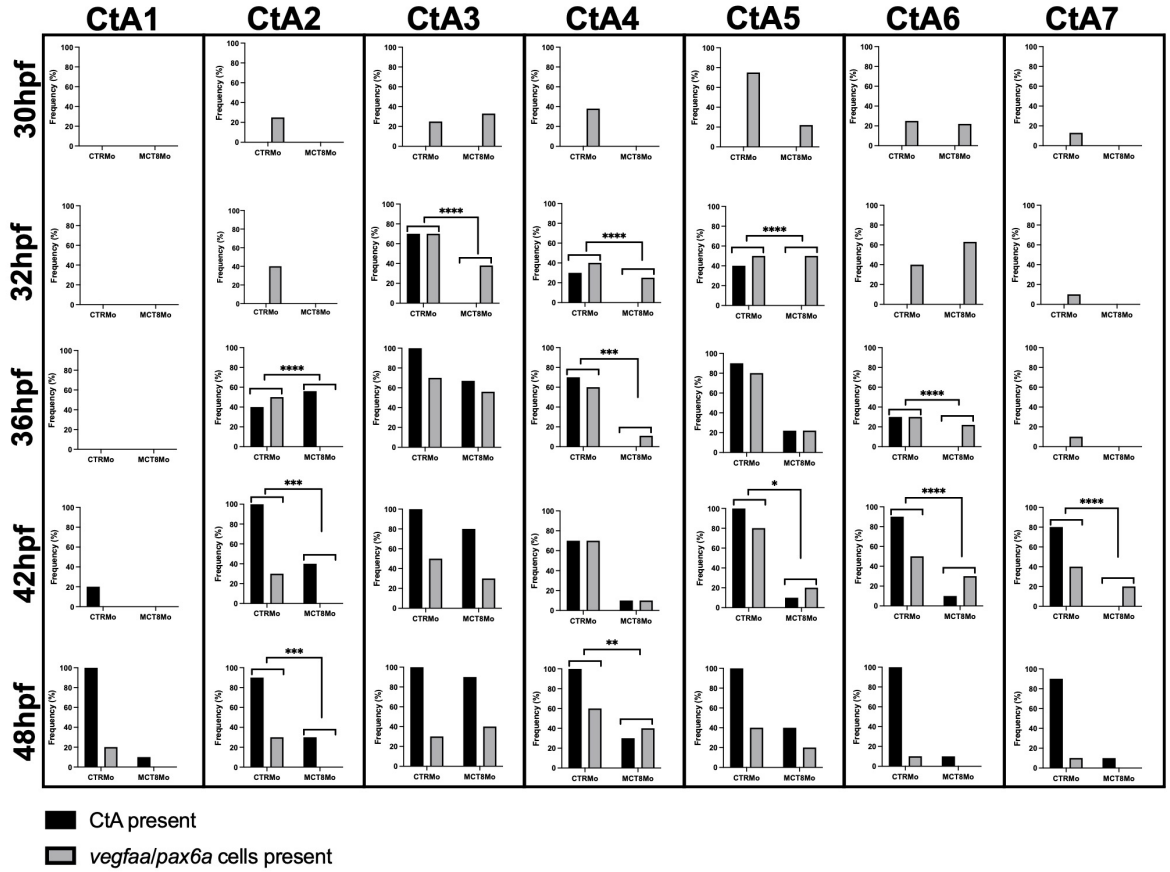

Figure 4.5 – *pax6a/vegfaa* co-expressing cells are needed for CtA development. During the different time points of BHB development, the presence and absence of CtAs and *pax6a*/*vegfaa* co-expressing cells were analysed and the correlation was analysed. CtAs 2, 4, 5 and 7 correlate with CtA development and *vegfaa/pax6a* co-

expressing cells. Statistical significance was determined using Fisher's exact test (n = 8 – 10). * p<0.05; ** p<0.01; *** p<0.001; **** p<0.0001.

4.2.4 *pax6a/vegfaa* co-expressing hindbrain cells influence central artery migration

Afterwards, we wanted to understand if the presence of *pax6a/vegfaa* co-expressing cells influences the direction of the growing CtA into the hindbrain. For that, the angle of the growing CtA was measured, using the primordial hindbrain channel (PHBC) as the basis (0 degrees). The angle was measured until the directional change of the CtA towards the basilar artery (BA) or its ipsilateral CtA neighbour. The CtAs that reached this point at a given embryonic stage are highlighted by the grey boxes in Fig. 4.6. In CTRMO zebrafish embryos, CtA 1 developed later in development (42 hpf; Fig. 4.6A), and this CtA was not attracted by the *pax6a/vegfaa* co-expressing cells. The growth angle between CTRMO and MCT8MO zebrafish embryos differed significantly because only 10% of the MCT8MO zebrafish embryos developed CtA 1 at 48 hpf (Fig. 4.6A). CtA 2 developed in most CTRMO embryos after 32 hpf (Fig. 4.6A) and at this developmental stage, *pax6a/vegfaa* co-expressing cells attracted this developing CtA towards its direction (Fig. 4.6 A and B). At 42 and 48 hpf, *pax6a/vegfaa* co-expressing cells were not influencing the directional growth of this CtA in CTRMO embryos (Fig. 4.6A). This was probably because the CtA already changed the directional migration, and thus the endothelial tip cells are likely not influenced by the *pax6a/vegfaa* co-expressing cells. In MCT8MO embryos, CtA 2 developed in some embryos, even without *pax6a/vegfaa* co-expressing cells (Fig. 4.6A). At 42 and 48 hpf, the angle of growth of CtA 2 differed significantly between CTRMO and MCT8MO zebrafish embryos (Fig. 4.6A). In CTRMO embryos, CtA 3 was attracted by *pax6a/vegfaa* co-expressing cells at 32 and 36 hpf (Fig. 4.6 A and B). At 42 and 48 hpf, this attraction was lost. The CtA grows in a different direction than the *pax6a/vegfaa* co-expressing cells (Fig. 4.6 A and B), probably because of the directional change of this CtA. Thus, the *pax6a/vegfaa* co-expressing cells do not influence the endothelial tip cells. In MCT8MO embryos, CtA 3 developed after 32 hpf. Although this CtA developed later than the control group, it grew towards the direction of the *pax6a/vegfaa* co-expressing cells until 48 hpf (Fig. 4.6 A and B). At 32 and 36 hpf, the angle of growth of CtA 3 between CTRMO and MCT8MO zebrafish embryos differed significantly (Fig. 4.6A), probably because of the late growth of this CtA in MCT8MO embryos. But at 42 and 48 hpf, this CtA developed

in the same direction in both experimental groups (Fig. 4.6 A and B). In CTRMO embryos, CtA 4 was attracted by *pax6a/vegfaa* co-expressing cells from 32 hpf to 48 hpf (Fig. 4.6 A and B). In MCT8MO embryos, *pax6a/vegfaa* co-expressing cells were almost absent during BHB development (Fig. 4.6A). A few cells appeared at 42 hpf and achieved to attract this CtA (Fig. 4.6 A and B). In CTRMO embryos, CtA 5 were attracted by *pax6a/vegfaa* co-expressing cells from 32 to 48 hpf (Fig. 4.6 A and B). The angle of CtA 5 migration and the location of *pax6a/vegfaa* co-expressing cells differed significantly between CTRMO and MCT8MO zebrafish embryos at 32, 36 and 42 hpf (Fig. 4.6A). Since *pax6a/vegfaa* co-expressing cells were almost absent in this rhombomere, this delayed the sprouting of this CtA. At 48 hpf, 50% of the MCT8MO embryos developed CtA 5. Although the growth angle was not statistically different between CTRMO embryos, we observed that the individual samples' growth angle was random (Fig. 4.6A). CtA 6 developed in CTRMO embryos after 32 hpf (Fig. 4.6A), and at 36 and 42 hpf, CtA 6 migrated towards the *pax6a/vegfaa* co-expressing cells (Fig. 4.6 A and B). At 48 hpf, CtA 6 migrated in the CTRMO embryos in a different direction than the *pax6a/vegfaa* co-expressing cells, which were almost absent at this developmental stage (Fig. 4.6A). Most MCT8MO embryos did not develop this CtA and *pax6a/vegfaa* co-expressing cells were also absent (Fig. 4.6 A). CtA 7 developed later during BHB development (Fig. 4.6A). At 42 hpf, this CtA grew towards the *pax6a/vegfaa* co-expressing cell, but at 48 hpf, the position of the cells and the growing CtA differed significantly in CTRMO embryos (Fig. 4.6 A and B). *pax6a/vegfaa* co-expressing cells were absent in MCT8MO embryos and CtA 7 did not develop until 48 hpf (Fig. 4.6A).

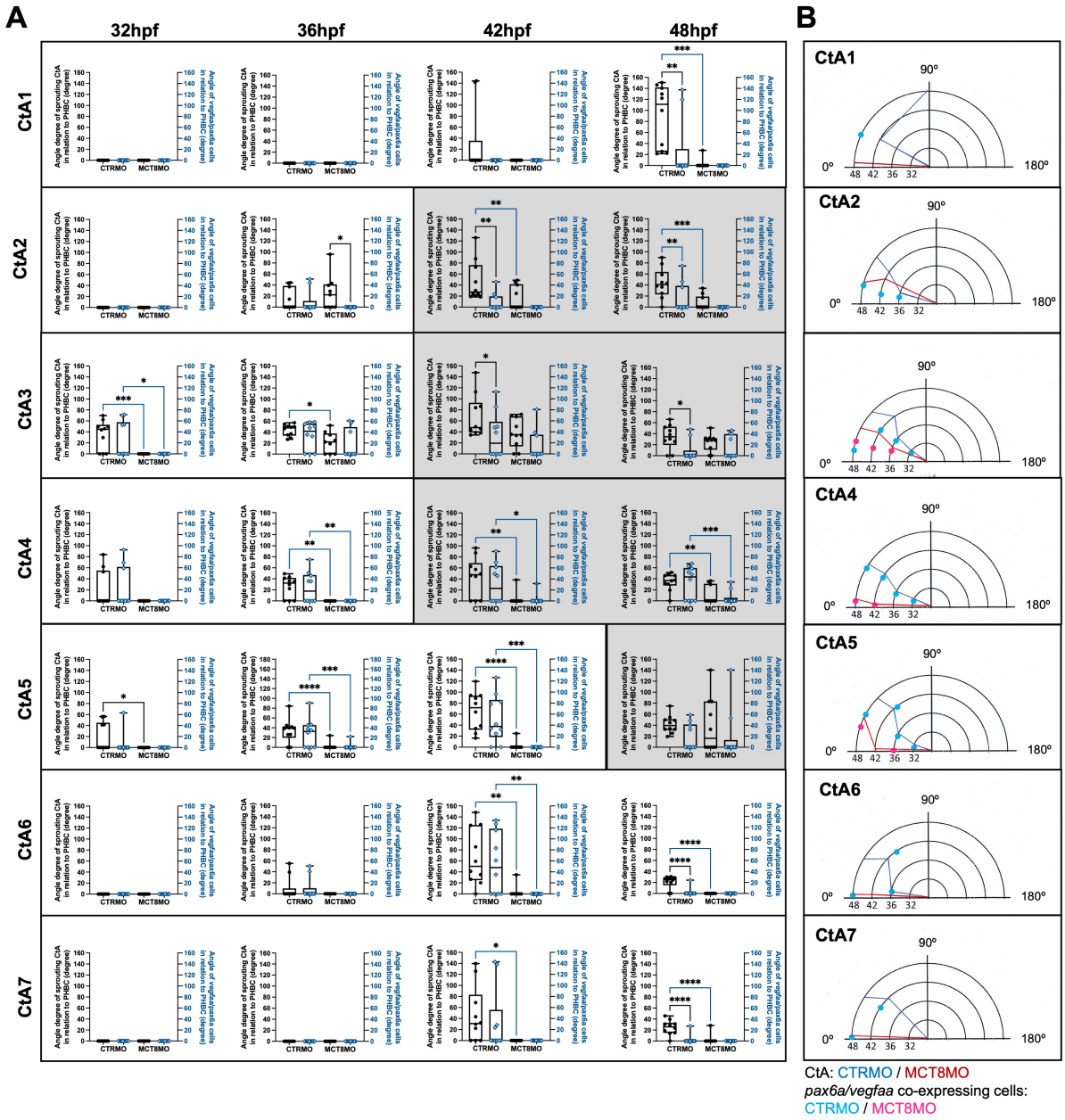

Figure 4.6 – *pax6a*/*vegfaa* co-expressing cells guide CtAs migration. A) The angle of the growing CtA was measured using the PHBC as the basis (0 degrees). The angle was measured before the turnover of the CtA towards the BA or directional change of the CtAs towards its ipsilateral neighbours. CtAs and *pax6a/vegfaa* co-expressing cells that were absent are indicated as 0º. Grey boxes show the CtAs that changed the directional migration during BHB development. Statistical significance was determined using 2-way ANOVA (n = 8 – 10). * $p<0.05$; ** $p<0.01$; *** $p<0.001$; **** $p<0.0001$. **B)** Graphical representation of the CtA directionality and the position of the *pax6a/vegfaa* co-expressing cells during BHB development. The mean values were used to construct these graphs.

4.2.5 Hindbrain *pax6a*+ cells express *thraa*, *thrab* and *mct8*

Expression of the zebrafish TH receptors *thraa* (Fig. 4.7), *thrab* (Fig. 4.8) and the TH membrane transporter *mct8* (Fig. 4.9) were detected by WISH in CTRMO and MCT8MO zebrafish embryos. Colocalisation analysis revealed that during BHB development, hindbrain *pax6a*+ cells express both receptors and the *mct8* transporter but at different time points and in different rhombomeres. In CTRMO zebrafish embryos *pax6a/thraa* colocalising cell were present in rhombomeres 3 to 7, mostly from 30 hpf to 36 hpf (Fig. 4.7). Colocalising *pax6a/thrab* cells were present in all 7 rhombomeres of CTRMO zebrafish embryos from 30 hpf until 48 hpf (Fig. 4.8). *pax6a/mct8* colocalising cells were present in rhombomeres 3 to 7 from 30hpf until 48 hpf in CTRMO zebrafish embryos (fig. 4.9).

Analysing the frequency in which *pax6a/thraa* co-expressing cells were present with the developing CtA during BHB development between CTRMO and MCT8MO embryos, we observed that CtAs 1, 2, and 7 were not being regulated by MT3 through *thraa* (Fig. 4.7 B). The absence of *pax6a/thraa* co-expressing cells in rhombomere 3 of MCT8MO embryos showed a relationship of these cells with CtA 3 development at 36 and 42 hpf (Fig. 4.7 A and B). However, CtA 3 developed in almost all MCT8MO zebrafish embryos, indicating probably that the absence of *pax6a/thraa* co-expressing cells could be important for the complete development of this CtA in all embryos analysed. In rhombomere 4, *pax6a/thraa* co-expressing cells were present at 32 and 36 hpf in CTRMO embryos, while these cells were absent in MCT8MO embryos (Fig. 4.7 A and B). The statistical analysis revealed a dependency of CtA 4 development and *pax6a/thraa* co-expressing cells at 36 hpf (Fig. 4.7 B), indicating that the initial expression of *pax6a/thraa* co-expressing cells in CTRMO embryos could be important for CtA 4 development. In rhombomeres 5 and 6, *pax6a/thraa* co-expressing cells were present, but the frequency of CtA development was low in MCT8MO embryos (Fig. 4.7 A and B). This might indicate that MT3 signals through *thraa* in *pax6a*+ hindbrain cells. However, another signalling cue is necessary for the sprouting of these CtAs.

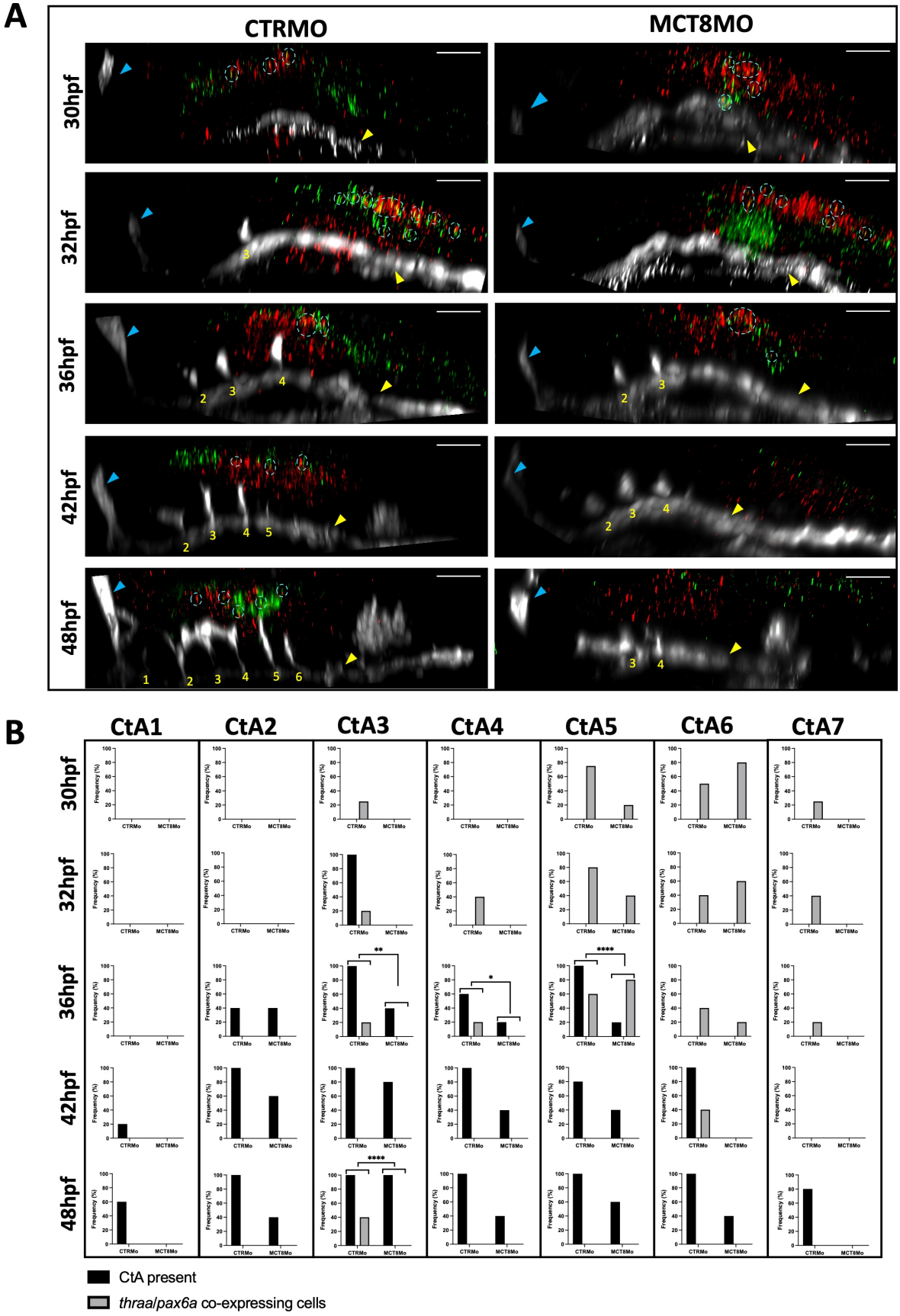
A
CTRMO
MCT8MO
30hpf
32hpf
36hpf
42hpf
48hpf
B
CtA1
CtA2
CtA3
CtA4
CtA5
CtA6
CtA7
Frequency (%)
CTRMo
MCT8Mo
CtA present
thraa/pax6a co-expressing cells

Figure 4.7 (previous page) – pax*6a*-expressing cells colocalise with TH receptor *thraa*. A) Fluorescent maximum projection images of double WISH of *pax6a* (green colour) and *thraa* (red colour) and IHC against GFP (endothelial cell marker, white colour) in CTRMO and MCT8MO zebrafish embryos at 30, 32, 36, 42 and 48 hpf are represented. The hindbrain of CTRMO and MCT8MO zebrafish embryos were analysed for colocalisation of *pax6a* and *thraa*-expressing cells (cyan dotted circles) during BHB development at different time points. Colocalisation was determined by using the colourmap colocalisation plugin of Fiji software in the region of every CtA. The blue arrowhead represents the mid-cerebral vein (MCeV), and the yellow arrowhead represents the primordial hindbrain channels (PHBC). Yellow numbers 1 – 7 indicate the CtA in its respective rhombomere. Scale bar: 50 µm. **B)** During the different time points of BHB development, the presence and absence of CtAs and *pax6a*/*thraa* co-expressing cells were analysed and the correlation was analysed. Statistical significance was determined using Fisher's exact test (n = 4 – 5). * $p<0.05$; ** $p<0.01$; *** $p<0.001$; **** $p<0.0001$.

Analysing the frequency in which *pax6a/thrab* co-expressing cells were present with the developing CtA during BHB development between CTRMO and MCT8MO zebrafish embryos, we observed that CtAs 1 and 7 were not being regulated by MT3 through *thrab* (Fig. 4.8 B). In rhombomere 3 of MCT8MO embryos, *pax6a/thrab* co-expressing cells were absent from 30 hpf until 36 hpf (Fig. 4.8 A and B). The statistical analysis revealed a dependency of *pax6a/thrab* co-expressing cells and CtA development at 36 hpf (Fig. 4.8 B). However, most of the MCT8MO embryos developed this CtA. In rhombomere 2, *pax6a/thrab* co-expressing cells were present in CTRMO embryos, while these cells were absent in MCT8MO embryos (Fig. 4.8 A and B). At 42 and 48 hpf we observed a significant dependency of CtA development and the presence of *pax6a/thrab* co-expressing cells (Fig 4.8 B), indicating that these cells were necessary for the development of CtA 2. The frequency of CtAs 4, 5, and 6 developments in MCT8MO embryos were low compared to CTRMO embryos. Statistical analysis revealed that the condition of *pax6a/thrab* co-expressing cells and CtA development was important. However, in these rhombomeres *pax6a/thrab* co-expressing cells were present (Fig. 4.8 A and B). This might indicate that another signalling mechanism regulates CtA development in these rhombomeres than through *pax6a/thrab* co-expressing cells.

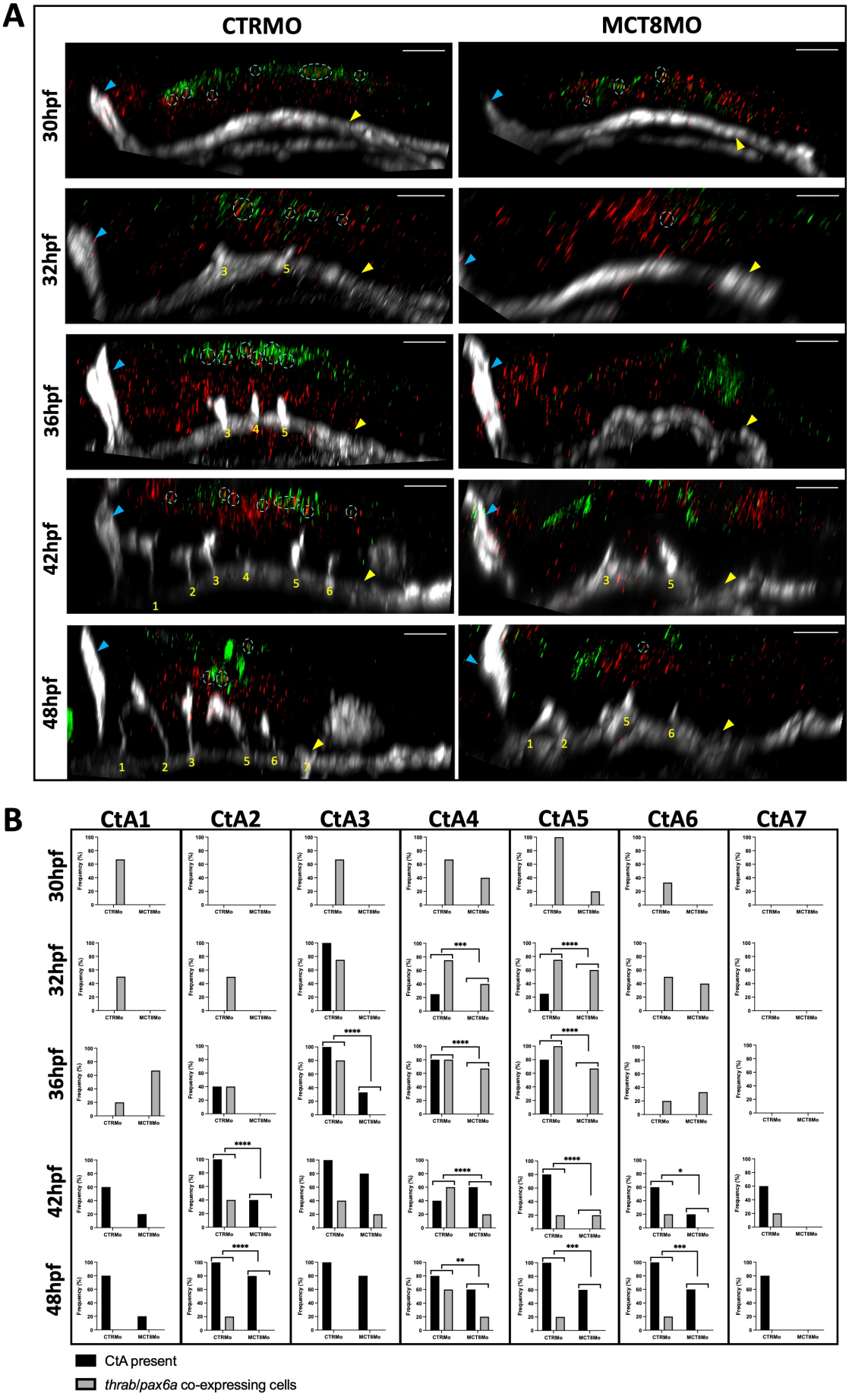
A
CTRMO
MCT8MO
30hpf
32hpf
36hpf
42hpf
48hpf
B
CtA1
CtA2
CtA3
CtA4
CtA5
CtA6
CtA7
Frequency (%)
CTRMo
MCT8Mo
CtA present
thrab/pax6a co-expressing cells

Figure 4.8 (previous page) – *pax6a*-expressing cells colocalise with TH receptor *thrab*. A) Fluorescent maximum projection images of double WISH of *pax6a* (green colour) and *thrab* (red colour) and IHC against GFP (endothelial cell marker, white colour) in CTRMO and MCT8MO zebrafish embryos at 30, 32, 36, 42 and 48 hpf are represented. The hindbrain of CTRMO and MCT8MO zebrafish embryos were analysed for colocalisation of *pax6a* and *thrab*-expressing cells (cyan dotted circles) during BHB development at different time points. Colocalisation was determined by using the colourmap colocalisation plugin of Fiji software in the region of every CtA. The blue arrowhead represents the mid-cerebral vein (MCeV), and the yellow arrowhead represents the primordial hindbrain channels (PHBC). Yellow numbers 1 – 7 indicate the CtA in its respective rhombomere. Scale bar: 50 µm. **B)** During the different time points of BHB development, the presence and absence of CtAs and *pax6a*/*thrab* co-expressing cells were analysed and the correlation was analysed. Statistical significance was determined using Fisher's exact test (n = 3 – 5). * $p<0.05$; ** $p<0.01$; *** $p<0.001$; **** $p<0.0001$.

Analysing the frequency in which *pax6a/mct8* co-expressing cells were present with the developing CtA during BHB development between CTRMO and MCT8MO zebrafish embryos, we observed that CtAs 1, 2, 6 and 7 were not being regulated by MT3 through *pax6a/mct8* co-expressing cells (Fig. 4.9 B). In MCT8MO embryos, *pax6a/mct8* co-expressing cells were absent in every rhombomere and every stage (Fig. 4.9 A and B). This is expected since the morpholino downregulates the *mct8* mRNA. In rhombomere 3, *pax6a/mct8* co-expressing cells were present at 36 and 48 hpf in CTRMO embryos (Fig. 4.9 A and B). The statistical analysis revealed that at these time points, CtA 3 development depends on these *pax6a/mct8* co-expressing cells (Fig. 4.9 B). However, most embryos developed CtA 3, which might indicate that the signalling through *mct8* might be required to potentiate CtA 3 development but is not the essential and necessary factor. In rhombomeres 4 and 5, the statistical analysis revealed that *pax6a/mct8* co-expressing cells were required for CtA development from 42 hpf onwards (Fig. 4.9 B).

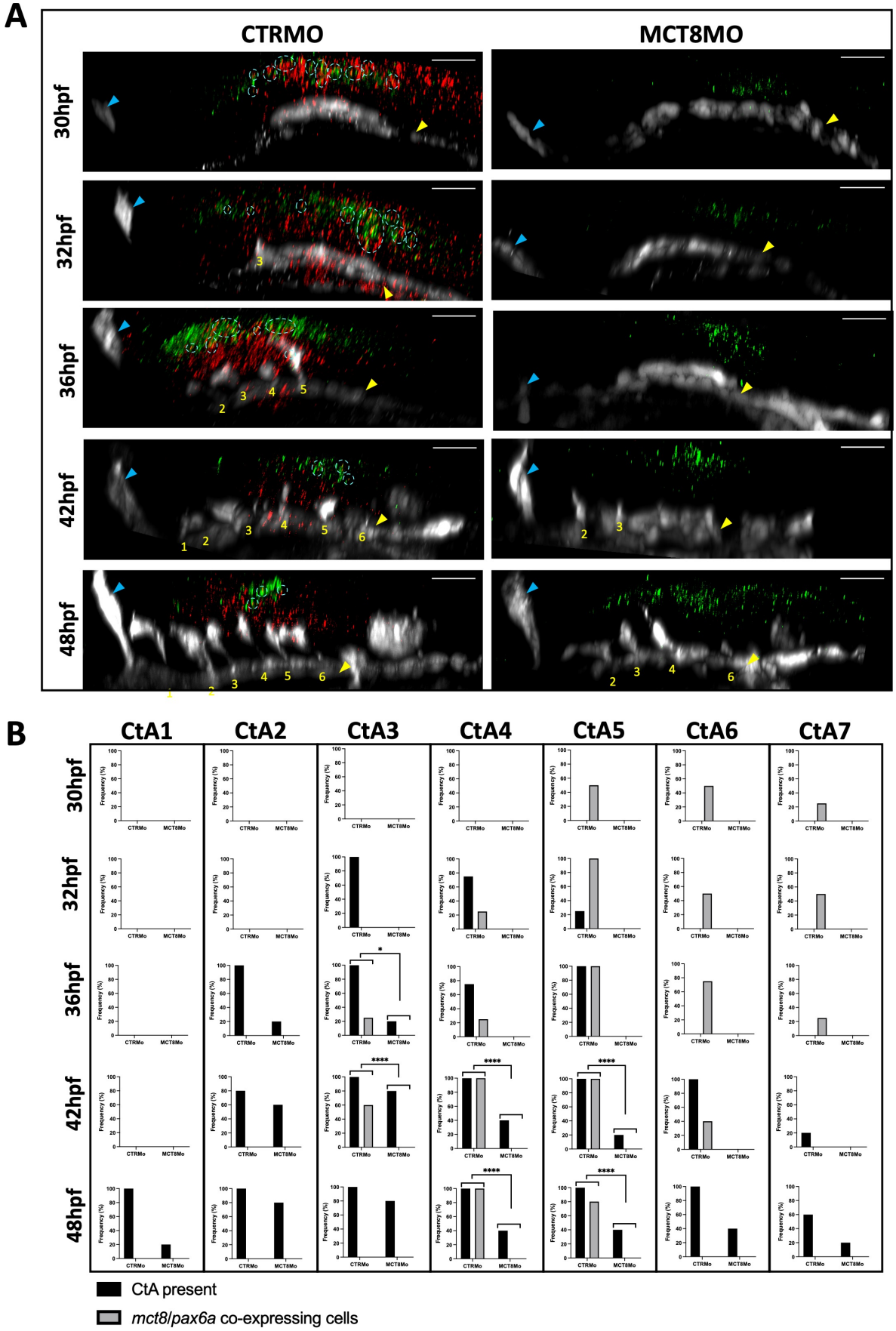
A
CTRMO
MCT8MO
30hpf
32hpf
36hpf
42hpf
48hpf
B
CtA1
CtA2
CtA3
CtA4
CtA5
CtA6
CtA7
Frequency (%)
CTRMo
MCT8Mo
CtA present
mct8/pax6a co-expressing cells

Figure 4.9 (previous page) – *pax6a*-expressing cells colocalise with TH transporter *mct8*. A) Fluorescent maximum projection images of double WISH of *pax6a* (green colour) and *mct8* (red colour) and IHC against GFP (endothelial cell marker, white colour) in CTRMO and MCT8MO zebrafish embryos at 30, 32, 36, 42 and 48 hpf are represented. The hindbrain of CTRMO and MCT8MO zebrafish embryos were analysed for colocalisation of *pax6a* and *mct8*-expressing cells (cyan dotted circles) during BHB development at different time points. Colocalisation was determined by using the colourmap colocalisation plugin of Fiji software in the region of every CtA. The blue arrowhead represents the mid-cerebral vein (MCeV) and the yellow arrowhead represents the primordial hindbrain channels (PHBC). Yellow numbers 1 – 7 indicate the CtA in its respective rhombomere. Scale bar: 50 μm. **B)** During the different time points of BHB development, the presence and absence of CtAs and *pax6a*/*mct8* co-expressing cells were analysed and the correlation was analysed. Statistical significance was determined using Fisher's exact test (n = 3 – 5). * $p<0.05$; ** $p<0.01$; *** $p<0.001$; **** $p<0.0001$.

4.2.6 Anti-Pax6 injection failed to knockdown *pax6* in the zebrafish hindbrain

To investigate the involvement of hindbrain *pax6a* progenitor cells in BHB development, a loss-of-function strategy by antibody-mediated knockdown was conducted (Lesaffre et al., 2007). This strategy was used by Lesaffre et al., (2007) to knockdown Pax6 function to study eye development. However, the intercellular injection of anti-Pax6 only affected eye development, while other structures dependent on Pax6 signalling, such as the hindbrain, remained unaffected (Lesaffre et al., 2007). For that reason, we increased the concentration of monoclonal anti-Pax6 (anti-mPax6; against Pax6a and Pax6b (DSHB, USA)) to 100 μg/ml, directly injected into the cell of 1-cell stage zebrafish eggs. We used zebrafish embryos that expressed mCherry under the regulatory region of the vascular endothelial growth factor receptor kdr-like (kdrl) (Fujita et al., 2011) and GFP under the regulatory region of the glial fibrillary acidic protein (GFAP) (Bernardos and Raymond, 2006) to view the effect of Pax6 in the vascular and nervous system simultaneously. At 48 hpf zebrafish embryos injected with anti-myc (DSHB, USA), which was used as a negative control for non-specific IgG reactions and that does not exist in zebrafish, presented a similar phenotype as control embryos (injected with 1×PBS) (Fig. 4.10 A and B). Zebrafish embryos injected with anti-mPax6 presented different phenotypes compared to control embryos (Fig. 4.10 A and C). Some zebrafish embryos presented a curved trunk, reduced eye diameter (eye diameter was not measured), and

the brain region showed malformations (Fig. 4.10 C). These zebrafish embryos presented a similar phenotype as the *pax6a*MO and *pax6(a+b)*MO from Coutinho et al., (2011). Live-imaging of anti-myc and anti-mPax6 injected embryos presented similar GFAP expression to control embryos (Fig. 4.10 D to F). Analysing the frequency of CtA development in the different experimental groups showed that injection with anti-myc and anti-mPax6 affected the same CtAs, CtAs 2, 3, 4, 5 and 7 compared to control embryos (Fig. 4.10 J). To confirm that Pax6 was absent in the zebrafish hindbrain, an IHC against α-mPax6 was conducted, which showed that Pax6 cells were still present in anti-mPax6 injected zebrafish embryos (Fig. 4.10 G – I). Overall, this knockdown experiment did not work for the zebrafish hindbrain, indicating that this method is not suitable for hindbrain loss-of-function study.

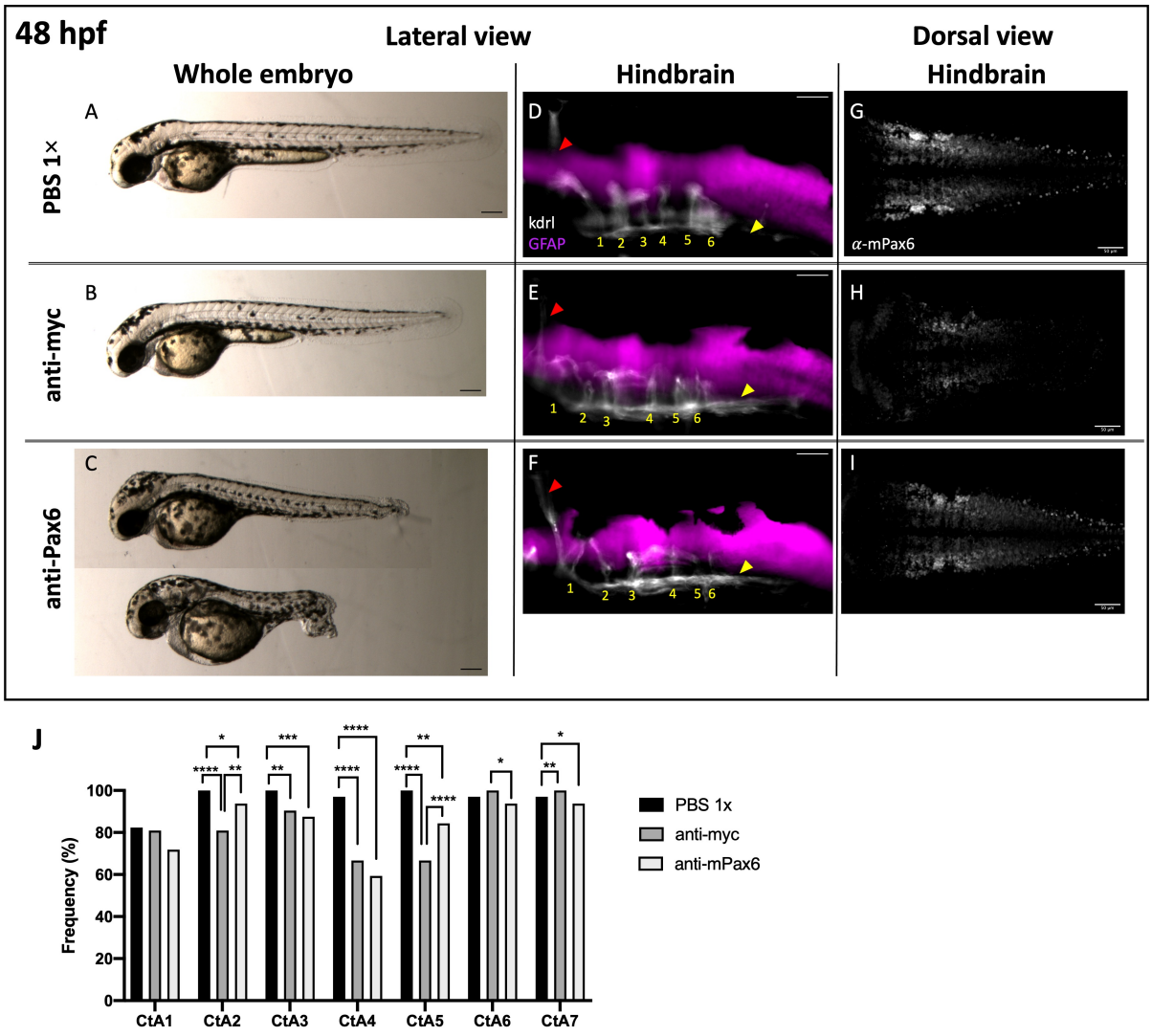

Figure 4.10 – Intercellular injection of anti-Pax6 monoclonal antibody did not affect CtA development. A - C) Lateral view of 48 hpf zebrafish embryos injected with 1× PBS (negative control), anti-myc antibody (non-specific IgG control) and anti-mPax6 antibody. Zebrafish embryos injected with 1× PBS and anti-myc antibody have

a similar phenotype. Zebrafish embryos injected with anti-mPax6 presented different phenotypes and differed from control (1× PBS) and anti-myc embryos. Scale bar: 200 μm. **D - F)** Live fluorescent images of 48 hpf zebrafish embryos expressing mCherry under the regulatory region of kdrl (endothelial cell marker, white colour) and expressing GFP under the regulatory region of GFAP (radial glial cell marker, magenta colour). No differences in CtA development and GFAP expression were observed in the different experimental conditions observed. The red arrowhead represents the mid-cerebral vein (MCeV), and the yellow arrowhead represents the primordial hindbrain channels (PHBC). Yellow numbers 1 – 7 indicate the CtA in its respective rhombomere. Scale bar: 50 μm. **G - I)** Dorsal view of fluorescent maximum projection images are represented. Immunohistochemistry against Pax6 (white colour) in 48 hpf zebrafish embryos shows that Pax6-expressing cells were present in all experimental groups. Zebrafish embryos injected with anti-mPax6 presented a slightly reduced expression of Pax6, while anti-myc injected embryos presented a high reduction in Pax6-expressing cells. n = 5 – 6. Scale bar: 50 μm. **J)** Graphical view of the frequency (%) of CtA development in the different experimental conditions. Intercellular injection of anti-mPax6 did not affect CtA development. Statistical analysis was performed using Fisher's exact test (n = 21 – 34). * $p<0.05$; ** $p<0.01$; *** $p<0.001$; **** $p<0.0001$.

4.2.7 Mutant *pax6a* CRISPER zebrafish present central arteries impaired development

After the unsuccessful knockdown experiment, we used the CRISPR/Cas9 technology to generate a *pax6a* mutant zebrafish. A guide RNA (gRNA) was designed against the zebrafish *pax6a* exon 7 locus (GGTTGAGGTTGTGCCCGAGG). Zebrafish embryos were injected with the *pax6a* gRNA and Cas9 protein (Weissman Institute, Israel) in 1-cell stage zebrafish embryos. The efficiency of the injection was verified by PCR using genomic DNA of the F0 *pax6a* mutant zebrafish embryos, which from here on are called crispants, and not injected control (CTR) embryos at 24 hpf. *pax6a* crispants were previously screened for positive *pax6a* mutation by selecting embryos with a small eye phenotype (Lesaffre et al., 2007). The PCR shows that *pax6a* crispants present a shorter exon 7 compared to CTR embryos (Fig. 4.11A). Sequence alignment analysis shows that CTR embryos share 99% of nucleotide homology with the canonical *pax6a* wildtype (wt) sequence (GenBank: BX004784.9), while the *pax6a* crispants share 94% of nucleotide homology with the canonical *pax6a* wt sequence. CTR and *pax6a* crispants share 96% of nucleotide homology. Most of the mutations present in the *pax6a* crispants were generated by deletions and point mutations in exon 7 (Fig. 4.11B). Exon 7 encodes the linker region between the paired domain and homeodomain (Dansault et al., 2007),

and the mutations generate a premature termination codon. It has been suggested by previous reports that this premature termination codon may result in a truncated protein, which lack the homeodomain and the PST domain, leading to the production of an inactive Pax6a protein (Qiu et al., 2019).

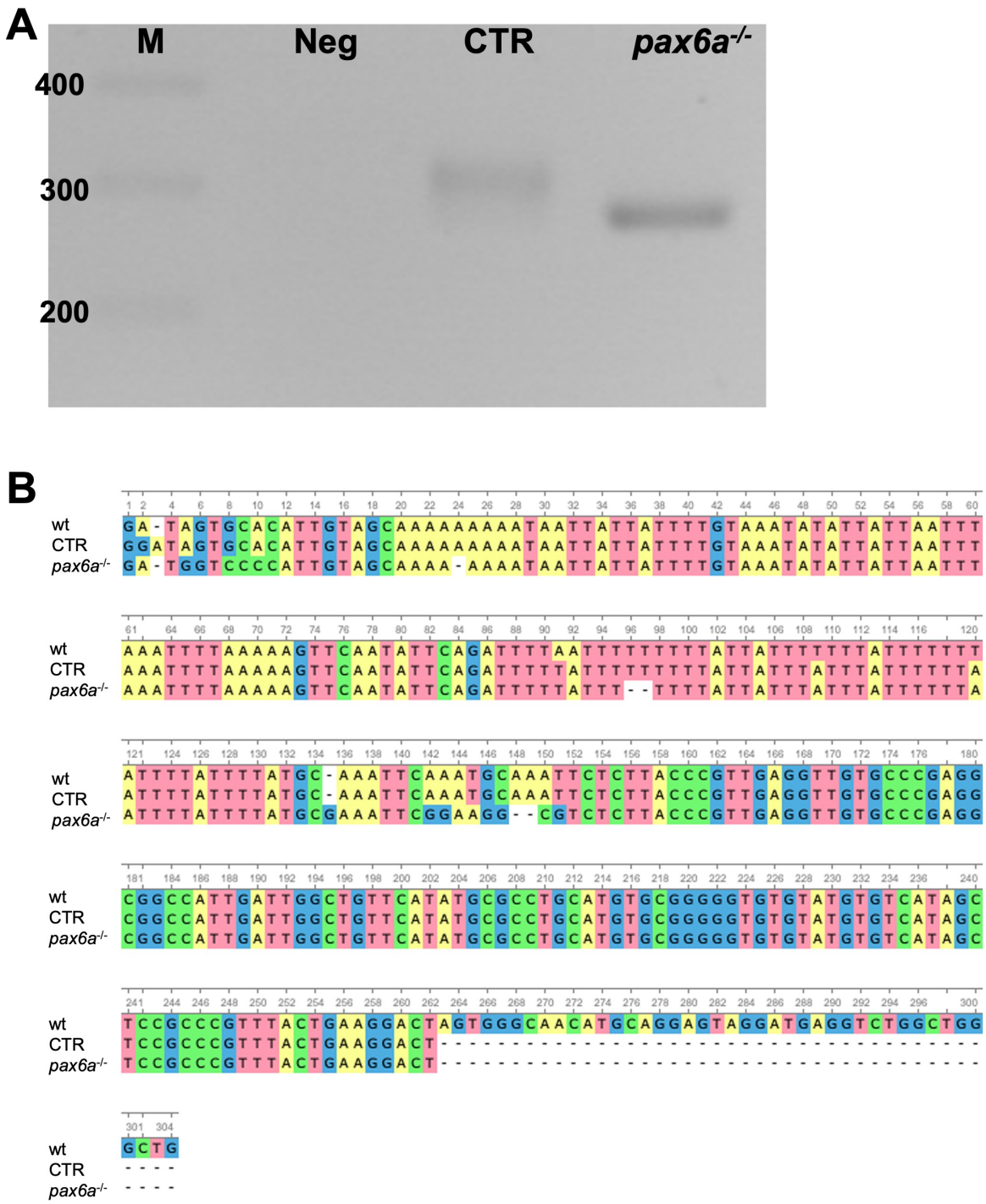

Figure 4.11 – CRISPR/Cas9 generated *pax6a* crispants gives rise to mutations in exon 7 that lead to the production of a truncated protein. A) PCR genotyping of not injected control embryos (CTR) and homozygotic *pax6a* mutant zebrafish embryos

(*pax6a*$^{-/-}$). M – Gene marker in base pair; Neg – Negative PCR control. **B)** Sequence alignment of the canonical *pax6a* wildtype (wt) exon 7 genomic region, with sequenced not injected control embryo (CTR), and homozygotic *pax6a* mutant embryo (*pax6a*$^{-/-}$).

Afterwards, *Tg(kdrl:CaaX-mCherry)* (Fujita et al., 2011) *pax6a* crispants were used to evaluate CtA development. Live imaging was conducted from 32 hpf onwards, focused on the hindbrain. We observed that *pax6a* crispants developed a normal PHBC (yellow arrowheads in Fig. 4.12A lower panel), mid-cerebral vein (MCeV, red arrowheads in Fig. 4.12A lower panel) and lateral dorsal aorta (LDA, green arrowhead in Fig. 4.12A lower panel). Like MCT8MO zebrafish embryos, *pax6a* crispants displayed a reduced number of CtAs compared to non-injected control embryos (Fig. 4.12A). In *pax6a* crispants the first CtAs sprouts were present at 36 hpf (Fig. 4.12A second panel). At 40 hpf, a third CtA developed, and these were the only CtAs that developed until 48 hpf (Fig. 4.12A second panel).

To compare the results with MCT8MO zebrafish embryos, we conducted the same live imaging experiment, using *Tg(fli1:EGFP)* zebrafish embryos (Lawson and Weinstein, 2002) (Fig. 4.12B). CtAs in CTRMO zebrafish embryos developed similarly to those in not-injected control embryos (Fig. 4.12 A and B, first panels). MCT8MO zebrafish embryos developed CtAs after 36 hpf, presenting 2 CtAs at 40 hpf (Fig. 4.12B second panel). At 44 hpf a third CtA developed, and these are the only CtAs that developed until 48 hpf (Fig. 4.12B, second panel). This shows that *pax6a* crispants and MCT8MO zebrafish embryos presented both CtA defects that arise in a similar chronological order (Fig. 4.11 A and B).

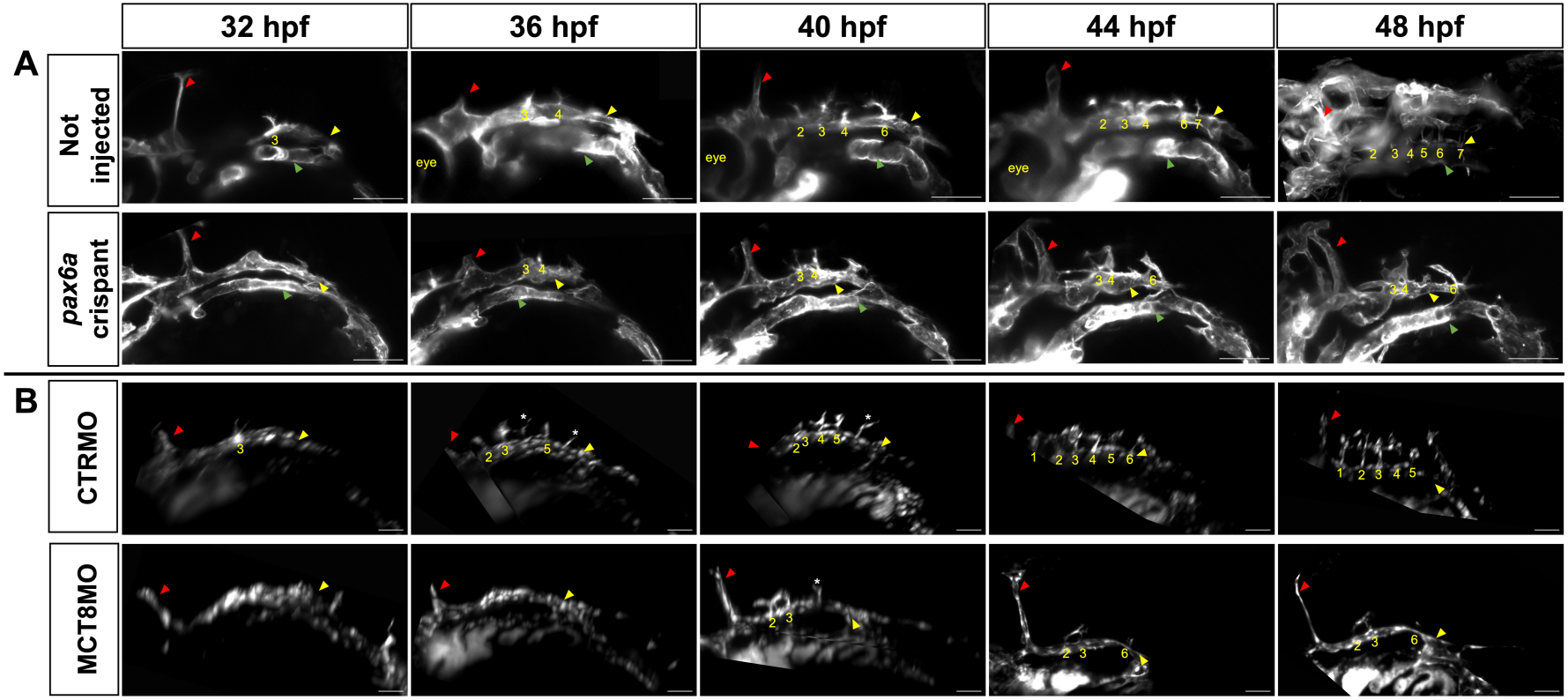

Figure 4.12 – *pax6a* mutant zebrafish embryos show a similar BHB development as MCT8MO zebrafish embryos. A) Live imaging of 32 hpf zebrafish embryo at the start of imaging (light sheet microscopy) between non-injected (control) and *pax6a* crispant zebrafish embryos are represented. The vascular system (*kdrl*) is shown in white (mCherry) in the reporter line *Tg(kdrl:CaaX-mCherry)*. Dorsal view of maximum projection images of the mentioned time points is shown. **B)** Life imaging of 32 hpf zebrafish embryo at the start of imaging between CTRMO and MCT8MO zebrafish embryos are represented. The vascular system is shown in white (GFP) in the reporter line *Tg(fli1:EGFP)*. Dorsal view of maximum projection images of the mentioned time point is shown. The red arrowhead represents the mid-cerebral vein (MCeV), the yellow arrowhead represents the primordial hindbrain channels (PHBC), and the green arrowhead represents the lateral dorsal aorta (LDA). White * represents sprouting projections of the PHBC to the BA (due to the inclination of the hindbrain imaging, we can visualise these structures). Yellow numbers 1 – 7 indicate the CtA in its respective rhombomere. n = 2. Scale bar: 50 µm.

Later we further confirmed in F2-generated zebrafish larvae at 4 days post-fertilization (dpf) the observations carried out using the F0-generated embryos for *pax6a* loss-of-function. The former showed an altered body and trunk development compared to wild-type control larvae (Fig. 4.13 A and B). They also showed defective hindbrain angiogenesis compared to control larvae, presenting reduced CtAs (Fig. 4.13 C and D).

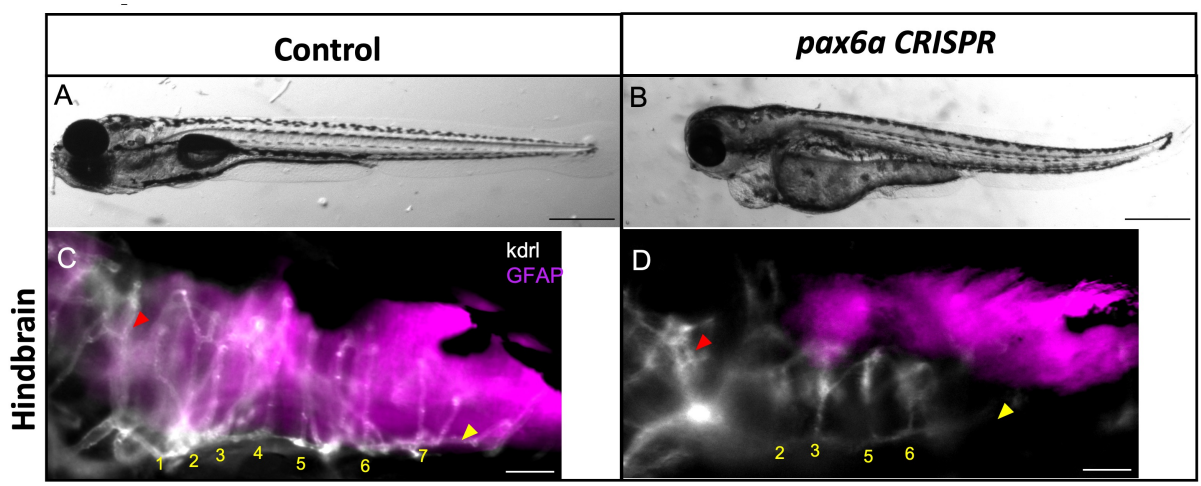

Figure 4.13 – *pax6a* knockout zebrafish larvae loose hindbrain central arteries. A-D) Comparison between control (not injected) and mutant *pax6a* CRISPR zebrafish larvae at 4 dpf are presented. **A-B)** Mutant *pax6a* knockout zebrafish larvae show a different phenotype than control larvae. Scale bar: 500 µm. **C-D)** The hindbrain of *pax6a* mutant zebrafish embryos presented only 4 CtAs, while the control zebrafish have 7 CtAs. The red arrowhead represents the mid-cerebral vein (MCeV), and the yellow arrowhead represents the primordial hindbrain channels (PHBC). Yellow numbers 1 – 7 indicate the CtA in its respective rhombomere. n = 5 – 9. Scale bar: 50 µm.

4.3 DISCUSSION

Several links have been made between the vascular and nervous systems over the last few years. The evidence that these two systems should be recognized as one functional unit is fundamental in understanding several diseases that combine the vascular and nervous systems, particularly in the brain (reviewed in Ridaura et al., 2021). During vertebrate brain development, NPC, including neuroepithelial cells and radial glia, regulate the expression of Vegfa for blood vessel ingression into the neural tissue (Haigh et al., 2003; Ma et al., 2013; Matsuoka et al., 2017; Raab et al., 2004). This ensures the delivery of oxygen and nutrients to the growing neural tissue. On the other hand, blood vessels modulate the balance between NPC proliferation and

differentiation. The relief of the hypoxic levels in the NPC niches leads to the differentiation of the NPC (Lange et al., 2016; Simon and Keith, 2008).

Previously we have shown that MT3 indirectly regulates the angiogenic sprouting of the hindbrain CtAs by regulating the expression of *vegfaa* in MT3-dependent hindbrain cells (Chapter 2). Here we show that MT3 via hindbrain *pax6a* progenitor cells, mediate the expression of *vegfaa* required for CtA development in a timely dependent manner.

4.3.1 MT3 regulates *pax6a* expression during zebrafish embryogenesis

Maintaining the balance between NPC self-renewal and neurogenesis is fundamental to generating the correct proportions of different classes of neurons (Sansom et al., 2009). One important gene that acts as a molecular switch between cell fate control and differentiation is *Pax6* (Bel-Vialar et al., 2007). *Pax6* is highly conserved between vertebrate and invertebrate species and has a fundamental role in developing the spinal cord, cerebral cortex, eyes, olfactory system, and pancreas (Hill et al., 1991; Klann and Seaver, 2019; Lesaffre et al., 2007; Osumi et al., 2008; St-Onge et al., 1997; van Heyningen and Williamson, 2002). Previous studies have shown that *Pax6* expression was downregulated in the developing neocortex in maternal TH-deficient mice. However, *Pax6* levels normalised at the peak of the first neurogenesis, indicating an indirect regulation of maternal THs on this transcription factor (Mohan et al., 2012). The transcriptome data (Chapter 2) indicated that this transcription factor was downregulated in 25 hpf MCT8MO zebrafish embryos (-0.575, $p<0.01$; FDR 5%, NCBI – BioProjects: PRJNA381309). Neurogenesis in zebrafish is ongoing at this point, since most neurons develop after neural tube closure from 18 hpf onwards (Schmidt et al., 2013). Analysing the expression pattern of *pax6a* by WISH demonstrated that this transcription factor was reduced in a cell-specific manner in the hindbrain and spinal cord of 25 and 48 hpf MCT8MO embryos compared to CTRMO embryos (Fig. 4.2). This data indicates that, unlike in mice, *pax6a* expression in zebrafish continues downregulated after the onset of neurogenesis. These facts may indicate differences between species in regulating *pax6a* by MT3. These results lead us to hypothesise that if some *pax6a*+ hindbrain cells are lost in MCT8MO embryos, are they responsible for CtA ingression during zebrafish embryonic development? During BHB developmental time window (32 – 48 hpf), *pax6a* expression was detected near the CtAs in CTRMO embryos. In CTRMO embryos *pax6a*-expressing cells increased in the

anterior hindbrain from 32 hpf to 48 hpf (Fig. 4.3). An increase in *pax6a* expression during CNS development might indicate that NPC initiates neuronal differentiation (Bel-Vialar et al., 2007). In MCT8MO embryos, *pax6a* expression was reduced in the hindbrain and spinal cord compared to CTRMO embryos (Fig. 4.2 and 4.3). In the hindbrain, ventral *pax6a*+ cells were more dependent on MT3 signalling than the more dorsal *pax6a*+ cells (Fig. 4.3). At the same time, in the spinal cord, the dorsal *pax6a*+ cells were more dependent on MT3 signalling (Fig. 4.2). This might indicate that MT3 acts differently in the different regions of the CNS and that all *pax6a*+ cells do not have the same identity. This is not unexpected since it has been previously demonstrated that MT3 acts in a developmental time and cell context-dependent manner (Silva and Campinho, 2023). In MCT8MO zebrafish embryos, rhombomere boundaries were also affected (Fig. 4.2). This has also been observed previously in *pax6a*MO zebrafish embryos (Nolte et al., 2006), in the hindbrain of chicken embryos (Peretz et al., 2016) and mice (Takahashi and Osumi, 2011).

In MCT8MO zebrafish embryos, the loss of Mct8 function leads to an underdeveloped vascularisation of the hindbrain (Campinho et al., 2014; Chapter 2). At 25 hpf, *pax6a* expression was already reduced in the MCT8MO zebrafish embryos, indicating that the loss of hindbrain *pax6a*-expressing cells was unlikely to be an effect caused by the underdeveloped vascularisation of the CNS. We hypothesise that most probably MT3 is 1) directly regulating *pax6a* expression in a cell-autonomous manner or 2) MT3 is regulating *pax6a* progenitor cells by regulating morphogenic signalling, such as SHH, FGF or RA signalling that are important for these cells to develop (del Corral and Morales, 2014; Diez del Corral et al., 2003; Diez del Corral and Morales, 2017; Ericson et al., 1997). Studies conducted in the developing brain of mice have shown that Shh is a direct target of T3 (Desouza et al., 2011; Gil-Ibañez et al., 2015; Gil-Ibáñez et al., 2014). *In vitro* studies of primary cultured cells from the embryonic mouse cerebral cortex and cerebellar astrocyte cultures showed that T3 regulates the expression of RA and FGF, respectively (Gil-Ibáñez et al., 2014; Mendes-De-Aguiar et al., 2008). However, we didn't look further into the indirect regulation of *pax6a* through these morphogenic signalling pathways in this thesis. Nonetheless, it is unlikely that MT3 regulates *pax6a* expression via *shh* given that there were no changes in expression in MCT8MO embryos (Campinho et al., 2014).

4.3.2 Hindbrain *pax6a*+ cells are responsible for the chemoattraction of the central arteries in a cell-autonomous way

In Chapter 2 we demonstrated that MT3 regulates the expression of *vegfaa* to induce the angiogenic sprouting and ingression of several hindbrain CtAs. In MCT8MO zebrafish embryos, *vegfaa* expression was reduced, and consequently, several CtAs were lost, showing that MT3 has a vital role in regulating hindbrain angiogenesis. First, we showed that *pax6a* and *vegfaa* expressing cells colocalise during BHB developmental time window and that these colocalising cells were juxtaposed to the developing CtAs (30 – 48 hpf, Fig. 4.4). We also observed that *pax6a/vegfaa* co-expressing cells favour the development of CtAs 2, 4, 5, 6, and 7 (Fig. 4.5). Curiously, in rhombomere 3, *pax6a/vegfaa* colocalising cells were present in MCT8MO embryos. This might indicate that vascularisation of this rhombomere is fundamental for BHB development and that MT3 was possibly not regulating the ingression of this CtA through *pax6a/vegfaa* signalling. We asked if these *pax6a/vegfaa* co-expressing cells influence CtA migration and if, in MCT8MO embryos, the migratory behaviour of the CtAs changes. In CTRMO embryos, CtAs migrated towards the *pax6a/vegfaa* co-expressing cells until CtA changed their direction towards the BA or CtA neighbour (Fig. 4.5). In MCT8MO embryos *pax6a/vegfaa* co-expressing cells were significantly reduced and the *pax6a/vegfaa* co-expressing cells localised in a different region that in CTRMO embryos, this consequently leads to an altered migratory behaviour of the sprouting CtAs (Fig. 4.5). The only exception was the migratory behaviour of CtA 3 in MCT8MO embryos that followed a similar route as observed in CTRMO zebrafish embryos, further suggesting that CtA3 develops independently of MT3 signalling.

Afterwards, we wanted to understand if MT3 regulates *pax6a* progenitor cells in a cell-autonomous way. The TH signalling machinery, such as transporters, receptors and deiodinases, have been described to be present in several neural cells (López-Espíndola et al., 2019; Vancamp et al., 2019). In the developing cerebral cortex of mice, *Mct8*, *Deiodinase 2* (*Dio2*) and *Thrα1* expression were detected in NPCs (Mohan et al., 2012). Here we show that TH machinery was also present in *pax6a* hindbrain progenitor cells during BHB development (Fig 4.7, 4.8 and 4.9). Vascularisation of rhombomeres 1, 3 and 7 were independent of the presence of *pax6a* progenitor cells that colocalise with *mct8*, *thraa* or *thrab* and thus independent of MT3 signalling (Fig. 4.7 – 4.9). Rhombomere 1 is the largest segment of the zebrafish hindbrain (reviewed in Moens and Prince, 2002), and this CtA usually interconnects

with the posterior communicating segments (PCSs) (Ulrich et al., 2011). Notwithstanding, the finding of *pax6a/thrab*+ cells but not *pax6a/mct8*+ cells suggests that in rhombomere 1 a subset of *pax6a*+ cells depend on *thrab* aporeceptor function to achieve its developmental outcome, which is not clear from our analysis. Rhombomere 7 also differs from rhombomeres 2 to 6, as it is twice as large and presents no visible caudal boundary to the spinal cord (Ma et al., 2009). Although CtA 7 development was independent of MT3 signalling, it is notable that both *pax6a/mct8*+ and *pax6a/thraa*+ cells existed from 30 – 36hpf strongly suggesting that these cells were responsive to MT3. The function of MT3 in rhombomere 7 is unclear, nor is the developmental outcome from MT3 on these *pax6a*+ progenitors, but this evidence clearly shows that MT3 is not involved in CtA 7 ingression. Given that CtA 3 developed irrespectively of *mct8* knockdown, it argues that *pax6a*/*mct8/thraa/thrab*+ cells and MT3 signalling does not participate in this CtA development. In fact, the presence in CTRMO embryos of *pax6a/mct8*+ cells in rhombomere 3 only from 36hpf onwards, after CtA 3 ingression at 32hpf further supports that *mct8* MT3-dependent signalling is not necessary. Nonetheless, *pax6a* was found to colocalise with *thrab* and *thraa* already at 30hpf suggesting that *TRalpha* aporeceptor function might be required for CtA 3 development. However, this has to be functionally analysed in the future. The exact role of MT3 in rhombomere 3 is unclear from this study. Notably, in rhombomere 2 *mct8* was not co-expressed with *pax6a* but *thrab* was and precedes vessel ingression. This suggests that *thrab* aporeceptor function might be required for the ingression of this CtA into the hindbrain.

During BHB development, *pax6a* progenitor cells colocalise with *mct8, thraa and thrab* in rhombomere 4 to 6 from 30 hpf until 48 hpf in CTRMO embryos (Fig. 4.7 - 4.9). In MCT8MO embryos, as expected, *pax6a/mct8* co-expressing cells were absent. Statistical analysis revealed a significant relationship between *pax6a/mct8* co-expressing cells and CtAs 4 to 6 (Fig. 4.9). In all these rhombomeres, *pax6a/mct8* co-expressing cells precedes or occurs at the time of CtA ingression. Moreover, *pax6a/thraa*+ and *pax6a/thrab*+ also preceded CtA development. Notably, CtAs 4 to 6 were the least frequent to develop in MCT8MO embryos, arguing that these depend on MT3-signalling. In CtA 4, but not 5 and 6, *thrab* was expressed already at 30hpf, before *mct8* and *thraa*. Moreover, CtA 4 only starts to develop when *pax6a/mct8*+ and *pax6a/thraa*+ cells were present thus suggesting that *thraa* is the main mediator of MT3-signalling for CtA4 ingression or that *pax6a* cells need to express both *thraa* and *thrab* to respond to MT3 in order to allow CtA 4 full ingression. Notably, in CtA 5 and 6 all MT3-signalling genes were already co-expressed in a subset of *pax6a* cells preceding CtA ingression,

further suggesting that both receptors are needed to allow MT3 signalling to drive vessel ingression.

4.4 CONCLUSIONS

Pax6a loss-of-functions studies proved that these cells are the origin of *vegfaa* needed for CtA development confirming observations made in *mct8* morphant zebrafish embryos. Notably, and in line with our observations in MCT8MO zebrafish embryos, *pax6a* crispants did not display any other vascular defects in the hindbrain and the PHBC, MCeV and LDA developed normally. We demonstrated that hindbrain *pax6a*+ progenitor cells coordinate the MT3-dependent ingression of CtAs during BHB development via *vegfaa*.

Our data showed the action of MT3 in CtAs ingression occurred via *pax6a* progenitor cells, in a rhombomere-specific manner and suggests that in CtAs 4, 5 and 6, both receptors were required for MT3-signalling. Even though MT3-signalling was not required (nor *pax6a/mct8*+ cells) for CtA 1, 2 and 3 development, *pax6a/thrab*+ cells occur in these rhombomeres, suggesting that aporeceptor function might have a role in the development of these vessels. For CtA 7 *thraa* but not *thrab* seems to be the aporeceptor. However, this evidence needs to be further functionally validated in the future. Nonetheless, our observations argue that the combinatorial nature of *TRalpha* receptors and *mct8* expression in *pax6a* MT3-responding cells might be essential for the ingression of CtAs 4, 5 and 6, thus providing a mechanistic rationale for the timely ingression of the different CtAs (Fig. 4.14).

Therefore, our data strongly argue that a specific population of hindbrain *pax6a* neural progenitor cells are the instructing origin of *vegfaa* that promotes specific CtAs hindbrain ingression to allow a fully functional BHB development.

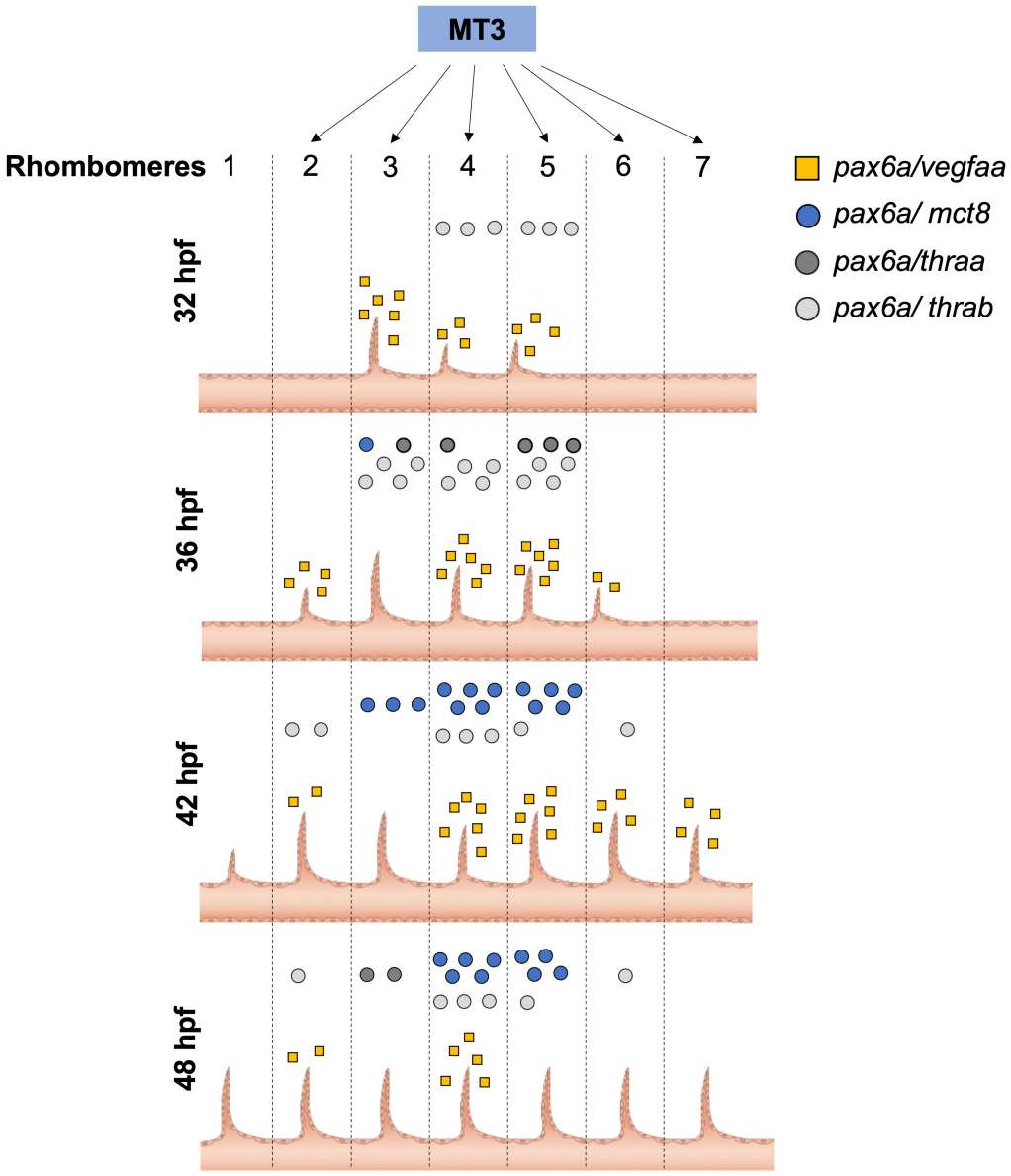

Figure 4.14 – Central arteries development is affected by the lack of MT3 in MCT8MO zebrafish embryos. Our data indicate that MT3 might regulate gene transcription in *pax6a*-T3 responsive cells for the timely supply of *vegfaa* for CtA development. In the schematic representation, CtAs development from 32 hpf onwards is shown. The frequency of CtA development verified in CTRMO embryos for every developmental stage is illustrated by the different lengths of the CtAs. In every developmental stage and rhombomere, the effect of *pax6a/vegfaa*, *pax6a/thraa*, *pax6a/thrab* and *pax6a/mct8* co-expressing on CtA development is illustrated. For example, at 32 hpf in rhombomere 4, CtA development is dependent on *pax6a/vegfaa* and *pax6a/thrab* co-expressing cells.

4.5 MATERIALS AND METHODS

4.5.1 Zebrafish maintenance

Adult zebrafish (*Danio rerio*) were maintained in a ZebTEC zebrafish housing system (Tecniplast, Italy) at 28 ºC in a 14h/10h light/dark cycle, in a fish facility laboratory at CCMAR, in the University of Algarve (Faro, Portugal). The breeding stocks were fed twice a day with granulated food (Tetra granules, Germany) and once with *Artemia nauplii*. Zebrafish lines used for egg production were wild-type (AB strain), *Tg(fli1:EGFP)* (Lawson and Weinstein, 2002), *Tg(kdrl:CaaX-mCherry)* (Fujita et al., 2011) and *Tg(gfap:GFP)* (Bernardos and Raymond, 2006). The night before egg collection, adult couples were placed in breeding tanks with a perforated bottom (Techniplast) and separated by a perspex screen. The separator was removed on the following day at the beginning of the light phase cycle. All experiments were carried out in accordance with the EU Directive 2010/63/EU on the protection of animals used for scientific purposes.

4.5.2 Morpholino injection and sampling

Upon spawning, embryos were immediately collected and microinjected at the 1-2-cell stage with 1 nL of morpholino solution containing either 0.8 pmol CTRMO (control morpholino) or MCT8MO (*mct8* morpholino) (Gene Tools, USA) as described in Campinho et al., (2014). Embryos were distributed on plastic Petri dishes (∅ 100mm) containing E3 medium (5 mM NaCl, 0.17 mM KCl, 0.33 mM CaCl, 0.33 mM MgSO4) and reared until sampling time at 28.5 ºC in an incubator (Sanyo, Germany) under 12h:12h light:dark cycles. Staging was done after Kimmel et al., (1995) by observing developmental landmarks in control embryos. Embryos were fixed at 30, 32, 36, 42 and 48 hpf in ice-cold 4% paraformaldehyde (PFA)/1×PBS overnight at 4 ºC. Samples were washed 2 × 5 min in 1×PBS/0.1% Tween-20 (PBT), depigmented with 0.3% H_2O_2/0.5% KOH/1×PBS and transferred into 100% methanol (MeOH) and stored at -20 ºC until use.

4.5.3 Analysis of mRNA expression

Five independent biological replicates (n = 5), pools of 10 wild-type embryos each, were sampled at 28, 30, 32, 36, 40, 44, 48, 54 and 72 hpf for each experimental condition (MCT8MO and CTRMO). Embryos were manually dechorionated, snap-frozen in liquid nitrogen and stored at -80 ºC until use.

RNA from the embryos were extracted manually with a glass mortar and E.Z.N.A® Total RNA kit I (Omega Biotek, USA) following the manufactures instructions. In order to remove contaminating DNA, total RNA was then treated with Ambion Turbo DNA-free™ kit (Life Sciences, USA) as described by the manufacturer. Afterwards RNA concentration and purity were determined using a NanoDrop ND-1000 spectrophotometer (NanoDrop Technologies Inc., USA). RNA with an A250/A280 ratio between 1.8 – 2.2 was considered satisfactory and used for further analysis. RNA quality was visualised on a 1% agarose gel containing 1× TEA buffer stained with SYBR Green nucleic acid gel stain (Thermo Fisher Scientific, USA). Immediately before electrophoresis, 200 ng of RNA sample was mixed with 100% formamide in the amount giving a final concentration of at least 50% (v/v) formamide. The samples were denatured by heating for 5 min at 65 ºC, immediately chilled on ice for 5 min, and loaded on the agarose gel.

500 ng of purified total RNA was reverse transcribed to complementary DNA (cDNA) in 20 µL of reaction using RevertAid First Stranded cDNA Synthesis kit and random hexamer primer (Thermo Fisher Scientific, USA) following the manufacturer's instructions. cDNA quality was confirmed by amplification of 18S ribosomal RNA (Forward primer: 5'-TCAAGAACGAAAGTCGGAGG-3' and Reverse primer: 5'-GGACATCTAAGGGCATCACA-3') using DreamTaq DNA Polymerase (Thermo Fisher Scientific, USA) according to the manufacturer's instructions. Afterwards, synthesized cDNA was diluted 1/5 in ultrapure water (Sigma-Aldrich, Germany) and stored at -20 ºC.

Primers of the target gene, *pax6a* and *rxrba*, were designed as follows: sequence variants obtained from the assembled transcriptome (NCBI – BioProjects: PRJNA381309) data were aligned in BioEdit (Hall, 2011) and primers were designed using Primer 3 Plus (Untergasser et al., 2012) in a common region of all sequence variance. Primers were produced by Stabvida (Portugal). Specificity and temperature optimization of primers for each gene was tested by PCR using DreamTaq DNA Polymerase (Thermo Fisher Scientific, USA) according to the

manufacturer's instructions. Afterwards, PCR products were amplified, purified using an E.Z.N.A. Gel Extraction kit (Omega Biotek, USA), quantified by NanoDrop ND-1000 spectrophotometer (NanoDrop Technologies Inc., USA), and sequenced at the Molecular Biology facility at CCMAR in the University of Algarve (Faro, Portugal) to confirm gene identity. Table 4.1 provides primer sequences and amplicon size for the *pax6a* and *rxrba* genes for quantitative real-time PCR (qRT-PCR) analysis.

Table 4.1 – Primer sequences of *pax6a* and *rxrba* used for qRT-PCR analysis.

Gene		Sequence 5' → 3'	Product size (bp)	Efficiency (r^2)
pax6a	*Forward*	GACAGCCCAATCAAGATGGT	107	97.1% (r^2=0.999)
	Reverse	CTGAAGCCTCATTTGGGTCTC		
rxrba	*Forward*	ACCGTGTCCATGTCAGGTCT	161	95.1% (r^2=0.999)
	Reverse	ACTCCATAGTGCTTGCCAGAG		

qRT-PCR for the target genes was performed in a CFX Touch Real-Time detection system (Bio-Rad, Portugal). Samples were run in a 384-well plate (Axygen, Life Sciences, USA) with 6 μL of reaction mixture per well. The final concentration of the reaction mixture consisted of 1 × SensiFAST™ SYBR, No-ROX Kit (Bioline, USA), 150 nM forward primer, 150 nM reverse primer, 1 μL cDNA (1/5), and ultrapure water (Sigma-Aldrich, USA). PCR cycling condition consisted of 95 ºC for 3 min, followed by 44 cycles of 95 ºC for 10 s and 60 ºC for 15 s. A standard melting curve was included, which consisted in a gradient temperature increment of 0.5 ºC for 5 s from 60 ºC to 95 ºC, to confirm the production of a single amplicon and the absence of primer dimers. Negative control was included to detect genomic DNA contamination. Each cDNA sample was run as two technical replicates and averaged for expression analysis. Every gene was analysed using a standard curve prepared from a purified PCR product of the target template and normalised to the input of the total RNA. Values are represented as fold change of relative gene expression between CTRMO and MCT8MO. PCR efficiency and coefficient of determination (r^2) were established and are listed in table 4.1.

4.5.4 Intercellular injection of anti-Pax6 monoclonal antibody

Intercellular injection of anti-mPax6 was carried out according to Lesaffre et al., (2007) with adaptations. Briefly, adult *Tg(kdrl:CaaX-mCherry)* and *Tg(gfap:GFP)* zebrafish were mated for egg collection. Upon spawning, embryos were immediately collected and microinjected at the 1-cell stage with hybridoma supernatants anti-mPax6 (DSHB, USA), anti-myc (DSHB, USA) and 1×PBS at a concentration of 100 µg/ml. At 48 hpf double transgenic embryos expressing the mCherry and GFP promoter were life imaged under a stereoscope (Olympus) coupled to an OPTICA 3.0 digital colour camera for central artery development assessment. Embryos were afterwards collected and fixed in ice-cold 4% PFA/1×PBS overnight at 4 ºC. Samples were washed 2 × 5 min in 1×PBS/0.1% Tween-20 (1×PBT), depigmented with 0.3% H_2O_2/0.5% KOH/1×PBS and transferred into 100% methanol (MeOH) and stored at -20 ºC until use.

4.5.5 Establishment of the mutant *pax6a* knockout line by CRISPR/Cas9 method

A guide RNA (gRNA) against the zebrafish *pax6a* locus was designed using the CRIPSRScan algorithm (Moreno-Mateos et al., 2015) against exon 7 (GGTTGAGGTTGTGCCCGAGG). gRNAs were *in vitro* transcribed as described by Moreno-Mateos et al., (2015), and purified by sodium acetate and ethanol precipitation. Afterwards, *pax6a* gRNA was injected (300ng/uL) with 600 ng of Cas9 protein (Weissman Institute, Israel) in 1-cell stage zebrafish embryos.

To verify the efficiency of the injection 8 embryos were collected at 24 hpf, dechorionated, and genomic DNA (gDNA) was extracted. Dechorionated embryos were placed in a microcentrifuge tube and E3 medium was removed. Afterwards, 50 µl/embryo of genomic extraction buffer (10 mM Tris pH 8.2, 10 mM EDTA, 200 mM NaCl, 0.5% SDS, 200 µg/ml proteinase K) was added and samples were incubated over-night at 50 ºC. 2 volumes of 100% ethanol were added, and samples were incubated for 30 min on ice. Afterwards, samples were centrifuged for 30 min at 4 ºC and 14’000 rpm. The supernatant was discarded and 1 mL of ice-cold 70% ethanol was added, briefly vortexed and centrifuged for 5 minutes at 4 ºC and 14’000

rpm. The supernatant was discarded, and gDNA was air-dried. Afterwards, the dried pellet was resuspended in 100 µl Tris-EDTA (TE) buffer.

To confirm the presence of mutagenesis in the *pax6a* locus, PCR was used using primers flanking the gRNA binding site (zf_gPax6aFw-GATAGTGCACATTGTAGCAA; zf_gPax6aRv-CAGCCCAGCCAGACCTCATCC). PCR reactions were performed using 1 µL of gDNA in 1x DreamTaq buffer, 0.2 µM of each primer, 0.2 mM dNTPs and 0.06 U of Dream Taq polymerase (Thermo Fisher Scientific, USA). The following PCR cycling program was used: 5 min 95 ºC, 35 cycles of 30 seconds 95 ºC, 30 seconds 58 ºC, 30 seconds 72 ºC, followed by a final 5 min step at 72 ºC. PCR products were fractioned in a 3.5% agarose/1×TAE gel. gDNA of a control wild-type embryo was used as a negative control.

After confirmation of successful mutagenesis in injected embryos, the remaining injected embryos were reared to adulthood. To identify F0 founders genotyping by tail-clip was carried out and the gDNA was extracted and genotyped as described above by PCR. F0 carriers were crossed with wild-type zebrafish to produce non-mosaic heterozygous F1 carriers. Identified F1 carriers (after fin-clip and PCR genotyping) were in-crossed to generate F2 homozygous *pax6a* knockout embryos.

4.5.6 Fluorescent immunohistochemistry

Microinjected samples with monoclonal anti-Pax6 (anti-mPax6), c-myc and 1×PBS were brought to room temperature and hydrated through a graded series of MeOH/1×PBS (75%, 50%, and 25% MeOH) for 5 min each, followed by 3 × 5 minutes in 1×PBS/0.1% Triton X-100 (Sigma-Aldrich, USA). Embryos were preincubated in 1×PBS/10% sheep serum (Sigma Aldrich, USA)/0.5% Triton X-100 at room temperature for 3 hours. Samples were incubated overnight at 4 ºC in rabbit anti-Pax6a+b (1/400, GeneTex, USA) primary antibody diluted in preincubation solution. Embryos were washed 6 × 30 minutes in 1×PBS/0.5% Triton X-100 (PBTr0.5%) and then blocked for 1 hour with preincubation solution. Samples were incubated overnight at 4 ºC in goat-anti-rabbit 594 (1/400, Sigma) secondary antibody and then washed 6 × 30 minutes in PBTr0.5%.

Lightsheet Z1 microscope (Zeiss, Germany) was used to acquire images. Samples were mounted in 1% low melt agarose (CarlRoth, Germany) and imaged using dual illumination and a z step of 1.758µm (optimal distance option) to acquire the complete hindbrain using 1× zoom. After image acquisition, dual illumination images were merged using Dual side Fusion (Zen Black, Zeiss). Images were then imported into Fiji (Schindelin et al., 2012) and analysed.

4.5.7 Riboprobe preparation

The *vegfaa* plasmid was kindly provided by Professor Brant Weinstein, the *thraa* and *thrab* probes were kindly provided by Dr Sachiko Takayama, and the *mct8* plasmid was kindly provided by the Singapore Genome Institute. Primers for *pax6a* (Table 4.2) were designed using as templates the sequences from the assembled transcriptome (NCBI – BioProjects: PRJNA381309). Isolation of the cDNA of *pax6a* was carried out using a DreamTaq PCR kit (Thermo Fisher Scientific, USA) following the manufacturer's recommendation, and the amplified fragment was isolated by agarose gel band extraction after electrophoresis and cloned into a pGemT easy vector (Promega) as described by the manufacturer. Isolated plasmid DNA was sequenced to confirm the identity and orientation.

Table 4.2 – Primer sequences used to isolate the zebrafish *mct8* and *pax6a* cDNA.

Gene	Primer Forward (5' → 3')	Primer Reverse (5' → 3')
mct8	ATGCACTCGGAAAGCGATGA	TCATATGTGTGTCTCCATGTC
pax6a	AGGCTGTTGGAACTATGCCTC	CGTCGCGTTCTCACTGTAGTC

Ten nanograms of plasmid DNA for zebrafish *pax6a* and *mct8* were used to PCR amplify the template and the T7 and SP6 RNA polymerase promoter in the flanking multiple cloning site using universal M13 forward and reverse primers. PCR protocol was 95 ºC for 5 min, 35 cycles of 95 ºC for 30 sec, 60 ºC for 30 sec and 1 min at 72C, followed by a final extension of 5 minutes at 72 ºC. PCR product was purified by agarose gel and extracted using a GFX gel band extraction kit (Omega Biotek, USA) according to the manufacturer's instructions. For the other zebrafish plasmids, five micrograms of plasmid DNA were linearized with Thermo Fisher

Scientific (USA) fast digest NotI (for *vegfaa*), HindIII (for *thraa*), and SpeI (for *thrab*), followed by phenol-chloroform extraction and sodium acetate and ethanol precipitation.

300 ng of purified linearized plasmid were used to prepare Digoxigenin or Fluorescein labelled antisense probes. These were synthesized by *in vitro* transcription with DIG-RNA labelling kit or Fluorescein-RNA labelling kit (Roche, Switzerland) according to the manufacturer's instructions. Probe for *vegfaa* was produced with T3 RNA polymerase (Fermentas, USA), probes for *pax6a and thraa* were produced with SP6 RNA polymerase (Fermentas, USA), and *thrab* probe was *in vitro* transcribed using T7 RNA polymerase (Fermentas, USA). Integrity of probes was determined by gel electrophoresis and stored in 50% RNAlater (Sigma, USA) at -20 ºC.

4.5.8 Whole-mount *in situ* hybridization (WISH)

WISH was carried out according to Thisse and Thisse (2008) with adaptations. Wild-type samples were brought to room temperature and hydrated through a graded series of MeOH/1×PBS (100% to 0% MeOH) and afterwards washed 3 × 5 min in 1×PBS/1×PBT. Embryos were permeabilized by digestion with proteinase K (1 μg/ml) in 1×PBS for 15 min. Proteinase K digestion was stopped by incubating the embryos for 20 min in 4% PFA/1×PBS. Samples were washed 4 × 5 min with PBT to remove the residual PFA and then pre-hybridized for 3 hours at 68 ºC in pre-heated hybridization mix (HybMix). HybMix was discarded and replaced with pre-heated HybMix containing 0.25 ng/ml of Dig-labelled cRNA *pax6a* probe and hybridized overnight at 68 ºC. Samples were subjected through a series of stringency washes at 68 ºC for 10 min in Hyb(–)/2×SSC (75%, 50% and 25% of Hyb(–)), 2×SSC/0.1% Tween-20 and finally washed twice in 0.2×SSC/0.1% Tween-20 (0.2×SSCT) for 30 minutes. Samples were then washed through a graded series in 0.2×SSCT/Malic acid buffer (MAB, Sigma-Aldrich, USA) (75%, 50% and 25% of 0.2×SSCT) and then washed 3 × 10 min in MAB/0.1% Triton X-100 (MABTr, Sigma-Aldrich, USA). Embryos were preincubated in blocking solution MAB/0.1% Triton X-100/10% sheep serum (Sigma-Aldrich, USA)/2% Blocking solution (Roche, Switzerland) for 2 hours at room temperature. Afterwards, the blocking solution was discarded and replaced with blocking solution containing anti-Dig-AP Fab fragments serum (1/5000, Roche, Switzerland) and incubated overnight at 4 ºC. Samples

were washed 6 × 30 min in MABTr. Afterwards, samples were washed 3 × 5 min in staining buffer (100 mM Tris HCl pH 9.5, 50 mM $MgCl_2$,100 mM NaCl, 2 mM Levimasol and 0.1% Tween-20) and then incubated in labelling solution containing nitro blue tetrazolium (NBT)/bromo-chloro-indolyl-phosphate (BCIP) diluted in staining solution for colour development. When the desired staining intensity was reached, reaction was stopped by washing the samples in stop solution (1× PBS pH 5.5, 1 mM EDTA, 0.1% Tween-20).

For image analysis samples were transferred to 100% glycerol and photographed under a stereoscope (Olympus) coupled to an OPTICA 3.0 digital colour camera. At least ten animals per stage and experimental condition were analysed.

4.5.9 Fluorescent *in situ* hybridization with immunohistochemistry

WISH was performed as described previously using *Tg(fli1:EGFP)* positive samples at 32, 36 and 48 hpf with some minor modifications. After the overnight blocking with blocking solution containing anti-Dig-AP Fab fragments serum (1/5000, Roche, Switzerland) samples were washed 6 × 30 min in MABTr and then briefly dried with absorbent paper. Afterwards, samples were incubated in FastRed TR/ Naphthol AS-MX tablets (Sigma, USA) for colour development, according to the manufacturer's instructions, followed by several washes in PBT.

For the immunohistochemistry, the samples were re-fixated in 4% PFA/1×PBS for 15 min and then washed 4 × 15 min in PBT. Embryos were preincubated in 1×PBS/10% sheep serum/0.5% Triton X-100 at room temperature for 1:30 hours. Samples were incubated overnight at 4 ºC with rabbit anti-GFP (1/500, abcam, UK) primary antibody diluted in preincubation solution. Samples were washed 6 × 30 minutes in 1×PBS/0.5% Triton X-100 (PBTr0.5%) and then blocked for 1 hour with preincubation solution. Samples were incubated overnight at 4 ºC with goat anti-rabbit IgG-488 HL (1:400, Jackson Labs) fluorescent labelling secondary antibody. Samples were then washed 6 × 30 minutes in PBTr0.5%.

Lightsheet Z1 (Zeiss, Germany) was used to acquire images. Samples were mounted in 1% low melt agarose (CarlRoth, Germany) and imaged using a 10× lens, dual illumination and a z step of 2 μm (optimal distance option) to acquire the complete hindbrain using 1× zoom. After image acquisition, dual illumination images were merged using Dual side Fusion (Zen Black, Zeiss).

Images were then imported into Fiji (Schindelin et al., 2012) and analysed. At least ten animals per stage and experimental condition were analysed.

4.5.10 Double fluorescent *in situ* hybridization with immunohistochemistry

WISH was performed as described previously using *Tg(fli1:EGFP)* positive samples at 30, 32, 36, 42 and 48 hpf with some minor modifications. Samples were incubated in pre-heated HybMix containing 1 ng/ml of Dig-labelled cRNA probe and 1 ng/ml of Fluorescein-labelled cRNA probe and hybridized overnight at 68 ºC. After the stringency washes probes were detected consecutive. **1st probe detection – anti-Dig-POD + Alexa 594 TSA detection:** Embryos were preincubated in blocking solution containing MAB/0.1% Triton X-100/10% sheep serum (Sigma-Aldrich, USA)/2% Blocking solution (Roche, Switzerland) for 2 hours at room temperature. Afterwards, the blocking solution was discarded and replaced with blocking solution containing anti-Dig-POD Fab fragments serum (1/500, Roche, Switzerland) and incubated overnight at 4 ºC. Samples were washed 6 × 30 min in PBT and then incubated in Alexa Fluor™ 594 Tyramide Reagent (Thermo Fisher Scientific, USA), 1:100 in amplification reagent (Perkin Elmer, USA) for fluorescent colour development, according to the manufacturer's instructions, followed by several washes in PBT. **2nd probe detection – anti-Fluorescein-POD + Fluorescein TSA detection:** Samples were incubated for 1hour in 3% H_2O_2/1×PBS to quench the peroxidase activity. Afterwards, samples were washed 6 × 5 min in PBS/0.1% Triton X-100 and then pre-incubated with blocking solution for 2 hours. Blocking solution was discarded and replaced with blocking solution containing anti-Fluorescein-POD fragments serum (1:500, Roche, Switzerland) and incubated over-night at 4 ºC. Samples were washed 6 × 30 min in PBT and then incubated in FITC-Tyramide (Perkin Elmer, USA) 1:100 in amplification reagent (Perkin Elmer, USA) for fluorescent colour development, according to the manufacturer's instructions, followed by several washes in PBT.

For the immunohistochemistry, the samples were preincubated in 1×PBS/10% sheep serum/0.5% Triton X-100 at room temperature for 1 hour. Afterwards, samples were incubated overnight at 4 ºC with rabbit anti-GFP (1/500, abcam, UK) primary antibody diluted in preincubation solution. Samples were washed 6 × 30 minutes in 1×PBS/0.5% Triton X-100

(PBTr0.5%) and then blocked for 1 hour with preincubation solution. Samples were incubated overnight at 4 ºC with goat anti-rabbit 633 (1:400, Sigma-Aldrich, USA) fluorescent labelling secondary antibody in preincubation solution. Samples were then washed 6 × 30 minutes in PBTr0.5%. Samples were stored in PBS containing 0.1% Dabco (CarlRoth, Germany).

Fluorescent imaging was carried out immediately to avoid bleaching of the fluorophores, using a Lighsheet Z1 (Zeiss, Germany) microscope. Samples were mounted in 1% low melt agarose (CarlRoth, Germany) and imaged using a 10× lens, dual illumination and a z step of 0.611μm (optimal distance option) to acquire the complete hindbrain using 1× zoom. After image acquisition, dual illumination images were merged using Dual side Fusion (Zen Black, Zeiss). Images were then imported into Fiji (Schindelin et al., 2012) and analysed.

4.5.11 Colocalisation analysis

Images acquired with Z1 microscope were imported into Fiji (Schindelin et al., 2012). The ImageJ "Colocalisation Colormap" plugin was used to find areas of colocalisation (Gorlewicz et al., 2020).

4.5.12 Live imaging of *pax6a* crispants, CTRMO and MCT8MO zebrafish embryos

Zebrafish *Tg(kdrl:CaaX-mCherry)* (Fujita et al., 2011) and wild-type AB were mated and eggs were injected at 1-cell stage with *pax6a* gRNA (300ng/uL) and 600 ng of Cas9 protein (Weissman Institute, Israel), as previously described. At 28 hpf, zebrafish embryos were screened for the membrane-bound Cherry fluorescent protein driven by the *kdrl* promoter, a marker for endothelial cells. Afterwards, embryos were screened for positive *pax6a* mutation by selecting embryos with a small eye (Lesaffre et al., 2007). These F0 embryos are called "crispants".

Zebrafish *Tg(fli1:EGFP)* (Lawson and Weinstein, 2002) and wild-type AB were mated and eggs were injected at 1-cell stage with 1 nL of morpholino solution containing either 0.8pmol CTRMO or MCT8MO (Gene Tools, USA) as previously described. At 28 hpf, zebrafish

embryos were screened for GFP fluorescent protein driven by the *fli1* promoter, a marker for endothelial cells.

Imaging was carried out by using a Lighsheet Z1 (Zeiss, Germany) microscope as described by Weber et al., (2014) with minor alterations. Briefly, embryos were anaesthetized and mounted alive in 0.3% (w/v) low-melting agarose (CarlRoth, Germany) in E3 medium containing tricaine (200 mg/l) into FEB tubes closed with a 1% low-melting agarose plug. 2 animals per group control (not injected embryos) and *pax6a* crispants were imaged in the same tube. Time lapses were performed starting at 32 hpf, with a z-step of 0.740 μm to acquire the complete hindbrain, and imaging was acquired every 20 min for 20 hours. The hindbrain was imaged with 10 × lens, 1 × zoom and dual illumination. Dual illumination images from Z1 were merged using Dual side Fusion (Zen Black, Zeiss, Germany). Images were imported into Fiji (Schindelin et al., 2012) and analysed. Maximum projection images were used to create a time-lapse video.

4.5.13 Statistical analysis

Student's t-test was performed to determine significant differences in absolute expression levels by qRT-PCR analysis between CTRMO and MCT8MO groups in stage-specific time points. Fisher's exact test was performed to determine the frequency of expression or CtA development between experimental groups in stage-specific time points. Statistical analysis was performed using GraphPad Prism version 8.4.0 software for Mac (San Diego, USA, www.graphpad.com).

CHAPTER 5

General discussion and conclusions

5.1 DISCUSSION

An established zebrafish Mct8 knockdown model was used to inhibit the cellular uptake of maternal thyroid hormones (THs), specifically maternal T3 (MT3), during the zebrafish embryonic development (Campinho et al., 2014; Silva et al., 2017). The specificity of Mct8 in transporting T3 exclusively at zebrafish physiological temperature (26 ºC) was shown by Arjona et al. (2011), highlighting the exclusive role of T3 as the major signalling TH metabolite in zebrafish embryogenesis. Here we provide evidence that blood-hindbrain barrier (BHB) development in the zebrafish depends on adequate MT3-dependent development of specific *pax6a* neural progenitor populations instructing central arteries (CtAs) ingression into the hindbrain. Our work highlights the integrative role of MT3 in embryonic development, where it is important not only for central nervous system (CNS) development (Campinho et al., 2014; Silva et al., 2017; Silva and Campinho, 2023) but also for the integration of the vasculature in the CNS to be able to give rise to a fully functional organism.

We demonstrated that, during zebrafish embryonic development, blood vessels in the hindbrain present an impaired development (Chapter 2). We observed that during development, the primordial hindbrain channels (PHBC) and basilar artery (BA) in MCT8MO zebrafish embryos have delayed development but were completely formed at 48 hpf. In control morphant (CTRMO) zebrafish embryos, 7 to 8 CtAs ingress into the hindbrain, but in *mct8* morphant (MCT8MO) embryos, an average of 2 CtAs form at 48 hpf. Although we did not analyse CtA development after 48 hpf, this phenotype was probably not a consequence of the late development of the MCT8MO embryos because other developmental landmarks, such as heart development, were synchronised with CTRMO zebrafish embryos. In fact, impaired brain vascularisation was also observed in MCT8MO zebrafish larvae at 120 hpf by De Vrieze et al. (2014), confirming that the vascular phenotype persists throughout development. Impaired brain vascularisation was also observed in induced hypothyroid rats after births (O'Shaughnessy et al., 2023; Zhang et al., 2010). This confirms that THs have a role in the morphogenesis and function of the endothelial cells involved in brain angiogenesis during embryonic development and after birth. Although no TH-signalling genes are expressed in the developing zebrafish vasculature until 48 hpf (Campinho et al., 2014), impaired MT3-signalling in the CNS affects BHB development and angiogenic-related developmental pathways. This is likely a consequence of impaired CNS development that affects the vascular endothelial growth factor (VEGF) ligand expression and secretion by neural progenitor cells (NPCs). We have

found evidence that supports such a statement. Most notably, a population of hindbrain *pax6a*+ NPCs were particularly dependent on MT3-signalling and express *mct8*, *thraa* and *thrab* during embryogenesis. Moreover, these cells are the source of *vegfaa* that we have found to be essential for CtA ingression into the hindbrain.

5.1.1 MT3 regulates hindbrain *vegfaa* expression for central arteries development

The fact that MT3 signalling impairment leads to hindbrain CtAs loss during zebrafish embryonic development argues that MT3 through Mct8 controls/regulates the angiogenic sprouting mechanism and/or the migration of the venous endothelial cells of the PHBCs involved in CtA development, which contribute to form a complete BHB. Brain angiogenesis strongly depends on VEGF and their endothelial tyrosine kinase receptors (VEGFR) (Ferrara et al., 2003; Lohela et al., 2009; Raab et al., 2004; Rossi et al., 2016; Wild et al., 2017). Our transcriptome data of 25 hpf MCT8MO zebrafish embryos showed that the sub-pathway Neuropilin interaction with VEGF and VEGFR has 75% of the genes regulated by MT3. The VEGF receptors *vegfr1*/*flt1*, *vegfr2*/*kdrl* and *vegfr3*/*flt4* were significantly upregulated in 25 hpf MCT8MO zebrafish embryos, as well as the co-receptors *neuropilin 1a* (*nrp1a*) and *nrp2a*. However, none of the Vegf ligands was differentially expressed in our transcriptome data. Of the Vegf ligands, Vegfa is the most potent ligand involved in angiogenesis (Liang et al., 1998). In zebrafish two Vegfa paralogues exist, *vegfaa* and *vegfab* (Bahary et al., 2007). Previous studies have shown that both ligands are important for CtA development but that *vegfaa* is the fundamental ligand involved in CtAs development. However, these mutant zebrafish embryos also displayed other brain and trunk vascular defects (Rossi et al., 2016), while in the MCT8MO zebrafish embryos, only the CtAs presented an impaired development. This evidence argues that the action of MT3 on vascular development is indirect and localised to the hindbrain. Our data further support this hypothesis.

First, we analysed the expression of *vegfaa* and *vegfab* by qRT-PCR; however, no significant changes were observed during BHB developmental time window (28 to 72 hpf). Gene expression analysis of *vegfaa* showed more variability than *vegfab*. This was also observed by WISH expression analysis that showed that both genes were reduced in the brain in MCT8MO embryos. However, in MCT8MO zebrafish embryos, *vegfab* was only mildly affected. At the

same time, *vegfaa* expression was significantly reduced in the hindbrain, indicating that MT3 regulates both *vegfa* paralogues but was affecting more the expression of *vegfaa*. The downregulation of the *vegfa* ligands was not verified in our transcriptome data directly, probably because the transcriptome was carried out at 25 hpf, a time when BHB development was not yet occurring and because, like the qRT-PCR expression analysis it was carried out in whole embryos. Nonetheless, the increased expression of the Vegf receptors *kdrl* (0.58 log2fold increase, $p < 0.01$, FDR < 0.0001) and *flt4* (0.43 log2fold increase, $p < 0.01$, FDR < 0.0001), which enhances angiogenesis, were responding in a way that precludes a compensatory mechanism for the reduced expression of the *vegfa* ligands to promote angiogenesis. Similarly to our results, the transcriptome data of the ventricular zone of hypothyroid mice treated with propylthiouracil (PTU) from in-utero life to postnatal day 2, also showed no significant changes in *Vegf* ligand expression. However, in their transcriptome data, *Flt4* and *Nrp1* were also not significantly expressed between PTU-treated and control neonate mice. Nonetheless, immunohistochemistry (IHC) analysis of blood-brain barrier (BBB) markers (cerebral microvasculature, COL IV, PECAM-1, F-actin) showed remarkable differences between control and PTU-treated mice (O'Shaughnessy et al., 2023). These results show that MT3 has a cell-specific action in blood-brain vessel angiogenesis in these vertebrate species and that these changes can only be observed by *in situ* analysis. To test if MT3 acts upstream of *vegfaa* signalling, which showed a promising expression in the region of CtA development, *vegfaa-165* mRNA was co-injected in MCT8MO zebrafish embryos and was able to partially rescue the MCT8MO hindbrain vasculature phenotype. At 48 hpf, an average of 4 CtAs developed in rescued zebrafish embryos, presenting a partially rescued phenotype compared to CTRMO and MCT8MO embryos. This revealed that MT3 through Mct8 regulates CtA development through *vegfaa* expression. However, due to the incapacity to completely rescue the seven CtAs, it argues that MT3 might regulate another angiogenic factor involved in CtA development. Rossi et al. (2016) showed that *vegfab* mutant zebrafish embryos also lose some CtAs, and since we showed that *vegfab* was also an MT3-dependent gene, the rescue with both *vegfa* ligands could restore the complete BHB. Another fact that can be responsible for the only partial rescue of the hindbrain CtAs, is the fact that the extracellular matrix (ECM) components were significantly affected in 25 hpf MCT8MO zebrafish embryos. ECM organisation was the most affected Reactome mother category pathway by MT3 deprivation in 25hpf MCT8MO zebrafish embryos. This was also shown in other transcriptomic analyses. Transcriptomic analysis of primary cerebrocortical cells of mice (Gil-Ibañez et al., 2015) and from microdissected brain tissues of the ventricular zone of hypothyroid rats (O'Shaughnessy et al., 2023) also identified

ECM proteins as one of the major groups regulated directly by T3. Vegfaa-165 isoform binds to the ECM (Lange et al., 2022) and the modification of the ECM components might affect the binding capacity of *vegfaa-165* to the ECM (Ruhrberg et al., 2002), which might lead to a lower concentration gradient or effectivity of *vegfaa* signalling to initiate the angiogenic sprouting of the endothelial cells of the venous PHBC. These results also highlighted that the hindbrain vasculature defects observed in MCT8MO zebrafish embryos result from an indirect regulation of MT3 on the endothelial cells' sprouting mechanism. MT3 is not directly regulating the endothelial cells sprouting and migration ability. Still, it regulates MT3-responsive hindbrain cells that express *vegfaa*, which provides the angiogenic cues for the angiogenic sprouting of the CtAs from the PHBC. Although it is not stated, previous studies using induced hypothyroid mice (treated with PTU from birth to postnatal day 21) indicated an indirect regulation of T3 over brain angiogenesis. In these PTU-treated mice, blood vessel development in the brain was reduced and presented a lower complexity and density of microvessels. The mRNA levels of *Vegfa* and *Flk1* (VEGFR2) in the cortex were significantly reduced compared to recovered mice (withdrawal of PTU at postnatal day 22) at postnatal day 90, arguing that the action of T3 on brain vessel development might also depend on a specific time-window to occur. They also showed by *in vitro* assays that rat brain endothelial (RBE4) cells stimulated with 10 nM of T3 increased VEGFA mRNA and protein levels, while *Flk1* mRNA levels remained unchanged (Zhang et al., 2010). These results highlighted the evidence of the direct regulation of T3 on *Vegfa* expression and that the reduced expression of *Flk1*, which is expressed in the endothelial cells (Liang et al., 2001), is affected due to the reduced microvessels in the brain, demonstrating an indirect regulation of T3 on blood vessel development in the brain.

5.1.2 MT3-responsive hindbrain cells

Maternal THs deficiency leads to an underdeveloped CNS. Several reports have highlighted the importance of maternal THs for NPC expansion, neurogenesis, and neuronal and glial cell differentiation, among others (Bernal, 2022; Mohan et al., 2012; Prezioso et al., 2018). In Chapters 3 and 4, we intended to identify the source of *vegfaa* signalling, for CtA development, by identifying MT3-dependent hindbrain CNS cells, such as neurons, glial cells or NPCs. Based on previous results, which showed that in mice (Himmels et al., 2017) and zebrafish (Wild et al., 2017), spinal cord vascularisation is promoted by neurons that coordinate the expression of

vegfaa and *sflt1*, we hypothesised that the effect of impaired cellular MT3 uptake leads to the loss of specific neurons. Given that BHB development happens at mid-development (around 20 hpf) and that the CtAs are the last vascular structures being formed in the zebrafish hindbrain from 32 to 72 hpf (Isogai et al., 2001; Quiñonez-Silvero et al., 2020; Ulrich et al., 2011) it is possible that neurons, which are already present at this developmental time (Kim et al., 1996), are also the instructing source of *vegfaa* for CtA development. However, we verified that *pax8* (inhibitory neuron marker) mutant zebrafish embryos presented a complete BHB and that *copine 4* (*cpne4*) interdigit innervating neurons do not express *vegfaa* and were, thus, not responsible for CtA development (Chapter 3). Nonetheless, we identified these neurons (*pax8* and *cpne4*) as MT3-responsive and likely their progenitor cells depend on MT3 for their differentiation.

In vertebrates, after perineural vascular plexus (PNVP) formation, the sprouting of the blood vessels into the neural tissue is promoted by NPCs that secret Vegf-A (Hogan et al., 2004; James et al., 2009; Matsuoka et al., 2017). In foetal hypothyroid rats, *Pax6* NPCs were reduced (Mohan et al., 2012), leading us to hypothesise if these are the source of *vegfaa* and responsible for CtA development in the zebrafish hindbrain. We verified that *pax6a* NPCs express *vegfaa* (Chapter 4). We also found a relationship between the migratory route of the sprouting CtAs with the *pax6a*/*vegfaa* co-expressing cells, which showed that before CtA turnover to the BA or its ipsilateral neighbour, the CtAs were attracted towards the *pax6a*/*vegfaa* co-expressing cells, while in MCT8MO zebrafish embryos the migratory route changed due to the loss or reduced presence of *pax6a/vegfaa* co-expressing cells. The only exception was CtA 3, which followed a similar migratory route as observed in CTRMO zebrafish embryos. CtA 3 was particularly different from the other CtAs. We observed that this CtA has the highest frequency of development in MCT8MO zebrafish embryos compared to the other CtAs. From the work performed in this thesis, we saw that in the different experiments analysed, 50 to 90% of MCT8MO zebrafish embryos at 48 hpf developed this CtA (Table 5.1). CtA 3 has the particularity to be the only CtA that always interconnects to the BA (Fujita et al., 2011; Ulrich et al., 2011). The interconnection of this CtA to the BA permits closing the circulatory loop of hindbrain vascularisation (Bussmann et al., 2011). In Chapter 2, we verified that *vegfaa* signalling, although significantly reduced compared to CTRMO zebrafish embryos, was still present in rhombomere 3 of MCT8MO embryos and in Chapter 4, we verified that in MCT8MO zebrafish embryos *pax6a/vegfaa* co-expressing cells were still present in rhombomere 3 (Table 5.1). Using the mutant *pax6a* zebrafish, generated by the CRISPR-Cas9 technology, we verified

that CtA 3 also developed, arguing that *pax6a* NPCs were not the instructing cells for CtA 3 development. However, these last results need further validation in future studies due to the low number of individuals used. These results indicate that MT3 signalling is not crucial for the development of this CtA but enhances its development, suggesting that another CNS cell type is responsible for the release of *vegfaa*, consequently leading to its development. CtA 1 develops in rhombomere 1, the largest segment of the zebrafish hindbrain (reviewed in Moens and Prince, 2002). In Chapter 2, *vegfaa-165* mRNA rescued this CtA to CTRMO levels. However, in Chapter 4, the statistical analysis revealed no correlation between *pax6a/vegfaa* co-expressing cells and CtA 1 development (Table 5.1). Because CtA 1 mostly interconnects to the posterior communicating segments (PCSs) (Ulrich et al., 2011), likely, another cell type that secret *vegfaa* and that might be under MT3 regulation is responsible for the development and migration of this CtA to the PCS. CtA 2 developed in 50% of the MCT8MO embryos analysed at 48 hpf (Table 5.1). The high frequency of development of this CtA was most likely the effect of the *vegfaa* signalling, although significantly reduced, that was still present in MCT8MO embryos (Table 5.1). Injection of *vegfaa-165* mRNA was able to rescue CtA2 development to CTRMO levels, and a correlation between this CtA with *pax6a/vegfaa* co-expressing cells was found, indicating that MT3 signalling regulates the development of this CtA. Vascularisation of rhombomere 4 was not rescued by the injection of *vegfaa-165* mRNA (Table 5.1). The statistical analysis revealed a correlation between the development of this CtA with the presence of *pax6a/vegfaa* co-expressing cells, showing that the loss of these cells leads to the loss of rhombomere 4 vascularisation. From the analysis, we also showed that this CtA was under the influence of *mct8* since the statistical analysis confirmed a spatial correlation between *pax6a/mct8* co-expressing cells and CtA development. This demonstrated that CtA 4 was a target of MT3 signalling via Mct8. However, the angiogenic factor regulating CtA 4 sprouting needs to be confirmed. Vascularisation of rhombomeres 5 and 6 could partially be rescued to CTRMO phenotype by injecting *vegfaa-165* mRNA (Table 5.1). However, *vegfaa* signalling was insufficient to rescue these rhombomeres' vascularisation completely. But the presence of *pax6a/vegfaa* co-expressing cells favours the development of these CtAs. The statistical analysis also revealed a spatial correlation between the development of CtA 5 and *pax6a/mct8* co-expressing cells, showing that this CtA was a target of MT3 signalling through Mct8. Nonetheless, another angiogenic factor, besides *vegfaa*, might be involved in the angiogenic sprouting and ingression of these two CtAs, which needs to be revealed. Vascularisation of rhombomere 7 was rescued in MCT8MO embryos by the co-injection of *vegfaa-165* mRNA (Table 5.1). The statistical analysis revealed a correlation between this CtA

with *pax6a/vegfaa* co-expressing cells, indicating that MT3 signalling regulates the development of this CtA through *pax6a* NPCs.

Table 5.1 – Relationship found between CtA development, *vegfaa* expression and *pax6a* neural progenitor cells in the present thesis under the effect of MT3 at 48 hpf. ° The values presented are the mean values obtained from the different experiments conducted in this thesis. * Statistically significant $p<0.05$.

	CtA development in MCT8MO embryos °	***vegfaa* signalling CTRMO vs. MCT8MO**	***vegfaa-165* mRNA rescued CtA development**	***pax6a/vegfaa* co-expressing cells and CtA development (CTRMO vs. MCT8MO)**	***pax6a/mct8* co-expressing cells and CtA development (CTRMO vs. MCT8MO)**
CtA 1	10%	*	yes	–	–
CtA 2	50%	*	yes	*	–
CtA 3	80%	*	yes	–	* before 48 hpf
CtA 4	40%	*	no	*	*
CtA 5	50%	*	partially	* before 48 hpf	*
CtA 6	40%		partially	* before 48 hpf	present before 48 hpf
CtA 7	10%		yes	* before 48 hpf	–

In mice, *Pax6* NPCs express thyroid hormone receptor alpha-1 (THRα1) (Mohan et al., 2012). Due to ancestral genome duplication events, two *TRalpha* genes were identified in zebrafish, the *thraa* and *thrab* (Darras et al., 2011). Analysing the expression of these two *TRalpha* genes, we verified that both were expressed in *pax6a* NPCs. These *TRs* were expressed in a spatiotemporal manner. Interesting was also the observation that both *TRalpha* receptors were present before rhombomere vascularization in all 7 CtAs, leading us to hypothesise that the presence of these *pax6a/thraa*+ or/and *pax6a/thrab*+ cells function as aporeceptors coordinating the sprouting and ingression of the CtAs for each rhombomere in a timely coordinated manner (Chapter 4). Nonetheless, these new evidence needs to be functionally

validated in future studies. This shows, that, as has been described by Ulrich et al., (2011), while CtAs sprouting is variable, it is not random, and that is shown by the appearance of the different *TRalpha* before and at the timings for CtA sprouting for each rhombomere and can function as aporeceptor or promote MT3 signalling for vessel ingression. Analysing the relation between the presence of the *TRalpha* and CtA development, we showed that most CtAs, except for CtAs 1 and 7 present a correlation with *pax6a/thrab* colocalizing cells from 32 hpf to 48 hpf. Correlation between *pax6a/thraa* colocalizing cells and CtA development has only been found for CtAs 3, 4 and 5 at 36 hpf. This shows that MT3 likely regulates *pax6a* NPC in a cell-autonomous way and that, most probably, T3 binds to the *TRalpha* receptors present in *pax6a* NPC in rhombomeres 2 to 6, thus regulating gene transcription. Further confirmation that *pax6a* hindbrain NPCs were essential to instruct BHB development and specifically CtAs ingression comes from our *pax6a* CRISPR/Cas9 knockout that has a similar BHB phenotype as observed in MCT8MO zebrafish embryos, confirming that these cells were responsible for the chemoattraction of some CtAs.

5.1.3 Relevance to Allan-Herndon-Dudley Syndrome

Vascular deficiency of the BBB has not been described in AHDS patients. Although this finding is not new since several studies in the past have shown a relationship between THs and BBB development. In adult dogs, it has been shown that chronic hypothyroidism leads to an increased BBB permeabilization (Pancotto et al., 2010, 2016). In rats rendered hypothyroid after exposure to the goitrogen PTU from birth to postnatal day 21, have reduced brain angiogenesis (Zhang et al., 2010). In zebrafish, an impaired BHB development has been shown in MCT8MO zebrafish embryos (Campinho et al., 2014) and larvae (De Vrieze et al., 2014). This clearly shows that THs influence BBB development and function. However, to date, this aspect has not been regarded in AHDS patients, and consequently, no data or studies are available to confirm this condition in human AHDS patients.

In cases where hypothyroidism develops only in post-natal life, the vascular defect in the brain can be recovered after TH supplementation therapy (Zhang et al., 2010). However, due to our morpholino model, which is a transient model used to study gene knockdown during embryonic development (Schulte-Merker and Stainier, 2014) we are unable to predict if in adult zebrafish TH supplementation therapy can restore brain angiogenesis. But most probably, the vascular

defects observed are not reversible. During embryonic development, we showed that MCT8MO zebrafish embryos lose ventral *pax6a* NPCs in the hindbrain, causing the loss of *vegfaa* signal that induces the angiogenic sprouting of the PHBCs endothelial cells (Chapter 4). The initial size of the NPC pool during brain development is defined during early embryonic development. It defines the number of neurons and glial cells constituting the CNS (Homem et al., 2015). The reduced number of *pax6a* NPCs results in fewer neurons and less neuron diversity (Silva and Campinho, 2023) developing in the brain. Consequently, this leads to irreversible neurological damage that cannot be recovered after birth (de Escobar et al., 2004). Thus, implementing TH supplementation therapy cannot recover the *pax6a* NPCs responsible for releasing *vegfaa* for CtA development. Most probably, the vascular defects can only be reversed by *vegfaa* analogue therapy. But that must be confirmed by future studies. Nonetheless, TH therapy applied to AHDS patients has only been shown to be (partially) effective if it occurs in the first weeks of gestation (Refetoff et al., 2021), thus further arguing that TH-supplementation or TH-mimetic drugs after birth will not be able to rescue the AHDS phenotype as previously shown (Di Cosmo et al., 2009; Grijota-Martínez et al., 2023; Groeneweg et al., 2019).

During embryonic development, neural stem cells (NSCs) and radial glial cells switch from cell proliferation to differentiation in a spatiotemporal manner that coincides with the angiogenic sprouting of blood vessels. In mice, it has been shown that the relief of the hypoxic levels in the neurogenic niches leads to radial glial cell differentiation (Lange et al., 2016). Thus, if *vegfaa* restores blood vessel development in the zebrafish hindbrain after birth, although we lose some *pax6a* NPCs, it is plausible that the remaining ones can differentiate. Angiogenesis of the blood vessels would also promote the differentiation and migration of the inhibitory interneurons since some authors have suggested that they need an intact vasculature to migrate (Barber et al., 2018; Tan et al., 2016; Won et al., 2013). Although we have seen that MT3 regulates the *pax8* inhibitory interneurons, some *pax8* inhibitory interneurons may be absent because of the defective hindbrain vasculature in the zebrafish hindbrain. Nonetheless, *pax8* neuron development precedes BHB development (Batista and Lewis, 2008; Campinho et al., 2014; Ikenaga et al., 2011), which argues against blood vessels' dependence on *pax8*+ neurons.

The pathogenic mechanism of MCT8 deficiency is not completely understood, and some controversy exists. It is clear that THs are fundamental for brain development and that the lack of T3 transport through the BBB and/or neurons causes poor regulation of TH-dependent genes (Groeneweg et al., 2020; Kersseboom et al., 2014). Some authors have suggested that the principal responsible for T3 deficiency in the brain is the BBB, which due to the defective

transport of T3, leads to brain hypothyroidism, leading to several neurological problems (Bernal et al., 2015; Ceballos et al., 2009). In this thesis, we showed, as previously suggested (Campinho et al., 2014; Silva and Campinho, 2023), that the neuronal defects observed in AHDS patients, precede BBB development. Evidence in zebrafish strongly argues that AHDS is due to decreased neural cells leading to decreased higher brain capacity (Silva and Campinho, 2023). The fact that the BHB is disrupted in zebrafish argues that brain permeabilisation is compromised, as has been observed in hypothyroid dogs (Pancotto et al., 2010, 2016), leading to the access of several factors/hormones/wastes to the brain. Nonetheless, the brain maintains a hypothyroid state while the peripheral tissues are in a hyperthyroid state (Bárez-López et al., 2019), suggesting that after BBB development, even malformed, it maintains some barrier function. In fact, this seems to be the case in zebrafish as well. We never observed any brain oedema in *mct8* morphant zebrafish embryos (Campinho et al., 2014), and although pericyte recruitment is delayed into the BHB it still occurs further arguing that in zebrafish the BHB permeability is maintained, at least in the end of embryogenesis (Chapter 2).

The BBB is a member of a greater functional unit, the neurovascular unit (NVU). The cross-talk between the different NVU constituents allows its function. Several studies have suggested that CNS diseases should imply an integrative approach, considering all the NVU members (Iadecola, 2017; Yu et al., 2020). That has been shown in several neurodegenerative diseases, such as Alzheimer's disease, Parkinson's disease, amyotrophic lateral sclerosis (ALS) and Huntington's disease, which also showed a compromised BBB (reviewed in Knox et al., 2022; Sweeney et al., 2018). Indeed, in these diseases, a higher risk of cerebral micro haemorrhages has been observed (Daida et al., 2018; de Reuck, 2012; Freeze et al., 2019). This can be due to a reduced expression of tight junction proteins in the BBB endothelial cells, reduced coverage of pericytes, alterations of the basement membrane, or the detachment of the astrocytic end-feet from the vascular basement membrane (Knox et al., 2022). However, to date, brain micro haemorrhage has not been observed in AHDS patients, and in MCT8MO zebrafish embryos, we also did not observe any blood leakage until 48 hpf. Indeed, we could observe blood circulation in the CtAs that developed in MCT8MO zebrafish embryos (results not shown). Tight junction proteins maintain BBB function and integrity and control the paracellular transport of molecules through the BBB (Zlokovic, 2008). In Alzheimer's disease, Parkinson's disease, AML and Huntington's disease, BBB integrity was shown to be affected by the reduced expression of the tight junction proteins claudin-5, occludin and ZO-1 (Chen et al., 2008; Drouin-Ouellet et al., 2015; Garbuzova-Davis et al., 2012; Yamazaki et al., 2019). In our

transcriptome data, the only tight junction protein with a differential expression was *claudin-5a* (*cldn5a* log2fold -0.332, p<0.01, FDR<0.05). Similarly, the transcriptome data of PTU-treated rats also showed a downregulation of claudin 5 (CDN5) (O'Shaughnessy et al., 2023). Immunohistochemistry analysis of CLD5 in the brain parenchyma of the ventricular zone of 2-day-old PTU-treated rats showed no significant changes compared to control neonates. The most significant changes were observed in the choroid plexus, where CLD5 was reduced and disorganised (O'Shaughnessy et al., 2023). BBB function is also regulated through the ion channels' and transporters' expression and function, regulating the synaptic function of the neuronal circuitry (Jones et al., 1998). The glucose transporter GLUT1, encoded by *SLC2A1A*, is the main glucose transporter in the BBB endothelial cells for brain metabolism (Winkler et al., 2015). In Alzheimer's disease, GLUT1 expression was downregulated (Mooradian et al., 1997), while in our transcriptome data, *slc2a1a* was upregulated (log2fold 0.748, p<0.01, FDR<0.05). In hypoxia-ischemia, GLUT1 expression also increased, which has been suggested to act as an energy-compensatory mechanism, thus acting as a neuroprotective effect after the cerebral ischemic attack (Li et al., 2013). Pericytes are important for blood vessel maturation and BBB stabilisation as they express tight junction proteins to promote vascular permeability (Daneman et al., 2010). In the BBB of Alzheimer's disease patients (Sengillo et al., 2013) and the blood–spinal cord barrier (BSCB) of ALS patients (Winkler et al., 2013), a reduced coverage of pericytes was identified. In Chapter 2, we showed that the disrupted development of the hindbrain vasculature in MCT8MO zebrafish embryos modified the migration behaviour of the pericytes to the different hindbrain vasculature structures. However, we showed that pericytes were not a direct target of MT3 and that the reduced number of pericytes in MCT8MO zebrafish embryos resulted from the defective development of the BHB vasculature. Thus, restoring the hindbrain vasculature would allow pericytes to migrate properly to the different vasculature structures and contribute to adequate BBB permeabilisation (Daneman et al., 2010). The basement membrane is also important to maintain BBB integrity (Obermeier et al., 2013). Laminins principally constitute the basement membrane (Parsons et al., 2002). In our transcriptome data, 4 laminins were differentially expressed (log2[fold-change] values): *laminin beta 1a* (*lamb1a* (0.543)), *laminin gamma 1* (*lamc1* (0.830)), *laminin gamma 2* (*lamc2* (0.985)) and *laminin beta 4* (*lamb4* (-0.905)). These laminins are expressed in various tissues during zebrafish embryonic development, including the brain at 24 hpf and 48 hpf (Carrara et al., 2019; Sztal et al., 2011). Overexpression of laminins has been found in several carcinomas (Chen et al., 2018; Patel et al., 2002). The *lamb4* was the only laminin that was significantly downregulated in 25 hpf MCT8MO zebrafish embryos. However, no studies are looking into

laminin's relevance in embryonic development. In the post-mortem cortex tissue of Alzheimer's and Parkinson's disease patients, an increase in the thickness of the basement membrane has been observed (Farkas et al., 2000). This can affect drug delivery capacity to the brain (Thomsen et al., 2017). The increased expression of the laminins in MCT8MO zebrafish embryos might also lead to an increased thickness of the vascular basement membrane due to the high expression levels of the laminins, but that must be confirmed in future studies. This shows clearly that MT3 is an important factor for neurodevelopment and has an important role in the angiogenic development of the vascular supporting system of the CNS, showing that it acts as an integrator to form a complete NVU.

In AHDS patients, an effective treatment that reverses the psycho-motor impairments remains to be found. So far, treatment with Triac only alleviates thyrotoxicosis in the peripheral tissues of AHDS patients (Groeneweg et al., 2020, 2019). If BBB impairment should be confirmed in AHDS patients, alternative strategies can be implemented to improve AHDS patients' life quality.

5.2 CONCLUSIONS

This thesis aimed to establish the MT3-dependent molecular and cellular determinants behind BHB development. Using the zebrafish Mct8 knockdown model, it was possible to establish the following conclusions:

1) Transcriptome analysis showed that MT3 regulates several developmental signalling pathways during zebrafish embryogenesis, including angiogenic-related pathways such as the VEGFA-VEGFR2 pathway.
2) MT3 regulates the hindbrain expression of *vegfaa* and *vegfab*.
3) MT3 signalling regulates the chemoattraction of the CtAs during zebrafish BHB development.
4) MT3 action on BHB development occurs indirectly by the action of MT3 in *pax6a* NPCs, which are the source of *vegfaa* required for CtA ingression into the hindbrain.
5) Vascularisation of rhombomeres 4, 5 and 6 are dependent on MT3 signalling.
6) Vascularisation of rhombomeres 1, 2, 3 and 7 are independent on MT3 signalling through *pax6a*/*mct8*+ cells. However, the presence of *pax6a*/*mct8*+ cells in rhombomere 7 in the stages before CtA development strongly suggests that these cells are responsive to MT3.
7) The presence of *pax6a*/*thraa*+ cells in rhombomere 7, the presence of *pax6a*/*thrab*+ cells in rhombomeres 1 and 2, and of both *TRalpha* in rhombomere 3 might indicate an aporeceptor function for the coordinated development of the CtAs

In conclusion, the presence of MT3 allows the survival and proliferation of specific *pax6a* NPCs in the zebrafish hindbrain, which are necessary for the timely ingression of the CtAs through the expression of the angiogenic factor *vegfaa*. The presence of the different TH signalling genes (*mct8*, *thraa* and *thrab*) in *pax6a* NPCs at the different time points and rhombomeres might indicate that MT3 is acting following the chronological order of CtA ingression, contributing to a fully functional BHB development. Figure 5.1 illustrates the mechanism of MT3 on CtA hindbrain ingression leading to BHB development. It would be of great interest to confirm that in human AHDS patients, the BBB is also disrupted to implement an alternative strategy to improve the life quality of these patients.

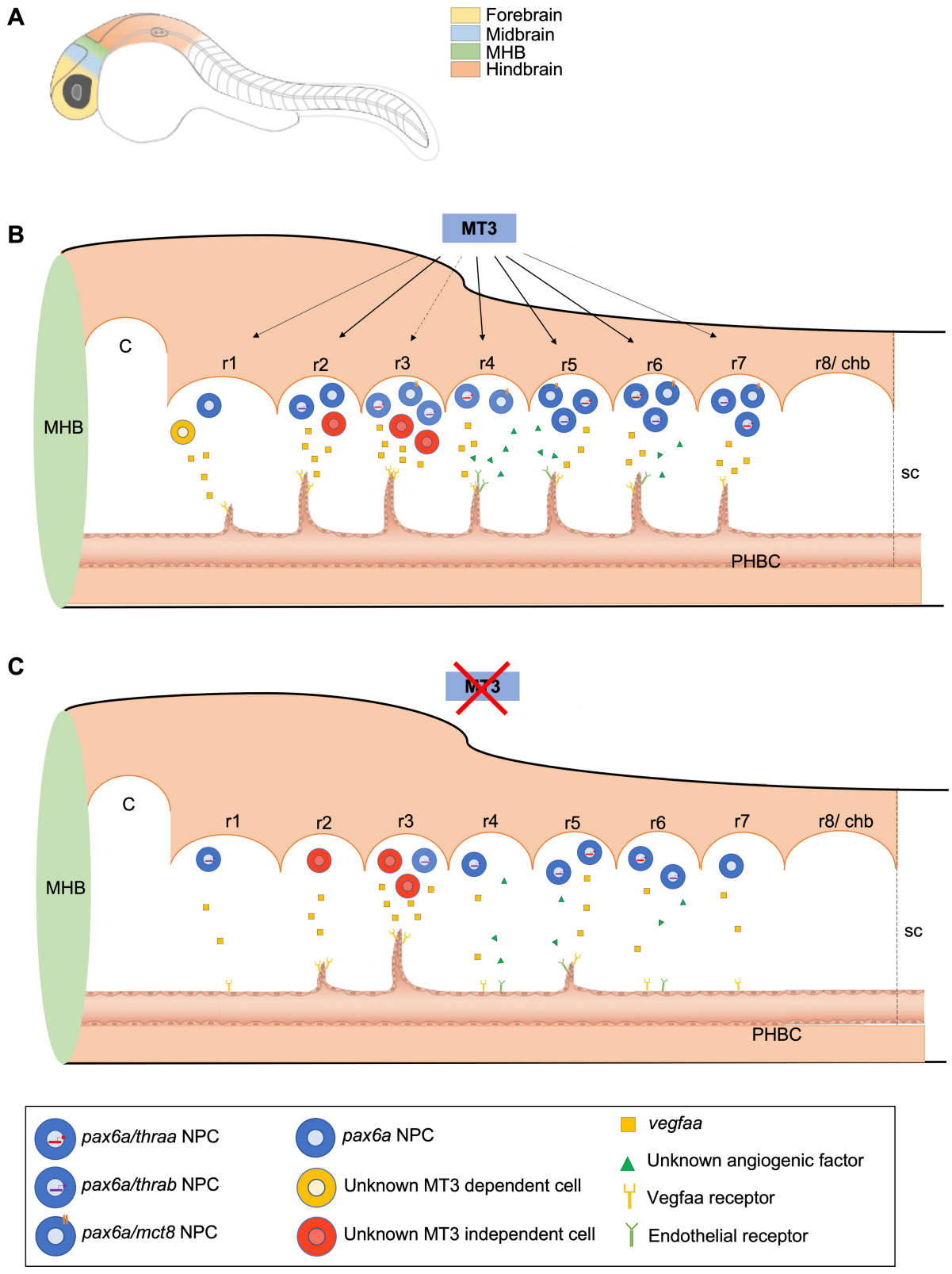

Figure 5.1 – The effect of MT3 through Mct8 on central arteries development for blood-hindbrain barrier development during zebrafish embryogenesis. A) Schematic illustration of the zebrafish brain at 30 hpf, a stage before CtA development. The different brain regions are highlighted in different colours: forebrain in yellow, midbrain in blue, midbrain-hindbrain boundary (MHB) in green, and hindbrain in

orange. Image adapted from Vaz et al., (2019). **B)** Illustration of a lateral view of the zebrafish hindbrain showing the influence of MT3 signalling through Mct8 on CtA development. The different *pax6a* neural progenitor cells (NPC) identified in the different rhombomeres with the TH machinery *mct8*, *thraa* and *thrab* are illustrated. In rhombomere 1 we suggest the involvement of another central nervous system (CNS) cell type that is MT3 dependent and the source of *vegfaa* required for CtA development. In rhombomere 3, *pax6a* NPCs are present, but MT3 signalling is not involved in CtA 3 development (dashed arrow line) but enhances its development. Vascularisation of rhombomeres 4, 5 and 6 suggests that, besides *vegfaa*, another angiogenic factor is involved in the angiogenic sprouting involved in CtA development. **C)** Illustration of a lateral view of the zebrafish hindbrain showing the effect of Mct8 knockdown and MT3-impaired signalling. The most frequently developed CtAs in the hindbrain of 48 hpf zebrafish embryos are represented. Although significantly reduced in rhombomere 2, *vegfaa* signalling is still present in MCT8MO zebrafish embryos, showing that another CNS cell type, independent of MT3 signalling, is responsible for releasing *vegfaa*. CtA 3 develops in rhombomere 3 independently on MT3 signalling. The inability to rescue the vascularisation of rhombomere 4 by *vegfaa-165* mRNA suggests that another angiogenic factor is necessary for its development. C: cerebellum; chb: caudal hindbrain; MHB: Midbrain-hindbrain boundary; MT3: maternal T3; PHBC: Primordial Hindbrain Channels; r1 – r8: rhombomere 1 – 8; sc – spinal cord.

5.3 FUTURE PERSPECTIVES

Transcriptome analysis revealed several signalling pathways affected by Mct8 ablation, showing the global effect of MTH action at 25 hpf during zebrafish embryogenesis. However, the developmental time window needed to be improved for studying the vascular defects observed during BHB development, given that this only occurs later in development. It would be useful to study a time window from 30 hpf onwards and apply transcriptome analysis only to the brain or hindbrain tissue. In the past years, single-cell transcriptomics has been revealed to be useful in studying single-cell gene expression profiles in zebrafish (Griffiths et al., 2018), such as to analyse the cell diversity of vascular endothelial cells (Gurung et al., 2022).

We showed that the injection of *vegfaa-165* mRNA partially rescued the development of CtAs 5 and 6, and CtA 4 could not be rescued. This shows that another angiogenic factor might be required to develop these CtAs. We propose to analyse the effect of *vegfab* on CtA development or even the combined effect of both *vegfa* ligands.

The availability of the *pax6a* KO F2 zebrafish line should be further explored to confirm which CtAs are effectively missing in these mutants and to confirm the results obtained in MCT8MO zebrafish embryos.

The generation of an Mct8 knockout zebrafish would help to study the effect of *vegfaa* therapy in adult zebrafish, confirming if it is possible to restore the vascular defects observed in MCT8MO zebrafish embryos, implementing an alternative strategy for AHDS.

CHAPTER 6

Bibliography

Abbott, N.J., 2004. Evidence for bulk flow of brain interstitial fluid: Significance for physiology and pathology. Neurochem. Int. 45, 545–552.

Abbott, N.J., Rönnbäck, L., Hansson, E., 2006. Astrocyte-endothelial interactions at the blood-brain barrier. Nat. Rev. Neurosci. 7, 41–53.

Abrams, E.W., Mullins, M.C., 2009. Early zebrafish development: It's in the maternal genes. Curr. Opin. Genet. Dev. 19, 396–403.

Abramsson, A., Lindblom, P., Betsholtz, C., 2003. Endothelial and nonendothelial sources of PDGF-B regulate pericyte recruitment and influence vascular pattern formation in tumors. J. Clin. Invest. 112, 1142–1151.

Adams, R.H., Alitalo, K., 2007. Molecular regulation of angiogenesis and lymphangiogenesis. Nat. Rev. Mol. Cell Biol. 8, 464–478.

Alabi, R.O., Farber, G., Blobel, X.C.P., 2018. Intriguing roles for endothelial ADAM10/NOTCH signaling in the development of organ-specific vascular beds. Physiol. Rev. 98, 2025–2061.

Alexander, T., Nolte, C., Krumlauf, R., 2009. Hox genes and segmentation of the hindbrain and axial skeleton. Annu. Rev. Cell Dev. Biol. 25, 431–456.

Alkaslasi, M.R., Piccus, Z.E., Hareendran, S., Silberberg, H., Chen, L., Zhang, Y., Petros, T.J., Le Pichon, C.E., 2021. Single nucleus RNA-sequencing defines unexpected diversity of cholinergic neuron types in the adult mouse spinal cord. Nat. Commun. 12, 1–14.

Allt, G., Lawrenson, J.G., 2001. Pericytes: Cell biology and pathology. Cells Tissues Organs 169, 1–11.

Álvarez-Aznar, A., Muhl, L., Gaengel, K., 2017. VEGF Receptor Tyrosine Kinases: Key Regulators of Vascular Function. Curr. Top. Dev. Biol. 123, 433–482.

Alvarez, J.I., Dodelet-Devillers, A., Kebir, H., Ifergan, I., Fabre, P.J., Terouz, S., Sabbagh, M., Wosik, K., Bourbonnière, L., Bernard, M., Van Horssen, J., De Vries, H.E., Charron, F., Prat, A., 2011. The hedgehog pathway promotes blood-brain barrier integrity and CNS immune quiescence. Science (80-.). 334, 1727–1731.

Alvarez, J.I., Katayama, T., Prat, A., 2013. Glial influence on the blood brain barrier. Glia 61, 1939–1958.

America, M., Bostaille, N., Eubelen, M., Martin, M., Stainier, D.Y.R., Vanhollebeke, B., America, M., Bostaille, N., Eubelen, M., Martin, M., Stainier, D.Y.R., 2022. An integrated model for Gpr124 function in Wnt7a / b signaling among vertebrates. Cell Rep. 39, 1–28.

Andersson, M., De Benoist, B., Delange, F., Zupan, J., 2007. Prevention and control of iodine deficiency in pregnant and lactating women and in children less than 2-years-old: Conclusions and recommendations of the Technical Consultation. Public Health Nutr. 10, 1606–1611.

Ando, K., Fukuhara, S., Izumi, N., Nakajima, H., Fukui, H., Kelsh, R.N., Mochizuki, N., 2016. Clarification of mural cell coverage of vascular endothelial cells by live imaging of zebrafish. Dev. 143, 1328–1339.

Andreone, B.J., Lacoste, B., Gu, C., 2015. Neuronal and vascular interactions. Annu. Rev.

Neurosci. 38, 25–46.

Anelli, V., Villefranc, J.A., Chhangawala, S., Martinez-Mcfaline, R., Riva, E., Nguyen, A., Verma, A., Bareja, R., Chen, Z., Scognamiglio, T., Elemento, O., Houvras, Y., 2017. Oncogenic BRAF disrupts thyroid morphogenesis and function via twist expression. Elife 6, 1–19.

Anne Galton, V., Cohen, J.S., 1980. Action of thyroid hormones in premetamorphic tadpoles: An important role for thyroxine? Endocrinology 107, 1820–1826.

Arjona, F.J., De Vrieze, E., Visser, T.J., Flik, G., Klaren, P.H.M., 2011. Identification and functional characterization of zebrafish solute carrier Slc16a2 (Mct8) as a thyroid hormone membrane transporter. Endocrinology 152, 5065–5073.

Armulik, A., Genové, G., Mäe, M., Nisancioglu, M.H., Wallgard, E., Niaudet, C., He, L., Norlin, J., Lindblom, P., Strittmatter, K., Johansson, B.R., Betsholtz, C., 2010. Pericytes regulate the blood-brain barrier. Nature 468, 557–561.

Attwell, D., Buchan, A.M., Charpak, S., Lauritzen, M., MacVicar, B.A., Newman, E.A., 2010. Glial and neuronal control of brain blood flow. Nature 468, 232–243.

Ausó, E., Lavado-Autric, R., Cuevas, E., Escobar Del Rey, F., Morreale De Escobar, G., Berbel, P., 2004. A moderate and transient deficiency of maternal thyroid function at the beginning of fetal neocorticogenesis alters neuronal migration. Endocrinology 145, 4037–4047.

Bagci, E., Heijlen, M., Vergauwen, L., Hagenaars, A., Houbrechts, A.M., Esguerra, C. V., Blust, R., Darras, V.M., Knapen, D., 2015. Deiodinase knockdown during early zebrafish development affects growth, development, energy metabolism, motility and phototransduction. PLoS One 10, 1–22.

Bahary, N., Goishi, K., Stuckenholz, C., Weber, G., LeBlanc, J., Schafer, C.A., Berman, S.S., Klagsbrun, M., Zon, L.I., 2007. Duplicate VegfA genes and orthologues of the KDR receptor tyrosine kinase family mediate vascular development in the zebrafish. Blood 110, 3627–3636.

Bakker, O., 2004. Thyroid hormone receptors. Encycl. Endocr. Dis. 4, 490–495.

Barber, M., Andrews, W.D., Memi, F., Gardener, P., Ciantar, D., Tata, M., Ruhrberg, C., Parnavelas, J.G., 2018. Vascular-derived VEGFA promotes cortical interneuron migration and proximity to the vasculature in the developing forebrain. Cereb. Cortex 28, 2577–2593.

Bárez-López, S., Grijota-Martínez, C., Ausó, E., Fernández-De Frutos, M., Montero-Pedrazuela, A., Guadaño-Ferraz, A., 2019. Adult Mice Lacking Mct8 and Dio2 Proteins Present Alterations in Peripheral Thyroid Hormone Levels and Severe Brain and Motor Skill Impairments. Thyroid 29, 1669–1682.

Bárez-López, S., Guadaño-Ferraz, A., 2017. Thyroid hormone availability and action during brain development in rodents. Front. Cell. Neurosci. 11, 1–7.

Bates, J.M., St. Germain, D.L., Galton, V.A., 1999. Expression profiles of the three iodothyronine deiodinases, D1, D2, and D3, in the developing rat. Endocrinology 140, 844–851.

Bath, S.C., Steer, C.D., Golding, J., Emmett, P., Rayman, M.P., 2013. Effect of inadequate iodine status in UK pregnant women on cognitive outcomes in their children: Results from the

Avon Longitudinal Study of Parents and Children (ALSPAC). Lancet 382, 331–337.

Batista, M.F., Lewis, K.E., 2008. Pax2/8 act redundantly to specify glycinergic and GABAergic fates of multiple spinal interneurons. Dev. Biol. 323, 88–97.

Bautch, V.L., James, J.M., 2009. Neurovascular development: The beginning of a beautiful friendship. Cell Adhes. Migr. 3, 199–204.

Bedell, V.M., Westcot, S.E., Ekker, S.C., 2011. Lessons from morpholino-based screening in zebrafish. Brief. Funct. Genomics 10, 181–188.

Bedell, V.M., Yeo, S.Y., Kye, W.P., Chung, J., Seth, P., Shivalingappa, V., Zhao, J., Obara, T., Sukhatme, V.P., Drummond, I.A., Li, D.Y., Ramchandran, R., 2005. Roundabout4 Is Essential for Angiogenesis in Vivo. Proc. Natl. Acad. Sci. U. S. A. 102, 6373–6378.

Begley, D.J., Brightman, M.W., 2003. Structural and functional aspects of the blood-brain barrier. Prog. Drug Res. 61, 39–78.

Bel-Vialar, S., Medevielle, F., Pituello, F., 2007. The on/off of Pax6 controls the tempo of neuronal differentiation in the developing spinal cord. Dev. Biol. 305, 659–673.

Bernal, J., 2007. Thyroid hormone receptors in brain development and function. Nat. Clin. Pract. Endocrinol. Metab. 3, 249–259.

Bernal, J., 2017. Thyroid hormone regulated genes in cerebral cortex development. J. Endocrinol. 232, R83–R97.

Bernal, J., 2022. Thyroid Hormones in Brain Development and Function. Endotext 1–27.

Bernal, J., Guadaño-Ferraz, A., Morte, B., 2015. Thyroid hormone transporters-functions and clinical implications. Nat. Rev. Endocrinol. 11, 406–417.

Bernal, J., Nuncez, J., 1995. Thyroid hormones and brain development. Eur. J. Endocrinol. 133, 390–398.

Bernal, J., Pekonen, F., 1984. Ontogenesis of the nuclear 3,5,3'-triiodothyronine receptor in the human fetal brain. Endocr. Soc. 114, 677–679.

Bernardos, R.L., Raymond, P.A., 2006. GFAP transgenic zebrafish. Gene Expr. Patterns 6, 1007–1013.

Bertrand, N., Medevielle, F., Pituello, F., 2000. FGF signalling controls the timing of Pax6 activation in the neural tube. Development 127, 4837–4843.

Betsholtz, C., 2018. Cell–cell signaling in blood vessel development and function. EMBO Mol. Med. 10, 2–5.

Bianco, A.C., da Conceição, R.R., 2018. The deiodinase trio and thyroid hormone signaling. Methods Mol. Biol. 1801, 67–83.

Bianco, A.C., Dumitrescu, A., Gereben, B., Ribeiro, M.O., Fonseca, T.L., Fernandes, G.W., Bocco, B.M.L.C., 2019. Paradigms of Dynamic Control of Thyroid Hormone Signaling. Endocr. Rev. 40, 1000–1047.

Bianco, A.C., Salvatore, D., Gereben, B., Berry, M.J., Larsen, P.R., 2002. Biochemistry,

cellular and molecular biology, and physiological roles of the iodothyronine selenodeiodinases. Endocr. Rev. 23, 38–89.

Blake, J.A., Ziman, M.R., 2014. Pax genes: Regulators of lineage specification and progenitor cell maintenance. Dev. 141, 737–751.

Blanco, R., Gerhardt, H., 2013. VEGF and Notch in tip and stalk cell selection. Cold Spring Harb. Perspect. Med. 3, 1–19.

Blanton, M.L., Specker, J.L., 2007. The hypothalamic-pituitary-thyroid (HPT) axis in fish and its role in fish development and reproduction. Crit. Rev. Toxicol. 37, 97–115.

Boccone, L., Dessì, V., Meloni, A., Loudianos, G., 2013. Allan-Herndon-Dudley syndrome (AHDS) in two consecutive generations caused by a missense MCT8 gene mutation. Phenotypic variability with the presence of normal serum T3 levels. Eur. J. Med. Genet. 56, 207–210.

Bochukova, E., Schoenmakers, N., Agostini, M., Schoenmakers, E., Rajanayagam, O., Keogh, J.M., Henning, E., Reinemund, J., Gevers, E., Sarri, M., Downes, K., Offiah, A., Albanese, A., Halsall, D., Schwabe, J.W.R., Bain, M., Lindley, K., Muntoni, F., Vargha-Khadem, F., Dattani, M., Farooqi, I.S., Gurnell, M., Chatterjee, K., 2012. A Mutation in the Thyroid Hormone Receptor Alpha Gene. N. Engl. J. Med. 366, 243–249.

Bolborea, M., Dale, N., 2013. Hypothalamic tanycytes: Potential roles in the control of feeding and energy balance. Trends Neurosci. 36, 91–100.

Bowler, E., Oltean, S., 2019. Alternative splicing in angiogenesis. Int. J. Mol. Sci. 20.

Bradley, D.J., Towle, H.C., Young, W.S., 1992. Spatial and temporal expression of α- and β-thyroid hormone receptor mRNAs, including the β2-subtype, in the developing mammalian nervous system. J. Neurosci. 12, 2288–2302.

Braun, D., Kinne, A., Brauer, A.U., Sapin, R., Klein, M.O., Köhrle, J., Wirth, E.K., Schweizer, U., 2011. Developmental and cell type-specific expression of thyroid hormone transporters in the mouse brain and in primary brain cells. Glia 59, 463–471.

Braun, D., Schweizer, U., 2018. Thyroid Hormone Transport and Transporters. Vitam. Horm.

Breier, G., Albrecht, U., Sterrer, S., Risau, W., 1992. Expression of vascular endothelial growth factor during embryonic angiogenesis and endothelial cell differentiation. Development 114, 521–532.

Briscoe, J., Wilkinson, D.G., 2004. Establishing neuronal circuitry: Hox genes make the connection. Genes Dev. 18, 1643–1648.

Brunton, P.J., Russell, J.A., 2011. Neuroendocrine control of maternal stress responses and fetal programming by stress in pregnancy. Prog. Neuro-Psychopharmacology Biol. Psychiatry 35, 1178–1191.

Bundgaard, M., Abbott, N.J., 2008. All vertebrates started out with a glial blood-brain barrier 4-500 million years ago. Glia 56, 699–708.

Burrow, G.N., Fisher, D.A., Larsen, P.R., 1994. Maternal and fetal thyroid function. N. Engl. J. Med. 1072–1078.

Bussmann, J., Lawson, N., Zon, L., Schulte-Merker, S., Ekker, M., Mullins, M., Postlethwait, J., Westerfield, M., 2008. Zebrafish VEGF receptors: A guideline to nomenclature. PLoS Genet. 4, 4–5.

Bussmann, J., Wolfe, S.A., Siekmann, A.F., 2011. Arterial-venous network formation during brain vascularization involves hemodynamic regulation of chemokine signaling. Development 138, 1717–1726.

Büyükgebiz, A., 2013. Newborn screening for congenital hypothyroidism. JCRPE J. Clin. Res. Pediatr. Endocrinol. 5, 8–12.

Caley, D.W., Maxwell, D.S., 1970. Development of the blood vessels and extracellular spaces during postnatal maturation of rat cerebral cortex. J. Comp. Neurol. 138, 31–47.

Calvo, R.M., Jauniaux, E., Gulbis, B., Asunción, M., Gervy, C., Contempré, B., De Escobar, G.M., 2002. Fetal tissues are exposed to biologically relevant free thyroxine concentrations during early phases of development. J. Clin. Endocrinol. Metab. 87, 1768–1777.

Calzolari, S., Terriente, J., Pujades, C., 2014. Cell segregation in the vertebrate hindbrain relies on actomyosin cables located at the interhombomeric boundaries. EMBO J. 33, 686–701.

Campinho, M.A., Saraiva, J., Florindo, C., Power, D.M., 2014. Maternal Thyroid Hormones Are Essential for Neural Development in Zebrafish. Mol. Endocrinol. 28, 1136–1149.

Campos-Barros, A., Hoell, T., Musa, A., Sampaolo, S., Stoltenburg, G., Pinna, G., Eravci, M., Meinhold, H., Baumgartner, A., 1996. Phenolic and tyrosyl ring iodothyronine deiodination and thyroid hormone concentrations in the human cental nervous system. J. Clin. Endocrinol. Metab. 81, 2179–2185.

Carmeliet, P., Ferreira, V., Breier, G., Pollefeyt, S., Kieckens, L., Gertsenstein, M., Fahrig, M., Vandenhoeck, A., Harpal, K., Eberhardt, C., Declercq, C., Pawling, J., Moons, L., Collen, D., Risaut, W., Nagy, A., 1996. Abnormal blood vessel development and lethality in embryos lacking a single VEGF allele. Nature.

Carrara, N., Weaver, M., Piedade, W.P., Vöcking, O., Famulski, J.K., 2019. Temporal characterization of optic fissure basement membrane composition suggests nidogen may be an initial target of remodeling. Dev. Biol. 452, 43–54.

Carvey, P.M., Hendey, B., Monahan, A.J., 2009. The blood-brain barrier in neurodegenerative disease: A rhetorical perspective. J. Neurochem. 111, 291–314.

Ceballos, A., Belinchon, M.M., Sanchez-Mendoza, E., Grijota-Martinez, C., Dumitrescu, A.M., Refetoff, S., Morte, B., Bernal, J., 2009. Importance of monocarboxylate transporter 8 for the blood-brain barrier-dependent availability of 3,5,3’ -triiodo-L-thyronine. Endocrinology 150, 2491–2496.

Chan, S., Kachilele, S., McCabe, C.J., Tannahill, L.A., Boelaert, K., Gittoes, N.J., Visser, T.J., Franklyn, J.A., Kilby, M.D., 2002. Early expression of thyroid hormone deiodinases and receptors in human fetal cerebral cortex. Dev. Brain Res. 138, 109–116.

Chan, S.Y., Martín-Santos, A., Loubière, L.S., González, A.M., Stieger, B., Logan, A., Mccabe, C.J., Franklyn, J.A., Kilby, M.D., 2011. The expression of thyroid hormone transporters in the human fetal cerebral cortex during early development and in N-Tera-2 neurodifferentiation. J. Physiol. 589, 2827–2845.

Chan, S.Y., Vasilopoulou, E., Kilby, M.D., 2009. The role of the placenta in thyroid hormone delivery to the fetus. Nat. Clin. Pract. Endocrinol. Metab. 5, 45–54.

Chandrasekhar, A., 2004. Turning Heads: Development of Vertebrate Branchiomotor Neurons. Dev. Dyn. 229, 143–161.

Chang, J., Wang, M., Gui, W., Zhao, Y., Yu, L., Zhu, G., 2012. Changes in Thyroid Hormone Levels during Zebrafish Development. Zoolog. Sci. 29, 181–184.

Chanoine, J.-P., Alex, S., Fang, S.L., Stone, S., Leonard, J.L., Körhle, J., Braverman, L.E., 1992. Role of transthyretin in the transport of thyroxine from the blood to the choroid plexus, the cerebrospinal fluid, and the brain. Endocr. Soc. 130, 933–938.

Chappell, J.C., Taylor, S.M., Ferrara, N., Bautch, V.L., 2009. Local Guidance of Emerging Vessel Sprouts Requires Soluble Flt-1. Dev. Cell 17, 377–386.

Chatonnet, F., Guyot, R., Benoît, G., Flamant, F., 2013. Genome-wide analysis of thyroid hormone receptors shared and specific functions in neural cells. Proc. Natl. Acad. Sci. 110, E766–E775.

Chen, J., Poskanzer, K.E., Freeman, M.R., Monk, K.R., 2020. Live-imaging of astrocyte morphogenesis and function in zebrafish neural circuits. Nat. Neurosci. 23, 1297–1306.

Chen, J., Zhang, H., Luo, J., Wu, X., Li, X., Zhao, X., Zhou, D., Yu, S., 2018. Overexpression of α3, β3 and γ2 chains of laminin-332 is associated with poor prognosis in pancreatic ductal adenocarcinoma. Oncol. Lett. 16, 199–210.

Chen, Q., Jiang, L., Li, C., Hu, D., Bu, J., Cai, D., Du, J., 2012. Haemodynamics-Driven Developmental Pruning of Brain Vasculature in Zebrafish. PLoS Biol. 10, 1–18.

Chen, X., Lan, X., Roche, I., Liu, R., Geiger, J.D., 2008. Caffeine protects against MPTP-induced blood-brain barrier dysfunction in mouse striatum. J. Neurochem. 107, 1147–1157.

Chen, Y., Young, M.A., 2010. Structure of a thyroid hormone receptor DNA-binding domain homodimer bound to an inverted palindrome DNA response element. Mol. Endocrinol. 24, 1650–1664.

Chen, Z.P., Hetzel, B.S., 2010. Cretinism revisited. Best Pract. Res. Clin. Endocrinol. Metab. 24, 39–50.

Cheng, S.Y., 2000. Multiple Mechanisms for Regulation of the Transcriptional Activity of Thyroid Hormone Receptors. Rev. Endocr. Metab. Disord. 1, 9–18.

Cheng, S.Y., Leonard, J.L., Davis, P.J., 2010. Molecular aspects of thyroid hormone actions. Endocr. Rev. 31, 139–170.

Cho, C., Smallwood, P.M., Nathans, J., 2017. Reck and Gpr124 Are Essential Receptor Cofactors for Wnt7a/Wnt7b-Specific Signaling in Mammalian CNS Angiogenesis and Blood-Brain Barrier Regulation. Neuron 95, 1056-1073.e5.

Choe, S.-K., Vlachakis, N., Sagerström, C.G., 2002. Meis family proteins are required for hindbrain development in the zebrafish. Development 129, 585–595.

Chowdhury, I., Chien, J.T., Chatterjee, A., Yu, J.Y.L., 2004. In vitro effects of mammalian leptin, neuropeptide-Y, β-endorphin and galanin on transcript levels of thyrotropin β and

common α subunit mRNAs in the pituitary of bighead carp (aristichthys nobilis). Comp. Biochem. Physiol. - B Biochem. Mol. Biol. 139, 87–98.

Citterio, C.E., Targovnik, H.M., Arvan, P., 2019. The role of thyroglobulin in thyroid hormonogenesis. Nat. Rev. Endocrinol. 15, 323–338.

Coenye, T., 2021. Do results obtained with RNA-sequencing require independent verification? Biofilm 3, 100043.

Colas, J.-F., Schoenwolf, G.C., 2001. Towards a cellular and molecular understanding of neurolation. Dev. Dyn. 221, 117–145.

Contempré, B., Jauniaux, E., Calvo, R., Jurkovic, D., Campbell, S., Morreale De Escobar, G., 1993. Detection of thyroid hormones in human embryonic cavities during the first trimester of pregnancy. J. Clin. Endocrinol. Metab. 77, 1719–1722.

Correale, J., Villa, A., 2009. Cellular elements of the blood-brain barrier. Neurochem. Res. 34, 2067–2077.

Coutinho, P., Pavlou, S., Bhatia, S., Chalmers, K.J., Kleinjan, D.A., Van Heyningen, V., 2011. Discovery and assessment of conserved Pax6 target genes and enhancers. Genome Res. 21, 1349–1359.

Covassin, L.D., Villefranc, J.A., Kacergis, M.C., Weinstein, B.M., Lawson, N.D., 2006. Distinct genetic interactions between multiple Vegf receptors are required for development of different blood vessel types in zebrafish. Proc. Natl. Acad. Sci. U. S. A. 103, 6554–6559.

Cowland, J.B., Carter, D., Bjerregaard, M.D., Johnsen, A.H., Borregaard, N., Lollike, K., 2003. Tissue expression of copines and isolation of copines I and III from the cytosol of human neutrophils. J. Leukoc. Biol. 74, 379–388.

Creutz, C.E., Tomsig, J.L., Snyder, S.L., Gautier, M.C., Skouri, F., Beisson, J., Cohen, J., 1998. The copines, a novel class of C2 domain-containing, calcium-dependent, phospholipid-binding proteins conserved from Paramecium to humans. J. Biol. Chem. 273, 1393–1402.

Croft, D., Mundo, A.F., Haw, R., Milacic, M., Weiser, J., Wu, G., Caudy, M., Garapati, P., Gillespie, M., Kamdar, M.R., Jassal, B., Jupe, S., Matthews, L., May, B., Palatnik, S., Rothfels, K., Shamovsky, V., Song, H., Williams, M., Birney, E., Hermjakob, H., Stein, L., D'Eustachio, P., 2014. The Reactome pathway knowledgebase. Nucleic Acids Res. 42, 472–477.

Cuevas, P., Gutierrez-Diaz, J.A., Reimers, D., Dujovny, M., Diaz, F.G., Ausman, J.I., 1984. Pericyte endothelial gap junctions in human cerebral capillaries. Anat. Embryol. (Berl). 170, 155–159.

Cvekl, A., Callaerts, P., 2017. PAX6: 25th anniversary and more to learn. Exp. Eye Res. 156, 10–21.

Daida, K., Tanaka, R., Yamashiro, K., Ogawa, T., Oyama, G., Nishioka, K., Shimo, Y., Umemura, A., Hattori, N., 2018. The presence of cerebral microbleeds is associated with cognitive impairment in Parkinson's disease. J. Neurol. Sci. 393, 39–44.

Daneman, R., Agalliu, D., Zhou, L., Kuhnert, F., Kuo, C.J., Barres, B.A., 2009. Wnt/β-catenin signaling is required for CNS, but not non-CNS, angiogenesis. Proc. Natl. Acad. Sci. U. S. A. 106, 641–646.

Daneman, R., Prat, A., 2015. The blood–brain barrier. Cold Spring Harb. Perspect. Biol. 7, 1–23.

Daneman, R., Zhou, L., Kebede, A.A., Barres, B.A., 2010. Pericytes are required for blood-brain barrier integrity during embryogenesis. Nature 468, 562–566.

Dansault, A., David, G., Schwartz, C., Jaliffa, C., Vieira, V., de la Houssaye, G., Bigot, K., Catin, F., Tattu, L., Chopin, C., Halimi, P., Roche, O., Van Regemorter, N., Munier, F., Schorderet, D., Dufier, J.L., Marsac, C., Ricquier, D., Menasche, M., Penfornis, A., Abitbol, M., 2007. Three new PAX6 mutations including one causing an unusual ophthalmic phenotype associated with neurodevelopmental abnormalities. Mol. Vis. 13, 511–523.

Darras, V.M., Van Herck, S.L.J., Heijlen, M., De Groef, B., 2011. Thyroid hormone receptors in two model species for vertebrate embryonic development: Chicken and zebrafish. J. Thyroid Res. 2011, 1–8.

Das Gupta, R.R., Scheurer, L., Pelczar, P., Wildner, H., Zeilhofer, H.U., 2021. Neuron-specific spinal cord translatomes reveal a neuropeptide code for mouse dorsal horn excitatory neurons. Sci. Rep. 11, 1–18.

Davis, P.J., Goglia, F., Leonard, J.L., 2016. Nongenomic actions of thyroid hormone. Nat. Rev. Endocrinol. 12, 111–121.

De Boer, A.G., Van der Sandt, I.C.J., Gaillard, P.J., 2003. The Role of Drug Transporters at the Blood-Brain Barrier. Annu. Rev. Pharmacol. Toxicol. 43, 629–656.

De Escobar, G.M., Obregón, M.J., Del Rey, F.E., 2004. Role of thyroid hormone during early brain development. Eur. J. Endocrinol. Suppl. 151, 25–37.

de Escobar, G.M., Obregón, M.J., Escobar del Rey, F., 2004. Maternal thyroid hormones early in prenancy and fetal brain development. Best Pract. Res. Clin. Endocrinol. Metab. 18, 225–248.

De Groef, B., Van Der Geyten, S., Darras, V.M., Kühn, E.R., 2006. Role of corticotropin-releasing hormone as a thyrotropin-releasing factor in non-mammalian vertebrates. Gen. Comp. Endocrinol. 146, 62–68.

de Reuck, J.L., 2012. The significance of small cerebral bleeds in neurodegenerative dementia syndromes. Aging Dis. 3, 307–312.

De Robertis, E.M., Kuroda, H., 2004. Dorsal-ventral patterning and neural induction in Xenopus embryos. Annu. Rev. Cell Dev. Biol. 20, 285–308.

De Vrieze, E., Van De Wiel, S.M.W., Zethof, J., Flik, G., Klaren, P.H.M., Arjona, F.J., 2014. Knockdown of monocarboxylate transporter 8 (mct8) disturbs brain development and locomotion in zebrafish. Endocrinology 155, 2320–2330.

del Corral, R., Morales, A., 2014. Retinoic Acid Signaling during Early Spinal Cord Development. J. Dev. Biol. 2, 174–197.

Delahunty, C., Falconer, S., Hume, R., Jackson, L., Midgley, P., Mirfield, M., Ogston, S., Perra, O., Simpson, J., Watson, J., Willatts, P., Williams, F., Dunlop, J., Kinmond, S., Lloyd, D., McFadyen, U., McArthur, A., Mitchell, S., Ray, M., Vallance, A., 2010. Levels of neonatal thyroid hormone in preterm infants and neurodevelopmental outcome at 5 1/2 years:

Millennium cohort study. J. Clin. Endocrinol. Metab. 95, 4898–4908.

Delange, F., 1997. Neonatal screening for congenital hypothyroidism: results and perspectives. Horm. Res. 48, 51–61.

Delong, G.R., Stanbury, J.B., Fierro-Benitez, R., 1985. Neurological signs in congenital iodine-deficiency disorder (endemic cretinism). Dev. Med. Child Neurol. 27, 317–324.

Dentice, M., Salvatore, D., 2011. Local impact of thyroid hormone inactivation. J. Endocrinol.

Desouza, L.A., Sathanoori, M., Kapoor, R., Rajadhyaksha, N., Gonzalez, L.E., Kottmann, A.H., Tole, S., Vaidya, V.A., 2011. Thyroid hormone regulates the expression of the sonic hedgehog signaling pathway in the embryonic and adult mammalian brain. Endocrinology 152, 1989–2000.

Development of the Neural Crest, 2014. , Reference Module in Biomedical Sciences, Elsevier. Elsevier.

Di Cosmo, C., Liao, X.H., Dumitrescu, A.M., Weiss, R.E., Refetoff, S., 2009. A thyroid hormone analog with reduced dependence on the monocarboxylate transporter 8 for tissue transport. Endocrinology 150, 4450–4458.

Dickson, B.J., Gilestro, G.F., 2006. Regulation of commissural axon pathfinding by Slit and its Robo receptors. Annu. Rev. Cell Dev. Biol. 22, 651–675.

Diez del Corral, R., Morales, A. V., 2017. The Multiple Roles of FGF Signaling in the Developing Spinal Cord. Front. Cell Dev. Biol. 5, 1–18.

Diez del Corral, R., Olivera-Martinez, I., Goriely, A., Gale, E., Maden, M., Storey, K., 2003. Opposing FGF and retinoid pathways control ventral neural pattern, neuronal differentiation, and segmentation during body axis extension. Cell Press 40, 65–79.

Dong, W., Macaulay, L.J., Kwok, K.W.H., Hinton, D.E., Stapleton, H.M., 2013. Using whole mount in situ hybridization to examine thyroid hormone deiodinase expression in embryonic and larval zebrafish: A tool for examining OH-BDE toxicity to early life stages. Aquat. Toxicol. 132–133, 190–199.

Dora, J.M., Machado, W.E., Rheinheimer, J., Crispim, D., Maia, A.L., 2010. Association of the type 2 deiodinase Thr92Ala polymorphism with type 2 diabetes: Case-control study and meta-analysis. Eur. J. Endocrinol. 163, 427–434.

Dratman, M.B., Crutchfield, F.L., Schoenhoff, M.B., 1991. Transport of iodothyronines from bloodstream to brain: contributions by blood:brain and choroid plexus:cerebrospinal fluid barriers. Brain Res. 554, 229–236.

Drouin-Ouellet, J., Sawiak, S.J., Cisbani, G., Lagacé, M., Kuan, W.L., Saint-Pierre, M., Dury, R.J., Alata, W., St-Amour, I., Mason, S.L., Calon, F., Lacroix, S., Gowland, P.A., Francis, S.T., Barker, R.A., Cicchetti, F., 2015. Cerebrovascular and blood-brain barrier impairments in Huntington's disease: Potential implications for its pathophysiology. Ann. Neurol. 78, 160–177.

Dumitrescu, A.M., Liao, X.H., Best, T.B., Brockmann, K., Refetoff, S., 2004. A Novel Syndrome Combining Thyroid and Neurological Abnormalities Is Associated with Mutations in a Monocarboxylate Transporter Gene. Am. J. Hum. Genet. 74, 168–175.

Ellertsdóttir, E., Lenard, A., Blum, Y., Krudewig, A., Herwig, L., Affolter, M., Belting, H.G., 2010. Vascular morphogenesis in the zebrafish embryo. Dev. Biol. 341, 56–65.

Engelhardt, B., Liebner, S., 2014. Novel insights into the development and maintenance of the blood-brain barrier. Cell Tissue Res. 355, 687–699.

Ericson, J., Rashbass, P., Schedl, A., Brenner-Morton, S., Kawakami, A., Van Heyningen, V., Jessell, T.M., Briscoe, J., 1997. Pax6 controls progenitor cell identity and neuronal fate in response to graded Shh signaling. Cell 90, 169–180.

Essner, J.J., Breuer, J.J., Essner, R.D., Fahrenkrug, S.C., Hackett, P.B., 1997. The zebrafish thyroid hormone receptor alpha 1 is expressed during early embryogenesis and can function in transcriptional repression. Differentiation. 62, 107–117.

Everaert, C., Luypaert, M., Maag, J.L.V., Cheng, Q.X., DInger, M.E., Hellemans, J., Mestdagh, P., 2017. Benchmarking of RNA-sequencing analysis workflows using whole-transcriptome RT-qPCR expression data. Sci. Rep. 7, 1–11.

Fanibunda, S.E., Desouza, L.A., Kapoor, R., Vaidya, R.A., Vaidya, V.A., 2018. Thyroid Hormone Regulation of Adult Neurogenesis, 1st ed, Vitamins and Hormones. Elsevier Inc.

Fantin, A., Lampropoulou, A., Gestri, G., Raimondi, C., Senatore, V., Zachary, I., Ruhrberg, C., 2015. Erratum to NRP1 Regulates CDC42 Activation to Promote Filopodia Formation in Endothelial Tip Cells [Cell Reports 11 (2015) 1577-1590]. Cell Rep. 13, 2037.

Fantin, A., Vieira, J.M., Gestri, G., Denti, L., Schwarz, Q., Prykhozhij, S., Peri, F., Wilson, S.W., Ruhrberg, C., 2010. Tissue macrophages act as cellular chaperones for vascular anastomosis downstream of VEGF-mediated endothelial tip cell induction. Blood 116, 829–840.

Farkas, E., De Jong, G.I., De Vos, R.A.I., Jansen Steur, E.N.H., Luiten, P.G.M., 2000. Pathological features of cerebral cortical capillaries are doubled in Alzheimer's disease and Parkinson's disease. Acta Neuropathol. 100, 395–402.

Feijóo, C.G., Saldias, M.P., De la Paz, J.F., Gómez-Skarmeta, J.L., Allende, M.L., 2009. Formation of posterior cranial placode derivatives requires the Iroquois transcription factor irx4a. Mol. Cell. Neurosci. 40, 328–337.

Fekete, C., Lechan, R.M., 2014. Central regulation of hypothalamic-pituitary-thyroid axis under physiological and pathophysiological conditions. Endocr. Rev. 35, 159–194.

Ferrara, N., Gerber, H.P., LeCouter, J., 2003. The biology of VEGF and its receptors. Nat. Med. 9, 669–676.

Filosa, J.A., Morrison, H.W., Iddings, J.A., Du, W., Kim, K.J., 2016. Beyond neurovascular coupling, role of astrocytes in the regulation of vascular tone. Neuroscience 323, 96–109.

Fischer, J., Kleinau, G., Müller, A., Kühnen, P., Zwanziger, D., Kinne, A., Rehders, M., Moeller, L.C., Führer, D., Grüters, A., Krude, H., Brix, K., Biebermann, H., 2015. Modulation of monocarboxylate transporter 8 oligomerization by specific pathogenic mutations. J. Mol. Endocrinol. 54, 39–50.

Fisher, D.A., Lehman, H., Lackey, C., 1964. Placental transport of thyroxine. J. Clin. Endocrinol. Metab. 24, 393–400.

Flamant, F., Baxter, J.D., Forrest, D., Refetoff, S., Samuels, H., Scanlan, T.S., Vennström, B., Samarut, J., 2006. International union of pharmacology. LIX. The pharmacology and classification of the nuclear receptor superfamily: Thyroid hormone receptors. Pharmacol. Rev. 58, 705–711.

França, M.M., German, A., Fernandes, G.W., Liao, X.H., Bianco, A.C., Refetoff, S., Dumitrescu, A.M., 2021. Human Type 1 Iodothyronine Deiodinase (DIO1) Mutations Cause Abnormal Thyroid Hormone Metabolism. Thyroid 31, 202–207.

Freeze, W.M., Bacskai, B.J., Frosch, M.P., Jacobs, H.I.L., Backes, W.H., Greenberg, S.M., van Veluw, S.J., 2019. Blood-brain barrier leakage and microvascular lesions in cerebral amyloid angiopathy Whitney. Stroke 50, 328–335.

Friesema, E.C.H., Docter, R., Moerings, E.P.C.M., Verrey, F., Krenning, E.P., Hennemann, G., Visser, T.J., 2001. Thyroid Hormone Transport by the Heterodimeric Human System L Amino Acid Transporter. Endocrinology 142, 4339–4348.

Friesema, E.C.H., Ganguly, S., Abdalla, A., Manning Fox, J.E., Halestrap, A.P., Visser, T.J., 2003. Identification of monocarboxylate transporter 8 as a specific thyroid hormone transporter. J. Biol. Chem. 278, 40128–40135.

Friesema, E.C.H., Grueters, P.A., Biebermann, H., Krude, H., Von Moers, A., Reeser, M., Barrett, T.G., Mancilla, E.E., Svensson, J., Kester, M.H.A., Kuiper, G.G.J.M., Balkassmi, S., Uitterlinden, A.G., Koehrle, P.J., Rodien, P., Halestrap, P.A.P., Visser, P.T.J., 2004. Association between mutations in a thyroid hormone transporter and severe X-linked psychomotor retardation. Lancet 364, 1435–1437.

Friesema, E.C.H., Jansen, J., Jachtenberg, J.W., Visser, W.E., Kester, M.H.A., Visser, T.J., 2008. Effective cellular uptake and efflux of thyroid hormone by human monocarboxylate transporter 10. Mol. Endocrinol. 22, 1357–1369.

Friesema, E.C.H., Jansen, J., Visser, T.J., 2005. Membrane transporters for thyroid hormone. Curr. Opin. Endocrinol. Diabetes 12, 371–380.

Friesema, E.C.H., Kuiper, G.G.J.M., Jansen, J., Visser, T.J., Kester, M.H.A., 2006. Thyroid hormone transport by the human monocarboxylate transporter 8 and its rate-limiting role in intracellular metabolism. Mol. Endocrinol. 20, 2761–2772.

Friesema, E.C.H., Visser, T.J., Borgers, A.J., Kalsbeek, A., Swaab, D.F., Fliers, E., Alkemade, A., 2012. Thyroid hormone transporters and deiodinases in the developing human hypothalamus. Eur. J. Endocrinol. 167, 379–386.

Fujita, M., Cha, Y.R., Pham, V.N., Sakurai, A., Roman, B.L., Gutkind, J.S., Weinstein, B.M., 2011. Assembly and patterning of the vascular network of the vertebrate hindbrain. Development 138, 1705–1715.

Fujiwara, M., Ghazizadeh, M., Kawanami, O., 2006. Potential role of the Slit/Robo signal pathway in angiogenesis. Vasc. Med. 11, 115–121.

Gaengel, K., Genové, G., Armulik, A., Betsholtz, C., 2009. Endothelial-mural cell signaling in vascular development and angiogenesis. Arterioscler. Thromb. Vasc. Biol. 29, 630–638.

Galton, V.A., 2017. The ups and downs of the thyroxine pro-hormone hypothesis. Mol. Cell. Endocrinol. 458, 105–111.

Garbuzova-Davis, S., Hernandez-Ontiveros, D.G., Rodrigues, M.C.O., Haller, E., Frisina-Deyo, A., Mirtyl, S., Sallot, S., Saporta, S., Borlongan, C. V., Sanberg, P.R., 2012. Impaired blood-brain/spinal cord barrier in ALS patients. Brain Res. 1469, 114–128.

Gaspard, N., Vanderhaeghen, P., 2010. Mechanisms of neural specification from embryonic stem cells. Curr. Opin. Neurobiol. 20, 37–43.

Gee, J.R., Keller, J.N., 2005. Astrocytes: Regulation of brain homeostasis via apolipoprotein E. Int. J. Biochem. Cell Biol. 37, 1145–1150.

Gelfand, M. V., Hagan, N., Tata, A., Oh, W.J., Lacoste, B., Kang, K.T., Kopycinska, J., Bischoff, J., Wang, J.H., Gu, C., 2014. Neuropilin-1 functions as a VEGFR2 co-receptor to guide developmental angiogenesis independent of ligand binding. Elife 3, e03720.

Gerdes, A.M., Ojamaa, K., 2016. Thyroid Hormone and Cardioprotection. Compr. Physiol. 6, 1199–1219.

Gereben, B., Zavacki, A.M., Ribich, S., Kim, B.W., Huang, S.A., Simonides, W.S., Zeöld, A., Bianco, A.C., 2008. Cellular and molecular basis of deiodinase-regulated thyroid hormone signaling. Endocr. Rev. 29, 898–938.

Gerhardt, H., Golding, M., Fruttiger, M., Ruhrberg, C., Lundkvist, A., Abramsson, A., Jeltsch, M., Mitchell, C., Alitalo, K., Shima, D., Betsholtz, C., 2003. VEGF guides angiogenic sprouting utilizing endothelial tip cell filopodia. J. Cell Biol. 161, 1163–1177.

Geudens, I., Gerhardt, O., 2011. Coordinating cell behaviour during blood vessel formation. Development 138, 4569–4583.

Ghassabian, A., Steenweg-de Graaff, J., Peeters, R.P., Ross, H.A., Jaddoe, V.W., Hofman, A., Verhulst, F.C., White, T., Tiemeier, H., 2014. Maternal urinary iodine concentration in pregnancy and children's cognition: Results from a population-based birth cohort in an iodine-sufficient area. BMJ Open 4.

Gil-Ibáñez, P., Bernal, J., Morte, B., 2014. Thyroid hormone regulation of gene expression in primary cerebrocortical cells: Role of thyroid hormone receptor subtypes and interactions with retinoic acid and glucocorticoids. PLoS One 9.

Gil-Ibañez, P., García-García, F., Dopazo, J., Bernal, J., Morte, B., 2015. Global Transcriptome Analysis of Primary Cerebrocortical Cells: Identification of Genes Regulated by Triiodothyronine in Specific Cell Types. Cereb. Cortex 8, bhv273.

Gilland, E., Baker, R., 2005. Evolutionary patterns of cranial nerve efferent nuclei in vertebrates. Brain. Behav. Evol. 66, 234–254.

Gleiser, C., Wagner, A., Fallier-Becker, P., Wolburg, H., Hirt, B., Mack, A.F., 2016. Aquaporin-4 in astroglial cells in the CNS and supporting cells of sensory organs-A comparative perspective. Int. J. Mol. Sci. 17.

Gore, A. V., Monzo, K., Cha, Y.R., Pan, W., Weinstein, B.M., 2012. Vascular Development in the Zebrafish. Cold Spring Harb. Perspect. Med. 2, a006684–a006684.

Gore, A. V., Swift, M.R., Cha, Y.R., Lo, B., McKinney, M.C., Li, W., Castranova, D., Davis, A., Yoh-suke, M., Weinstein, B.M., 2011. Rspo1/wnt signaling promotes angiogenesis via vegfc/vegfr3. Development 138, 4875–4886.

Gorlewicz, A., Krawczyk, K., Szczepankiewicz, A.A., Trzaskoma, P., Mulle, C., Wilczynski, G.M., 2020. Colocalization Colormap -an ImageJ Plugin for the Quantification and Visualization of Colocalized Signals. Neuroinformatics 18, 661–664.

Gothié, J.D., Vancamp, P., Demeneix, B., Remaud, S., 2020. Thyroid hormone regulation of neural stem cell fate: From development to ageing. Acta Physiol. 228, 1–24.

Götz, M., Huttner, W.B., 2005. The cell biology of neurogenesis. Nat. Rev. Mol. Cell Biol. 6, 777–788.

Gouti, M., Metzis, V., Briscoe, J., 2015. The route to spinal cord cell types: A tale of signals and switches. Trends Genet. 31, 282–289.

Gridley, T., 2010. Notch signaling in the vasculature. Curr. Top. Dev. Biol. 92, 277–309.

Griffiths, J.A., Scialdone, A., Marioni, J.C., 2018. Using single-cell genomics to understand developmental processes and cell fate decisions. Mol. Syst. Biol. 14, e8046.

Grijota-Martínez, C., Montero-Pedrazuela, A., Hidalgo-Álvarez, J., Bárez-López, S., Guadaño-Ferraz, A., 2023. Intracerebroventricular High Doses of 3,3′,5-Triiodothyroacetic Acid at Juvenile Stages Improve Peripheral Hyperthyroidism and Mediate Thyromimetic Effects in Limited Brain Regions in a Mouse Model of Monocarboxylate Transporter 8 Deficiency. https://home.liebertpub.com/thy 33, 501–510.

Groeneweg, S., Peeter, R.P., Moran, C., Stoupa, A., Auriol, F., Tonduti, D., Dica, A., Paone, L., 2019. Effectiveness and safety of Triac in children and adults with MCT8 deficiency : an international, multicentre, single group, open-label, phase 2 trial. Lancet Diabetes Endocrinol. 7, 695–706.

Groeneweg, S., Van Geest, F.S., Peeters, R.P., Heuer, H., Visser, W.E., 2020. Thyroid Hormone Transporters. Endocr. Rev.

Grupp, L., Wolburg, H., Mack, A.F., 2010. Astroglial structures in the zebrafish brain. J. Comp. Neurol. 518, 4277–4287.

Guadaño-Ferraz, A., Obregón, M.J., St. Germain, D.L., Bernal, J., 1997. The type 2 iodothyronine deiodinase is expressed primarily in glial cells in the neonatal rat brain. Proc. Natl. Acad. Sci. U. S. A. 94, 10391–10396.

Guénet, J.L., 2005. The mouse genome. Genome Res. 15, 1729–1740.

Gumieniak, O., Perlstein, T.S., Williams, J.S., Hopkins, P.N., Brown, N.J., Raby, B.A., Williams, G.H., 2007. Ala92 type 2 deiodinase allele increases risk for the development of hypertension. Hypertension 49, 461–466.

Guo, C., Chen, X., Song, H., Maynard, M.A., Zhou, Y., Lobanov, A. V., Gladyshev, V.N., Ganis, J.J., Wiley, D., Jugo, R.H., Lee, N.Y., Castroneves, L.A., Zon, L.I., Scanlan, T.S., Feldman, H.A., Huang, S.A., 2014. Intrinsic expression of a multiexon type 3 deiodinase gene controls zebrafish embryo size. Endocrinol. (United States) 155, 4069–4080.

Gurung, S., Restrepo, N.K., Chestnut, B., Klimkaite, L., 2022. Single - cell transcriptomic analysis of vascular endothelial cells in zebrafish embryos. Sci. Rep. 12, 1–13.

Hagan, N., Ben-Zvi, A., 2015. The molecular, cellular, and morphological components of

blood-brain barrier development during embryogenesis. Semin. Cell Dev. Biol. 38, 7–15.

Hagenbuch, B., Dawson, P., 2004. The sodium bile salt cotransport family SLC10. Pflugers Arch. Eur. J. Physiol. 447, 566–570.

Haigh, J.J., Morelli, P.I., Gerhardt, H., Haigh, K., Tsien, J., Damert, A., Miquerol, L., Muhlner, U., Klein, R., Ferrara, N., Wagner, E.F., Betsholtz, C., Nagy, A., 2003. Cortical and retinal defects caused by dosage-dependent reductions in VEGF-A paracrine signaling. Dev. Biol. 262, 225–241.

Hall, T., 2011. BioEdit: An important software for molecular biology. GERF Bull. Biosci. 2, 60–61.

Hallmann, R., Horn, N., Selg, M., Wendler, O., Pausch, F., Sorokin, L.M., 2005. Expression and function of laminins in the embryonic and mature vasculature. Physiol. Rev. 85, 979–1000.

Hardwick, L.J.A., Ali, F.R., Azzarelli, R., Philpott, A., 2015. Cell cycle regulation of proliferation versus differentiation in the central nervous system. Cell Tissue Res. 359, 187–200.

Häring, M., Zeisel, A., Hochgerner, H., Rinwa, P., Jakobsson, J.E.T., Lönnerberg, P., La Manno, G., Sharma, N., Borgius, L., Kiehn, O., Lagerström, M.C., Linnarsson, S., Ernfors, P., 2018. Neuronal atlas of the dorsal horn defines its architecture and links sensory input to transcriptional cell types. Nat. Neurosci. 21, 869–880.

Harrington, M.J., Hong, E., Brewster, R., 2009. Comparative analysis of neurulation: First impressions do not count. Mol. Reprod. Dev. 76, 954–965.

Harvey, C.B., Williams, G.R., 2002. Mechanism of thyroid hormone action. Thyroid 12, 441–6.

Heijlen, M., Houbrechts, A.M., Bagci, E., Van Herck, S.L.J., Kersseboom, S., Esguerra, C. V., Blust, R., Visser, T.J., Knapen, D., Darras, V.M., 2014. Knockdown of type 3 iodothyronine deiodinase severely perturbs both embryonic and early larval development in zebrafish. Endocrinology 155, 1547–1559.

Heijlen, M., Houbrechts, A.M., Darras, V.M., 2013. Zebrafish as a model to study peripheral thyroid hormone metabolism in vertebrate development. Gen. Comp. Endocrinol. 188, 289–296.

Hellström, M., Gerhardt, H., Kalén, M., Li, X., Eriksson, U., Wolburg, H., Betsholtz, C., 2001. Lack of pericytes leads to endothelial hyperplasia and abnormal vascular morphogenesis. J. Cell Biol. 152, 543–553.

Hellström, M., Phng, L.K., Hofmann, J.J., Wallgard, E., Coultas, L., Lindblom, P., Alva, J., Nilsson, A.K., Karlsson, L., Gaiano, N., Yoon, K., Rossant, J., Iruela-Arispe, M.L., Kalén, M., Gerhardt, H., Betsholtz, C., 2007. Dll4 signalling through Notch1 regulates formation of tip cells during angiogenesis. Nature 445, 776–780.

Hennemann, G., Docter, R., Friesema, E.C.H., Jong, M. DE, Krenning, E.P., Visser, T.J., 2001. Plasma membrane transport of thyroid hormones and its role in thyroid hormone metabolism and bioavailability. Endocr. Rev. 22, 451–476.

Herbert, S.P., Stainier, D.Y.R., 2011. Molecular control of endothelial cell behaviour during

blood vessel morphogenesis. Nat. Rev. Mol. Cell Biol. 12, 551–564.

Hernandez-Miranda, L.R., Müller, T., Birchmeier, C., 2017. The dorsal spinal cord and hindbrain: From developmental mechanisms to functional circuits. Dev. Biol. 432, 34–42.

Heuer, H., 2007. The importance of thyroid hormone transporters for brain development and function. Best Pract. Res. Clin. Endocrinol. Metab. 21, 265–276.

Hill, R.E., Favor, J., Hogan, B.L.M., Ton, C.C.T., Saunders, G.F., Hanson, I.M., Prosser, J., Jordan, T., Hastie, N.D., van Heyningen, V., 1991. Mouse small eye results from mutations in a paired-like homeobox-containing gene. Nature 354, 522–525.

Himmels, P., Paredes, I., Adler, H., Karakatsani, A., Luck, R., Marti, H.H., Ermakova, O., Rempel, E., Stoeckli, E.T., Ruiz De Almodóvar, C., 2017. Motor neurons control blood vessel patterning in the developing spinal cord. Nat. Commun. 8, 1–16.

Hogan, B.M., Schulte-Merker, S., 2017. How to Plumb a Pisces: Understanding Vascular Development and Disease Using Zebrafish Embryos. Dev. Cell 42, 567–583.

Hogan, K.A., Ambler, C.A., Chapman, D.L., Bautch, V.L., 2004. The neural tube patterns vessels developmentally using the VEGF signaling pathway. Development 131, 1503–1513.

Homem, C.C.F., Repic, M., Knoblich, J.A., 2015. Proliferation control in neural stem and progenitor cells. Nat. Rev. Neurosci. 16, 647–659.

Hübner, K., Cabochette, P., Diéguez-Hurtado, R., Wiesner, C., Wakayama, Y., Grassme, K.S., Hubert, M., Guenther, S., Belting, H.G., Affolter, M., Adams, R.H., Vanhollebeke, B., Herzog, W., 2018. Wnt/β-catenin signaling regulates VE-cadherin-mediated anastomosis of brain capillaries by counteracting S1pr1 signaling. Nat. Commun. 9.

Iadecola, C., 2017. The Neurovascular Unit Coming of Age: A Journey through Neurovascular Coupling in Health and Disease. Neuron 96, 17–42.

Ikenaga, T., Urban, J.M., Gebhart, N., Hatta, K., Kawakami, K., Ono, F., 2011. Formation of the spinal network in zebrafish determined by doman-specific Pax genes. J. Comp. Neurol. 519, 1562–1579.

Ishikawa, Y., Yamamoto, N., Yoshimoto, M., Ito, H., 2012. The primary brain vesicles revisited: Are the three primary vesicles (forebrain/midbrain/hindbrain) universal in vertebrates? Brain. Behav. Evol. 79, 75–83.

Isogai, S., Horiguchi, M., Weinstein, B.M., 2001. The vascular anatomy of the developing zebrafish: An atlas of embryonic and early larval development. Dev. Biol. 230, 278–301.

Jain, R.K., 2003. Molecular regulation of vessel maturation. Nat. Med. 9, 685–693.

James, J.M., Gewolb, C., Bautch, V.L., 2009. Neurovascular development uses VEGF-A signaling to regulate blood vessel ingression into the neural tube. Development 136, 833–841.

James, J.M., Mukouyama, Y. suke, 2011. Neuronal action on the developing blood vessel pattern. Semin. Cell Dev. Biol. 22, 1019–1027.

Janesick, A., Wu, S.C., Blumberg, B., 2015. Retinoic acid signaling and neuronal differentiation. Cell. Mol. Life Sci. 72, 1559–1576.

Jauniaux, E., Gulbis, B., 2000. Fluid compartments of the embryonic environment. Hum. Reprod. Update 6, 268–278.

Jeong, J.Y., Kwon, H.B., Ahn, J.C., Kang, D., Kwon, S.H., Park, J.A., Kim, K.W., 2008. Functional and developmental analysis of the blood-brain barrier in zebrafish. Brain Res. Bull. 75, 619–628.

Jho, S.H., Vouthounis, C., Lee, B., Stojadinovic, O., Im, M.J., Brem, H., Merchant, A., Chau, K., Tomic-Canic, M., 2005. The book of opposites: The role of the nuclear receptor co-regulators in the suppression of epidermal genes by retinoic acid and thyroid hormone receptors. J. Invest. Dermatol. 124, 1034–1043.

Jia, P.P., Ma, Y.B., Lu, C.J., Mirza, Z., Zhang, W., Jia, Y.F., Li, W.G., Pei, D.S., 2016. The effects of disturbance on Hypothalamus-Pituitary-Thyroid (HPT) axis in zebrafish larvae after exposure to DEHP. PLoS One 11, 1–11.

Jin, D., Zhu, D., Fang, Y., Chen, Y., Yu, G., Pan, W., Liu, D., Li, F., Zhong, T.P., 2017. Vegfa signaling regulates diverse artery / vein formation in vertebrate vasculatures. J. Genet. Genomics 44, 483–492.

Jin, S., Hansson, E.M., Tikka, S., Lanner, F., Sahlgren, C., Farnebo, F., Baumann, M., Kalimo, H., Lendahl, U., 2008. Notch signaling regulates platelet-derived growth factor receptor-β expression in vascular smooth muscle cells. Circ. Res. 102, 1483–1491.

Johnson, K., Barragan, J., Bashiruddin, S., Smith, C.J., Tyrrell, C., Parsons, M.J., Doris, R., Kucenas, S., Downes, G.B., Velez, C.M., Schneider, C., Sakai, C., Pathak, N., Anderson, K., Stein, R., Devoto, S.H., Mumm, J.S., Barresi, M.J.F., 2016. Gfap-Positive Radial Glial Cells Are an Essential Progenitor Population for Later-Born Neurons and Glia in the Zebrafish Spinal Cord. Glia 64, 1170–1189.

Jones, H.C., Keep, R.F., Butt, A.M., 1998. The development of ion regulation at the blood-brain barrier. Prog. Brain Res. 91, 123–131.

Joutel, A., Haddad, I., Ratelade, J., Nelson, M.T., 2016. Perturbations of the cerebrovascular matrisome: A convergent mechanism in small vessel disease of the brain? J. Cereb. Blood Flow Metab. 36, 143–157.

Karapanou, O., Papadimitriou, A., 2011. Thyroid hormone transporters in the human. Hormones 10, 270–279.

Kawakami, K., Abe, G., Asada, T., Asakawa, K., Fukuda, R., Ito, A., Lal, P., Mouri, N., Muto, A., Suster, M.L., Takakubo, H., Urasaki, A., Wada, H., Yoshida, M., 2010. ZTrap: Zebrafish gene trap and enhancer trap database. BMC Dev. Biol. 10, 105.

Kendall, E.C., 1919. Iodine Compound in Thyroid. J. Biol. Chem. 40, 265–334.

Kersseboom, S., Horn, S., Edward Visser, W., Chen, J., Friesema, E.C.H., Vaurs-Barrière, C., Peeters, R.P., Heuer, H., Visser, T.J., 2014. In vitro and mouse studies supporting therapeutic utility of triiodothyroacetic acid in MCT8 deficiency. Mol. Endocrinol. 28, 1961–1970.

Kim, C.H., Ueshima, E., Muraoka, O., Tanaka, H., Yeo, S.Y., Huh, T.L., Miki, N., 1996. Zebrafish elav/HuC homologue as a very early neuronal marker. Neurosci. Lett. 216, 109–112.

Kimmel, C.B., Ballard, W.W., Kimmel, S.R., Ullmann, B., Schilling, T.F., 1995. Stages of

embryonic development of the zebrafish. Dev. Dyn. 203, 253–310.

Kimmel, C.B., Kane, D.A., Walker, C., Warga, R.M., Rothman, M.B., 1989. A mutation that changes cell movement and cell fate in the zebrafish embryo. Nature.

Kintner, C., Hemmati-Brivanlou, A., 2013. Neural Induction Embryonic Stem Cells, Patterning and Cell Type Specification in the Developing CNS and PNS. Elsevier Inc.

Kintner, C., Koyano-Nakagawa, N., 2013. Neurogenesis in the Vertebrate Embryo, Second Edi. ed, Handbook of Stem Cells. Elsevier Inc.

Klann, M., Seaver, E.C., 2019. Functional role of pax6 during eye and nervous system development in the annelid Capitella teleta. Dev. Biol. 456, 86–103.

Kleinau, G., Schweizer, U., Kinne, A., Köhrle, J., Grüters, A., Krude, H., Biebermann, H., 2011. Insights into molecular properties of the human monocarboxylate transporter 8 by combining functional with structural information. Thyroid Res. 4, S4.

Kleinjan, D.A., Bancewicz, R.M., Gautier, P., Dahm, R., Schonthaler, H.B., Damante, G., Seawright, A., Hever, A.M., Yeyati, P.L., Van Heyningen, V., Coutinho, P., 2008. Subfunctionalization of duplicated zebrafish pax6 genes by cis-regulatory divergence. PLoS Genet. 4, 1–14.

Knox, E.G., Aburto, M.R., Clarke, G., Cryan, J.F., O'Driscoll, C.M., 2022. The blood-brain barrier in aging and neurodegeneration. Mol. Psychiatry 27, 2659–2673.

Koch, S., Claesson-Welsh, L., 2012. Signal transduction by vascular endothelial growth factor receptors. Cold Spring Harb Perspect Med. July, 1–21.

Kolte, D., McClung, J.A., Aronow, W.S., 2016. Vasculogenesis and Angiogenesis, Translational Research in Coronary Artery Disease: Pathophysiology to Treatment. Elsevier Inc.

Kooij, G., Van Horssen, J., De Vries, E., 2005. Tight junctions of the blood-brain barrier. Blood-Brain Barrier its Microenviron. Basic Physiol. to Neurol. Dis. 38, 47–69.

Korn, J., Christ, B., Kurz, H., 2002. Neuroectodermal origin of brain pericytes and vascular smooth muscle cells. J. Comp. Neurol. 442, 78–88.

Krumlauf, R., Wilkinson, D.G., 2022. Segmentation and patterning of the vertebrate hindbrain. Development 148, 1–38.

Kurz, H., 2009. Cell lineages and early patterns of embryonic CNS vascularization. Cell Adhes. Migr. 3, 205–210.

Lacomme, M., Medevielle, F., Bourbon, H.M., Thierion, E., Kleinjan, D.J., Roussat, M., Pituello, F., Bel-Vialar, S., 2018. A long range distal enhancer controls temporal fine-tuning of PAX6 expression in neuronal precursors. Dev. Biol. 436, 94–107.

Lacoste, B., Comin, C.H., Ben-zvi, A., Kaeser, P.S., Xu, X., Costa, L.F., Gu, C., 2014. Sensory-related eural activity regulates the structure of vascular networks in the cerbral cortex. Neuron 83, 1117–1130.

LaFranchi, S.H., Austin, J., 2007. How should we be treating children with congenital hypothyroidism? J. Pediatr. Endocrinol. Metab. 20, 559–578.

Lafrenière, R.G., Carrel, L., Willard, H.F., 1994. A novel transmembrane transporter encoded by the XPCT gene in Xq13.2, Human Molecular Genetics.

Landers, K., Richard, K., 2017. Traversing barriers – How thyroid hormones pass placental, blood-brain and blood-cerebrospinal fluid barriers. Mol. Cell. Endocrinol. 458, 22–28.

Lange, C., Turrero Garcia, M., Decimo, I., Bifari, F., Eelen, G., Quaegebeur, A., Boon, R., Zhao, H., Boeckx, B., Chang, J., Wu, C., Le Noble, F., Lambrechts, D., Dewerchin, M., Kuo, C.J., Huttner, W.B., Carmeliet, P., 2016. Relief of hypoxia by angiogenesis promotes neural stem cell differentiation by targeting glycolysis. EMBO J. 35, 924–941.

Lange, M., Ohnesorge, N., Hoffmann, D., Rocha, S.F., Benedito, R., Siekmann, A.F., 2022. Zebrafish mutants in vegfab can affect endothelial cell proliferation without altering ERK phosphorylation and are phenocopied by loss of PI3K signaling. Dev. Biol. 486, 26–43.

Langmead, B., Salzberg, S.L., 2012. Fast gapped-read alignment with Bowtie 2. Nat. Methods 9, 357–359.

Lara-Ramirez, R., Peŕez-Gonzaĺez, C., Anselmi, C., Patthey, C., Shimeld, S.M., 2019. A notch-regulated proliferative stem cell zone in the developing spinal cord is an ancestral vertebrate trait. Dev. 146.

Larrivée, B., Freitas, C., Suchting, S., Brunet, I., Eichmann, A., 2009. Guidance of vascular development: Lessons from the nervous system. Circ. Res. 104, 428–441.

Lavado-Autric, R., Ausó, E., García-Velasco, J.V., del Carmen Arufe, M., Escobar del Rey, F., Berbel, P., Morreale de Escobar, G., 2003. Early maternal hypothyroxinemia alters histogenesis and cerebral cortex cytoarchitecture of the progeny. J. Clin. Invest. 111, 1073–1082.

Lawson, N.D., Weinstein, B.M., 2002. In vivo imaging of embryonic vascular development using transgenic zebrafish. Dev Biol 248, 307–318.

Lazar, M.A., Berrodin, T.J., Harding, H.P., 1991. Differential DNA binding by monomeric, homodimeric, and potentially heteromeric forms of the thyroid hormone receptor. Mol. Cell. Biol. 11, 5005–5015.

Le Dréau, G., Martí, E., 2012. Dorsal-ventral patterning of the neural tube: A tale of three signals. Dev. Neurobiol. 72, 1471–1481.

Lee, S., Chen, T.T., Barber, C.L., Jordan, M.C., Murdock, J., Desai, S., Ferrara, N., Nagy, A., Roos, K.P., Iruela-arispe, M.L., 2007. Autocrine VEGF Signaling Is Required for Vascular Homeostasis. Cell 130, 691–703.

Lee, S., Privalsky, M.L., 2005. Heterodimers of retinoic acid receptor and thyroid hormone receptors display unique combinatorial regulatory properties. Mol. Endocrinol. 19, 863–878.

Lee, S.W., Kim, W.J., Choi, Y.K., Song, H.S., Son, M.J., Gelman, I.H., Kim, Y.J., Kim, K.W., 2003. SSeCKS regulates angiogenesis and tight junction formation in blood-brain barrier. Nat. Med. 9, 900–906.

Lesaffre, B., Joliot, A., Prochiantz, A., Volovitch, M., 2007. Direct non-cell autonomous Pax6 activity regulates eye development in the zebrafish. Neural Dev. 2.

Leslie, J.D., Ariza-McNaughton, L., Bermange, A.L., McAdow, R., Johnson, S.L., Lewis, J.,

2007. Endothelial signalling by the Notch ligand Delta-like 4 restricts angiogenesis. Development 134, 839–844.

Li, X., Han, H., Hou, R., Wei, L., Wang, G., Li, C., Li, D., 2013. Progesterone treatment before experimental hypoxia-ischemia enhances the expression of glucose transporter proteins GLUT1 and GLUT3 in neonatal rats. Neurosci. Bull. 29, 287–294.

Li, Yuanbin, Shan, Z., Teng, W., Yu, X., Li, Yushu, Fan, C., Teng, X., Guo, R., Wang, H., Li, J., Chen, Y., Wang, W., Chawinga, M., Zhang, L., Yang, L., Zhao, Y., Hua, T., 2010. Abnormalities of maternal thyroid function during pregnancy affect neuropsychological development of their children at 25 – 30 months. Clin. Endocrinol. (Oxf). 72, 825–829.

Liang, D., Chang, J.R., Chin, A.J., Smith, A., Kelly, C., Weinberg, E.S., Ge, R., 2001. The role of vascular endothelial growth factor (VEGF) in vasculogenesis, angiogenesis, and hematopoiesis in zebrafish development. Mech. Dev. 108, 29–43.

Liang, D., Xu, X., Chin, A.J., Balasubramaniyan, N. V., Teo, M.A.L., Lam, T.J., Weinberg, E.S., Ge, R., 1998. Cloning and characterization of vascular endothelial growth factor (VEGF) from zebrafish, Danio rerio. Biochim. Biophys. Acta - Gene Struct. Expr. 1397, 14–20.

Liebner, S., Corada, M., Bangsow, T., Babbage, J., Taddei, A., Czupalla, C.J., Reis, M., Felici, A., Wolburg, H., Fruttiger, M., Taketo, M.M., Von Melchner, H., Plate, K.H., Gerhardt, H., Dejana, E., 2008. Wnt/β-catenin signaling controls development of the blood - brain barrier. J. Cell Biol. 183, 409–417.

Liebner, S., Plate, K., 2010. Differentiation of the brain vasculature: The answer came blowing by the Wnt. J. Angiogenes. Res. 2, 1–10.

Lieschke, G.J., Currie, P.D., 2007. Animal models of human disease: Zebrafish swim into view. Nat. Rev. Genet. 8, 353–367.

Lindblom, P., Gerhardt, H., Liebner, S., Abramsson, A., Enge, M., Hellström, M., Bäckström, G., Fredriksson, S., Landegren, U., Nyström, H.C., Bergström, G., Dejana, E., Östman, A., Lindahl, P., Betsholtz, C., 2003. Endothelial PDGF-B retention is required for proper investment of pericytes in the microvessel wall. Genes Dev. 17, 1835–1840.

Liu, X., Zheng, N., Shi, Y.N., Yuan, J., Li, L., 2014. Thyroid hormone induced angiogenesis through the integrin avb3/protein kinase D/histone deacetylase 5 signaling pathway. J. Mol. Endocrinol. 52, 245–254.

Liu, Y., Wada, R., Yamashita, T., Mi, Y., Deng, C.X., Hobson, J.P., Rosenfeldt, H.M., Nava, V.E., Chae, S.S., Lee, M.J., Liu, C.H., Hla, T., Spiegel, S., Proia, R.L., 2000. Edg-1, the G protein-coupled receptor for sphingosine-1-phosphate, is essential for vascular maturation. J. Clin. Invest. 106, 951–961.

Liu, Y.W., Chan, W.K., 2002. Thyroid hormones are important for embryonic to larval transitory phase in zebrafish. Differentiation 70, 36–45.

Logan, C.Y., Nusse, R., 2004. The Wnt signaling pathway in development and disease. Annu. Rev. Cell Dev. Biol. 20, 781–810.

Lohela, M., Bry, M., Tammela, T., Alitalo, K., 2009. VEGFs and receptors involved in angiogenesis versus lymphangiogenesis. Curr. Opin. Cell Biol. 21, 154–165.

López-Espíndola, D., García-Aldea, Á., Gómez de la Riva, I., Rodríguez-García, A.M., Salvatore, D., Visser, T.J., Bernal, J., Guadaño-Ferraz, A., 2019. Thyroid hormone availability in the human fetal brain: novel entry pathways and role of radial glia. Brain Struct. Funct. 224, 2103–2119.

López-Espíndola, D., Morales-Bastos, C., Grijota-Martínez, C., Liao, X.H., Lev, D., Sugo, E., Verge, C.F., Refetoff, S., Bernal, J., Guadaño-Ferraz, A., 2014. Mutations of the thyroid hormone transporter MCT8 cause prenatal brain damage and persistent hypomyelination. J. Clin. Endocrinol. Metab. 99, E2799–E2804.

López-Muñoz, E., Mateos-Sánchez, L., Mejía-Terrazas, G.E., Bedwell-Cordero, S.E., 2019. Hypothyroidism and isolated hypothyroxinemia in pregnancy, from physiology to the clinic. Taiwan. J. Obstet. Gynecol. 58, 757–763.

Lowery, L.A., Sive, H., 2004. Strategies of vertebrate neurulation and a re-evaluation of teleost neural tube formation. Mech. Dev. 121, 1189–1197.

Lu, P., Takai, K., Weaver, V.M., Werb, Z., 2011. Extracellular Matrix degradation and remodeling in development and disease. Cold Spring Harb. Perspect. Biol. 3, 1–24.

Luidens, M.K., Mousa, S.A., Davis, F.B., Lin, H.Y., Davis, P.J., 2010. Thyroid hormone and angiogenesis. Vascul. Pharmacol. 52, 142–145.

Lumsden, A., 1990. The cellular basis of segmentation in the developing hindbrain. Trends Neurosci. 13, 329–335.

Luongo, C., Dentice, M., Salvatore, D., 2019. Deiodinases and their intricate role in thyroid hormone homeostasis. Nat. Rev. Endocrinol.

Ma, L.H., Gilland, E., Bass, A.H., Baker, R., 2010. Ancestry of motor innervation to pectoral fin and forelimb. Nat. Commun. 1, 1–8.

Ma, L.H., Punnamoottil, B., Rinkwitz, S., Baker, R., 2009. Mosaic hoxb4a neuronal pleiotropism in zebrafish caudal hindbrain. PLoS One 4.

Ma, S., Kwon, H.J., Johng, H., Zang, K., Huang, Z., 2013. Radial Glial Neural Progenitors Regulate Nascent Brain Vascular Network Stabilization Via Inhibition of Wnt Signaling. PLoS Biol. 11.

Machado, D.S., Sabet, A., Santiago, L.A., Sidhaye, A.R., Chiamolera, M.I., Ortiga-Carvalho, T.M., Wondisford, F.E., 2009. A thyroid hormone receptor mutation that dissociates thyroid hormone regulation of gene expression in vivo. Proc. Natl. Acad. Sci. U. S. A. 106, 9441–9446.

Maia, A.L., Kim, B.W., Huang, S.A., Harney, J.W., Larsen, P.R., 2005. Type 2 iodothyronine deiodinase is the major source of plasma T3 in euthyroid humans. J. Clin. Invest. 115, 2524–2533.

Malaeb, S.N., Cohen, S.S., Virgintino, D., Stonestreet, B.S., 2012. Core concepts: Development of the blood-brain barrier. Neoreviews 13, e241–e250.

Mancuso, M.R., Kuhnert, F., Kuo, C.J., 2008. Developmental angiogenesis of the central nervous system. Lymphat. Res. Biol. 6, 173–180.

Marchand, O., Safi, R., Escriva, H., Van Rompaey, E., Prunet, P., Laudet, V., 2001. Molecular

cloning and characterization of thyroid hormone receptors in teleost fish. J. Mol. Endocrinol. 26, 51–65.

Marelli, F., Carra, S., Agostini, M., Cotelli, F., Peeters, R., Chatterjee, K., Persani, L., 2016. Patterns of thyroid hormone receptor expression in zebrafish and generation of a novel model of resistance to thyroid hormone action. Mol. Cell. Endocrinol. 424, 102–117.

Marelli, F., Carra, S., Rurale, G., Cotelli, F., Persani, L., 2017. *In vivo* Functional Consequences of Human *THRA* Variants Expressed in the Zebrafish, Thyroid.

Marsili, A., Zavacki, A.M., Harney, J.W., Larsen, P.R., 2011. Physiological role and regulation of iodothyronine deiodinases: A 2011 update. J. Endocrinol. Invest. 34, 395–407.

Martino, M.M., Brkic, S., Bovo, E., Burger, M., Schaefer, D.J., Wolff, T., Gürke, L., Briquez, P.S., Larsson, H.M., Gianni-Barrera, R., Hubbell, J.A., Banfi, A., 2015. Extracellular matrix and growth factor engineering for controlled angiogenesis in regenerative medicine. Front. Bioeng. Biotechnol. 3, 1–8.

Martins, L.F., Brambilla, I., Motta, A., de Pretis, S., Bhat, G.P., Badaloni, A., Malpighi, C., Amin, N.D., Imai, F., Almeida, R.D., Yoshida, Y., Pfaff, S.L., Bonanomi, D., 2022. Motor neurons use push-pull signals to direct vascular remodeling critical for their connectivity. Neuron 110, 4090-4107.e11.

Masnada, S., Sarret, C., Antonello, C.E., Fadilah, A., Krude, H., Mura, E., Mordekar, S., Nicita, F., Olivotto, S., Orcesi, S., Porta, F., Remerand, G., Siri, B., Wilpert, N.M., Amir-Yazdani, P., Bertini, E., Schuelke, M., Bernard, G., Boespflug-Tanguy, O., Tonduti, D., 2022. Movement disorders in MCT8 deficiency/Allan-Herndon-Dudley Syndrome. Mol. Genet. Metab. 135, 109–113.

Mathiisen, T.M., Lehre, K.P., Danbolt, N.C., Ottersen, O.P., 2010. The perivascular astroglial sheath provides a complete covering of the brain microvessels: An electron microscopic 3D reconstruction. Glia 58, 1094–1103.

Matsuoka, R.L., Marass, M., Avdesh, A., Helker, C.S.M., Maischein, H.M., Grosse, A.S., Kaur, H., Lawson, N.D., Herzog, W., Stainier, D.Y.R., 2016. Radial glia regulate vascular patterning around the developing spinal cord. Elife 5, 1–24.

Matsuoka, R.L., Rossi, A., Stone, O.A., Stainier, D.Y.R., 2017. CNS-resident progenitors direct the vascularization of neighboring tissues. Proc. Natl. Acad. Sci. U. S. A. 114, 10137–10142.

Mayerl, S., Müller, J., Bauer, R., Richert, S., Kassmann, C.M., Darras, V.M., Buder, K., Boelen, A., Visser, T.J., Heuer, H., 2014. Transporters MCT8 and OATP1C1 maintain murine brain thyroid hormone homeostasis. J. Clin. Invest. 124, 1987–1999.

McConnell, H.L., Kersch, C.N., Woltjer, R.L., Neuwelt, E.A., 2017. The translational significance of the neurovascular unit. J. Biol. Chem. 292, 762–770.

Mellitzer, G., Xu, Q., Wilkinson, D.G., 1999. Eph receptors and ephrins restrict cell intermingling and communication. Nature 400, 77–81.

Mellström, B., Naranjo, J.R., Santos, A., Gonzalez, A.M., Bernal, J., 1991. Independent expression of the α and β c-erba genes in developing rat brain. Mol. Endocrinol. 5, 1339–1350.

Mendelsohn, A.I., Dasen, J.S., Jessell, T.M., 2017. Divergent Hox Coding and Evasion of

Retinoid Signaling Specifies Motor Neurons Innervating Digit Muscles. Neuron 93, 792-805.e4.

Mendelson, K., Zygmunt, T., Torres-Vázquez, J., Evans, T., Hla, T., 2013. Sphingosine 1-phosphate receptor signaling regulates proper embryonic vascular patterning. J. Biol. Chem. 288, 2143–2156.

Mendes-De-Aguiar, C.B.N., Costa-Silva, B., Alvarez-Silva, M., Tasca, C.I., Trentin, A.G., 2008. Thyroid hormone mediates syndecan expression in rat neonatal cerebellum. Cell. Mol. Neurobiol. 28, 795–801.

Moens, C.B., Prince, V.E., 2002. Constructing the hindbrain: Insights from the zebrafish. Dev. Dyn. 224, 1–17.

Mohan, V., Sinha, R.A., Pathak, A., Rastogi, L., Kumar, P., Pal, A., Godbole, M.M., 2012. Maternal thyroid hormone deficiency affects the fetal neocorticogenesis by reducing the proliferating pool, rate of neurogenesis and indirect neurogenesis. Exp. Neurol. 237, 477–488.

Molyneaux, B.J., Arlotta, P., Fame, R.M., MacDonald, J.L., MacQuarrie, K.L., Macklis, J.D., 2009. Novel subtype-specific genes identify distinct subpopulations of callosal projection neurons. J. Neurosci. 29, 12343–12354.

Moog, N.K., Entringer, S., Heim, C., Wadhwa, P.D., Kathmann, N., Buss, C., 2017. Influence of maternal thyroid hormones during gestation on fetal brain development. Neuroscience 342, 68–100.

Mooradian, A.D., Chung, H.C., Shah, G.N., 1997. GLUT-1 expression in the cerebra of patients with Alzheimer's disease. Neurobiol. Aging 18, 469–474.

Moreno-Mateos, M.A., Vejnar, C.E., Beaudoin, J.-D., Fernandez, J.P., Mis, E.K., Khokha, M.K., Giraldez, A.J., 2015. CRISPRscan: designing highly efficient sgRNAs for CRISPR/Cas9 targeting in vivo. Nat. Methods 12, 982–988.

Morreale De Escobar, G., Obregon, M.J., Escobar Del Rey, F., 2000. Clinical perspective: Is neuropsychological development related to maternal hypothyroidism or to maternal hypothyroxinemia? J. Clin. Endocrinol. Metab. 85, 3975–3987.

Morte, B., Gil-Ibáñez, P., Bernal, J., 2018. Regulation of Gene Expression by Thyroid Hormone in Primary Astrocytes: Factors Influencing the Genomic Response. Endocrinology 159, 2083–2092.

Murakami, Y., Tanaka, M., 2011. Evolution of motor innervation to vertebrate fins and limbs. Dev. Biol. 355, 164–172.

Murao, N., Noguchi, H., Nakashima, K., 2016. Epigenetic regulation of neural stem cell property from embryo to adult. Neuroepigenetics 5, 1–10.

Nagy, J.I., Rash, J.E., 2003. Astrocyte and oligodendrocyte connexins of the glial syncytium in relation to astrocyte anatomical domains and spatial buffering. Cell Commun. Adhes. 10, 401–406.

Niazi, A., Kalra, S., Irfan, A., Islam, A., 2011. Thyroidology over the ages. Indian J. Endocrinol. Metab. 15, 121–126.

Nolte, C., Rastegar, M., Amores, A., Bouchard, M., Grote, D., Maas, R., Kovacs, E.N., Postlethwait, J., Rambaldi, I., Rowan, S., Yan, Y.L., Zhang, F., Featherstone, M., 2006. Stereospecificity and PAX6 function direct Hoxd4 neural enhancer activity along the antero-posterior axis. Dev. Biol. 299, 582–593.

Nornes, S., Clarkson, M., Mikkola, I., Pedersen, M., Bardsley, A., Martinez, J.P., Krauss, S., Johansen, T., 1998. Zebrafish contains two Pax6 genes involved in eye development1The sequence reported in this paper has been deposited in the GenBank data base (accession no. AF061252).1. Mech. Dev. 77, 185–196.

Noten, A.M.E., Loomans, E.M., Vrijkotte, T.G.M., Van De Ven, P.M., Paul Van Trotsenburg, A.S., Rotteveel, J., Van Eijsden, M., Finken, M.J.J., 2015. Maternal hypothyroxinaemia in early pregnancy and school performance in 5-year-old offspring. Eur. J. Endocrinol. 173, 563–571.

Novara, F., Groeneweg, S., Freri, E., Estienne, M., Reho, P., Matricardi, S., Castellotti, B., Visser, W.E., Zuffardi, O., Visser, T.J., 2017. Clinical and Molecular Characteristics of SLC16A2 (MCT8) Mutations in Three Families with the Allan–Herndon–Dudley Syndrome. Hum. Mutat. 38, 260–264.

Novitch, B.G., Wichterle, H., Jessell, T.M., Sockanathan, S., 2003. A requirement for retinoic acid-mediated transcriptional activation in ventral neural patterning and motor neuron specification. Neuron 40, 81–95.

O'Brown, N.M., Pfau, S.J., Gu, C., 2018. Bridging barriers: A comparative look at the blood-brain barrier across organisms. Genes Dev. 32, 466–478.

O'Shaughnessy, K.L., Mcmichael, B.D., Sasser, A.L., Bell, K.S., Riutta, C., Ford, J.L., Stoker, T.E., Grindstaff, R.D., Pandiri, A.R., Gilbert, M.E., Bastian, T., 2023. Thyroid hormone action controls multiple components of cell junctions at the ventricular zone in the newborn rat brain. Front. Endocrinol. (Lausanne). 1–16.

Obermeier, B., Daneman, R., Ransohoff, R.M., 2013. Development, maintenance and disruption of the blood-brain barrier. Nat. Med. 19, 1584–1596.

Obregon, M., Calvo, R., Escobar Del Rey, F., Morreale De Escobar, G., 2007. Ontogenesis of thyroid function and interactions with maternal function. Endocr. Dev. 10, 86–98.

Oetting, A., Yen, P.M., 2007. New insights into thyroid hormone action. Best Pract. Res. Clin. Endocrinol. Metab. 21, 193–208.

Okano, H., Temple, S., 2009. Cell types to order: temporal specification of CNS stem cells. Curr. Opin. Neurobiol. 19, 112–119.

Ono, E., Ariga, M., Oshima, S., Hayakawa, M., Imai, M., Ochiai, Y., Mochizuki, H., Namba, N., Ozono, K., Miyata, I., 2016. Three novel mutations of the MCT8 (SLC16A2) gene: individual and temporal variations of endocrinological and radiological features. Clin. Pediatr. Endocrinol. 25, 23–35.

Opitz, R., Antonica, F., Costagliola, S., 2013. New Model Systems to Illuminate Thyroid Organogenesis. Part I: An Update on the Zebrafish Toolbox. Eur. Thyroid J. 2, 229–242.

Opitz, R., Köhrle, J., 2017. Editorial: Get inspired - Lessons learned from evolution of thyroid hormone signaling in developmental processes. Mol. Cell. Endocrinol. 459, 1–4.

Oppenheimer, J.H., Schwartz, H.L., 1997. Molecular basis of thyroid hormone-dependent brain development. Endocr. Rev. 18, 462–475.

Ortiga-Carvalho, T.M., Chiamolera, M.I., Pazos-Moura, C.C., Wondisford, F.E., 2016. Hypothalamus-pituitary-thyroid axis. Compr. Physiol. 6, 1387–1428.

Osumi, N., Shinohara, H., Numayama-Tsuruta, K., Maekawa, M., 2008. Concise Review: Pax6 Transcription Factor Contributes to both Embryonic and Adult Neurogenesis as a Multifunctional Regulator. Stem Cells 26, 1663–1672.

Pancotto, T., Rossmeisl, J.H., Panciera, D.L., Zimmerman, K.L., 2010. Blood-brain-barrier disruption in chronic canine hypothyroidism. Vet. Clin. Pathol. 39, 485–493.

Pancotto, T.E., Rossmeisl, J.H., Huckle, W.R., Inzana, K.D., Zimmerman, K.L., 2016. Evaluation of endothelin-1 and MMPs-2, -9, -14 in cerebrospinal fluid as indirect indicators of blood–brain barrier dysfunction in chronic canine hypothyroidism. Res. Vet. Sci. 105, 115–120.

Panicker, V., Cluett, C., Shields, B., Murray, A., Parnell, K.S., Perry, J.R.B., Weedon, M.N., Singleton, A., Hernandez, D., Evans, J., Durant, C., Ferrucci, L., Melzer, D., Saravanan, P., Visser, T.J., Ceresini, G., Hattersley, A.T., Vaidya, B., Dayan, C.M., Frayling, T.M., 2008. A common variation in deiodinase 1 gene DIO1 is associated with the relative levels of free thyroxine and triiodothyronine. J. Clin. Endocrinol. Metab. 93, 3075–3081.

Pardridge, W.M., 2003. Blood-brain barrier drug targeting: the future of brain drug development. Mol. Interv. 3, 90–105.

Paredes, I., Himmels, P., Almodo, C.R. De, 2018. Neurovascular Communication during CNS Development. Dev. Cell 45, 10–32.

Paridaen, J.T., Huttner, W.B., 2014. Neurogenesis during development of the vertebrate central nervous system. EMBO Rep. 15, 351–364.

Park, K.W., Morrison, C.M., Sorensen, L.K., Jones, C.A., Rao, Y., Chien, C. Bin, Wu, J.Y., Urness, L.D., Li, D.Y., 2003. Robo4 is a vascular-specific receptor that inhibits endothelial migration. Dev. Biol. 261, 251–267.

Parker, M.W., Xu, P., Li, X., Vander Kooi, C.W., 2012. Structural basis for selective vascular endothelial growth factor-A (VEGF-A) binding to neuropilin-1. J. Biol. Chem. 287, 11082–11089.

Parsons, M.J., Pollard, S.M., Saúde, L., Feldman, B., Coutinho, P., Hirst, E.M.A., Stemple, D.L., 2002. Zebrafish mutants identify an essential role for laminins in notochord formation. Development 129, 3137–3146.

Patel, J., Landers, K., Li, H., Mortimer, R.H., Richard, K., 2011. Thyroid hormones and fetal neurological development. J. Endocrinol. 209, 1–8.

Patel, Jatin, Landers, K., Li, H., Mortimer, R.H., Richard, K., 2011. Delivery of maternal thyroid hormones to the fetus. Trends Endocrinol. Metab. 22, 164–170.

Patel, V., Aldridge, K., Ensley, J.F., Odell, E., Boyd, A., Jones, J., Gutkind, S., Yeudall, W.A., 2002. Laminin-γ2 overexpression in head-and-neck squamous cell carcinoma. Int. J. Cancer 99, 583–588.

Peeters, R.P., Van Den Beld, A.W., Attalki, H., Van Toor, H., De Rijke, Y.B., Kuiper, G.G.J.M., Lamberts, S.W.J., Janssen, J.A.M.J.L., Uitterlinden, A.G., Visser, T.J., 2005. A new polymorphism in the type II deiodinase gene is associated with circulating thyroid hormone parameters. Am. J. Physiol. - Endocrinol. Metab. 289, 75–81.

Peeters, R.P., Van Toor, H., Klootwijk, W., De Rijke, Y.B., Kuiper, G.G.J.M., Uitterlinden, A.G., Visser, T.J., 2003. Polymorphisms in thyroid hormone pathway genes are associated with plasma TSH and iodothyronine levels in healthy subjects. J. Clin. Endocrinol. Metab. 88, 2880–2888.

Peretz, Y., Eren, N., Kohl, A., Hen, G., Yaniv, K., Weisinger, K., Cinnamon, Y., Sela-Donenfeld, D., 2016. A new role of hindbrain boundaries as pools of neural stem/progenitor cells regulated by Sox2. BMC Biol. 14, 1–20.

Phng, L.K., Gerhardt, H., 2009. Angiogenesis: A Team Effort Coordinated by Notch. Dev. Cell 16, 196–208.

Pinto, L., Götz, M., 2007. Radial glial cell heterogeneity-The source of diverse progeny in the CNS. Prog. Neurobiol. 83, 2–23.

Plessis, A.J. du, Volpe, J.J., 2018. Chapter 1 - Neural Tube Development. In: Volpe's Neurology of the Newnorn (Sixth Edition). pp. 3–33.

Porazzi, P., Calebiro, D., Benato, F., Tiso, N., Persani, L., 2009. Thyroid gland development and function in the zebrafish model. Mol. Cell. Endocrinol. 312, 14–23.

Potente, M., Gerhardt, H., Carmeliet, P., 2011. Basic and therapeutic aspects of angiogenesis. Cell 146, 873–887.

Préau, L., Fini, J.B., Morvan-Dubois, G., Demeneix, B., 2015. Thyroid hormone signaling during early neurogenesis and its significance as a vulnerable window for endocrine disruption. Biochim. Biophys. Acta - Gene Regul. Mech. 1849, 112–121.

Prezioso, G., Giannini, C., Chiarelli, F., 2018. Effect of thyroid hormones on neurons and neurodevelopment. Horm. Res. Paediatr. 90, 73–81.

Protze, J., Braun, D., Hinz, K.M., Bayer-Kusch, D., Schweizer, U., Krause, G., 2017. Membrane-traversing mechanism of thyroid hormone transport by monocarboxylate transporter 8. Cell. Mol. Life Sci. 74, 2299–2318.

Qiu, J.-J., Zhang, Q., Geng, Z., Liu, M., Chen, J., Liu, F., 2019. Identification of a novel PAX6 mutation in a Chinese family with aniridia. BMC Ophthalmol. 19, 10–15.

Quiñonez-Silvero, C., Hübner, K., Herzog, W., 2020. Development of the brain vasculature and the blood-brain barrier in zebrafish. Dev. Biol. 457, 181–190.

Raab, S., Beck, H., Gaumann, A., Yüce, A., Gerber, H.P., Plate, K., Hammes, H.P., Ferrara, N., Breier, G., 2004. Impaired brain angiogenesis and neuronal apoptosis induced by conditional homozygous inactivation of vascular endothelial growth factor. Thromb. Haemost. 91, 595–605.

Rastogi, M. V., LaFranchi, S.H., 2010. Congenital hypothyroidism. Orphanet J. Rare Dis. 5, 1–22.

Redzic, Z.B., Segal, M.B., 2004. The structure of the choroid plexus and the physiology of the choroid plexus epithelium. Adv. Drug Deliv. Rev. 56, 1695–1716.

Refetoff, S., Bassett, J.H.D., Beck-Peccoz, P., Bernal, J., Brent, G., Chatterjee, K., De Groot, L.J., Dumitrescu, A.M., Jameson, J.L., Kopp, P.A., Murata, Y., Persani, L., Samarut, J., Weiss, R.E., Williams, G.R., Yen, P.M., 2014. Classification and proposed nomenclature for inherited defects of thyroid hormone action, cell transport, and metabolism. Thyroid 24, 407–409.

Refetoff, S., Dumitrescu, A.M., 2007. Syndromes of reduced sensitivity to thyroid hormone: genetic defects in hormone receptors, cell transporters and deiodination. Best Pract. Res. Clin. Endocrinol. Metab. 21, 277–305.

Refetoff, S., Pappa, T., Williams, M.K., Matheus, M.G., Liao, X.H., Hansen, K., Nicol, L., Pierce, M., Blasco, P.A., Jensen, M.W., Bernal, J., Weiss, R.E., Dumitrescu, A.M., Lafranchi, S., 2021. Prenatal Treatment of Thyroid Hormone Cell Membrane Transport Defect Caused by MCT8 Gene Mutation. Thyroid 31, 713–720.

Remerand, G., Boespflug-Tanguy, O., Tonduti, D., Touraine, R., Rodriguez, D., Curie, A., Perreton, N., Des Portes, V., Sarret, C., Afenjar, A., Burglen, L., Castellotti, B., Cuntz, D., Desguerre, I., Doummar, D., Estienne, M., Freri, E., Heron, D., Moutard, M.L., Novara, F., Orcesi, S., Saletti, V., Zibordi, F., 2019. Expanding the phenotypic spectrum of Allan–Herndon–Dudley syndrome in patients with SLC16A2 mutations. Dev. Med. Child Neurol. 61, 1439–1447.

Reuss, M.L., Paneth, N., Pinto-Martin, J.A., Lorenz, J.M., Susser, M., 1996. The Relation of Transient Hypothyroxinemia in Preterm Infants to Neurologic Development at Two Years of Age. Obstet. Gynecol. Surv. 51, 470–472.

Reyahi, A., Nik, A.M., Ghiami, M., Gritli-Linde, A., Pontén, F., Johansson, B.R., Carlsson, P., 2015. Foxf2 Is Required for Brain Pericyte Differentiation and Development and Maintenance of the Blood-Brain Barrier. Dev. Cell 34, 19–32.

Ridaura, I.E., Sorrentino, S., Moroni, L., 2021. Parallels between the Developing Vascular and Neural Systems: Signaling Pathways and Future Perspectives for Regenerative Medicine. Adv. Sci. 8.

Risau, W., Hallmann, R., Albrecht, U., 1986. Differentiation-dependent expression of proteins in brain endothelium during development of the blood-brain barrier. Dev. Biol. 117, 537–545.

Robbins, J. and Rall, J.E., 1960. Proteins associated with the thyroid hormones. Physiol. Rev. 40, 415–489.

Roberts, L.M., Woodford, K., Zhou, M., Black, D.S., Haggerty, J.E., Tate, E.H., Grindstaff, K.K., Mengesha, W., Raman, C., Zerangue, N., 2008. Expression of the thyroid hormone transporters monocarboxylate transporter-8 (SLC16A2) and organic ion transporter-14 (SLCO1C1) at the blood-brain barrier. Endocrinology 149, 6251–6261.

Robinson, M.D., McCarthy, D.J., Smyth, G.K., 2009. edgeR: A Bioconductor package for differential expression analysis of digital gene expression data. Bioinformatics 26, 139–140.

Rogers, C.D., Moody, S.A., Casey, E.S., 2009. Neural induction and factors that stabilize a neural fate. Birth Defects Res. Part C - Embryo Today Rev. 87, 249–262.

Rossi, A., Gauvrit, S., Marass, M., Pan, L., Moens, C.B., Stainier, D.Y.R., 2016. Regulation of

Vegf signaling by natural and synthetic ligands. Blood 128, 2359–2366.

Roti, E., Fang, S.L., Green, K., Braverman, L.E., Emerson, C.H., 1981. Human placenta is an active site of thyroxine and 3, 3′, 5-triiodothyronine tyrosyl ring deiodination. Endocrinology 53, 498–501.

Ruhrberg, C., Bautch, V.L., 2013. Neurovascular development and links to disease. Cell. Mol. Life Sci. 70, 1675–1684.

Ruhrberg, C., Gerhardt, H., Golding, M., Watson, R., Ioannidou, S., Fujisawa, H., Betsholtz, C., Shima, D.T., 2002. Spatially restricted patterning cues provided by heparin-binding VEGF-A control blood vessel branching morphogenesis. Genes Dev. 16, 2684–2698.

Sainson, R.C.A., Aoto, J., Nakatsu, M.N., Holderfield, M., Conn, E., Koller, E., Hughes, C.C.W., 2005. Cell-autonomous notch signaling regulates endothelial cell branching and proliferation during vascular tubulogenesis. FASEB J. 19, 1027–1029.

Salvatore, D., Low, S.C., Berry, M., Maia, A.L., Harney, J.W., Croteau, W., St. Germain, D.L., Larsen, P.R., 1995. Type 3 iodothyronine deiodinase: Cloning, in vitro expression, and functional analysis of the placental selenoenzyme. J. Clin. Invest. 96, 2421–2430.

Sansom, S.N., Griffiths, D.S., Faedo, A., Kleinjan, D.J., Ruan, Y., Smith, J., Van Heyningen, V., Rubenstein, J.L., Livesey, F.J., 2009. The level of the transcription factor Pax6 is essential for controlling the balance between neural stem cell self-renewal and neurogenesis. PLoS Genet. 5, 20–23.

Saunders, N.R., Dreifuss, J.J., Dziegielewska, K.M., Johansson, P.A., Habgood, M.D., Møllgård, K., Bauer, H.C., 2014. The rights and wrongs of blood-brain barrier permeability studies: A walk through 100 years of history. Front. Neurosci. 8, 1–26.

Saunders, N.R., Dziegielewska, K.M., Møllgård, K., Habgood, M.D., 2018. Physiology and molecular biology of barrier mechanisms in the fetal and neonatal brain. J. Physiol. 596, 5723–5756.

Schindelin, J., Arganda-Carreras, I., Frise, E., Kaynig, V., Longair, M., Pietzsch, T., Preibisch, S., Rueden, C., Saalfeld, S., Schmid, B., Tinevez, J.Y., White, D.J., Hartenstein, V., Eliceiri, K., Tomancak, P., Cardona, A., 2012. Fiji: An open-source platform for biological-image analysis. Nat. Methods 9, 676–682.

Schmidt, R., Strähle, U., Scholpp, S., 2013. Neurogenesis in zebrafish - from embryo to adult. Neural Dev. 8, 1–13.

Schuermann, A., Helker, C.S.M., Herzog, W., 2014. Angiogenesis in zebrafish. Semin. Cell Dev. Biol. 31, 106–114.

Schulte-Merker, S., Stainier, D.Y.R., 2014. Out with the old, in with the new: reassessing morpholino knockdowns in light of genome editing technology. Development 141, 3103–3104.

Schussler, G.C., 2000. The Thyroxine-Binding Proteins. Mary Ann Liebert, Inc 10, 141–149.

Schwartz, C.E., May, M.M., Carpenter, N.J., Rogers, R.C., Martin, J., Bialer, M.G., Ward, J., Sanabria, J., Marsa, S., Lewis, J.A., Echeverri, R., Lubs, H.A., Voeller, K., Simensen, R.J., Stevenson, R.E., 2005. Allan-Herndon-Dudley Syndrome and the Monocarboxylate Transporter 8 (MCT8) Gene. Am. J. Hum. Genet. 77, 41–53.

Schwartz, C.E., Stevenson, R.E., 2007. The MCT8 thyroid hormone transporter and Allan--Herndon-- Dudley syndrome. Best Pract. Res. Clin. Endocrinol. Metab. 21, 307–321.

Schweizer, U., Johannes, J., Bayer, D., Braun, D., 2014. Structure and function of thyroid hormone plasma membrane transporters. Eur. Thyroid J. 3, 143–153.

Segura, I., De Smet, F., Hohensinner, P.J., Almodovar, C.R. de, Carmeliet, P., 2009. The neurovascular link in health and disease: an update. Trends Mol. Med. 15, 439–451.

Sengillo, J.D., Winkler, E.A., Walker, C.T., Sullivan, J.S., Johnson, M., Zlokovic, B. V., 2013. Deficiency in mural vascular cells coincides with blood-brain barrier disruption in alzheimer's disease. Brain Pathol. 23, 303–310.

Shalaby, F., Janet, R., Yamaguchi, T.P., Gertsenstein, M., Wu, X.F., Breitman, M.L., Schuh, A.C., 1995. Failure of blood-island formation and vasculogenesis in Flk-1-deficient mice. Nature.

Shparberg, R., Glover, H., Morris, M.B., 2019. Modelling mammalian commitment to the neural lineage using embryos and embryonic stem cells. Front. Physiol. 10.

Siekmann, A.F., Lawson, N.D., 2007. Notch signalling limits angiogenic cell behaviour in developing zebrafish arteries. Nature 445, 781–784.

Silva, N., 2020. Maternal thyroid hormones role in zebrafish neural development.

Silva, N., Campinho, M.A., 2023. In a zebrafish biomedical model of human Allan-Herndon-Dudley syndrome impaired MTH signaling leads to decreased neural cell diversity. Front. Endocrinol. (Lausanne). 1–22.

Silva, N., Louro, B., Trindade, M., Power, D.M., Campinho, M.A., 2017. Transcriptomics reveal an integrative role for maternal thyroid hormones during zebrafish embryogenesis. Sci. Rep. 7, 1–11.

Simic, N., Asztalos, E. V., Rovet, J., 2009. Impact of neonatal thyroid hormone insufficiency and medical morbidity on infant neurodevelopment and attention following preterm birth. Thyroid 19, 395–401.

Simon, M.C., Keith, B., 2008. The role of oxygen availability in embryonic development and stem cell function. Nat. Rev. Mol. Cell Biol. 9, 285–296.

Sinha, R.A., Singh, B.K., Yen, P.M., 2014. Thyroid hormone regulation of hepatic lipid and carbohydrate metabolism. Trends Endocrinol. Metab. 25, 538–545.

Sixt, M., Engelhardt, B., Pausch, F., Hallmann, R., Wendler, O., Sorokin, L.M., 2001. Endothelial cell laminin isoforms, laminins 8 and 10, play decisive roles in T cell recruitment across the blood-brain barrier in experimental autoimmune encephalomyelitis. J. Cell Biol. 153, 933–945.

Skah, S., Uchuya-Castillo, J., Sirakov, M., Plateroti, M., 2017. The thyroid hormone nuclear receptors and the Wnt/β-catenin pathway: An intriguing liaison. Dev. Biol. 422, 71–82.

Smallridge, R.C., 1980. Thyroid Hormone Effects on the Heart. Hear. Hear. Organs 93–160.

Soker, S., Miao, H.Q., Nomi, M., Takashima, S., Klagsbrun, M., 2002. VEGF165 mediates formation of complexes containing VEGFR-2 and neuropilin-1 that enhance VEGF165-

receptor binding. J. Cell. Biochem. 85, 357–368.

Song, J., Lu, Y., Cheng, X., Shi, C., Lou, Q., Jin, X., He, J., Zhai, G., Yin, Z., 2021. Functions of the thyroid-stimulating hormone on key developmental features revealed in a series of zebrafish dyshormonogenesis models. Cells 10.

St-Onge, L., Sosa-Pineda, B., Chowdhury, K., Mansouri, A., Gruss, P., 1997. Pax6 is required for differentiation of glucagon-producing α-cells in mouse pancreas. Nature.

Stamatovic, S., Keep, R., Andjelkovic, A., 2008. Brain Endothelial Cell-Cell Junctions: How to "Open" the Blood Brain Barrier. Curr. Neuropharmacol. 6, 179–192.

Stenman, J.M., Rajagopal, J., Carroll, T.J., Ishibashi, M., McMahon, J., McMahon, A.P., 2008. Canonical Wnt signaling regulates organ-specific assembly and differentiation of CNS vasculature. Science (80-.). 322, 1247–1250.

Stepien, B.K., Huttner, W.B., 2019. Transport, metabolism, and function of thyroid hormones in the developing mammalian brain. Front. Endocrinol. (Lausanne). 10, 1–16.

Stern, C.D., 2005. Neural induction: Old problem, new findings, yet more questions. Development 132, 2007–2021.

Streisinger, G., Walker, C., Dower, N., Knauber, D., Singer, F., 1981. Production of clones of homozygous diploid zebra fish (Brachydanio rerio). Nat. Publ. Gr. 291, 293–296.

Strømme, P., Groeneweg, S., Lima De Souza, E.C., Zevenbergen, C., Torgersbråten, A., Holmgren, A., Gurcan, E., Meima, M.E., Peeters, R.P., Visser, W.E., Høneren Johansson, L., Babovic, A., Zetterberg, H., Heuer, H., Frengen, E., Misceo, D., Visser, T.J., 2018. Mutated thyroid hormone transporter OATP1C1 associates with severe brain hypometabolism and juvenile neurodegeneration. Thyroid 28, 1406–1415.

Styne, D.M., 2016. Pediatric endocrinology: A clinical handbook, Pediatric Endocrinology: A Clinical Handbook.

Sun, T., Pringle, N.P., Hardy, A.P., Richardson, W.D., Smith, H.K., 1998. Precursors in the Ventral Neural Tube. Mol. Cell. Neurosci. 239, 228–239.

Swanson, O.K., Maffei, A., 2019. From hiring to firing: Activation of inhibitory neurons and their recruitment in behavior. Front. Mol. Neurosci. 12, 1–9.

Sweeney, M.D., Sagare, A.P., Zlokovic, B. V., 2018. Blood-brain barrier breakdown in Alzheimer disease and other neurodegenerative disorders. Nat. Rev. Neurol. 14, 133–150.

Sztal, T., Berger, S., Currie, P.D., Hall, T.E., 2011. Characterization of the laminin gene family and evolution in zebrafish. Dev. Dyn. 240, 422–431.

Takahashi, M., Osumi, N., 2011. Pax6 regulates boundary-cell specification in the rat hindbrain. Mech. Dev. 128, 289–302.

Takahashi, T., Takase, Y., Yoshino, T., Saito, D., Tadokoro, R., Takahashi, Y., 2015. Angiogenesis in the developing spinal cord: Blood vessel exclusion from neural progenitor region is mediated by VEGF and its antagonists. PLoS One 10, 1–20.

Takayama, S., Hostick, U., Haendel, M., Eisen, J., Darimont, B., 2008. An F-Domain Introduced by Alternative Splicing Regulates Activity of the Zebrafish Thyroid Hormone

Receptor α: Role of zebrafish TRα F-domain. Gen. Comp. Endocrinol. 155, 176–189.

Tallafuss, A., Hale, L.A., Yan, Y.L., Dudley, L., Eisen, J.S., Postlethwait, J.H., 2006. Characterization of retinoid-X receptor genes rxra, rxrba, rxrbb and rxrg during zebrafish development. Gene Expr. Patterns 6, 556–565.

Tam, S.J., Richmond, D.L., Kaminker, J.S., Modrusan, Z., Martin-McNulty, B., Cao, T.C., Weimer, R.M., Carano, R.A.D., vanBruggen, N., Watts, R.J., 2012. Death Receptors DR6 and TROY Regulate Brain Vascular Development. Dev. Cell 22, 403–417.

Tam, S.J., Watts, R.J., 2010. Connecting Vascular and Nervous System Development: Angiogenesis and the Blood-Brain Barrier. Annu. Rev. Neurosci. 33, 379–408.

Tambalo, M., Mitter, R., Wilkinson, D.G., 2020. A single cell transcriptome atlas of the developing zebrafish hindbrain. Dev. 147.

Tammela, T., Zarkada, G., Wallgard, E., Murtomäki, A., Suchting, S., Wirzenius, M., Waltari, M., Hellström, M., Schomber, T., Peltonen, R., Freitas, C., Duarte, A., Isoniemi, H., Laakkonen, P., Christofori, G., Ylä-Herttuala, S., Shibuya, M., Pytowski, B., Eichmann, A., Betsholtz, C., Alitalo, K., 2008. Blocking VEGFR-3 suppresses angiogenic sprouting and vascular network formation. Nature 454, 656–660.

Tan, X., Liu, W.A., Zhang, X.J., Shi, W., Ren, S.Q., Li, Z., Brown, K.N., Shi, S.H., 2016. Vascular Influence on Ventral Telencephalic Progenitors and Neocortical Interneuron Production. Dev. Cell 36, 624–638.

Tata, M., Ruhrberg, C., 2018. Cross-talk between blood vessels and neural progenitors in the developing brain. Neuronal Signal. 2, 1–13.

Tata, M., Ruhrberg, C., Fantin, A., 2015. Vascularisation of the central nervous system. Mech. Dev. 138, 26–36.

Taverna, E., Götz, M., Huttner, W.B., 2014. The cell biology of neurogenesis: toward an understanding of the development and evolution of the neocortex, Annual review of cell and developmental biology.

Teng, W., Shan, Z., Patil-Sisodia, K., Cooper, D.S., 2013. Hypothyroidism in pregnancy. Lancet Diabetes Endocrinol. 1, 228–237.

Thanas, C., Ziros, P.G., Chartoumpekis, D. V, Renaud, C.O., Sykiotis, G.P., 2020. The Keap1/Nrf2 Signaling Pathway in the Thyroid-2020 Update. Antioxidants 9, 1–14.

Thisse B, Thisse C (2004) Fast release clones: a high throughput expression analysis. Available at: http://zfin.org/cgi-bin/webdriver?MIval¼aa-pubview2. apg&OID¼ZDB-PUB-040907–1. Accessed: 16 January 2008.

Thisse, C., Degrave, A., Kryukov, G.V.G. V., Gladyshev, V.N., Obrecht-Pflumio, S., Krol, A., Thisse, B., Lescure, A., 2003. Spatial and temporal expression patterns of selenoprotein genes during embryogenesis in zebrafish. Gene Expr. Patterns 3, 525–532.

Thisse, C., Thisse, B., 2008. High-resolution in situ hybridization to whole-mount zebrafish embryos. Nat. Protoc. 3, 59–69.

Thomsen, M.S., Routhe, L.J., Moos, T., 2017. The vascular basement membrane in the healthy

and pathological brain. J. Cereb. Blood Flow Metab. 37, 3300–3317.

Thorpe-Beeston, J.G., Nicolaides, K.H., Felton, C. V., Butler, J., McGregor, A.M., 1991. Maturation of the secretion of thyroid hormone and thyroid-stimulating hormone in the fetus. N. Engl. J. Med. 329, 532–536.

Thummel, R., Enright, J.M., Kassen, S.C., Montgomery, J.E., Bailey, T.J., Hyde, D.R., 2010. Pax6a and Pax6b are required at different points in neuronal progenitor cell proliferation during zebrafish photoreceptor regeneration. Exp. Eye Res. 90, 572–582.

Timme-Laragy, A.R., Karchner, S.I., Hahn, M.E., 2012. Gene knockdown by morpholino-modified oligonucleotides in the zebrafish (danio rerio) model: Applications for developmental toxicology. Methods Mol. Biol. 889, 51–71.

Trajkovic, M., Visser, T.J., Mittag, J., Horn, S., Lukas, J., Darras, V.M., Raivich, G., Bauer, K., Heuer, H., 2007. Abnormal thyroid hormone metabolism in mice lacking the monocarboxylate transporter 8. J. Clin. Invest. 117, 627–635.

Tramontin, A.D., García-Verdugo, J.M., Lim, D.A., Alvarez-Buylla, A., 2003. Postnatal development of radial glia and the ventricular zone (VZ): A continuum of the neural stem cell compartment. Cereb. Cortex 13, 580–587.

Trapnell, C., Roberts, A., Goff, L., Pertea, G., Kim, D., Kelley, D.R., Pimentel, H., Salzberg, S.L., Rinn, J.L., Pachter, L., 2013. Differential gene and transcript expression analysis of RNA-seq experiments with TopHat and Cufflinks. Nat. Protoc. 7, 562–578.

Tu, H.M., Legradi, G., Bartha, T., Salvatore, D., Lechan, R.M., Larsen, P.R., 1999. Regional expression of the type 3 iodothyronine deiodinase messenger ribonucleic acid in the rat central nervous system and its regulation by thyroid hormone. Endocrinology 140, 784–790.

Ulrich, F., Carretero-Ortega, J., Menéndez, J., Narvaez, C., Sun, B., Lancaster, E., Pershad, V., Trzaska, S., Véliz, E., Kamei, M., Prendergast, A., Kidd, K.R., Shaw, K.M., Castranova, D.A., Pham, V.N., Lo, B.D., Martin, B.L., Raible, D.W., Weinstein, B.M., Torres-Vázquez, J., 2016. Reck enables cerebrovascular development by promoting canonical Wnt signaling. Dev. 143, 147–159.

Ulrich, F., Ma, L.H., Baker, R.G., Torres-V??zquez, J., 2011. Neurovascular development in the embryonic zebrafish hindbrain. Dev. Biol. 357, 134–151.

Umans, R.A., Henson, H.E., Mu, F., Parupalli, C., Ju, B., Peters, J.L., Lanham, K.A., Plavicki, J.S., Taylor, M.R., 2017. CNS angiogenesis and barriergenesis occur simultaneously. Dev. Biol. 425, 101–108.

Untergasser, A., Cutcutache, I., Koressaar, T., Ye, J., Faircloth, B.C., Remm, M., Rozen, S.G., 2012. Primer3-new capabilities and interfaces. Nucleic Acids Res. 40, 1–12.

Urbán, N., Guillemot, F., 2014. Neurogenesis in the embryonic and adult brain: Same regulators, different roles. Front. Cell. Neurosci. 8, 1–19.

Utiger, R., 1999. Maternal hypothyroidism and fetal development. N. Engl. J. Med. 341, 321–354.

van Heyningen, V., Williamson, K.A., 2002. PAX6 in sensory development. Hum. Mol. Genet. 11, 1161–1167.

van Mullem, A., van Heerebeek, R., Chrysis, D., Visser, E., Medici, M., Andrikoula, M., Tsatsoulis, A., Peeters, R., Visser, T.J., 2012. Clinical phenotype and mutant TRα1. N. Engl. J. Med. 366, 1451–1453.

Van Wassenaer, A.G., Kok, J.H., 2004. Hypothyroxinaemia and thyroid function after preterm birth. Semin. Neonatol. 9, 3–11.

Vancamp, P., Darras, V.M., 2017. Dissecting the role of regulators of thyroid hormone availability in early brain development: Merits and potential of the chicken embryo model. Mol. Cell. Endocrinol. 459, 71–78.

Vancamp, P., Houbrechts, A.M., Darras, V.M., 2019. Insights from zebrafish deficiency models to understand the impact of local thyroid hormone regulator action on early development. Gen. Comp. Endocrinol. 279, 45–52.

Vanderpas, J.B., Rivera-Vanderpas, M.T., Bourdoux, P., Luvivila, K., Lagasse, R., Perlmutter-Cremer, N., Delange, F., Lanoie, L., Ermans, A.M., Thilly, C.H., 1986. Reversibility of severe hypothyroidism with supplementary iodine in patients with endemic cretinism. N. Engl. J. Med. 315, 791–795.

Vatine, G.D., Zada, D., Lerer-Goldshtein, T., Tovin, A., Malkinson, G., Yaniv, K., Appelbaum, L., 2013. Zebrafish as a model for monocarboxyl transporter 8-deficiency. J. Biol. Chem. 288, 169–180.

Vaz, R., Hofmeister, W., Lindstrand, A., 2019. Zebrafish models of neurodevelopmental disorders: Limitations and benefits of current tools and techniques. Int. J. Mol. Sci. 20.

Vella, K.R., Hollenberg, A.N., 2017. The actions of thyroid hormone signaling in the nucleus. Mol. Cell. Endocrinol. 458, 127–135.

Vergauwen, L., Cavallin, J.E., Ankley, G.T., Bars, C., Gabriëls, I.J., Michiels, E.D.G., Fitzpatrick, K.R., Periz-Stanacev, J., Randolph, E.C., Robinson, S.L., Saari, T.W., Schroeder, A.L., Stinckens, E., Swintek, J., Van Cruchten, S.J., Verbueken, E., Villeneuve, D.L., Knapen, D., 2018. Gene transcription ontogeny of hypothalamic-pituitary-thyroid axis development in early-life stage fathead minnow and zebrafish. Gen. Comp. Endocrinol. 266, 87–100.

Verloop, H., Dekkers, O.M., Peeters, R.P., Schoones, J.W., Smit, J.W.A., 2014. Genetics in endocrinology: Genetic variation in deiodinases: A systematic review of potential clinical effects in humans. Eur. J. Endocrinol. 171, R123–R135.

Vigone, M.C., Caiulo, S., Di Frenna, M., Ghirardello, S., Corbetta, C., Mosca, F., Weber, G., 2014. Evolution of thyroid function in preterm infants detected by screening for congenital hypothyroidism. J. Pediatr. 164, 1296–1302.

Visser, W.E., Wong, W.S., van Mullem, A.A.A., Friesema, E.C.H., Geyer, J., Visser, T.J., 2010. Study of the transport of thyroid hormone by transporters of the SLC10 family. Mol. Cell. Endocrinol. 315, 138–145.

Vulsma, T., Gons, M.H., de Vijlder, J.J. m., 1989. Maternal-Fetal Transfer of Thyroxine in Congenital Hypothyroidism Due to a Total Organification Defect or Thyroid Agenesis. N. Engl. J. Med. 321, 13–16.

Walter, K.M., Miller, G.W., Chen, X., Yaghoobi, B., Puschner, B., Lein, P.J., 2019. Effects of thyroid hormone disruption on the ontogenetic expression of thyroid hormone signaling genes

in developing zebrafish (Danio rerio). Gen. Comp. Endocrinol. 272, 20–32.

Wang, Y.F., Liu, C., Xu, P.F., 2021. Deciphering and reconstitution of positional information in the human brain development. Cell Regen. 10, 1–13.

Wang, Y.Y., Pan, L.Y., Moens, C.B., Appel, B., 2014. Notch3 establishes brain vascular integrity by regulating pericyte number. Dev. 141, 307–317.

Watts, M.E., Pocock, R., Claudianos, C., 2018. Brain energy and oxygen metabolism: Emerging role in normal function and disease. Front. Mol. Neurosci. 11, 1–13.

Weber, M., Mickoleit, M., Huisken, J., 2014. Multilayer mounting for long-term light sheet microscopy of zebrafish. J. Vis. Exp. 1–8.

Weinstein, D.C., Hemmati-Brivanlou, A., 1999. Neural induction. Annu. Rev. Cell Dev. Biol. 15, 411–433.

Wild, R., Klems, A., Takamiya, M., Hayashi, Y., Strähle, U., Ando, K., Mochizuki, N., Van Impel, A., Schulte-Merker, S., Krueger, J., Preau, L., Le Noble, F., 2017. Neuronal sFlt1 and Vegfaa determine venous sprouting and spinal cord vascularization. Nat. Commun. 8.

Williams, G.R., 2000. Cloning and Characterization of Two Novel Thyroid Hormone Receptor β Isoforms. Mol. Cell. Biol. 20, 8329–8342.

Williams, G.R., 2008. Neurodevelopmental and neurophysiological actions of thyroid hormone. J. Neuroendocrinol. 20, 784–794.

Willoughby, K.A., McAndrews, M.P., Rovet, J.F., 2014. Effects of maternal hypothyroidism on offspring hippocampus and memory. Thyroid 24, 576–584.

Winkler, E.A., Bell, R.D., Zlokovic, B. V., 2014. Central nervous system pericytes in health and disease. Nat. Neurosci. 14, 1398–1405.

Winkler, E.A., Nishida, Y., Sagare, A.P., Rege, S. V., Bell, R.D., Perlmutter, D., Sengillo, J.D., Hillman, S., Kong, P., Nelson, A.R., Sullivan, J.S., Zhao, Z., Meiselman, H.J., Wendy, R.B., Soto, J., Abel, E.D., Makshanoff, J., Zuniga, E., De Vivo, D.C., Zlokovic, B. V., 2015. GLUT1 reductions exacerbate Alzheimer's disease vasculoneuronal dysfunction and degeneration. Nat. Neurosci. 18, 521–530.

Winkler, E.A., Sengillo, J.D., Sullivan, J.S., Henkel, J.S., Appel, S.H., Zlokovic, B. V., 2013. Blood-spinal cord barrier breakdown and pericyte reductions in amyotrophic lateral sclerosis. Acta Neuropathol. 125, 111–120.

Wirth, E.K., Roth, S., Blechschmidt, C., Hölter, S.M., Becker, L., Racz, I., Zimmer, A., Klopstock, T., Gailus-Durner, V., Fuchs, H., Wurst, W., Naumann, T., Bräuer, A., de Angelis, M.H., Köhrle, J., Grüters, A., Schweizer, U., 2009. Neuronal 3',3,5-triiodothyronine (T3) uptake and behavioral phenotype of mice deficient in Mct8, the neuronal T3 transporter mutated in Allan-Herndon-Dudley syndrome. J. Neurosci. 29, 9439–9449.

Wirth, E.K., Schweizer, U., Köhrle, J., 2014. Transport of thyroid hormone in brain. Front. Endocrinol. (Lausanne). 5, 1–7.

Won, C., Lin, Z., Kumar T., P., Li, S., Ding, L., Elkhal, A., Szabó, G., Vasudevan, A., 2013. Autonomous vascular networks synchronize GABA neuron migration in the embryonic

forebrain. Nat. Commun. 4.

Wu, Y., Koenig, R.J., 2000. Gene regulation by thyroid hormone. Trends Endocrinol. Metab. 11, 207–211.

Xing, G., Zhao, T., Zhang, X., Li, H., Li, X., Cui, P., Li, M., Li, D., Zhang, N., Jiang, W., 2020. Astrocytic Sonic Hedgehog Alleviates Intracerebral Hemorrhagic Brain Injury via Modulation of Blood-Brain Barrier Integrity. Front. Cell. Neurosci. 14, 1–15.

Yamanishi, E., Takahashi, M., Saga, Y., Osumi, N., 2012. Penetration and differentiation of cephalic neural crest-derived cells in the developing mouse telencephalon. Dev. Growth Differ. 54, 785–800.

Yamazaki, Y., Shinohara, Mitsuru, Shinohara, Motoko, Yamazaki, A., Murray, M.E., Liesinger, A.M., Heckman, M.G., Lesser, E.R., Parisi, J.E., Petersen, R.C., Dickson, D.W., Kanekiyo, T., Bu, G., 2019. Selective loss of cortical endothelial tight junction proteins during Alzheimer's disease progression. Brain 142, 1077–1092.

Yan, Y., Wang, Q., 2021. BMP Signaling: Lighting up the Way for Embryonic Dorsoventral Patterning. Front. Cell Dev. Biol. 9, 1–16.

Yen, P., 2001. Physiological and Molecular Basis of Thyroid Hormone Action. Physiol. Rev. 81, 1097–1143.

Yeo, S.Y., Chitnis, A.B., 2007. Jagged-mediated Notch signaling maintains proliferating neural progenitors and regulates cell diversity in the ventral spinal cord. Proc. Natl. Acad. Sci. U. S. A. 104, 5913–5918.

Yoshimasa, Y., Hamada, S., 1983. Thyroxine action on the rat liver nuclear thyroid-hormone receptors. Biochem. J. 210, 331–337.

Yu, X., Ji, C., Shao, A., 2020. Neurovascular Unit Dysfunction and Neurodegenerative Disorders. Front. Neurosci. 14, 1–8.

Zacchigna, S., Lambrechts, D., Carmeliet, P., 2008. Neurovascular signalling defects in neurodegeneration. Nat. Rev. Neurosci. 9, 169–181.

Zada, D., Blitz, E., Appelbaum, L., 2017. Zebrafish – An emerging model to explore thyroid hormone transporters and psychomotor retardation. Mol. Cell. Endocrinol. 459, 53–58.

Zada, D., Tovin, A., Lerer-Goldshtein, T., Appelbaum, L., 2016. Pharmacological treatment and BBB-targeted genetic therapy for MCT8-dependent hypomyelination in zebrafish. Dis. Model. Mech. 9, 1339–1348.

Zada, D., Tovin, A., Lerer-Goldshtein, T., Vatine, G.D., Appelbaum, L., 2014. Altered Behavioral Performance and Live Imaging of Circuit-Specific Neural Deficiencies in a Zebrafish Model for Psychomotor Retardation. PLoS Genet. 10.

Zenker, D., Begley, D., Bratzke, H., Rübsamen-Waigmann, H., von Briesen, H., 2003. Human blood-derived macrophages enhance barrier function of cultured primary bovine and human brain capillary endothelial cells. J. Physiol. 551, 1023–1032.

Zhang, B., Dietrich, U.M., Geng, J.G., Bicknell, R., Esko, J.D., Wang, L., 2009. Repulsive axon guidance molecule Slit3 is a novel angiogenic factor. Blood 114, 4300–4309.

Zhang, K., Xi, H., Wang, X., Guo, Y., Huang, S., Zheng, Z., Zhang, F., Gao, X., 2012. A Family-based Association Study of DIO2 and children mental retardation in the Qinba region of China. J. Hum. Genet. 57, 14–17.

Zhang, L., Cooper-Kuhn, C.M., Nannmark, U., Blomgren, K., Kuhn, H.G., 2010. Stimulatory effects of thyroid hormone on brain angiogenesis in vivo and in vitro. J. Cereb. blood flow Metab. 30, 323–335.

Zhang, X., Hoffmann, B., Tran, P.B.V., Graupner, G., Pfahl, M., 1992. Retinoid X receptor is an auxiliary protein for thyroid hormone and retinoid acid receptors. Nature 355, 441–446.

Zhou, Y., Nathans, J., 2014. Gpr124 controls CNS angiogenesis and blood-brain barrier integrity by promoting ligand-specific canonical Wnt signaling. Dev. Cell 31, 248–256.

Zlokovic, B. V., 2008. The Blood-Brain Barrier in Health and Chronic Neurodegenerative Disorders. Neuron 57, 178–201.

Zoeller, R.T., Rovet, J., 2004. Timing of Thyroid Hormone Action in the Developing Brain: Clinical Observations and Experimental Findings. J. Neuroendocrinol. 16, 809–818.

Zoeller, R.T., Tan, S.W., Tyl, R.W., 2007. General background on the hypothalamic-pituitary-thyroid (HPT) axis. Crit. Rev. Toxicol. 37, 11–53.